UILU-ENG-82-2006

CIVIL ENGINEERING STUDIES

STRUCTURAL RESEARCH SERIES NO. 498

RESPONSE OF PRESTRESSED CONCRETE PLATE-EDGE COLUMN CONNECTIONS

By
HARIANTO SUNIDJA
DOUGLAS A. FOUTCH
WILLIAM L. GAMBLE

UNIVERSITY OF ILLINOIS
at URBANA-CHAMPAIGN
URBANA, ILLINOIS
MARCH 1982

50272-101

REPORT DOCUMENTATION PAGE	1. REPORT NO. UILU-ENG-82-2006	2.	3. Recipient's Accession No.

4. Title and Subtitle

RESPONSE OF PRESTRESSED CONCRETE PLATE-EDGE COLUMN CONNECTIONS

5. Report Date

6.

7. Author(s)

Harianto Sunidja, Douglas A. Foutch, William L. Gamble

8. Performing Organization Rept. No. SRS 498

9. Performing Organization Name and Address

10. Project/Task/Work Unit No.

11. Contract(C) or Grant(G) No.

(C)

(G)

12. Sponsoring Organization Name and Address

13. Type of Report & Period Covered

14.

15. Supplementary Notes

16. Abstract (Limit: 200 words)

The main objective of this investigation was to study experimentally the strength and behavior of prestressed plate-edge column connections with unbonded tendons representative of those used in prestressed flat plate buildings. To achieve the objective, four two-thirds scale, flat plate-edge column specimens were constructed and subjected to static loadings in which both the shear and moment transferred between the slab and the column were increased proportionately until failure occurred. The experimental variables considered in this program were the direction of the banded tendons and the moment-shear ratio. Three models for predicting the strength of prestressed concrete flat plate-edge column connections were investigated. The problems associated with predicting the tendon stress were discussed and several models for predicting the tendon stress were presented and evaluated with respect to measured values.

17. Document Analysis a. Descriptors

bonded reinforcement, deflection, moment, plate, prestressed concrete, rotation, shear, slab, stiffness, strength, torsion, unbonded tendon

b. Identifiers/Open-Ended Terms

c. COSATI Field/Group

18. Availability Statement	19. Security Class (This Report) UNCLASSIFIED	21. No. of Pages 232
	20. Security Class (This Page) UNCLASSIFIED	22. Price

ACKNOWLEDGMENT

The work described in this report was conducted at the Nathan M. Newmark Civil Engineering Laboratory of the University of Illinois at Urbana-Champaign. The work was sponsored by MUCIA-AID-Indonesian Higher Education Development Training Project and by the University of Illinois Civil Engineering Department.

Appreciation is expressed for the kind and patient assistance of many who were involved with this work, several of whom are mentioned below.

This report was prepared as a doctoral dissertation by Harianto Sunidja, under the direction of Dr. D. A. Foutch, Assistant Professor of Civil Engineering, and Dr. W. L. Gamble, Professor of Civil Engineering. They are thanked for their invaluable suggestions and supervision of the work described in this report. The author is especially indebted to Dr. D. A. Foutch, for his guidance and stimulating encouragement during all phases of the author's study program at the University of Illinois.

Mr. G. H. Lafenhagen and Mr. D. C. Hines Jr. offered generous assistance in setting up instrumentation and data recording circuits. Mr. O. H. Ray and his staff helped in fabricating test specimens and hardware. The advice of D. G. Morrison and the assistance during testing of D. Hoedajanto, B. Hariandja, Indra Djati, and D. Honegger are gratefully

acknowledged.

The author would like to express his appreciation to the University of Indonesia for providing him the time away from his duties to study in the United States, and to Dr. Jean S. Taylor and her staff of MUCIA-AID-Indonesian Higher Education Development Training Project at Madison, for their assistance and guidance during his entire study program.

Finally, this undertaking could never have been completed without the encouragement, patience and understanding of his family, Maria, Karman and Didit. The author sincerely hopes that their efforts and sacrifices are well rewarded.

TABLE OF CONTENTS

LIST OF TABLES

LIST OF FIGURES

1. INTRODUCTION

1.1 General Remarks

A flat plate floor is supported by a series of columns, which are normally positioned in a square or rectangular pattern. There are no beams spanning from column to column in either direction. Flat plate floor construction is widely used for commercial and residential buildings because it results in aesthetically pleasing architectural lines, minimum floor to floor height, simple formwork, minimum obstruction to utility and duct placement, reduction of construction time, and good fire-resistance properties.

With the increasing demand for longer spans, the flexural stiffness of the flat plate system is reduced to the point where serviceability may become a critical factor in design. Prestressing the flat plate has been used to overcome this critical factor. Prestressing can be used effectively to control deflections, to minimize the chances of cracking, and to improve the punching resistance of the slab-column connection. Thus, since prestressed flat plates do not require drop panels or column capitals, they retain all of the beneficial aspects mentioned above.

The majority of prestressed flat plates are constructed using unbonded post-tensioned tendons because of speed of construction and other economic considerations. In recent years, the use of a banded tendon arrangement to simplify

construction has become popular even though this differs from the present ACI Building Code (ACI 318-77) [1] requirements and the tentative recommendations prepared by ACI-ASCE Committee 423 [6]. The tendons in this type of construction are grouped in a narrow band over the column line in one direction, while the tendons in the transverse direction are uniformly distributed. Fig. 1.1 shows the typical layout of the banded tendon arrangement for a two-thirds scale model slab.

Although the study of slab-column connections has received considerable attention, uncertainties still exist concerning the response of prestressed flat plates, even when this structural system is loaded statically. One of the major problems encountered in the design of flat plate structures lies in the connections between the plate and its supporting columns. Large bending moments as well as shearing forces are generally concentrated at the connection, and the connection is generally susceptible to punching shear failure. For edge columns in particular the presence of the free edge adds further to the concentrated stress condition at the connection. The complexity of the three-dimensional stress distribution in the portion of a plate immediately adjacent to a column and the large number of interdependent parameters have precluded development of a general analytical solution for calculating the strength of these connections. All available methods for designing these connections employ either approximate theoretical solutions which utilize

experimentally determined constants or purely empirical expressions which satisfy experimental results.

Extensive investigations have been made in an attempt to understand the behavior of slab-column connections, and they have focused primarily on typical interior columns. In contrast, most practical structures have more edge and corner columns than interior columns. Since very limited experimental or theoretical research has been carried out on post-tensioned plate-edge column connections subjected to combined shear and unbalanced moment, it is clear that further research is required in this area.

1.2 Object and Scope

In a typical flat plate floor carrying gravity loads, shear and unbalanced bending moment will be present at the edge column connections. The transfer of unbalanced bending moment causes the distribution of shear stress in the slab around the column to become nonuniform and reduces the shear strength of the connection. The main objective of this investigation was to study experimentally under static loading the strength and behavior of prestressed plate-edge column connections with unbonded tendons representative of those used in prestressed flat plate buildings.

To achieve the objective, four two-thirds scale, flat plate-edge column connections were constructed and subjected to loadings in which both the shear and moment transferred between the slab and the column were increased proportionately

until failure occurred. The experimental variables considered in this program were the direction of the banded tendons and the moment-shear ratio.

The specific objectives of this investigations were as follows:

1. To study the effect of the moment-shear ratio on the response of the connections.

2. To study the increase in stress in the unbonded tendons at ultimate load.

3. To study the basic mechanism of failure in the connections.

4. To develop a simple design procedure for predicting the ultimate strength of the connection.

Based on the results of experimental investigations of this study and investigations carried out by other investigators, practical recommendations are made for the design of prestressed flat plate-edge column connections.

2. REVIEW OF PREVIOUS RESEARCH

2.1 Introduction

Because prestressed concrete behaves similarly to reinforced concrete, with only a few special differences, this chapter will review the state of knowledge of the behavior of prestressed concrete as well as reinforced concrete slab-column connections. Numerous studies have been made in the attempt to understand the way in which the slab-column connection transfers load. In the discussion to follow, some of the methods of analysis based on these studies are discussed in detail so that their application to the present study can be easily followed.

This review is concerned principally with studies on transfer of shear and moment from flat plates to columns. Even for uniform gravity loading, there is always moment transfer at the edge column connections. The existing methods of analysis of slab-column connections transferring shear and unbalanced bending moment have progressed from an elastic plate theory to that of a limit design. These methods can be placed in four catagories: (1) analyses based on linear variation in shear stress, (2) analyses based on elastic plate theory, (3) beam analogies, and (4) yield line analysis.

2.2 Analyses Based on Linear Variation of Shear Stress

The methods for calculating the strength of the slab-

column connections reviewed in this section are related to each other in that they each assume a linear variation of vertical shear stress from the centroidal axis of the critical section. They differ in the assumed location of the critical sections and in the selection of the factor K which is the portion of the total unbalanced moment producing shear stresses on the critical section. These are important parameters because the transfer of any moment reduces the capacity of the connection in direct shear. Fig. 2.1 shows an assumed critical section and the linear distribution of shear stress for an exterior column connection.

In 1960, DiStasio and Van Buren [15] published a method for determining stresses at the connection between a flat plate and a column under combined shear and unbalanced moment. Prior to this, structural designers had no generally recognized method of analysis for designing the connections. Although the actual stress distribution on the critical section is extremely complex, DiStasio and Van Buren assumed that shear stresses on the critical section varied linearly with distance from the centroidal axis of the perimeter and were induced by the shear force and part of the unbalanced bending moment. The critical section was taken at a distance $(h - 1\frac{1}{2})$ in. from the column periphery as shown in Fig. 2.2a. The concept of an equivalent polar moment of inertia of the critical peripheral section was used to determined the shear stresses induced by the moment. The remainder of the

unbalanced moment was assumed to be carried by flexure in the slab and to be dependent on the amount of the flexural reinforcement through the critical section. Stresses were limited to those permitted under Working Stress Design.

An extensive test series using 43 slab-column specimens was reported by Moe [34] in 1961. He developed an ultimate strength analysis for moment transfer at an interior column by performing tests on twelve 6 ft. square, 6 in. thich slabs which were simply supported along all four edges. The load was applied at different eccentricities through a centrally located square column stub. The critical section governing the ultimate shear strength was taken at the column face as is shown in Fig. 2.2b. From his experimental test data, Moe concluded that approximately one-third of the total unbalanced moment was transferred by shear stresses. Following this semi-empirical approach, the portion of the unbalanced moment transferred by shear was then assumed to be constant and independent of the amount of the flexural reinforcement through the critical area. Moe also concluded that the shear strength was dependent on $\sqrt{f'_c}$. He believed that shear failures were controlled primarily by tensile splitting; and the tensile strength is generally assumed proportional to $\sqrt{f'_c}$.

To develop design recommendations for the 1963 ACI Code, ACI-ASCE Committee 326 [5] published a report, "Shear and Diagonal Tension," in 1962. The recommendations for slab

shear analysis contained in the report drew heavily from DiStasio and Van Buren's and Moe's investigations, and in addition took into account some preliminary information on Hanson and Hanson's [18] work. The Committee 326 report had great influence on the provisions adopted for the 1963 ACI Code. Three principal variables recognized as affecting the shear strength were the concrete strength, the relative size of the column compared to the slab thickness, and the magnitude of the bending moment near the column. The Committee found that Moe's equation for ultimate shear stress of concrete slabs could not be applied to connections with either very large or very small values of C/d, where C = side length of a square column and d = effective depth of the slab. To satisfy the above conditions, Committee 326 selected a hyperbolic equation.

$$v_u = 4\sqrt{f'_c}\ (d/C + 1)\ \text{psi} \qquad (2.1)$$

where f'_c is the compressive cylinder strength of concrete in psi. Based on the evaluation of 25 test results, and adopting a procedure similar to that suggested by Moe, the Committee recommended limiting the shear stress to $4\sqrt{f'_c}$ on a design critical section located at a distance d/2 from the column face and the portion of the unbalanced moment transferred by shear was taken as a constant value K = 0.2. The location of the critical section is shown in Fig. 2.2c.

The Commentary to the 1963 ACI Code includes a slightly modified form of the DiStasio and Van Buren Working Stress Design Method. It retains the concept that only the moment which cannot be transferred by flexural steel need be considered when examining the shear stress.

In 1968 Hanson and Hanson [18] reported the results of 17 tests on slab-column connections. Their principal interest was moment transfer at interior columns. Consequently, they tested only one specimen simulating conditions at an exterior column. The principal variables were the loading arrangement and the location of voids adjacent to the column. They concluded from their test data and interaction diagrams that the ultimate strength design method recommended by ACI-ASCE Committee 326 would give a good prediction of the strength of the slab-column connection when the moment reduction factor K was changed from 0.2 to 0.4.

A design recommendation was included for the first time in ACI 318-71 [3]. During preparation of a proposed revision of the 1963 ACI Code, it was noted that most test data considered by Hanson and Hanson involved square columns. In practice, however, rectangular columns are frequently used. It is logical to assume that the portion of moment transferred by flexure increases as the width of the face of the critical section resisting the moment increases. Accordingly, the fraction of the moment given by:

$$K = 1 - \frac{1}{1 + \frac{2}{3}\sqrt{\left(\frac{C_1 + d}{C_2 + d}\right)}} \qquad (2.2)$$

was considered transferred by shear about the centroid of the critical section. C_1 is the size of the rectangular column measured in direction of the moment, and C_2 the size of the rectangular column measured transverse to the direction of the moment. For square columns $C_1 = C_2 = C$ and $K = 0.4$ as suggested by Hanson and Hanson. The shear stress was limited to $4\sqrt{f'_c}$ on the critical section.

In Sections 11.11 and 11.12, the ACI Building Code [1] recommends a design procedure for reinforced concrete slab-column connections transferring shear and unbalanced bending moment without shear reinforcement. The Commentary to the 1977 ACI Code [2] gives the background to the present ACI Code recommendations. In 1974, ASCE-ACI Committee 426 [7] presented a comprehensive state-of-the-art report on the shear strength of slab-column connections.

An ASCE-ACI Committee 426 report published in 1977 [8] suggested revisions to the shear provisions of the 1971 ACI Code. The suggested revisions introduced comprehensive design provisions for moment transfer at slab-column connections. The ACI 318-77 Code does not contain all the revisions suggested in the ASCE-ACI Committee 426 report, but it is evident that the report is a valuable supplementary

design guide to the Code. The procedure recommended in the present ACI Code 318-77 is based on investigations by Hanson and Hanson and others reviewed in the ASCE-ACI Committee 426 state-of-the-art report. The critical section is taken as being a distance d/2 from the column periphery. The location of the critical section is shown in Fig. 2.2f. The analysis assumes that shear stresses on a critical perimeter vary linearly with distance from the centroidal axis of the critical section and are induced by the shear force and part of the unbalanced bending moment. The method is semiempirical, and the fraction of the unbalanced moment transferred by shear is assumed to be a function of the column geometry and is given by:

$$K = \gamma_v = 1 - \frac{1}{1 + \frac{2}{3}\sqrt{\left(\frac{C_1 + d}{C_2 + d}\right)}} \qquad (2.2)$$

The remainder of the unbalanced bending moment is carried by flexure at the front face of the column. The nominal shear strength of the connection is reached when the maximum shear stress at the critical section reaches:

$$v_c = \left(2 + \frac{4}{\beta_c}\right)\sqrt{f'_c}\ \text{psi} \leq 4\sqrt{f'_c}\ \text{psi} \qquad (2.3)$$

where β_c is the ratio of long side to short side of column, and f'_c the compressive cylinder strength of concrete in psi.

The above maximum shear stress was developed to facilitate calculation of the punching shear strength and to reflect the reduction in shear strength which occurs as the aspect ratio of a column section increases above 2.0.

2.3 Analyses Based on Elastic Plate Theory

The classical elastic plate theory assumes that the material of the slab is homogeneous and isotropic, and much of the early research into the strength of the slab-column connection transferring moment and shear used this elastic plate approach. At low levels of load the slab is uncracked and the distribution of forces can be computed from the elastic theory using the uncracked flexural stiffness of the slab. However, after cracking of the concrete and inelastic deformations have commenced, the stress distribution will change from that given by elastic theory and significant redistribution of internal actions can occur before the ultimate load is reached.

Long [29] reported a theoretical analysis of the punching shear problem of slabs containing two-way flexural reinforcement and no shear reinforcement. Elastic isotropic theory with several approximations was used to compute the stresses in the concrete compression zone at the column face even at failure. The failure load was found using an octahedral shear failure criterion for concrete. Several correction factors were also employed. Masterson [32] extended Long's work using a finite element plate bending analysis. His

analysis is, however, only applicable to slabs which yield before punching.

Mast [31] attempted to compare results from an elastic Navier solution of the isolated slab-column connection with an applied moment at the column to experimental results reported by Hanson and Hanson. Integration of these complex distributions to determine shear and torsional forces was simplified by the use of tables. Stresses computed by Mast's

the details of the various beam analogies may differ, the concept is the same. In calculating the strength of the slab-column connection, the beam analogy transforms a three dimensional problem into a two dimensional one. As a two dimensional analysis, the beam analogy provides a convenient method for determining the strength of slab-column connections transferring shear and unbalanced bending moment. An estimate of the strength of slab-column connections without shear reinforcement may be obtained from a beam analogy in which the slab adjacent to the column is assumed to act as beams running in two directions at right angles into the column faces. Fig. 2.3 shows faces of the critical section of an exterior slab-column connection with a square column. The slab strips which represent the beams are subjected to bending moment, torsional moment and shear force. Redistribution of these actions is assumed to be able to occur between the beams. Compatibility restrictions are ignored and each beam is assumed to deform sufficiently for the development of the governing ultimate bending moment, torsional moment, or shear for the beam. The strength equations can be based on the ACI 318-77 predictions for beams with an allowance for interaction effects. The strength of the connection is calculated by summing the contributions of the strengths of the beams.

Hawkins and Corley [21] developed an ultimate strength procedure for interior and exterior slab-column connections

based on a beam analogy. The strength of the edge connection is governed by either combined flexure and torsion, or combined shear and torsion. The moment-torsion failure is likely to control when the shear transferred to the column is relatively small. For a moment-torsion failure, significant rotations occur near the column prior to ultimate load. These rotations are sufficient to permit the top bars passing into the front face to yield in negative bending moment. The balance of the applied moment is taken in torsion on the side faces. The shear-torsion failure mode dominates when the shear transferred is significant. For a shear-torsion failure, the rotations will be less than those for a moment-torsion failure. The applied moment will be resisted initially at the front face of the column. The flexural strength of this face in negative moment must be exhausted before the balance of this moment can be distributed as torsion to the side faces. The distribution of shears is more difficult to establish. It is reasonable to expect that once the shear on the front face is close to its ultimate value, additional shears can be transferred to the side faces until a failure condition is also reached on these faces.

Park and Islam [40] developed a simpler beam analogy for interior slab-column connections, with or without shear reinforcement, which assumes that sufficient ductility in bending, torsion, and shear is available at the critical faces to allow development of the ultimate flexural,

torsional, and shear capacities as required.

Zaghlool and de Paiva [45] conducted tests on 21 edge and corner column specimens. Their analysis indicated that punching was a secondary phenomenon that occurred after the steel in the vicinity of the connection yielded. Punching developed because the compression zone of the slab was destroyed when the concrete stress reached its limiting strength for combined normal and shear stresses.

In order to verify the realism of the ultimate torsional shear stress on the side faces of a slab-column connection, Kanoh and Yoshizaki [26] tested eight slab-column specimens. The approach followed by Kanoh and Yoshizaki employs a beam analogy similar to that of Park and Islam. In their experimental study they applied a torque to the edge of 1/2.5 scale model test specimens as shown in Fig. 2.4. As the stub of the column was cast to the edge of the slab with only the face of the column able to transfer load, the flexural and shear components of moment in the complete specimen were effectively eliminated. From these tests, they concluded that an ultimate torsional shear stress of $24\sqrt{f'_c}$ may be used which is far greater than the value assumed in the ACI 318-77 Code. It seems that the increase in strength is due to the critical section of the slab being restrained by the continuum around it. Greater torsional strengths are to be expected for the critical sections of slab-column connections because the restraints are larger and transverse reinforcement is

continuous through the column.

2.5 Yield Line Analysis

In the design of flat plate floors it is important to insure that shear failures at slab-column connections do not precede a flexural failure. The yield line approach is a useful way of obtaining the flexural capacity of a slab-column connection. Since the yield line theory is an upper bound method, it is necessary to examine all possible collapse mechanisms around the connections. Under combined shear and unbalanced bending moment, the yield line pattern can be either a local mechanism in the slab surrounding the column involving fans of yield lines or a folding type collapse mechanism with yield lines extending across the slab. The high shear and torsional stresses at the slab-column connection indicate that the mode of failure is predominately governed by considerations of shear and torsion.

Park and Islam [40] have derived the folding type yield line pattern by considering a mechanism made up of negative yield lines at the faces of an interior column, as they must be if the yield lines are straight. For this pattern to dominate the failure of the connection, the unbalanced bending moment must be the main contributor to failure, and shear should therefore be relatively small.

The local yield line pattern for isotropic slabs has been considered by Park and Islam [40] by using circular fans centered on the column corners. For orthotropic slabs,

Gesund and Goli [16,17] used a more complex expression for the radius of the corner fans. The critical pattern depends on the ratio of the unbalanced bending moment to vertical shear forces to be transferred by the connection. Therefore, from the analysis of yield line pattern, it is possible to judge the behavior of the slab-column connection. It is always necessary to examine all possible collapse mechanisms to ensure that the load carrying capacity is not overestimated.

2.6 Prestressed Concrete Slabs

In the discussion to follow, past investigations concerned primarily with the strength and behavior of prestressed concrete slabs will be reviewed. The state of knowledge on the behavior of prestressed concrete flat plates has been summarized by ACI-ASCE Committee 423 [6] and 426 [7], and by the Post-Tensioning Institute [14]. The Post-Tensioning Institute publication "Design of Post-Tensioned Slabs," summarizes the research rather completely and most of the recommendations by Burns [9,23] are mentioned in that publication.

The ACI 318-77 Code does not provide detailed provisions for the design of prestressed concrete slabs. Some additional guidance is given in the Commentary to the ACI Code [2]. However, it is clear from the Commentary that the principal design guide is the "Tentative Recommendations for Prestressed Concrete Flat Plates," which was prepared by ACI-ASCE Committee

423 on Prestressed Concrete.

A significant feature of a prestressed concrete structure is that it is crack free under service loads, and whatever cracks may be developed under moderate overloads will be closed up as soon as the load is removed. This feature enchances the serviceability when the structure is exposed to weather because elimination of cracks prevents corrosion and greatly reduces deterioration of the structure when exposed to freeze-thaw action. Also as a direct result of not having cracks at service loads, a prestressed slab is stiffer than a normal reinforced concrete slab having the same span and thickness, since the stiffness is that of a full depth cross-section rather than of a cracked section. Prestressing also allows the use of a thinner slab for the same span, with accompanying savings in the dead load of the structure. However, there is a lower bound on the slab thickness that would be governed by deflections, vibration problems and the Code-specified minimum thickness.

For flat plate structures, shear often determines floor load capacity, and the initial estimate of slab thickness may be such as to satisfy shear strength requirements at the columns. Prestressing the slab increases the shear strength of the connection. Based on a review of available test results, ACI-ASCE Committees 423 and 426 have recommended that Eq. (11-13) of ACI 318-77,

$$V_{cw} = (3.5\sqrt{f'_c} + 0.3f_{pc})b_w d + V_p \quad \text{lb.} \qquad (2.4)$$

be used to determine the shear strength of connections transferring shear only. In Eq. (2.4) f'_c is the compressive cylinder strength of concrete in psi, f_{pc} is the compression stress in slab in psi, b_w and d are the effective width and depth of the slab in inches, and V_p is the vertical component of effective prestress force at the critical section. Because a prestressed slab is relatively thin, V_p is usually very small. Therefore, the term V_p may be conservatively neglected and the recommended design shear stress is:

$$v_{cw} = 3.5\sqrt{f'_c} + 0.3f_{pc} \quad \text{psi} \qquad (2.5)$$

As the average prestress level, f_{pc}, is increased, the load for flexural cracking usually increases at a faster rate than the load for shear failure. Further, because of the reduction in the degree of cracking, more of the input energy is stored as elastic strain energy. Thus, the ductility prior to failure will generally decrease, and the violence of failure will generally increase, as the f_{pc} value is increased.

Most unbonded prestressed flat plates will have bonded bar reinforcement at least in the negative moment regions over the columns. A minimum amount of bonded reinforcement

was also recommended by ACI-ASCE Committee 423.

Compression reinforcement has a negligible effect on a slab's ultimate flexural strength. Compression reinforcement continuous through the column has been recommended by researchers because, when properly detailed, it acts as a suspension net that may hold the slab together even after punching failure. However, due to the added expense, compression reinforcement is seldom used in practice.

The prestressing tendons are seldom grouted, and the lack of bond introduces some problems. A code expression for predicting the tendon stress at the ultimate load for the slab should lead to either the correct or to a conservative value. The equation recommended by ACI for predicting the stress in the prestressing steel in a slab was derived from the results of tests of beams, and is a lower bound to that test data. A study by Mojtahedi and Gamble [35] demonstrated that the ultimate steel stress in thin unbonded post-tensioned slabs often does not reach the expected stress predicted using the equation contained in the 1977 ACI Code. They [36] also reported a preliminary series of tests of four one-way slabs with the span-depth ratio as the main parameter. Although the tests were not conclusive about the effects of the span-depth ratio in the lightly reinforced specimens, the steel stresses reached at extremely large deformations exceeded substantially those predicted using the method given in the 1977 ACI Code.

Cook, Park, and Yong [11] described the results of tests on nine prestressed concrete slabs with unbonded tendons in which the span-depth ratio was considered as a variable. To provide a comparison, further tests were also carried out on three prestressed concrete slabs with bonded tendons which were identical in all other respects to three slabs with unbonded tendons. The measured values were compared to predicted values using Pannell's method [38] for calculating the flexural strength which takes into account the span-depth ratio. However, there was still a large scatter of results using this approach. They suggested that the scatter resulted from differences in the load arrangement and in the duct material for the tendons, from inaccuracies in the prestress load measuring techniques and from deviations between the proposed and actual profiles. In view of this uncertainty they recommended the use of the more conservative equation for f_{ps} from the ACI 318-63 Code.

Burns and Hemakom [9] reported a series of multi-panel tests at the University of Texas, Austin. The primary objective of the investigation was to determine the physical behavior of the prestressed flat plate structure over the total range of loading up to the point of collapse. The investigation intended to answer some questions about distribution of cracking, the contribution of bonded reinforcement to strength, the stress increase in unbonded tendons as a slab is loaded to ultimate, and the adequacy

of present design methods. The safety of the prestressed concrete slabs against punching shear failure was also investigated very closely.

Hawkins and Trongtham [42] have presented a report on the testing of five unbonded post-tensioned flat plate specimens. Four of the specimens simulated interior slab-column connections and one represented a typical exterior slab-column connection. The exterior column specimen was loaded with shear and moment in step increments. The direction of the load was also cycled. They confirmed the applicability of the ACI 318-77 approach for calculating the shear capacity of connections transferring moment as well as shear.

3. EXPERIMENTAL PROGRAM

3.1 Introduction

The purpose of this investigation was to simulate the performance of an actual unbonded post-tensioned flat plate-edge column connection. The overall configuration of the test specimens was governed by equipment, modeling limitations, and by the objectives of the tests. The connection specimens tested in this program were based on the design of a two-thirds scale model of the prototype structure. The layout of the model is as shown in Fig. 1.1. The model structure design specified 11-3/8 in. diameter tendons per bay and an average prestress of about 240 psi. The specimens were models of the edge column connections and the adjacent slab area as indicated by dashed lines of sections A and B in Fig. 1.1. The material properties in the two-thirds scale specimens were expected to give a faithful representation of full-scale prestressed concrete flat plate connection. Thus, any possible size effects were assumed to be avoided.

Two major variables selected in this test program were:

1. The distribution of prestressed reinforcement in the vicinity of a column, which depends on the directions of the banded and the uniformly distributed tendons.

2. The effect of moment-shear ratio on the response of the connection.

Since the predicted flexural strength of a slab is primarily a function of the number of tendons in a particular

direction and is not strongly influenced by their distribution, all tendons in one direction are generally grouped in a narrow band over the column line, while the tendons in the orthogonal direction are uniformly distributed. The design concept is that the closely spaced tendons are thought of as forming beams in one direction, while the slab then acts as a one-way slab between these beams in the other direction. This arrangement is common in practice since it simplifies the placing and jacking sequence of the tendons.

In all, four specimens were constructed and tested. These specimens will be referred to as S1 to S4. In the first two specimens the banded tendons were perpendicular to the direction of the exterior edge of the slab, while in the next two specimens the banded tendons were parallel to the exterior edge of the slab. Specimens S1 and S2 and specimens S3 and S4 are represented in Fig. 1.1 by A and B respectively.

The effect of moment-shear ratio on the behavior of the statically loaded specimens was investigated by applying the load at different distances from the column face. Details of the loading arrangements will be given later.

3.2 Description of Specimens

Plan and elevation views of the test specimens are shown in Fig. 3.1. Each specimen consisted of a 60-in. square prestressed concrete slab 4-in. in thickness, and a 12-in. square column located adjacent to and centered along

the edge of the slab. Thus, the geometry of each specimen was the same. The concrete slab was prestressed in both directions, and represented a two-way flat plate in which the tendons in one direction were banded in a narrow strip over the column, and the tendons in the other direction were uniformly spaced. In addition, No. 3 bars were used as non-prestressed reinforcement in the slab in the vicinity of the column as suggested by ACI-ASCE Committee 423. Figs. 3.2 through 3.4 show the reinforcement patterns for the slabs. The column had hinged reaction points 38 in. above and below the surfaces of the slab. In the prototype structure these points are at midheight of the column. The columns were reinforced with eight No. 6 deformed bars so as to make the flexural capacity of the column greater than of the slab to avoid a column failure. Fig. 3.5 shows the reinforcement details of the columns. The chosen specimen configuration includes the immediate edge column connection area and an adjacent portion of the slab. The slab area is approximately that located within the negative moment area around the edge column.

The conditions at the boundary of any model of a continuous structure should ideally be identical to those at the corresponding location in the structure being modeled. These boundary conditions often cannot be satisfied exactly for plates without testing the entire structure. The main reason for the use of isolated connection models is the

simplicity and ease of testing relative to the much more complex and expensive multi-panel models.

The interaction of internal actions around the connection is quite complex for even an elastic plate, but the complexities are confined to a localized portion of the slab in the vicinity of the column. The stress concentrations in this region are very high, but decrease rapidly with increase of distance from the column. Therefore, the strengths observed in these specimens are thought to closely approximate the strengths of the connections in an actual slab system.

The locations and shapes of the contraflexure lines are not constant in a prestressed concrete slab system. Cracking of the slab produces changes in the relative stiffness of various sections and directions. Redistribution of moments can and does take place in the slab system, causing the location of the contraflexure lines to shift. Reproducing these conditions would be very difficult, and the isolated connection models do not include these effects of continuity in the studies of slab-column connections.

3.3 Specimen Materials

(a) Concrete

Type I Portland Cement, river sand and 3/4-in. maximum size gravel were used for all the specimens. The mix proportions, by weight, used for each specimen are listed in Table 3.1. Measured slumps ranged from 1 to 1-3/4-in. for S1 and S2, and from 2 to 2-3/4-in. for S3 and S4. To provide

better workability of the concrete, it was decided to use a higher water-cement ratio for the last two specimens (S3 and S4). The concrete was mixed in a 2200-lb. capacity horizontal rotating type mixer. Two batches of concrete were required to cast each specimen and its test cylinders. Six standard 6 by 12 in. concrete cylinders were cast from the first batch, and three were cast from the second batch. Of these, three cylinders of the first batch were tested on the day of tensioning the tendons, and the remaining six were tested on the day of testing of the particular specimen. Splitting tension tests were carried out on three 6 by 6 in. cylinders taken from each of the two batches. Flexural beam tests were carried out on three 6 by 6 by 20 in. beams taken from the first batch. The splitting tension and flexural beam specimens were tested on the day of testing of the particular specimen. The concrete strengths listed in Table 3.1 are averages of the test results obtained by this method. A typical stress-strain curve for the concrete is shown in Fig. 3.6.

(b) Bonded Reinforcing Steel

All bonded bars used in the specimens were deformed bars taken from the laboratory stock. No. 3 bars were placed in the plate and concentrated directly over and immediately adjacent to the column. The columns were reinforced with No. 6 bars, and the ties were made from No. 3 bars. Measured mechanical characteristics of coupons cut from the steel bars are listed

in Table 3.2. A typical stress-strain curve for the bonded reinforcing steel is shown in Fig. 3.7.

(c) Prestressing Strand

The tendons used in this program were 3/8-in. diameter, 7-wire strands meeting the requirement of ASTM Specification A-416. The specific minimum ultimate strength was 270 ksi, and the average apparent Young's modulus was 28,300 ksi. A typical stress-strain curve is shown in Fig. 3.8. The tendons were inserted into $\frac{1}{2}$-in. inside diameter polyethylene tubing to prevent bonding to the concrete.

(d) Strand Anchorage

The end anchorages used were Supreme brand reusable strand chucks, model number 600XX. This system developed an anchorage in which the tendons are gripped by frictional-type split-cone wedges. The advantages of this system are its convenience in gripping the tendon at any point along its length and in removing the chuck from the tendon upon completion of the test. The jacking end grips were threaded externally and installed with nuts. Therefore, the slip of the grips wedges could be overcome by tightening the nuts against a bearing plate located between the specimen and the chuck. To provide a safety allowance, the maximum recommended jacking load is only 18,400 lb., whereas the ultimate strand force is 22,950 lb.

3.4 Fabrication of Specimens

(a) Forming, Casting, and Curing

The specimens were cast in a form made primarily of wood. The base, side forms, and the column form were constructed of 3/4-in. plywood and stiffened with 2 x 2 in. timber. The formwork was supported on a rigid steel platform to provide stability during casting of the specimens. The side form extended exactly 4 in. above the surface of the base form. Holes of 5/8-in. diameter were drilled through the side forms at the proper heights at the prestressing tendon locations. The forms were carefully aligned and leveled, and the joints were caulked to assure water tightness. Aluminium conduits with 1-$\frac{1}{2}$-in. inside diameter were placed in the slab to form the holes for the loading bars to pass through. The form was oiled with light form oil prior to placing of the reinforcement.

The columns were reinforced with eight No. 6 deformed bars, placed at the two sides of the column which were parallel to the free edge of the slab. Ties made from No. 3 deformed bars, spaced at 4 to 8 in. center to center, were used in the column outside the slab region. A 12 x 12 x 1 in. steel plate was welded to the bottom end of the column reinforcement, and then the column reinforcement cage was placed in the center of the column form.

The bonded slab reinforcement consisting of No. 3 deformed bars was placed next. The reinforcing mats were

tied together and the bars passing through the column were also tied to the column reinforcement to help prevent movement during casting. The top bars were positioned in the forms and were supported by bar chairs.

In both directions, polyethylene tubing was fitted through the holes in the side forms of the specimen. The tendons were then inserted into the polyethylene tubing used to prevent bonding to the concrete. The tendons in the banded direction were placed first, and the plastic encased tendons were securely tied to the bar chairs and to the bonded bars. The tendons in the orthogonal direction were placed next. The tendons passing through the column were tied to the vertical bars of the column cage, and this formed a very rigid mat which resisted any displacement during casting. Typical photographs of the specimens with all reinforcement in place are shown in Figs. 3.9 and 3.10.

Two batches of concrete were required to cast each specimen and its test cylinders. The concrete in each batch was placed in the forms in the following sequence:

1. The first batch was placed in the lower column and in the slab immediately around the column.

2. The second batch was placed in the remaining slab and in the upper column.

An electric vibrator was used to consolidate the concrete. The surface of the slab was leveled with a wooden screed supported on the side forms of the slab. The surface was

finished using a steel trowel. The entire casting and finishing of the slab took about two hours.

About six hours after the concrete was placed, the slab surface was covered with wet burlap and plastic sheets. This moist curing continued for seven days.

Side forms and the column forms were stripped 24 hours after casting. At the same time, all of the cylinders and beams were taken out of the steel molds, and were cured in the same way as the slab-column specimen.

The top steel plate of the column was set in place with cement paste three days after casting, and was welded to the main reinforcement the following day.

(b) Prestressing

Before the stressing operation began, steel bearing plates were placed around the tendon at each end of the specimen. A thin layer of molding plaster was provided between the plate and the concrete to give a uniform bearing on the concrete surface.

The slabs were post-tensioned when they were one week old providing that the concrete strength was not less than 4,500 psi. The tendons were prestressed individually by means of a 30-ton hydraulic jack which was placed between a prestressing yoke and an anchorage plate. A schematic drawing of the prestressing set-up is shown in Fig. 3.11.

Prestressing force was measured with aluminium sleeve load cells which were placed between the anchorage plates

and end grips. At the time of stressing, one load cell was also placed at the jacking end so that the friction losses could be calculated from load cell readings. However, these losses were found to be insignificant. The aluminium load cells were instrumented with bonded wire electrical resistance strain gages, with the four gages on each sleeve arranged as a 4-arm bridge. The sleeves were of 6060-T6 aluminium, 1-3/8-in. outside diameter, 5/8-in. inside diameter, and 6-in. long. The average sensitivity of the load cells was about 4.8 lbs. per micro-strain division on a portable strain indicator.

Since the slabs were relatively short, the losses accompanying transfer of the post-tensioning force from the hydraulic jack to the tendon were relatively important and had to be minimized by special procedures. The prestressing operation was begun by applying a desired force to the tendon, pushing the grip at the jacking end to the bearing plate, and then releasing the jack force completely in order to allow the wedge-type anchor to grip the tendon firmly at both ends. After the tendon was retensioned to about 16.0 kips, the nut on the outside of the grip at the jacking end was screwed down to the bearing plate, and then the jack force was released again. The last step was sometimes repeated several times to overcome the problem of slip at the grips, and to insure that the prestressing force was adequate after release of the jack force. The hydraulic

jack was then removed at the completion of stressing. The losses following this procedure were quite small, and the desired prestressing force could be controlled to an adequate degree. Approximately half of the tendons were stressed at each face of the slab in order to alternate the jacking end and holding end forces and to equalize the stress distribution. The stressing sequence is shown in Fig. 3.12.

3.5 Test Setup and Procedures

After the test specimen was prestressed to the required prestress force, it was then moved to the test frame. The specimen was supported by bolting the base of the column to a steel pivot that provided a hinged end condition. The upper end of the column was connected to the test frame by a horizontal steel bar which also produced a hinged end condition. The test frame was braced to minimize sidesway. The test frame with a specimen in position is shown schematically in Fig. 3.1.

Strain gages were applied on the concrete surfaces after the concrete surfaces were thoroughly dry. The location of these gages is shown in Fig. 3.13.

The unbalanced moment transferred from the slab to the column was obtained by applying a downward load to the slab through the use of two 30-ton hydraulic rams and a whiffle-tree loading mechanism. This type of loading system consisted of a series of small simple beams, and produced four point loads to the slab. A thin layer of molding plaster

was applied to the concrete surface to ensure uniform contact between the steel loading plates and the concrete slab. The location of the loading points for each specimen is shown in Fig. 3.1. The loads were measured by means of load cells placed between the hydraulic rams and their reactions. The rams were connected to a common manifold that operated from a single pump so that each ram simultaneously produced the same force. All specimens were instrumented to provide detailed data on their behavior throughout their entire loading history.

The zero readings for deflections and strains were recorded with the specimen in position loaded only by its own weight.

To apply a load increment, the hydraulic pressure in the loading rams were raised to a desired value. The deflection was then held constant, and during this time data on deflections, loads in the rams, prestress forces in the tendons, strains and cracks were recorded. The magnitude of load increments was reduced at load levels near failure. The loading of specimen S1 could not be completed in a single day, and had to be continued on the following day. In total, the test of S1 took approximately 12 hours up to failure. For each of the other three specimens, the test was completed up to failure approximately seven hours after the first load was applied.

3.6 Instrumentation

Each specimen was instrumented to provide detailed data on its behavior throughout its entire loading history. The instrumentation was designed to obtain the following information.

(a) Loads

The load was applied to the specimens by means of two 30-ton capacity center-hole hydraulic rams, acting on 1-in. diameter high-strength pull bars through a whiffle-tree loading mechanism and anchored to the testing floor. The forces in the rams were monitored using load cells positioned at locations shown in Figs 3.1 and 3.14. The load cells had a sensitivity of 8.2 lbs. per micro-strain on a portable strain indicator.

(b) Prestress Forces

As described earlier in Section 3.4(b), aluminium load cells were placed at the holding ends of each prestressing tendon. The change in tendon forces due to each load increment was monitored through these load cells. Figs. 3.11 and 3.14 show the position of the load cells.

(c) Horizontal Displacement

Three mechanical dial gages with an accuracy of 0.001 in. were used to determine the horizontal displacements of the column with respect to an independent steel frame fixed to the laboratory floor. The positions of those gages are shown in Fig. 3.1. They are identified by numerals 22, 23, and 24.

(d) Deflection at Various Points

Vertical deflections along the East-West centerline were measured by five mechanical dial gages, and the twisting angles of the slab in the North-South direction were measured by eight mechanical dial gages on each side of the column. All dial gages were located above the top surface of the slab at positions shown in Fig. 3.15. The dial gages were attached to a specially designed steel frame which was fixed to the upper column, but independent of the slab and its loading system. The accuracy of each gage was 0.001 in. or 0.0001 in.

(e) Strains

Electrical resistance strain gages were used at selected locations on the surface of the concrete and on the bonded top reinforcement. These strain gages are shown in Figs. 3.13 and 3.16, respectively. Five 1-in. long SR-4 gages were placed on the bottom surface, and two were placed on the top surface of the concrete slab 2-in. from the faces of the column. Eight, EA-06-250BG-120 Micro-Measurements gages were mounted on the No. 3 bonded bars prior to placing the bars in the form, to measure bar behavior during each stage of loading until failure. After being placed on the bars, the gages were covered carefully with a waterproofing compound.

(f) Data Recording and Reduction

Electrical impulses from the load cells and strain gages were scanned and amplified by a Vidar data acquisition system and were then recorded by a teletype where the strain readings

were typed on paper and punched on paper tape. Calibration of the data was provided by inserting a known equivalent gage output into the circuitry of each channel. Once the calibration factors for each gage were determined, the data were manually scaled and plotted.

4. TEST RESULTS

Four slab-edge column connections with varying tendon arrangements and loading positions were tested to failure. The details of the specimens and the experimental methodology were given in Chapter 3. A summary of the overall dimensions and prestressing stresses for each specimen is given in Table 4.1.

A large quantity of data, in the form of dial gage measurements, electrical strain gage measurements on the bonded reinforcing bars and the concrete surfaces, tendon forces, and crack patterns, was accumulated from the tests. In order to facilitate the comparison of the behavior of the four specimens, the data for each type of measurement will be presented and discussed as a unit for all four specimens.

4.1 Moment-Deflection Relationships

The specimens were loaded by increments, and the moment at each load increment was obtained by multiplying the total applied load by the distance from the applied load to the face of the column. The location of the loading points for each specimen is shown in Fig. 3.1.

The deformation of the specimens under applied load was measured by dial gages at locations shown in Fig. 3.15. The deflections shown are the increases measured during the test and do not include the dead load of the concrete slab or the loading frame. The deflections plotted in the moment-

deflection curves are the deflections measured at dial gage No. 13 shown in Fig. 3.15, which was located at a distance of 42 in. from the face of the column or 6 in. from the east edge of the specimen. This will be referred to as the edge deflection in the subsequent discussion. The curves of moment versus deflection for all four specimens are shown in Fig. 4.1. The moment, shear and the edge deflections at peak load for these four specimens along with the observed failure modes are tabulated in Tables 4.2 and 4.3.

(a) Specimen S1

Initially, the slab was uncracked, and the moment-deflection curve was almost linear. The slope of the curve changed as cracking of concrete developed on the tensile surface of the slab. After cracking a decrease in stiffness of the connection was evident. The curve of Fig. 4.2 shows the recovery of the slab with removal of the applied load.

Following reloading, the specimen behavior appeared to be unchanged. A second decrease in the stiffness began with the yielding of the top bonded reinforcement. The transitions between these stages were gradual because of gradual spread of both cracking and yielding throughout the slab. The load was again released, and the residual deflection of the slab was about 0.111 in., which was approximately twice the residual deflection after the first removal of the applied load.

During the third loading sequence, the deflection curve again indicates that the flexural stiffness was approximately

the same as it would have been if the slab had been loaded up to these loads initially. As the ultimate moment was approached, crushing was noticed at the intersection of the bottom surface of the slab and the east column face. Once crushing developed at the front column face, the capacity decreased with increasing displacements. The ultimate moment of 43.23 k-ft was accompanied by an edge deflection of about 1.449 in. The load was then released after the maximum load was reached. At zero load after unloading, the residual deflection at the edge of the slab was about 0.381 in.

The specimen was reloaded for the fourth time, and again the deflection curve indicates that the flexural stiffness was approximately the same as when it was terminated in the third loading sequence. The moment decreased with increasing slab deflection. It is apparent that considerable rotation occurred directly at the face of the column. This contributed greatly to the edge deflection. Since the deflection was quite large, the test was terminated due to concern for possible catastrophic failure of the connection. The behavior of the specimen was quite ductile, and the final residual deflection at the conclusion of the test was about 1.145 in.

It appears that the ultimate load and the behavior of the slab during testing were not unfavorably affected by the repeated loading.

A photograph of specimen S1 at completion of testing is shown in Fig. 4.3, and it is apparent that the slab folded

down markedly along a yield line passing along the face of the column. This will be more clearly shown in a later section when deflection profiles are plotted.

(b) Specimen S2

Specimen S2 was essentially identical to specimen S1 in the amounts and distribution of the reinforcement, and in its slab thickness and column size. The principal variable was the location of the loading points.

The moment-deflection curve for specimen S2 is also shown in Fig. 4.1. At the early stages of loading the specimen exhibited the same behavior as specimen S1 and the deflections were nearly the same. Some difference in the response resulted from their slightly differing concrete strengths and prestressing forces. After yielding of the top bonded reinforcement, the behavior of specimens S1 and S2 differed considerably. This specimen, as compared with specimen S1, exhibited significantly lower ultimate moment. The ultimate moment of 37.01 k-ft was accompanied by an edge deflection of 0.919 in. Just before failure, the stiffness of the connection decreased rather significantly. Specimen S2 exhibited a rather brittle behavior, and failed in shear by a sudden collapse of the compression zone below the inclined cracks. The slab failed along a surface formed by inclined cracks in the immediate vicinity of the column. The failure surface had a shape approximating the surface of a truncated cone spreading from the column. As soon as shear failure

occurred, the pressure in the hydraulic system relieved itself and the load decreased to about 1.8 k. A photograph of the specimen after completion of the test is shown in Fig. 4.4.

Since the details of S1 and S2 were nearly identical, the moment capacities of the slabs should have been the same. A comparison of the moment-deflection curves for S1 and S2 in Fig. 4.1 indicates that the presence of the higher shear stresses for S2 resulted in a connection failure at a moment significantly lower than the flexural capacity of the slab.

(c) Specimen S3

Specimen S3 had a different reinforcing pattern than S1 and S2. Therefore, its flexural capacity was significantly lower. However, at early stages of loading the specimens exhibited similar behavior, and deflections were very nearly the same as those for the first two specimens. As cracking developed, the behavior of the specimens with the two reinforcing patterns differed considerably. A second decrease in the stiffness began with the start of significant yielding of the top bonded reinforcement. The moment-deflection curve became nearly horizontal as yielding of the reinforcement extended throughout the slab. The transition between these three stages was gradual because of gradual spread of both cracking and yielding throughout the slab. The behavior of specimen S3 as the failure load was approached was quite ductile and was very similar to that of S1 as shown by the

moment-deflection curve of Fig. 4.1.

The ultimate moment of 29.79 k-ft was accompanied by an edge deflection of 1.511 in. It appeared that at their respective peak loads, the edge deflections of specimens S3 and S1 were very close to each other. The final deflection at the conclusion of the test was 2.055 in. Very large deflection occurred in the slab, and the test was terminated due to concern for catastrophic failure of the connection. The strength of the specimen was controlled by flexure in the slab rather than by the shear capacity of the connection. A photograph of the specimen after testing is presented in Fig. 4.5.

(d) Specimen S4

Specimen S4 was nearly identical to specimen S3 except for the location of the applied load. Therefore, their flexural capacities should have been identical. The moment-deflection curve for specimen S4 is also shown in Fig. 4.1. At the early stages of loading the specimen exhibited the same behavior, and deflections were very nearly the same as those for specimen S3. Some difference in the response resulted from their differing concrete strengths and pre-stressing forces. As the peak load was approached, specimen S4 exhibited a sudden failure in shear at the front column face. As with S2, the detrimental effect of high shear stresses in the connection region on the ability of the slab to transmit moment to the column was evident. Unlike S2, no

crushing was observed at the slab-column intersection on the east, bottom face of the specimen prior to failure. The ultimate moment of 26.39 k-ft was accompanied by an edge deflection of 0.837 in. At peak loads the edge deflections of specimens S4 and S2 were very close to each other. As soon as shear failure occurred, the pressure in the hydraulic system relieved itself and the load decreased to about 13.14 k. A photograph of the specimen after completion of testing is shown in Fig. 4.6.

4.2 Slab Deflection Profiles

The deflected profiles of the slabs along their central west-east axis for several critical load stages are shown in Figs. 4.7 through 4.10. These profiles are of importance in comparing the response of the connections at several critical load stages.

The rigid body rotation of the slabs relative to the columns caused by the initial cracking at the front face of the column can be seen in the slab deflection profiles of all specimens. Increasing the load produced additional rotations due to gradual spread of both cracking and yielding throughout the slab.

The deflection profiles reveal the basic difference in the nature of the two types of failures, flexural and shear, that were investigated in this series of tests. As the failure load was approached for specimens S1 and S3, considerable rotation occurred at the front face area of the

column and this resulted in a folding action of the slab. The rigid-body-type rotation of the slab relative to the column that resulted from these flexural failures is apparent in Figs. 4.7 and 4.9. The profiles associated with shear failures are shown in Figs. 4.8 and 4.10. As would be expected with punching, the failure cone intersecting the top surface of the slab is clearly defined. The broken lines on these figures indicate where the failure cone intersected the top surfaces of the slabs of specimens S2 and S4.

Because of the concentration of tendons over the column the flexural stiffness of specimen S2 was much greater than of specimen S4. As expected, the ultimate moment of specimen S2 measured at the face of the column was also larger than that of S4. Therefore, the local failure of specimen S2 around the connection was accompanied by significant crushing of the compression zone of the slab, while no crushing was observed on the bottom face of specimen S4. The absence of bottom steel in the slab passing through the column and the crushing of the compression zone of specimen S2 were the main causes of the significant movement of the slab down the column after shear failure had occurred. The top steel is not effective in providing post-punching resistance because it tends to tear out a substantial area of the concrete cover of the slab. Therefore, the failure region of specimen S2 was more pronounced than S4.

4.3 Internal Cracking

The slabs generally experienced major shear distress at the area of the column corners, and cracking appears to have developed first in the slab near the corners. Since the initiation of the inclined cracking in the slab could not be precisely detected, the development of inclined cracking in the vicinity of the column was detected indirectly by observing the change in the pattern of the deflections of the slab at locations No. 5 and No. 14 as shown in Fig. 3.16. This indirect method, while not highly sensitive, is thought to provide qualitative information on internal cracking of the specimens. The curves of moment versus deflection are shown in Figs. 4.11 and 4.12. Since the measured deflections at those two locations were very small, it would be expected that they would differ somewhat from each other especially when those two locations were crossed by flexural or torsional cracks. However, by observing the trends in the deflections at those points, some general statements about internal cracking may be made.

Comparison of those curves shows consistently a very distinct behavior of the specimens at those two locations. The change in direction of deflections generally occurred immediately before or at the time when the maximum applied load was recorded. For specimens S1 and S3, which failed in flexure, the moment-deflection curves for those two locations are gradual throughout the tests, and the change in direction

of deflections occurred before the maximum applied loads were recorded. For specimens S2 and S4, which failed in shear, a distinct change in the direction of deflection was observed at one of the two locations, and it occurred at the time when the maximum applied load was recorded. This evidence is thought to correspond to the pronounced opening of the inclined cracks in the vicinity of the column, and suggests a failure mechanism for specimens S2 and S4. Before cracking, the shear stress in the slab should follow closely the parabolic shear stress distribution. Consequently, the inclined cracking begins near the center of the slab. The nature of the punching shear failure for a slab is generally progressive. The slab failed first at one of the corners, and the shear capacity of this region was lost. The inclined crack opened and propagated to the compression surface, and the slab area adjacent to this column face became ineffective in transferring the load. Punching followed as the areas remaining to transfer the shear were unable to do so and the formation of the crack forming the failure cone was quickly completed.

4.4 Concrete Strain

Concrete strains were measured at various locations on the tensile and compressive surfaces of the slab as described in Section 3.6(e). The measured concrete strains are plotted as a function of the applied moment in Figs. 4.13 through 4.20.

The tensile and compressive strains increased linearly up to the cracking load. After cracking had occurred at the

top surface of the slab, no meaningful data could be obtained from the tensile strain gages. The compressive strains increased further as the moment increased until near failure. It appears that the readings of the compressive strain of specimen S1 was not unfavorably affected by the repeated loadings. At the ultimate load, the compressive strains of specimens S1 and S2, at points located at a distance of 2 in. from the column face, were about 0.003. Since the strain in the concrete increases directly with the bending moments in the slab, the actual strain at the column face of specimens S1 and S2 must have been greater than 0.003, and it was thus greater than the usual limiting compressive strain recommended by ACI for unconfined concrete. This observation was confirmed by the crushing of the compression surface as the ultimate applied load was approached. For specimen S3 the strain recorded at peak load was about 0.0022, and as failure was approached the maximum strain recorded was about 0.0036. For the same reason, it appeared that the limiting compressive strain was also approached in specimen S3, and crushing was also observed. Since the bending moment in S4 was relatively small, the maximum compressive strain recorded was only about 0.0008, and it is no surprise that no crushing was observed on the bottom surface of specimen S4.

4.5 Steel Strain

Strain gages were attached to the top bonded reinforcement at several locations as described in Section 3.6(e).

These gages provided information on how far yielding of the section had spread across the width of the specimen. One gage was damaged while casting each of specimens S1, S2 and S3.

The measured strains are plotted as a function of the applied moments in Figs 4.21 through 4.24. Initially, the moment-strain curves were almost linear until the slab began to crack. The strain in the bars passing through the column increased more than the others. The load was increased and yielding occurred in the top bars. It is interesting to note that the steel strain in specimen S2 followed the curve for specimen S1 very closely up to the load at which shear failure took place. The same phenomenon happened for specimens S3 and S4. A sudden increase of strains was recorded in the final seconds before failure of the specimen. It is apparent that the strain in the top bars was well beyond the yield strain. Yielding had developed probably to the edges of the specimen. Yielding of the reinforcement results in a concentration of rotation along the line of the slab-column interface, and the majority of the edge deflection of the slab was the result of this rotation. As expected, bars passing through the column in the direction transverse to moment transfer were never highly stressed.

4.6 Tendon Stress

The tendon stresses were measured during the tests by means of load cells placed at the holding ends of the tendons.

The increase in tendon stress was greatest for tendons passing through the column. A plot of the increase in tendon stress versus moment for the tendon in each specimen that experienced the largest stress increase is shown in Fig. 4.25.

During the early stages of loading, the increase in tendon stress was not significant. The stress began to increase when cracking developed, and the deflection of the slab was large enough to cause elongation in the unbonded tendon. The tendon stress increased gradually with load until yielding developed in the bonded bars, after which it increased at a greater rate. This is generally observed in members with unbonded tendons. As the applied load approached the failure load, larger increases in tendon stress were obtained at the expense of very large deflections. Major cracking developed before this stage of behavior. As might be expected, very little change of tendon stress was recorded in the direction transverse to the direction of moment transfer.

A tabulation of initial stresses at the beginning of the tests, the ACI prediction of stress increase, and the measured stress increases based on the load cell measurements are shown in Tables 4.4 and 4.5. The results gave some indications of how the tendon stress increases varied across the specimens. As previously mentioned, the stress in the tendons passing through the column increased more than for the tendons outside the column. This is reasonable since the greatest slab curvature occurred in the region near the column. The results

shown in Tables 4.4 and 4.5 also indicate that the ACI equation greatly overestimated the increase in tendon stress for all four specimens. This problem will be addressed in the next chapter of this report.

The tendon stress increase versus moment curves have similar shapes to the moment versus deflection curves for their respective tests. This observation led to the plotting of tendon stress increase versus rotation as shown in Fig. 4.26. The rotation at each load increment was obtained by dividing the deflection of the slab at the location of the loading point by the distance from the applied load to the face of the column. After yielding of the bonded bars, the relationship between tendon stress increase and rotation is relatively linear until the ultimate moment is reached. This result is not particularly unexpected, since it appears that the tendon stress increase is primarily a geometrical problem depending on the initial geometry of the system and on the total rotation in the hinging region. The tendon stress increase is directly related to the total change in length of the concrete slab at the level of the tendon. It is interesting to note that the rotation, and therefore the increase in tendon stress, of specimens S1 and S3 at peak load are very close to each other, and they both failed in flexure. This observation is also valid for specimens S2 and S4, which failed in shear. Since specimens S1 and S3 which failed in flexure experienced larger rotations before failure than did

S2 and S4 which failed in shear, it follows that the increase in tendon stress was also larger for S1 and S3 than for S2 and S4.

4.7 Cracking

The specimens were loaded by increments, and the cracks were marked as they appeared. Numbers were written on the crack lines to indicate the load step number at which the crack became visible. The crack width at some specific points was measured by means of a 7-power optical comparator having a set of lines of various widths on a glass reticle.

The crack patterns for each specimen at various loadings are shown in Figs. 4.27 through 4.45. The failure modes were relatively complex, and the crack patterns tended to vary somewhat, but certain common features were still noticeable.

(a) Specimen S1

In all specimens, the first crack to become visible originated at the N-E and S-E column corners, and developed gradually over the front face of the column. This crack could be described as a typical flexural crack, and occurred at the tension surface of the slab once the tensile strength of the concrete was exceeded. Loading beyond this produced additional flexural cracks at greater distances from the column face. When the load was released for the first time the cracks closed completely. The first unloading was prior to yielding of the bonded steel.

During the next loading sequence, flexural cracks appeared

at the north and south edges of the specimen. With a further increase in the load the cracks beginning at the edge of the specimen and those at the center of the slab propagated towards each other and eventually developed over the entire width of the slab. Also during this stage of loading, torsion cracks developed in the slab to the north and south sides of the column. Torsional cracking could be easily identified by crack formation extending backwards from the inner column corners towards the slab edge. The crack pattern on the top surface for S1 at about the time that the bonded steel yielded is shown in Fig. 4.27. The load was again released, but the residual tensile strain existed in the steel. This permanent elongation remaining in the steel did not allow the cracks to close completely.

During the third loading sequence, more flexural and torsional cracks developed as the load approached the ultimate capacity of the slab. The crack widths gradually increased, and the maximum crack width at the maximum applied load was about 0.6 mm. or 0.024 in. Torsion cracks progressed down the free edge of the slab at an angle of approximately 35 degrees to the horizontal, and proceeded up the bottom surface of the slab. The column was generally unaffected during the test, except for splitting near the surface of the slab. Crushing was also observed at the intersection of the bottom face of the slab and the east column face. Once crushing developed at the front face, the capacity decreased with

increasing displacements. The loading of specimen S1 could not be completed in a single day, and the load was released after the maximum load had been reached. Again the cracks did not close completely at zero load after unloading. The crack pattern at peak load is shown in Fig. 4.28.

On the following day, the specimen was reloaded, but the previous maximum load could not be reached in this loading sequence. It is apparent that considerable rotation occurred directly at the face of the column, and that this contribution to the edge deflection was large. In attempting to retain a doubly-curved shape, tensile stresses resulted in a crack at the top W-E centerline of the slab. Extensive crushing developed at the east column face, and spalling also occurred along the torsion cracks on the bottom face of the slab. When evidence of incipient failure became visible, the test was terminated. It is apparent from Figs. 4.29 through 4.31 that flexural and torsional cracking were well developed on both the top and bottom surfaces by the completion of the test.

(b) Specimen S2

At the early stages of loading, specimen S2 exhibited nearly the same behavior and crack patterns as for specimen S1. The crack patterns consisted primarily of flexural and torsional cracks throughout the top surface of the slab. The crack pattern at yield is shown in Fig. 4.32. With a further increase in the load crushing was observed at the intersection of the bottom face of the slab and the east

column face. The punching failure quickly followed as the areas remaining to transfer the shear were unable to do so. The failure was sudden, occurring when a truncated pyramid of concrete around the column "punched" through the slab. After the shear crack had formed, the reinforcement attempted to carry the applied load by dowel action. This caused a splitting action of the concrete along the tensile reinforcement which resulted in the surface cracks that were visible on the top surface at failure. Considerable amounts of concrete cover were torn off along the failure crack. Inclined cracks forming the failure surface originated inside the slab and spread to both faces. Spalling also occurred along the torsion cracks on the bottom face of the slab. The crack patterns at failure of S2 are shown in Figs 4.34 through 4.36.

After yielding of the top bonded reinforcement part of the unbalanced moment was transmitted to the side faces as torsional moments. Since the moment-shear ratio of specimen S2 was smaller as compared to specimen S1, the unbalanced bending moment was also smaller. Consequently, part of the unbalanced bending moment transmitted to the side faces as torsional moment was also smaller, and therefore, specimen S2 exhibited less extensive torsion cracks.

(c) Specimen S3

It is apparent from the test results of S3 and S4 that the use of different reinforcing patterns does not change the gross behavior of the connection at the early stages of

loading. The first crack to become visible for S3 also originated at the N-E and S-E column corners. With increasing load, flexural and torsional cracks developed throughout the slab. The torsional cracking extended to the free edge, continued across the free edge, and proceeded across the bottom surface of the slab, as can be seen in Figs. 4.37 through 4.41. At loads beyond yield torsional cracks were quite wide, and the test was terminated due to concern for possible complete collapse of the specimen. As the failure load was approached, crushing was observed at the intersection of the bottom surface of the slab and the east column face due to the large rotation of the connection. In this lightly reinforced specimen, the strength of the connection was primarily controlled by yielding of the bonded bars in the connection area.

(d) Specimen S4

Initially, this specimen exhibited nearly the same crack pattern as did specimen S3. As the peak load was approached, specimen S4 failed in shear along a surface formed by inclined cracks in the immediate vicinity of the column. As the moment-shear ratio was small, the shear force was more significant than the bending moment. The surface cracks at the failure location were not flexural cracks, but resulted from a splitting action of the top concrete cover after the shear crack had formed. In this specimen, the punching failure occurred without any prior sign of crushing or spalling of

the concrete. The crack patterns for S4 are shown in Figs. 4.42 through 4.45.

4.8 Twist

Vertical displacements along two lines parallel to the exterior edge of the slab were measured at various times during testing. The location of the dial gages is shown in Fig. 3.15. The tangent of the twisting angle of the portion of the slab to the side of the column was obtained from the corresponding difference in the vertical displacement of the slab measured along the two parallel lines divided by the distance between the two lines. The twisting angles plotted in the twisting angle-moment curves are the twisting angles determined from the displacements measured by dial gages No. 4 and No. 8 as shown in Fig. 3.15. The twisting angle-moment curves for all four specimens are shown in 4.46.

The twisting angle-moment relationships for the four specimens were quite similar. The twisting measured before yielding of the top bonded steel was relatively small. After the steel yielded, the twisting angle increased rapidly until the specimens failed. In addition, torsional cracking of the slabs was not prominent prior to yielding. Therefore, it appears that after yielding of the bonded steel, the percentage of the unbalanced moment transmitted to the column as torsional moments on the side faces increased.

The variation of the twisting angles along the edges of the slabs were also plotted for several critical load stages.

These curves are shown in Figs. 4.47 through 4.50. It can be seen that the rate of change in the twisting angles was greatest near the side face of the column. This also corresponds to the region that experienced the most torsional cracking. Therefore, these measured twisting angles can provide some qualitative information on the distribution of torsion of the slab at the various loading stages.

4.9 Summary of Test Results

Four slab-edge column specimens with varying tendon arrangement and loading positions were loaded incrementally until failure occurred. The bonded reinforcement was identical for all four specimens. Two of the specimens had 11-3/8 in. diameter tendons (heavily reinforced) and two had 4-3/8 in. diameter tendons (lightly reinforced) running perpendicular to the direction of the exterior edge of the slabs. The following phenomena were observed during the four stages of specimen behavior:

Before Cracking

1. The moment-deflection relationship was linear for all specimens and the stiffness of each was approximately the same.

2. The stress in the tendons remained constant.

From Cracking to Yield

1. A gradual decrease in stiffness for all specimens was observed. The decrease in stiffness was more rapid for the lightly reinforced specimens.

2. A series of flexural cracks developed in all four specimens. Small torsional cracks appeared in the heavily reinforced specimens.

3. Small twist angles were observed opposite the side faces of the column.

4. The increase in the tendon stresses was proportional to the edge deflections of the slabs.

From Yield to Peak Load

1. Yielding of the bonded steel occurred for each specimen at approximately the same edge deflection.

2. The stiffness of the specimens decreased rapidly until the peak load was reached.

3. The edge deflections of the specimens resulted mainly from a rotation of the slab about a yield line that formed along one of the flexural cracks.

4. Torsional cracks became more apparent for all specimens but were most extensive for the heavily reinforced specimens. The torsional cracking was accompanied by increasing twist angles.

5. The increase in the tendon stresses was still proportional to the rotation of the slabs.

From Peak Load to Failure

1. Highly developed torsional cracks were present on all specimens and were accompanied by very large twisting angles.

2. Crushing occurred at the intersection of the

compression side of the slab and the column for three of the specimens. Crushing began at about the same slab rotation for each of these, and this corresponded to the rotation at the peak load for the two specimens that failed in flexure. The fourth specimen failed in shear before it reached this level of slab rotation.

3. The peak loads of the two specimens that failed in shear occurred at about the same slab rotation. The specimens that failed in flexure experienced the same phenomenon, but this occurred at larger rotation as compared to the specimens that failed in shear.

4. The relationship between the increase in the tendon stress and the slab rotation was no longer linear.

5. The specimens that failed in flexure exhibited more ductility than those that failed in shear.

5. MODELS FOR PREDICTING THE STRENGTH OF PRESTRESSED CONCRETE PLATE-EDGE COLUMN CONNECTIONS

5.1 Introduction

In this chapter three models for predicting the strength of prestressed concrete flat plate-edge column connections are discussed. The strengths and behavior predicted by the models are compared with measured strengths and the observed behavior of the four specimens tested in this investigation and of several specimens tested by other investigators.

All of the models for predicting the flexural strength of a member with unbonded tendons require a prediction of the stress in the tendons at the ultimate moment of the member. The problems associated with predicting the tendon stress are discussed and several models for predicting the tendon stress are presented and evaluated with respect to measured values.

Results of a linear finite element analysis of one of the specimens are also presented. These are helpful in determining the state of stress in the specimen after prestressing and in understanding the behavior of the specimen before cracking occurs.

5.2 ACI Code Approach

5.2.1 Flexural Strength

As recommended in the 1977 ACI Building Code, the ultimate strength of a section containing both bonded

reinforcement and unbonded post-tensioned tendons can be calculated from the following expression:

$$M_u = [A_{ps} f_{ps} (d_{ps} - a/2) + A_s f_y (d_s - a/2)] \text{ lb-in} \qquad (5.1)$$

where

A_{ps} = area of unbonded tendons in slab strip of width b, sq. in.

f_{ps} = stress in unbonded tendon at failure in flexure, psi

d_{ps} = depth of unbonded tendon, in.

a = depth of equivalent rectangular compression zone, in.

b = width of section being considered, in.

A_s = area of bonded reinforcement in slab strip of width b, sq. in.

f_y = yield stress of bonded reinforcement, psi

d_s = depth of bonded reinforcement, in.

Because slipping occurs between the unbonded tendons and the concrete, the stress in the tendons at failure, f_{ps}, cannot be accurately computed. Eq. (18-4) of the ACI Building Code may be used for predicting the stress in the tendons when the ultimate moment of the slab is reached:

$$f_{ps} = f_{se} + 10{,}000 + \frac{f'_c}{100\rho_p} \text{ ,psi} \qquad (5.2)$$

$$f_{ps} \leq f_{py} \tag{5.3}$$

$$f_{ps} \leq f_{se} + 60{,}000 \text{ , psi} \tag{5.4}$$

where

f_{se} = effective prestress at service load, after losses, psi

f_{py} = yield stress of prestressed reinforcement, psi

ρ_p = reinforcement ratio of unbonded tendons.

These equations, which were derived from tests of post-tensioned beams, yield unconservative values of tendon stress when the span-depth ratio of a member is typical for that of slabs. A revision of Eq. (5.2) to be applied to members with span-depth ratios greater than 35 is currently under consideration by ACI Committee 318. A discussion of this phenomenon is given in Section 5.3.

5.2.2 Shear Strength

Provisions in the ACI Building Code for analyzing moment transfer to columns are given only for reinforced concrete slabs with no recommendations given for the design of prestressed slabs. The analysis of shear stress on the critical section is based on an elastic model which assumes that the total shear stress distribution may be approximated as the superposition of the uniform shear stress caused by the shear force and the nonuniform shear stress produced by the portion of the total unbalanced moment assumed to be

transmitted to the column by shear. The shear stresses produced by the unbalanced moment are assumed to vary linearly with distance from the centroidal axis of the critical section. The remainder of the unbalanced bending moment is transmitted directly to the column by flexure in the slab. This approach is semiempirical, and is based on investigations by Hanson and Hanson [18]. The assumed critical section is taken as being a distance d/2 from the column periphery. Fig. 2.1 shows the assumed critical section and distribution of shear stress in the slab when moment is transferred normal to the edge of the slab. The shear stress in the slab at face AB, and at points C and D of the critical section are given by

$$v_{AB} = \frac{V_u}{A_c} + \frac{\gamma_v (M_u - V_u g) C_{AB}}{J_c} \quad \text{psi} \qquad (5.5)$$

$$v_C = v_D = \frac{V_u}{A_c} - \frac{\gamma_v (M_u - V_u g) C_{CD}}{J_c} \quad \text{psi} \qquad (5.6)$$

where

V_u = ultimate shear force, acting at the centroidal axis of the column section, lb

M_u = ultimate unbalanced bending moment, acting about the centroidal axis of the column section, lb-in.

C_{AB} = distance from face AB of the critical section to centroidal axis CC, in.

$$C_{AB} = \frac{[C_1 + d/2]^2 \, d}{A_c} \qquad (5.7)$$

C_{CD} = distance from points C and D of the critical section to centroidal axis CC, in.

$$C_{CD} = [C_1 + d/2] - C_{AB} \tag{5.8}$$

g = distance between the centroidal axis of the critical section, and the centroidal axis of the column, in.

A_c = area of concrete at critical section, sq. in.

$$A_c = d\,[2C_1 + C_2 + 2d] \tag{5.9}$$

γ_v = fraction of unbalanced moment transferred by shear stresses at slab-column connections

J_c = property of section analogous to polar moment of inertia, in^4.

$$J_c = \frac{2d\,[C_1 + d/2]^3}{12} + \frac{2\,[C_1 + d/2]\,d^3}{12} + [C_2 + d]\,d\,C_{AB}^2 + 2\,[C_1 + d/2]\,d\,\left[\frac{(C_1 + d/2)}{2} - C_{AB}\right]^2 \tag{5.10}$$

In Eqs. (5.5) and (5.6), the first term is the uniform shear stress and the second term is the shear stress resulting from the unbalanced moment. The nominal shear strength of the connection of a reinforced concrete slab is reached when the maximum shear stress at the critical section, v_{AB}, v_C or v_D, reaches v_c, where for normal weight concrete

$$v_c = (2 + 4/\beta_c)\,\sqrt{f'_c} \text{ psi} \leq 4\sqrt{f'_c} \text{ psi} \tag{5.11}$$

where

β_c = ratio of long side to short side of the column

f'_c = compressive cylinder strength of concrete, psi.

Although ACI Building Code does not provide detailed provisions for the design of prestressed concrete slabs, it is clear from the Commentary [2] that the principal design guide is the "Tentative Recommendations for Prestressed Concrete Flat Plates," which was prepared by ACI-ASCE Committee 423 on Prestressed Concrete. This report recommends that the limiting shear stress on the critical section of a prestressed slab is given by

$$v_{cw} = 3.5\sqrt{f'_c} + 0.3f_{pc} \text{ ,psi} \qquad (5.12)$$

where

f'_c = compressive cylinder strength of concrete, psi

f_{pc} = average compressive stress in concrete due to effective prestress force only, psi.

However, when using Eq. (5.12) f_{pc} is limited to 500 psi and f'_c to 5,000 psi since these are the limits for which test data is available. The above expression was originally developed for web-shear cracking in prestressed beams. This type of cracking is associated with principal tensile stresses in the area of the web where there are no flexural cracks and near the centroid of the beam where the principal tensile

stresses are the greatest. Since the state of stress in the web of a prestressed beam is quite different from that of a two-way slab where f_{pc} could be substantially different in the two directions and where high confining stresses are able to develop normal to the flexural stress, Eq. (5.12) should be quite conservative. This phenomenon will be discussed further in Section 5.4.

The value of f_{pc} to use for an edge column is not clear, particularly when the level of prestress differs appreciably in the two directions. For interior column connections the average value of f_{pc} for the slab is used. At the edge column the actual value of f_{pc} could be quite different from the average and would depend on the location of the tendons with respect to the critical section. If some tendons are passing through the columns, ACI-ASCE Committee 423 recommends using the average value. A proposal to use Eq. (5.11) for evaluating v_c for edge column connections of prestressed slabs is currently being considered as a requirement in the 1983 ACI Building Code.

5.2.3 Comparison of Measured and Computed Strengths

In order to evaluate the model for predicting connection strength recommended by ACI, the observed strengths of the four test specimens were compared to values computed using the ACI model. Since the relationship between shear and moment is dictated by the geometry and loading position of each specimen, M_u may be written as a function of V_u and

substituted into Eqs. (5.5) and (5.6). The ultimate shear force may then be found as a function of the ultimate shear stress. The comparison of measured and predicted connection strengths is shown in Table 5.1 for two values of v_c, one using Eq. (5.12) and one using Eq. (5.11). When Eq. (5.12) was used for estimating v_{cw}, the actual value of f_{pc} for each specimen was used in the calculation. The values shown for M_u are the ultimate moment at the column centerline, and they were determined from the computed value of V_u and the position of the load for each specimen.

All of the predicted connection strengths were lower than the observed values and those which were based on v_c using Eq. (5.11) were the most conservative. For specimens S1 and S3 the actual shear strengths are unknown since flexural failures occurred in the slabs before the connection failed in shear. Therefore, the observed values may be thought of as lower bounds on the actual connection strengths.

The results for these four specimens suggest that the ACI method of predicting connection strength is conservative but not consistently so. The error in the calculated values of V_u ranged from 2.9 % for S2 to 18.5 % for S1. Ironically, the error was smallest for specimens S2 and S4 that actually had shear failures.

In addition to being conservative, the ACI model does not reflect the observed failure mechanism of the specimens. For specimen S2 the strength of the connection is governed

by Eq. (5.6) which implies that the failure should begin on the critical section at the free edge of the slab. The actual failure began at or near the face of the column opposite the free edge. However, a model for use in design need not actually reflect the precise failure mode provided that it is conservative (but not overly so) and reasonably consistent. It should not be surprising that the ACI model does not accurately predict the failure mode since it is based on an elastic theory.

The ultimate flexural strengths of the slabs calculated using Eq. (5.1) are shown in Table 5.2. The width of the section, b, used in the calculation was the entire width of the specimens. Since the geometry and loading position of each specimen is known, the ultimate moment at the column centerline M_u could be determined from the flexural strength of the slabs calculated at the face of the column. Although it appears that the ultimate flexural strengths calculated by the ACI method were close to the observed strengths, the actual stresses at ultimate load in the bonded reinforcement and in the unbonded tendons were quite different from the stresses specified by the ACI Code. These stresses are also shown in Table 5.2. All of the observed stresses in the tendons were smaller than the ACI predicted stresses, while the observed stresses in the bonded reinforcement were higher than the actual yield stress. And for this reason, the calculated flexural strengths were reasonably close to the

observed strengths.

Since the ACI equation for predicting the stress in the tendon at flexural strength, f_{ps}, is unconservative for slabs, it will be discussed in more detail in Section 5.3 to provide a better understanding of the problem.

5.3 Stress in Unbonded Tendon

5.3.1 Introduction

When a prestressed concrete flat plate with unbonded tendons is loaded, slipping occurs between the tendon and the surrounding concrete. Compatibility of strain between the tendon and the concrete does not exist, and therefore, it is difficult to predict accurately the stress in the tendon when the flexural strength of the slab is reached. Since the deformation of the unbonded tendon resulting from the applied load is distributed throughout the entire length of the tendon, the tendon stress increases more slowly than it would in a similar member with bonded tendons.

The current design practice for predicting the stress, f_{ps}, in the tendon at ultimate moment of the slab is to use Eq. (5.2). Since this equation was derived from the results of tests of beams with small span-depth ratios compared with those typical of slabs, Eq. (5.2) may not be valid when applied to slabs. Data from available tests summarized by Mojtahedi and Gamble [35] shows that Eq. (5.2) may overestimate the stress in the unbonded tendon if the span-thickness ratio is about 45. They demonstrated that at

least one additional factor, the span-depth ratio, needs to be introduced into the prediction equation for the tendon stress, f_{ps}, as its effect on the increase in stress is pronounced.

The purpose of this section is twofold: (1) to describe an approach for evaluating the relationship which exists between stress increase in the tendon and rotations of the slab at failure, thus providing a tool for predicting the tendon stress increase in flat plate structures; and (2) to present the results obtained by applying this approach to several previous tests, thus giving some insight into the nature of this relationship.

In Section 4.6 it was observed that the stress in the tendons passing through the column increased more than in the tendons outside the column. The following approach will focus on the stress increase of tendons passing through the column.

5.3.2 Basic Formula for Predicting Tendon Stress

The experimental results presented in Section 4.6 indicate that the tendon stress increase is primarily a function of geometry depending on the initial geometry of the tendon and on the deformation of the slab. The tendon stress increase is proportional to the total increase in length of the unbonded tendon. In order to predict the elongation of the tendon, the deformation of the flat plate structure or the rotations at the plastic hinges must first

be determined. However, the calculation of deflections of two-way slabs is complicated by the large number of significant parameters, as well as by the cracking and the time-dependent nature of the material response. In spite of these complications, if a correct collapse mechanism of the structure and a rational estimate of the rotations at the plastic hinges can be obtained, the elongation of the tendon can be calculated. The effect of shear deformation is assumed to be negligible compared to the deformations mentioned previously.

Cracking of the slab may be assumed to occur at several discrete locations when the tensile stress at the extreme fiber of a section exceeds the tensile strength of the concrete. A representation of the slab with flexural crack elements is shown in Fig. 5.1a. For the purpose of analysis, the band of intense cracking is represented by a single yield line, and all rotation is considered to occur along that line as shown in Fig. 5.1b. Since the plastic deformations along the yield lines are much greater than the elastic deformations of the slab segments between the yield lines, it is reasonable to assume that the slab segments between the yield lines are plane. At the final stage of loading, which corresponds to ultimate, the cracks have propagated deep into the slab. The elongation of the tendon between the crack presented in Fig. 5.1b, can be expressed directly from the rotation:

$$\Delta L_{ps} = R\ (d_{ps} - a) \quad \text{in.} \tag{5.13}$$

where

R = rotation at a plastic hinge, rad.

d_{ps} = effective depth of unbonded tendon, in.

a = depth of equivalent rectangular compression zone, in.

Several simplifying assumptions must be made in the calculation of the equivalent depth, a, for a slab with unbonded tendons. Because the stress in the unbonded tendon at ultimate is an unknown value, in calculating the equivalent depth, a, the stress f_{ps} can be replaced by the effective prestress, f_{se}, without significantly affecting the estimate. The strain hardening of the bonded reinforcement is also not taken into account, and therefore, the stress f_s can be replaced by the yield stress f_y. The equivalent depth, a, may then be written as

$$a = \frac{A_{ps}f_{se} + A_s f_y}{0.85 f'_c \, C} \text{ in.} \qquad (5.14)$$

where

A_{ps} = area of tendons passing through the column, sq. in.

A_s = area of bonded reinforcement passing through the column, sq. in.

f_{se} = effective prestress at service load, after losses, psi

f_y = yield stress of bonded reinforcement, psi

f'_c = compressive cylinder strength of concrete, psi

C = width of column, in.

Tam and Pannell [41] reported the results of tests on eight unbonded beams with varying span-depth ratios and reinforcing. All specimens were tested as simply supported beams subjected to a single central point load. As the ultimate load was approached, the cracks under the loading points for the beams were much wider than the rest of the cracks and thus, it was evident that plastic hinging occurred at the midspan of the beams as would be expected.

Tam and Pannell proposed a method for predicting f_{ps} similar to the one proposed here. They assumed that the beams remained elastic up to failure except in a zone of plastic hinging of width W_h, where

$$W_h = \emptyset \ (a/\beta_1) \quad \text{in.} \tag{5.15}$$

where

$\emptyset$ = plastic hinge width parameter

a = depth of equivalent rectangular compression zone, in.

β_1 = ratio of equivalent depth to neutral axis depth.

The equivalent depth, a, is generally small in a slab structure, and since several simplifying assumptions have been made in the calculation of the equivalent depth in Eq. (5.14), it may have little significance if the neutral

axis depth is assumed to be equal to the equivalent depth a. Therefore, the plastic hinge width can then be replaced by:

$$W_h = \phi\, a \quad \text{in.} \tag{5.16}$$

They also assumed that the lengthening of concrete at the level of the tendon in the elastic zone was negligible compared with the lengthening in the plastic zone. Their basis for determining the stress in the unbonded tendon at ultimate was based on the elongation of the tendon at the plastic hinge. A value of $\epsilon_c = 0.003$ was used as a limit of the concrete strain in the compression zone of the member at ultimate. From the strain diagram shown in Fig. 5.2,

$$\epsilon_{cp} = \frac{d_{ps} - a}{a}\, \epsilon_c \tag{5.17}$$

Finally, the change in length of the tendon may be written as

$$\Delta L_{ps} = \epsilon_{cp}\, \phi a \quad \text{in.} \tag{5.18}$$

or

$$\Delta L_{ps} = \phi\, \epsilon_c\, (d_{ps} - a) \quad \text{in.} \tag{5.19}$$

It is possible that the parameter ϕ is a variable depending upon A_{ps}, A_s, f_{ps}, f_y, f'_c, ϵ_c, the span-depth ratio, and even the loading arrangement. From the beams tested by Tam and Pannell the variation of ϕ was between 8.15 and 13.32.

For members with span-depth ratios typical of slabs, it may be more conservative if a lower value of $\emptyset$ around 9 be used for the purpose of analysis.

Comparing Eq. (5.13) to Eq. (5.19) for calculating ΔL_{ps}, we can conclude that the rotation of the plastic hinge is

$$R = \emptyset \epsilon_c \quad \text{rad.} \tag{5.20}$$

Substituting the limiting values of $\emptyset = 9$ and $\epsilon_c = 0.003$ suggest that

$$R = 0.027 \text{ rad.} \tag{5.21}$$

Since the rotation at the plastic hinges can only be approximated at present, more research is needed to find the ultimate rotation of a plastic hinge region.

To obtain the total elongation of the tendon within a particular strip of a flat plate structure that contains more than one yield line, all crack mechanisms at which plastic deformations occur must be taken into account. The total elongation due to plastic deformations at n discrete locations may be written as

$$\Delta L_{ps\ Total} = \sum_{i=1}^{n} \Delta L_{ps} \quad \text{in.} \tag{5.22}$$

If the strain in the tendon at the time of testing is

designated as ϵ_{se}, and if the increase of strain in the tendon as the load varies from zero to ultimate is $\Delta\epsilon_{ps}$, the total strain in the tendon at failure can be expressed as:

$$\epsilon_{ps} = \epsilon_{se} + \Delta\epsilon_{ps} \tag{5.23}$$

where

$$\epsilon_{se} = \frac{f_{se}}{E_{ps}} \tag{5.24}$$

$$\Delta\epsilon_{ps} = \frac{\Delta L_{ps\ Total}}{L_{ps}} \tag{5.25}$$

When the total strain in the unbonded tendon at ultimate, ϵ_{ps}, is smaller than the yield strain ϵ_{py}, the stress increase in the tendon can be determined by a single expression:

$$\Delta f_{ps} = \Delta\epsilon_{ps}\, E_{ps} \quad \text{psi} \tag{5.26}$$

or

$$\Delta f_{ps} = \frac{\Delta L_{ps\ Total}}{L_{ps}} E_{ps} \quad \text{psi} \tag{5.27}$$

where

$\Delta L_{ps\ Total}$ = total increase in length of tendon at ultimate, in.

L_{ps} = initial length of tendon, in.

E_{ps} = modulus of elasticity of tendon, psi.

For a simply supported beam with a single concentrated load, n would be 1 and the predicted tendon stress increase would be

$$\Delta f_{ps} = \phi \epsilon_c \left(1 - \frac{a}{d_{ps}}\right) \frac{d_{ps}}{L_{ps}} E_{ps} \quad \text{psi} \qquad (5.28)$$

Therefore, the tendon stress increase is expressed explicitly as a function of the span-depth ratio. The stress in the unbonded tendon at ultimate may then be expressed in the following general form

$$f_{ps} = f_{se} + \Delta f_{ps} \text{ ,psi} \qquad (5.29)$$

When the strain at failure ϵ_{ps} is larger than the yield strain ϵ_{py}, the behavior of the tendon is not linearly elastic at this stage. Using the value of ϵ_{ps} obtained from Eq. (5.23), the corresponding stress in the tendon at ultimate, f_{ps}, can be obtained from the stress-strain relationship for the prestressing reinforcement.

One problem with the model just described is that the prediction of stress increase in the tendons depends on the prediction of the total rotation along a yield line. Unfortunately, this rotation is not easy to predict. The expression for rotation employed by this model is purely empirical. Very few tests have been conducted to substantiate

the value of $\emptyset$ that should be used; in fact, the variables that effect $\emptyset$ are unknown. In spite of these shortcomings, if a lower bound of $\emptyset = 9$ is used in the model, a reasonable prediction of stress increase may be obtained for flat plate structures. Ideally, a rational method of computing the rotation would be preferred. In the next section, a method for predicting the rotation along a yield line crossing near an edge column is proposed.

5.3.3 Rotation at End Support

It was noted in Section 4.2 that the rotations of the slabs tested under this program were mainly concentrated at the front face of the columns. The contribution of the rotations at the plastic hinges to the deformations of the slabs was, by far, the most significant factor. It would also be expected that the plastic deformation near the edge column of a flat plate structure would contribute significantly to the stress increases of the tendons.

Fig. 5.3 shows the model that will be used in calculating the rotation of the slab and the elongation of the tendon along the crack due to the bond-slip of the tensile reinforcement along its embedded length in the anchorage zone. The bond stress is assumed to be constant along the development length, with a magnitude u. From the equilibrium of forces, the development length L_d required for a given f_s becomes

$$L_d = \frac{D\ f_s}{4\ u} \quad \text{in.} \tag{5.30}$$

When the strength method is used for design, f_s of Eq. (5.30) becomes f_y. Thus the development length L_d required is

$$L_d = \frac{D\ f_y}{4\ u} \quad \text{in.} \tag{5.31}$$

where

D = diameter of reinforcing bar, in.

f_s = stress in bonded reinforcement, psi

f_y = yield stress of bonded reinforcement, psi

u = average bond stress, psi.

The average ultimate bond stress for No. 11 and smaller bars is taken as follows [4]:

$$u = \frac{9.5\sqrt{f'_c}}{D} \leq 800 \quad \text{psi} \tag{5.32}$$

As the bond stress is assumed constant over the development length, the stress in the bonded reinforcement decreases linearly with distance and becomes zero at the distance of the development length. The elongation of the reinforcement over the development length will be:

$$\Delta L_s = \frac{L_d\ \epsilon_s}{2} \quad \text{in.} \tag{5.33}$$

where

ϵ_s = maximum strain in the bonded reinforcement.

If no crushing of the compression zone occurs and the joint concrete is assumed to be rigid, the rotation at the plastic hinge due to the bond-slip of the tensile reinforcement can be approximated by the expression:

$$R = \frac{\Delta L_s}{(d_s - a)} \text{ rad.} \qquad (5.34)$$

The elongation of the tendon between the crack at the front face of the column due to the bond-slip effect can then be calculated directly from the rotation:

$$\Delta L_{ps} = \frac{(d_{ps} - a)}{(d_s - a)} \frac{L_d \epsilon_s}{2} \text{ in.} \qquad (5.35)$$

where

d_{ps} = effective depth of unbonded tendon, in.

d_s = effective depth of bonded reinforcement, in.

a = depth of equivalent rectangular stress block, in.

L_d = development length, in.

ϵ_s = maximum strain in the bonded reinforcement.

The increase of strain in the tendon can then be calculated using Eq. (5.25), and thus, the stress increase in the unbonded tendon can also be determined.

But the problem with the model just described is that the prediction of stress increase depends on the prediction of the increase in strain in the bonded reinforcement, which is not easy to predict. A conservative prediction of the

maximum strain, ϵ_s, may be obtained by limiting the concrete strain in the compression zone to $\epsilon_c = 0.003$.

5.3.4 Comparison with Test Results

The four specimens tested during this investigation provided measured values of tendon stress increase with which the predicted values could be compared. Three tendons were passing through the columns in specimens S1 and S2, and two in specimens S3 and S4. The comparisons are shown in Table 5.3.

All the proposed models for predicting tendon stress increase rely on the assumption that a direct and predictable relationship exists between the rotation at a yield line and the increase in the tendon stress. To substantiate this the measured values of Δf_{ps} from the four specimens were compared with predicted values using the actual measured rotations. Each calculated value shown under the third column of Table 5.3 was determined using Eqs. (5.13), (5.14), (5.25), and (5.27), along with the measured rotation which was approximated as the slab deflection measured at gage No. 9, as shown in Fig. 3.15, divided by the distance between the point of measurement and the column face. The calculated results are close to the measured values even for specimens S2 and S4 which failed in shear. This suggests that one can predict the tendon stress increase with reasonable accuracy provided that the rotations at the plastic hinges are known. This is also substantiated by the near-linear behavior of the measured Δf_{ps} vs. rotation data shown in Fig. 4.26.

Calculated values of Δf_{ps} using the bond-slip model are also given in Table 5.3 for two values of strain in the bonded steel: the measured strain and the strain predicted by limiting ϵ_c to 0.003. When measured strain in the bonded reinforcement was used in the bond-slip model, the results were close to the measured values. But, if the strains in the bonded reinforcement were calculated based on the limiting strain $\epsilon_c = 0.003$, the results were very conservative. This evidence indicates that either the concrete strain in the compression zone must be larger than the assumed limiting strain, $\epsilon_c = 0.003$, or that compatibility of strains does not exist.

The tendon stress increases of specimens S1 and S3 which failed in flexure were also predicted using the modified Tam and Pannell approach with $\emptyset = 9$ and $\epsilon_c = 0.003$. The results are close to the measured values. This suggests that the Tam and Pannell model may be useful in design.

Finally, the stress increases were also predicted using ACI Code equations. It is not a surprise that the results are much larger than the measured stresses.

In order to further investigate the proposed models, measured tendon stress increases from tests conducted by other investigators are compared with predicted values in Table 5.4. The tests were conducted on beams as well as on thin slabs and multipanel flat plate structures. From the reported load-deflection curves, the approximate deformations of the specimens could be determined. By applying a reasonable

collapse mechanism to the structure, the rotations along the plastic hinges could be calculated by the ordinary methods of geometry. Using the calculated rotations, the total elongation of the tendons passing through the column could be obtained, and the tendon stress increase could easily be calculated.

The predicted values of Δf_{ps} derived from measured deflections were very good when compared with measured values from tests conducted using mid-point or uniform loading. In addition, the specimens tested by Hemakom and by Winter contained more than one yield line, thus allowing the validity of Eq. (5.22) to be verified. For simply supported specimens loaded at two points only, the measured values of Δf_{ps} were consistently smaller than the predicted ones. The calculated values were reasonably good for specimens with small reinforcing ratio (Cooke specimens 3, 6 and 9) or with large span-depth ratios (Mojtahedi specimens). Evidently, the large region of constant moment associated with two point loading affects the tendon stress increase. Unlike the specimens with a single point or uniform loading, several large cracks formed in these specimens as opposed to well-defined yield lines.

Also given in Table 5.4 are the predicted values using the modified Tam and Pannell approach with $\phi = 9$ and $\epsilon_c = 0.003$. The predictions were quite close to the measured values except for the four specimens tested by Mojtahedi and Gamble for which the predictions were quite conservative.

This data along with that shown in Table 5.3 suggests that the modified Tam and Pannell approach may be very useful for the design of prestressed slabs.

Finally, the ACI Code predictions are also shown in Table 5.4. The results are not consistently predicted by Eq. (5.2). In some of the specimens the predicted values were reached, while in others the increases were far from the predicted values. In some of the slab specimens the predicted values were extremely unconservative. On the average, the modified Tam and Pannell method was a much better predictor of Δf_{ps}.

5.4 Beam Analogy

5.4.1 Introduction

This section presents a beam analogy approach for the determination of the shear and unbalanced moment capacity of prestressed concrete slab-edge column connections without shear reinforcement. The use of a beam analogy for predicting the capacity of slab-column connections is not mentioned in ACI 318-77 nor in its Commentary. It is, however, recommended by ACI-ASCE Committee 426 as an alternative approach to the ACI procedure.

The current beam analogies were derived for determining the strength of nonprestressed reinforced concrete slab-column connections. Park and Islam [40] have developed a beam analogy for predicting the strength of reinforced concrete interior column connections. The modified beam analogy proposed here

introduces a number of changes in Park and Islam's beam analogy for application to prestressed concrete slab-edge column connections. The strength predictions from this model are then compared with test results.

5.4.2 Beam Analogy

The beam analogy is an ultimate strength procedure for predicting the strengths of slab-column connections. The slab sections framing into each column face are idealized as beam sections. There is a sweeping approximation in the assumption that the three "beams" framing into the column can each deform sufficiently for the simultaneous development of their strengths. Compatibility restrictions are ignored and each beam is assumed to be able to developed its ultimate bending moment, torsional moment and shear force.

The connection is in equilibrium under the forces shown in Fig. 5.4b. The strength of the connection is calculated by summing the contribution of the strengths of the three beams.

$$V_u \leq V_{AB} + V_{BC} + V_{AD} \tag{5.36}$$

$$M_u \leq M_{AB} + (T_{BC} + T_{AD}) + V_{AB}(C/2 + d/2) + (V_{BC} + V_{AD})d/4 \tag{5.37}$$

where

V_u = ultimate shear, lb

M_u = ultimate unbalanced bending moment to be transferred, acting about the axis at the centroid of the column, lb-in.

V_{AB}, V_{BC}, V_{AD} = shear forces acting on faces AB, BC, and AD, lb

M_{AB} = bending moment acting on face AB, lb-in.

T_{BC}, T_{AD} = torsional moments acting on faces BC and AD, lb-in.

C = width of square column, in.

d = effective depth of prestressed concrete slab, but not less than 0.8h, in.

The actual behavior of the cracked prestressed concrete slab around the column is extremely complex, primarily because of the combined flexural and diagonal tension cracking, and the three-dimensional nature of the problem. Therefore, it is necessary to make simplifications in order to derive the strength terms of the above equilibrium equations. A discussion of each assumption required to formulate the model follows:

1. The location of the critical section is important with slabs because the predicted shear stress distribution and the allowable shear stress will depend on the location of the assumed critical section. The calculated maximum shear is only a convenient and relative measure of the critical shear stresses. It is indicative of neither the actual distribution nor the absolute magnitude of the true critical stresses. The assumed critical section is located at a distance d/2 from the column face as shown in Fig. 5.4a. This is the same location as assumed in the ACI model.

2. The ultimate flexural capacity on face AB, M_{AB}, is assumed to be governed only by the reinforcing passing through this face and thus may be written as

$$M_{AB} = [A_{ps}f_{ps}(d_{ps} - a/2) + A_s f_y(d_s - a/2)] \text{ lb-in.} \qquad (5.38)$$

where

A_{ps} = area of unbonded tendons passing through face AB of the critical section, sq. in.

A_s = area of bonded reinforcement passing through face AB of the critical section, sq. in.

f_{ps} = stress in unbonded tendon at failure, psi

f_y = yield stress of bonded reinforcement, psi

d_{ps} = effective depth of unbonded tendon, in.

d_s = effective depth of bonded reinforcement, in.

a = depth of equivalent rectangular compression zone, in.

The presence of shear on face AB is assumed not to reduce M_{AB}.

3. Face AB is the critical face for vertical shear stress. The part of M_u transferred by the torsional moments, T_{BC} and T_{AD}, produces shear stresses on face AB that add to those produced by V_{AB}. Therefore, the total shear stress is maximum on face AB of the critical section. The shear stress on this face is assumed to be uniformly distributed over the effective depth of the slab. For an interior prestressed concrete slab-column connection, the maximum vertical shear stress is

limited to the value given by Eq. (5.12). This value was recommended by ACI-ASCE Committee 423 and the ACI Code. It was noted in Section 5.2.2 that there currently is some concern that the prestress is not fully effective around the perimeter of the critical section of an exterior slab-column connection. Therefore, it has been recommended that Eq. (5.11) be used at these locations. Both values will be considered in this investigation.

4. The distribution of shear stress on the side faces BC and AD is difficult to establish at ultimate. It was mentioned in Section 4.8 that after yielding of the top bonded reinforcement passing through the column, changes developed in the distribution of forces on the critical section. After yielding, a greater percentage of the applied moment was carried by torsion on the side faces of the column. The exact percentage of the total moment carried by these torsional moments is unknown and undoubtedly depends on several variables. Until additional data is collected to clarify this uncertainty, the combined reinforcement index described in Section 18.8.1 of the ACI Code will therefore be used as a qualitative indicator of the magnitude of the torsional moment transferred to the side faces BC and AD of the critical section. For prestressed concrete members without compression reinforcement, the combined reinforcement index of

$$\omega + \omega_p \leq 0.3 \qquad (5.39)$$

is used as the dividing line between the under-reinforced and over-reinforced members, where

$$\omega = \frac{\frac{A_s}{bd} f_y}{f'_c} \tag{5.40}$$

$$\omega_p = \frac{\frac{A_{ps}}{bd} f_{ps}}{f'_c} \tag{5.41}$$

The simultaneous application of shear and torsion on the side faces will cause a non-uniform distribution of the shear stress. It is expected that under-reinforced slabs will transfer smaller torsional moments to the side faces than over-reinforced slabs. Proposed distributions of shear stress for over-reinforced and under-reinforced slabs are shown in Figs. 5.5 and 5.6 respectively. It is assumed for both cases that on the region of non-uniform shear stress the positive and negative stresses produce equal but opposite, forces. Therefore, the shear forces on the side faces, V_{BC} and V_{AD}, are carried by the regions of uniform shear stress. Interaction between torsion and shear will produce strength reduction. Therefore, it is expected that sections with larger torsional moments will carry less shear force, while members with smaller torsional moments will carry more shear force. It is proposed that the shear stress for over-reinforced sections be assumed to be uniformly distributed

over a distance d/2 from the inner corners of the critical section as shown in Fig. 5.5. The shear force may then be written as

$$V_{BC} = V_{AD} = v_{cw}(d/2 \cdot d) \text{ lb} \qquad (5.42)$$

For under-reinforced sections, the shear stress is assumed to be uniformly distributed over a distance C_{AB} from the inner corners of the critical section as shown in Fig. 5.6. For this case the shear force may be written as

$$V_{BC} = V_{AD} = v_{cw}(C_{AB} \cdot d) \text{ lb} \qquad (5.43)$$

where

C_{AB} = distance from face AB of the critical section to the centroidal axis, CC, in.

5. The torsional strength of a beam without web reinforcement is assumed to be exhausted when the maximum torsional stress, v_t, equals the maximum principal tensile stress because pure torsion is assumed to give a pure shear stress condition. On this basis, Hsu [24] proposed for the ultimate torsional capacity of a rectangular beam of prestressed concrete the following equation

$$T_u = 6\sqrt{f'_c}\sqrt{1 + 10f_{pc}/f'_c}\,\Sigma(\alpha x^2 y) \text{ lb-in.} \qquad (5.44)$$

where

$f_t \approx 6\sqrt{f'_c}$ = tensile strength of concrete, psi

$\sqrt{1 + 10f_{pc}/f'_c}$ = prestress factor

f_{pc} = average prestress on section, psi

f'_c = compressive cylinder strength of concrete, psi

α = shape factor

$$\alpha = \frac{0.35}{0.75 + (x/y)} \qquad (5.45)$$

x = smaller cross-sectional dimension, in.

y = larger cross-sectional dimension, in.

Even though ultimate strength is the basis for design, it is convenient to compute maximum torsional shear stress in the same manner as for the elastic homogeneous section. Therefore, the maximum torsional shear stress may be approximated by

$$v_t = \frac{T_u}{\Sigma(\alpha x^2 y)} = 6\sqrt{f'_c}\ \sqrt{1 + 10f_{pc}/f'_c} \text{ psi} \qquad (5.46)$$

In slabs the critical section is restrained by the continuum around it, and the transverse reinforcement is generally continuous through to the other side of the column. Therefore, one might expect to reach a greater nominal shear stress than that measured for beams. This was confirmed by Kanoh and Yoshizaki [26]. Based on tests of eight slab-column connection specimens, they recommended the use of $24\sqrt{f'_c}$ as the ultimate shear stress. In lieu of more experimental data, it is

proposed that the maximum torsional stress, v_t, be limited to 75 % of this higher value,

$$v_t \leq 18\sqrt{f'_c}\ \sqrt{1 + 10f_{pc}/f'_c} \quad \text{psi} \qquad (5.47)$$

Therefore, in absence of shear force, the torsional strength of the side faces BC and AD may then be written as

$$T_{BCO} = T_{ADO} = 18\sqrt{f'_c}\ \sqrt{1 + 10f_{pc}/f'_c}\ \Sigma(\alpha x^2 y) \text{ lb-in.} \qquad (5.48)$$

The simultaneous application of shear forces and torques on the side faces will produce an interaction that will reduce the strength compared with what it would be if they were acting alone. The exact relationship is unknown. A simple, but undoubtedly conservative, straight line interaction between shear and torsion is recommended for the strength prediction. It can be expressed by the formula,

$$\frac{V_{BC}}{V_{BCO}} + \frac{T_{BC}}{T_{BCO}} = 1 \qquad (5.49)$$

or

$$T_{BC} = T_{BCO}\left(1 - \frac{V_{BC}}{V_{BCO}}\right) \text{ lb-in.} \qquad (5.50)$$

where V_{BC} and T_{BC} are respectively the shear force and torque carried by face BC. V_{BCO} is the ultimate shear force that could be carried by BC if no torque was present and is given by

$$V_{BCO} = v_{cw} [d \cdot (C + d/2)] \quad \text{lb} \qquad (5.51)$$

It is also assumed that $V_{BC} = V_{AD}$ and $T_{BC} = T_{AD}$.

5.4.3 Comparison with Test Results

The measured strengths of the connections for the four specimens tested in this investigation and the calculated strengths using the beam analogy model are given in Table 5.5. The predicted strengths shown in Table 5.5 were evaluated for two values of v_c, one using Eq. (5.12) and one using Eq. (5.11). The combined reinforcement index for each of the specimens was as follows: S1, 0.32; S2, 0.37; S3, 0.24; and S4, 0.20. Since the value of 0.30 is used as the dividing line, specimens S1 and S2 were over-reinforced members while specimens S3 and S4 were under-reinforced members. Therefore, Eq. (5.42) was used for the calculation of the shear forces, V_{BC} and V_{AD}, on the side faces of specimens S1 and S2, and Eq. (5.43) for specimens S3 and S4. The shear force to be transferred to the column cannot exceed the summation of the shear strengths as described by Eq. (5.36).

Since the validity of the model was being checked, the measured stresses of f_{ps} and f_s were used in Eq. (5.38) for

the calculation of the ultimate bending moment, M_{AB}, on face AB of the critical section. Substituting Eqs. (5.38), (5.42) or (5.43), (5.48) and (5.50) into Eq. (5.37) gave the unbalanced bending moment strength of the slab-column connection.

The values shown for M_u are the governing ultimate moment at the column centerline, and they were determined either by the predicted value of V_u from Eq. (5.36) and the position of the load for each specimen, or directly from Eq. (5.37). If Eq. (5.37) governed, the ultimate shear force, V_u, was calculated from the predicted value of M_u and the known position of the load.

The predicted strength of specimen S1 was governed by the unbalanced bending moment strength Eq. (5.37), for both values of v_c. It is evident that the predicted strength of the connection was not significantly effected by the value of v_c that was used. If Eq. (5.37) governs the strength, the value of v_c is only used for the calculation of V_{BCO}, and its effect is insignificant. The predicted strengths were smaller than but close to the measured strengths. The predicted mode of failure was also confirmed by the observed failure of the specimen in flexure at the front face, AB, and in torsion on the side faces, BC and AD. The torsional moments, T_{BC} and T_{AD}, contributed significantly in the flexural strength of the connection. This suggests that the ultimate torsional strength predicted by Eqs. (5.48) and

(5.50) is realistic.

The mode of failure of specimen S2 predicted by the beam analogy model was dependent upon the value chosen for v_c. When Eq. (5.11) was used to determine v_c, the correct failure mode, punching shear, was predicted and the value of V_u predicted by Eq. (5.36) was very close to the measured value. When Eq. (5.12) was used to find v_c, Eq. (5.37) governed, thus, indicating that flexure controlled. The predicted strength, however, was still very good.

As for specimen S1, the predicted strength of specimen S3 was governed by the flexural strength equation for both values of v_c which was also in agreement with the observed mode of failure. The predicted strengths were larger than but still close to the measured strength.

Finally, the predicted strength of specimen S4 was governed by the shear strength equation for both values of v_c. The predicted strength using Eq. (5.12) for the value of v_c gave larger value as compared to the measured strength, but if Eq. (5.11) was used the predicted strength gave a better result. Again, this might indicate that the use of Eq. (5.11) in the beam analogy method can give a better prediction if the strength of the connection is governed by shear.

Table 5.6 shows a comparison of the predicted strength of a prestressed concrete slab-edge column connection with that measured in a test conducted by Hawkins [20]. The measured strength was only about 94 % of the predicted

strength. However, it is likely that the cyclic loading applied to the connection caused strength degradation, and therefore the lower strength was observed.

Since it is possible that the maximum contribution from each effect may not occur simultaneously, calculating the strength of the connection by summing the contributions of the strengths of the beams should represent an upper bound value. That this was not the case for the four specimens reported here highlights the fact that the model is approximate. However, the predicted strengths computed using the beam analogy approach are found to be easily obtained but still in good agreement with the measured strengths. Although one may not make broad and general conclusions based on this small sample of data, the accuracy of the model demonstrated here indicates that the beam analogy approach should be investigated further.

5.5 Yield Line Theory

5.5.1 Introduction

In order to prevent shear failures of slab-column connections it is essential to know the ultimate flexural strength of the flat plate floors. Once this is known it is possible to design the slab such that the collapse load would produce ductile yielding throughout the slab rather than the more brittle shear failure of the connections. The yield line theory provides a convenient method for evaluating a slab's flexural strength. However, it is an upper bound method.

Therefore, it is always necessary to examine all the possible collapse mechanisms to ensure that the load carrying capacity of the slab is not over-estimated. Two types of yield line patterns, folding and local, will be investigated here.

5.5.2 Folding Yield Line Pattern

The first yield line pattern is shown in Fig. 5.7. It represents a folding-type collapse mechanism of the slab, involving one negative-moment yield line running along the front face of the column and transverse to the direction of bending. For a multipanel flat plate structure that experienced a folding-type collapse in one of its bays, there would, in general, be a negative-moment yield line running along each column line and a positive-moment yield line passing through the slab at approximately midspan of the bay.

If the column rotates by an angle θ_1 for the specimen shown in Fig. 5.7, causing a unit upward displacement at the negative-moment yield line, the collapse mechanism gives

$$\theta_1 = 1/C \tag{5.52}$$

$$\theta_2 = 1/D \tag{5.53}$$

and

$$\theta = \theta_1 + \theta_2 = (1/C + 1/D) \tag{5.54}$$

where

C = width of square column, in.

D = distance between point load and the face of the column, in.

The total internal work done by the negative-moment yield line is

$$m_x L\ \theta = m_x L\ (1/C + 1/D) \tag{5.55}$$

and the total external work done by the unbalanced bending moment M_u and the shear V_u is

$$\text{External Work} = M_u\ \theta_1 + V_u\ 1/2 \tag{5.56}$$

Equating the total internal work to the total external work, and substituting the relationship $M_u = V_u\ (C/2 + D)$ will reduce the equation to

$$V_u = \frac{m_x L}{D}\ \text{lb} \tag{5.57}$$

and

$$M_u = m_x L\ (1 + \frac{C}{2D})\ \text{lb-in.} \tag{5.58}$$

where

m_x = negative yield moment per unit length provided by the reinforcement running in the X direction, lb-in/in.

L = width of the specimen, in.

C = width of the square column, in.

D = distance from the front face of the column to the loading point, in.

5.5.3 Local Yield Line Pattern

Gesund and Goli [16] have shown yield line patterns for a local collapse mechanism of the slab around an internal column. The yield line pattern consists of a mixed pattern of straight lines and fan-shaped mechanisms centering on the column corners. Since the curved yield line cannot be determined for the general case, a logarithmic spiral was assumed as an approximation for orthotropic slabs.

For edge column connections, the back face of the column is also the free edge of the slab, and no yielding could then be present at the free edge. Therefore, some adjustment must be made to Gesund's model. The proposed yield line pattern for this mode is shown in Fig. 5.8.

Since the slab is orthotropic, a coefficient of orthotropy is defined as follows:

$$\mu = \frac{m_x + m_x'}{m_y + m_y'} \tag{5.59}$$

$$\Sigma m = (m_x + m_x') + (m_y + m_y') \tag{5.60}$$

Consequently,

$$(m_x + m_x') = \frac{\mu \Sigma m}{1 + \mu} \tag{5.61}$$

$$(m_y + m_y') = \frac{\Sigma m}{1 + \mu} \tag{5.62}$$

where

m_x = negative yield moment per unit length provided by the reinforcement running in the X direction, lb-in/in.

m_x' = positive yield moment per unit length provided by the reinforcement running in the X direction, lb-in/in.

m_y = negative yield moment per unit length provided by the reinforcement running in the Y direction, lb-in/in.

m_y' = positive yield moment per unit length provided by the reinforcement running in the Y direction, lb-in/in.

The moment per unit length acting along a positive or a negative yield line making an angle ϕ with the X-axis can be written as

$$m_\phi^+ = m_x' \sin^2\phi + m_y' \cos^2\phi \tag{5.63}$$

and

$$m_{\phi}^{-} = m_x \sin^2\phi + m_y \cos^2\phi \qquad (5.64)$$

The equation of the assumed logarithmic spiral is

$$R_{\phi} = R\ e^{\gamma\phi} \qquad (5.65)$$

where

$\gamma = 1/\tan\theta$ = constant

θ = angle between the radial and the circumferential yield lines

Assume that the column rotates through an angle 1/C. Then the total external work done by M_u and V_u is

$$\text{External Work} = M_u\ 1/C + V_u\ 1/2 \qquad (5.66)$$

The total internal work can be written as:

1. The internal work of the front trapezoid:

$$(m_x + m_x')\ [C + 2Re^{\gamma(\pi/2-\theta)}\sin(\pi/2-\theta)]\ \frac{1}{Re^{\gamma(\pi/2-\theta)}\cos(\pi/2-\theta)} =$$

$$\frac{\mu}{1+\mu}\ \Sigma m\ \{\frac{\sqrt{(1+\gamma^2)}}{\beta\ \exp[\gamma(\pi/2-\theta)]} + 2\gamma\} \qquad (5.67)$$

where

$$\beta = R/C \qquad (5.68)$$

2. The internal work done by the shaded segment as shown in Fig. 5.9 is

$$(m^{+}_{\phi+\theta} + m^{-}_{\phi+\theta}) \frac{Re^{\gamma\phi}\, d_{\phi}}{\sin\theta} \frac{1}{Re^{\gamma\phi}\sin\theta} \tag{5.69}$$

Therefore, the internal work done by the two fan segments is

$$2 \int_{(\pi/2-\theta)}^{\phi_1} [(m^{+}_{\phi+\theta} + m^{-}_{\phi+\theta}) \frac{Re^{\gamma\phi} d_{\phi}}{\sin\theta} \frac{1}{Re^{\gamma\phi}\sin\theta}] =$$

$$\{\frac{1-\mu}{1+\mu}[(\gamma^2 - 1)\sin\phi_1\cos\phi_1 + \gamma(\cos^2\phi_1 - \sin^2\phi_1)] +$$

$$(1+\gamma^2)(\phi_1 + \theta - \pi/2)\}\,\Sigma m \tag{5.70}$$

Equating the total internal work and the total external work,

$$\frac{M_u}{C} + \frac{V_u}{2} = K\,\Sigma m \tag{5.71}$$

where

C = width of square column, in.

$$K = \frac{\mu}{1+\mu}\{\frac{\sqrt{(1+\gamma^2)}}{\beta \exp[\gamma(\pi/2-\theta)]} + 2\gamma\}$$

$$+ \frac{1-\mu}{1+\mu}[(\gamma^2 - 1)\sin\phi_1\cos\phi_1 + \gamma(1 - 2\sin^2\phi_1)]$$

$$+ (1+\gamma^2)(\phi_1 + \theta - \pi/2) \tag{5.72}$$

The correct failure mechanism corresponds to the one that gives the minimum value of K. Therefore, Eq. (5.72)

would have to be minimized with respect to ϕ_1 and γ within the constraint that $\pi/2 \leq \phi_1 \leq \pi$. In order to simplify Eq. (5.72) for this study, a circular arc was used to approximate the assumed logarithmic spiral. This implies

$$\theta = \pi/2 \tag{5.73}$$

or

$$\gamma = 0 \tag{5.74}$$

and

$$1/\beta = C/R = -\cos\phi_1 \tag{5.75}$$

Therefore, the coefficient K becomes

$$K = -\left(\frac{\mu}{1+\mu}\right)\cos\phi_1 - \left(\frac{1-\mu}{1+\mu}\right)\frac{\sin 2\phi_1}{2} + \phi_1 \tag{5.76}$$

5.5.4 Comparison with Test Results

The measured strengths of the connections for the four specimens tested in this investigation and the calculated strengths using the yield line theory are given in Table 5.8. The predicted strengths were evaluated for two yield line patterns, one using the folding-type and one using the local yield line pattern.

The predicted strengths for the folding-type yield line pattern were obtained from Eqs. (5.57) and (5.58). It is apparent that since the strain-hardening effect of the bonded reinforcement was not taken into account in the calculation

of the yield strength, $m_x L$, the predicted strength of the slab-edge column would be smaller than the measured value. In fact, if the actual stress in the bonded bars had been used, the calculated strengths would have been nearly identical to the measured values. But the strengths calculated here were still close to the measured strengths, even for specimens S2 and S4 which failed in shear. However, for both of these specimens the bonded bars yielded before the shear failure occurred. Therefore, yield lines had already formed in the specimens. Strictly speaking, the yield line methods are only applicable to flexural collapse mechanisms.

For a prestressed concrete slab that does not have uniform tendon spacing, the exact widths over which to calculate m_x and m_y to be used in the local yield line pattern were not clearly defined. Since the mechanism is localized in the column region, a width of approximately three column widths along the free edge and two column depths normal to the free edge would be reasonable. For calculating the strengths of these specimens, the observed crack patterns led to the values used. The cracks on the side faces of the column were observed to pass through the weakest sections of the slab, e.g. close to the locations where the tendons ended. Fig. 5.10 shows the approximate yield line patterns used for specimens S1 and S2 and for specimens S3 and S4. Thus, the widths of the slabs considered in the X and Y directions for computing m_x and m_y for specimens S1 and S2 were 36 in. and

30 in., and the widths for specimens S3 and S4 were 40 in. and 33 in. The calculated unit moments needed for the calculation of connection strengths are tabulated in Table 5.7. Using the same assumptions and observed crack patterns, the value ϕ_1 can also be obtained. The values K were determined from Eq. (5.76); and upon substituting these values of K in Eq. (5.71) the strengths of the connections were obtained. The predicted strengths were larger than the observed values. This was not surprising, given the fact that none of the specimens failed by developing a local yield line mechanism.

The analysis using the local yield line pattern involved some approximations that were not fully justified. The calculations were also done by estimating K from charts given by Gesund [16] for interior columns and then subtracting contributions to K that would not be present at an edge column. The results were similar to those in Table 5.8. Therefore, the calculated values are believed to be reasonable estimates of the values that would be obtained by minimizing Eq. (5.72). Since this type of failure mechanism frequently occurs [23], especially for edge columns, this method of analysis should be investigated further.

5.6 Finite Element Method

5.6.1 Introduction

At low levels of load the slab elements are uncracked and the actions and deformations could be computed from elastic theory using the uncracked flexural stiffness of the slab

elements. An uncracked slab may be treated as isotropic, regardless of the orientation and the orthotropy of the reinforcement in the slab. The finite element method would then be the logical choice for the analysis of slab-column connections.

Cracking reduces the overall flexural stiffness of the connection, causing a nonlinear increase in deflection per unit of load. Deflections calculated on the basis of uncracked section will result in smaller values than actually occur. After cracking, the stiffness of the cracked section, as opposed to an uncracked section, depends greatly on the percentage of the reinforcement in the slab. For an isotropic reinforced slab, the crack orientation is normal to the major principal moment direction. But, this is not normally the case for an orthotropically reinforced slab. The solution may be trivial, because moment and shear redistribution due to inelastic behavior can occur before the ultimate applied load is reached. Therefore, the finite element analysis presented herein is limited to only the elastic load range.

5.6.2 Description of the Finite Element Mesh

Prestressed concrete slabs are subjected both to bending and membrane forces. For this reason the RFSHELL element was selected for the analysis of specimen S1. The RFSHELL element is a four node, flat rectangular element that allows both bending and membrane forces. It is constructed by combining a plane RECTANGLE element and a RPB12 plate bending

element. As a result, within each RFSHELL element, membrane and bending actions uncouple. Each node is defined to have six degrees of freedom in the element XYZ system. These are U, V, W, θ_x, θ_y, and θ_z.

The element mesh used to model half of specimen S1 is shown in Fig. 5.11. Small elements in the immediate area around the column and larger elements in the other areas have been selected to improve the accuracy of the solution in the critical region with reasonable computational effort. The prestress forces were defined to be uniformly distributed along the outer edge of the elements where the tendons were located. Specimen S1 was subjected to the weight of the slab, plus a total applied load of 4.20 kips located at 42 in. from the front face of the column. The load was the measured applied load at loading step No. 8, and was smaller than the cracking load. Half of this applied load was then uniformly distributed over the shaded elements as shown in Fig. 5.11. For the uncracked slab, the Young's modulus and Poisson's ratio were taken as 4.2×10^6 psi and 0.15, respectively.

The problem was then solved using a computer program known as "FINITE" developed at the University of Illinois at Urbana-Champaign. The major computational effort expended in the analysis involved generating and solving the equilibrium equations to determine nodal displacements. In general, the system will perform any back-substitution calculations necessary to satisfy output requests.

5.6.3 Calculated Response of S1

Stresses acting across different cross-sections are shown in Figs. 5.12 through 5.14. The stresses plotted are the average of stresses at the corners of the elements meeting at the particular nodes.

Fig. 5.12 shows the stress distribution at the top surface of the slab caused by prestressing only. The section numbers in this figure refer to Fig. 5.11. It can be seen that the stresses are not uniformly distributed over the cross-sections. Compressive stresses are distributed rather uniformly over the column strip, while some tensile stresses are also noticeable in areas near the edge of the specimen. Although the stress distribution in a full slab would be somewhat different, the effect of banding the tendons in the vicinity of the column can be seen. The membrane prestress will be much higher than the average value, P/A, near the columns at the free edges and will be small at some distance away from the column. This stress concentration will gradually dissipate and become a uniform stress across the slab.

The stress distribution at the top surface of the slab caused by the prestress forces and the applied load is shown in Fig. 5.13. As shown in Section I-I, a concentration of tensile stresses occurs near the corners of the column. This calculated result confirms the observations from tests that the first crack originated at the inner column corners. Due to the nonuniformity of the prestress, the tensile stress

due to bending is also nonuniform as seen in Section II-II through IV-IV. Note the high tensile stress at the outer edge of the specimen in Section II-II. This behavior is supported by the observed formation of cracks at this location as described in Section 4.7. It is apparent from the comparison of stresses in the X and Y direction that the stresses in the X direction are much smaller than the stresses in the Y direction. This is also confirmed by the observation pointed out in Section 4.5 that the bars in the direction transverse to the moment transfer were never highly stressed.

The calculated stresses at the bottom surface of the slab in the Y direction are plotted in Fig. 5.14. The compressive stresses are concentrated near the front face of the column. The maximum compressive stress also occurred at the corner of the column.

Since the finite element analysis presented here assumed linear material behavior, the results are of limited value. The general agreement between locations where calculated tensile stresses were high and where cracking initiated provides qualitative information about the specimen behavior in the elastic response range. As more sophisticated elements are developed that allow cracking due to a three-dimensional stress state, this technique may be a very powerful tool for investigating the punching shear phenomenon.

6. SUMMARY AND CONCLUSIONS

6.1 Object and Scope

The main objective of this investigation was to study experimentally the strength and behavior of prestressed plate-edge column connections with unbonded tendons representative of those used in prestressed flat plate buildings. To achieve the objective, four two-third scale, flat plate-edge column specimens were constructed and subjected to static loadings in which both the shear and moment transferred between the slab and the column were increased proportionately until failure occurred. The experimental variables considered in this program were the direction of the banded tendons and the moment-shear ratio.

6.2 Description of the Experimental Program

6.2.1 Test Specimens

The specimens were models of the edge column and the surrounding slab area. The slab area was approximately that located within the negative moment area around the edge column. The model structure design specified 11-3/8 in. diameter tendons per bay and an average prestress of about 240 psi.

Each specimen consisted of a 60-in. square prestressed concrete slab 4-in. in thickness, and a 12-in. square column located adjacent to and centered along one edge of the slab. The concrete slab was prestressed in both directions, and

represented a two-way flat plate in which the tendons in one direction were banded in a narrow strip over the column, and the tendons in the other direction were uniformly spaced. In addition, No. 3 bars were used as non-prestressed reinforcement in the slab in the vicinity of the column as suggested by ACI-ASCE Committee 423. The columns were reinforced with eight No. 6 deformed bars so as to make the flexural capacity of the column much greater than that of the slab to avoid a column failure.

6.2.2 Test Setup and Procedures

The specimen was supported by bolting the base of the column to a steel pivot that provided a hinged end condition. The upper end of the column was connected to the test frame by a horizontal steel bar which also produced a hinged end condition. The test frame was braced to minimize sidesway.

The unbalanced moment transferred from the slab to the column was obtained by applying a downward load to the slab through the use of hydraulic rams and a whiffle-tree loading mechanism. The rams were connected to a common manifold that operated from a single pump so that each ram simultaneously produced the same force. All specimens were instrumented to provide detailed data on their behavior throughout their entire loading history.

To apply a load increment, the hydraulic pressure in the loading rams was raised until the desired value of load or deflection was reached. The deflection was then held constant,

and during this time data on deflections, loads in the rams, prestress forces in the tendons, strains and cracks were recorded.

6.3 Test Results

Four slab-edge column specimens with varying tendon arrangement and loading positions were loaded incrementally until failure occurred. The following phenomena were observed during the four stages of specimen behavior:

a) Before Cracking

1. The moment-deflection relationship was linear for all specimens and the stiffness of each was approximately the same.

2. The stress in the tendons remainded constant.

b) From Cracking to Yield

1. A gradual decrease in stiffness for all specimens was observed. The decrease in stiffness was more rapid for the lightly reinforced specimens.

2. A series of flexural cracks developed in all four specimens. Small torsional cracks appeared in the slabs near the side faces of the columns in the heavily reinforced specimens.

3. Small twist angles were also observed opposite the side faces of the column.

4. The increase in the tendon stresses was proportional to the edge deflections of the slabs.

c) From Yield to Peak Load

1. Yielding of the bonded steel occurred for each specimen at approximately the same edge deflection.

2. The stiffness of the specimens decreased rapidly until the peak load was reached.

3. The edge deflections of the specimens resulted mainly from a rotation of the slab about a yield line that formed along one of the flexural cracks.

4. Torsional cracks became more apparent for all specimens but were more extensive for the heavily reinforced specimens. The torsional cracking was accompanied by an increase of the twist angles.

5. The increase in the tendon stresses was still proportional to the rotation of the slabs.

d) From Peak Load to Failure

1. Highly developed torsional cracks were present on all specimens and were accompanied by very large twist angles.

2. Crushing occurred at the intersection of the compression side of the slab and the column for three of the specimens. Crushing began at about the same slab rotation for each of these, and this corresponded to the rotation at the peak load for the two specimens that failed in flexure. The fourth specimen failed in shear before it reached this level of slab rotation.

3. The peak loads of the two specimens that failed in shear occurred at about the same slab rotation. The specimens

that failed in flexure also failed at about the same slab rotation, but this occurred at larger rotation as compared to the specimens that failed in shear.

4. The relationship between the increase in the tendon stress and the slab rotation was no longer linear.

5. The specimens that failed in flexure exhibited more ductility than those that failed in shear.

6.4 Discussion Related to the Use of Simple Models

The ACI model does not accurately predict the failure mode since it is based on an elastic theory. However, it did predict the strengths reasonably well. The actual stresses at ultimate load in the bonded reinforcement and in the unbonded tendons were quite different from the stresses specified by the ACI Code. The stresses in the tendons were smaller than the ACI predicted stresses, while the observed stresses in the bonded reinforcement were higher than the yield stress specified by the Code, because of strain hardening. For this reason, the errors counteracted each other and the calculated flexural strengths were reasonably close to the observed strengths.

All the proposed models suggested in this investigation for predicting tendon stress increase rely on the assumption that a direct and predictable relationship exists between the rotation at a yield line and the increase in the tendon stress. This hypothesis was substantiated by the test results obtained in this study as well as others reported in the literature. Therefore, one can predict the tendon

stress increase with reasonable accuracy provided that the rotations at the plastic hinges are known. On the average, the modified Tam and Pannell method was the best predictor of the tendon stress increase, Δf_{ps}, and it may be very useful for the design of prestressed slabs.

The modified beam analogy proposed in this investigation introduces a number of changes in Park and Islam's beam analogy for application to prestressed concrete slab-edge column connections. The predicted strengths computed using the beam analogy approach are found to be easily obtained but still in good agreement with the measured strengths. Although one may not make broad and general conclusions based on this small sample of data, the accuracy of the model indicates that the beam analogy approach should be investigated further.

Two types of yield line patterns, folding and local, were examined to study the strength of the connections. The predicted strengths using the folding-type yield line pattern were close to the measured strengths, even for specimens which failed in shear. For those specimens, the bonded bars yielded before the shear failure occurred. The analysis using the local yield line mechanism involved some adjustment to Gesund's model. The predicted strengths were larger than the observed values. This was reasonable since none of the specimens failed in this manner.

The application of finite element technique to the connections over the elastic loading range was also

investigated. The general agreement between the locations where the calculated tensile stresses were high and where the cracking initiated provides qualitative information about the specimen behavior in the elastic response range. As more sophisticated elements are developed that allow cracking due to a three dimensional stress state, this technique may be a very powerful tool for investigating the punching shear phenomenon.

6.5 Conclusions

On the basis of the reported test results and analyses, the following conclusions and recommendations can be made about the prestressed concrete plate-edge column specimens:

1. As the shear transmitted from the slab to the column increases, the ultimate bending moment that can be transmitted to the column and the ductility of the response decrease.

2. The concentration of prestressing tendons in the region of the edge column increases the strength of the connection and also increases the load at which cracking occurs. Before cracking there was no significant difference in the stiffness of the four specimens.

3. At ultimate load, the actual stresses in the bonded reinforcement were significantly higher than specified by the ACI Code and those in the unbonded tendons were significantly lower than the predicted values. However, the predicted flexural strengths were reasonably close to the measured strengths since the errors compensated for each other. This

is an undesirable situation for designers since these errors cannot always be relied upon to compensate for each other and unconservative estimates of connection strength may result.

4. The equation recommended by ACI for predicting the increase in tendon stress for unbonded tendons is inadequate since it does not contain the variables that influence this behavior. The equation can be extremely unconservative for slabs which have large span-depth ratios.

5. The increase in stress in the unbonded tendons is directly related to the span-depth ratio and to the rotation of the slab at a yield line which it crosses. The modified Tam and Pannell method was the best predictor of the tendon stress increase, and it may be very useful for the design of prestressed concrete slabs.

6. The accuracy of the beam analogy proposed in this investigation indicates that this approach can be used as a practical design method for calculating the strength of prestressed concrete slab-edge column connections transferring moments and shears.

7. The yield line theory provides a convenient method for evaluating the ultimate flexural strength of prestressed flat plate floors.

8. The development of the cracks as well as the effects of these cracks on the ultimate behavior of an edge column connection are complex three-dimensional problems which have no simple solutions. Additional data and new experimental

methods are required if a true understanding of these phenomena is to be attained.

6.6 Recommendations for Future Research

Since the behavior of prestressed concrete slab-column connections has not been adequately explored, many questions still exist and need more detailed clarification. Several areas that require further research are as follows:

1. Additional experimental data needs to be obtained to further clarify the effect of the interaction between moment and shear at the connection. In particular, additional specimens where shear governs the connection strengths need to be tested. This data will also clarify which models for predicting connection strength are most suitable.

2. Additional research needs to be done before an adequate understanding of the initiation and propagation of cracks associated with punching shear failures can be obtained. In addition, it is not known what influence, if any, the presence of flexural cracks has on the punching shear resistance of a slab.

3. The rotation of a slab at the plastic hinges is an important factor that influences the stress increase in the unbonded tendons. Therefore, to predict the stress increase it is necessary to investigate the ultimate rotation capacity of the slabs at the plastic hinges. The effect of span-depth ratio on the stress increase also needs to be clarified.

4. More research should be done to clarify the

percentages of the unbalanced bending moment to be transmitted as flexural moment at the front face and as torsional moments at the side faces of the critical section. Also the ultimate torsional capacity of the slab and the parameters that influence this capacity should be investigated further.

5. The beam analogy presented in the previous chapter appears to be a reasonably good model for predicting the strength of the slab-column connection. However, several uncertanties in the model still exist that need to be investigated further. The model assumes that the ultimate strengths of the equivalent beams may be reached simultaneously. It is uncertain what detailing practices would be required for this assumptions to be true. The distribution of shear stresses at the critical section at ultimate needs to be clarified. The use of the combined reinforcement index as a qualitative indicator for the distribution of shear on the side faces of the column should also be investigated. Since the critical section is restrained by the continuum around it, the ultimate torsional shear stress is expected to be greater than the torsional shear capacity in beams. More data is required to clarify the capacity of the slab in carrying torsion. The simultaneous application of shear forces and torques at the side faces, and shear forces and moments at the front face of the critical section will produce interactions that will reduce the strength compared with what it would be if they were acting alone. More

experimental research is required to identify the nature of this interaction.

6. The local yield line theory appears to be a very promising analytical tool for investigating the local flexural failures in slabs. This is particularly important at edge column connections, since experiments conducted on multi-panel specimens indicate that these types of failures are more likely to occur than a general folding-type yield line failure. For prestressed concrete slabs that do not have uniform tendon spacing, it is necessary to investigate the widths over which to calculate the unit moments to be used in the yield line analysis.

7. The development of finite element techniques that allow three-dimensional cracking would provide a very powerful tool for investigating the punching shear phenomenon.

Table 3.1 Properties of Concrete

PARAMETER	SPECIMEN			
	S1	S2	S3	S4
Mix by Weight	1:2.98:2.78	1:2.98:2.78	1:2.98:2.78	1:2.98:2.78
W/C by Weight	0.576	0.576	0.598	0.598
Slump (in.)	1-1/4	1-7/8	2	2-1/2
<u>At Time of Stressing</u>				
Age (days)	8	7	7	7
Compressive Strength, f'_c (psi)	4,700	5,300	4,600	4,900
<u>At Time of Testing</u>				
Age (days)	33	24	47	28
Compressive Strength, f'_c (psi)	7,300	6,200	6,100	7,000
Tensile Strength, f_{sp} (psi)	528	561	493	400
Modulus of Rupture, f_r (psi)	726	627	702	628

Table 3.2 Properties of Bonded Reinforcement

PARAMETER	BAR SIZE	
	#3 (Slab)	#6 (Column)
Yield Stress, f_y (Ksi)	72.73	72.73
Yield Strain, ϵ_y	0.0025	0.0025
ϵ_h	0.0060	0.0050
Maximum Stress, f_u (Ksi)	126.7	120.5
Strain at Maximum Stress ϵ_u	0.100	

ϵ_y: measured yield strain

ϵ_h: strain at initiation of strain hardening

Table 4.1 Dimensions and Details of Specimens

SPECIMEN	CROSS SECTION b x h, $in.^2$	NUMBER OF Ø3/8"-TENDONS		$F_{se}/A_{specimen}$, KSI	
		W-E DIRECTION	N-S DIRECTION	W-E DIRECTION	N-S DIRECTION
S1	60 x 4	11	5	0.650	0.246
S2	60 x 4	11	5	0.691	0.325
S3	60 x 4	4	6	0.260	0.385
S4	60 x 4	4	6	0.264	0.368

Table 4.2 Measured and Calculated Ultimate Moment at Face of Column

SPECIMEN	MOMENT DUE TO D.L. SLAB + LOADING FR.	MOMENT DUE TO APPLIED LOAD	MEASURED MOMENT	CALCULATED MOMENT ACI 318-77	CALCULATED MOMENT BASED ON MEAS. INTERNAL FORCES	MODE OF FAILURE
S1	2.86	40.37	43.23	40.95	41.65	Flexure
S2	2.49	34.52	37.01	37.10	36.47	Shear
S3	2.49	27.30	29.79	27.90	29.29	Flexure
S4	2.25	24.14	26.39	24.68	26.09	Shear

Moment in units of k-ft.

Table 4.3 Ultimate Shear and Moment at Centerline of Columns

SPECIMEN	SHEAR DUE TO			MOMENT DUE TO			DEFLECTION
	D.L. SLAB + LOADING FR.	APPLIED LOAD	TOTAL LOAD	D.L. SLAB + LOADING FR.	APPLIED LOAD	TOTAL LOAD	AT EDGE OF SLAB
S1	1.45	11.53	12.98	3.50	46.12	49.62	1.449
S2	1.45	17.26	18.71	3.12	43.15	46.27	0.919
S3	1.45	13.65	15.10	3.12	34.12	37.24	1.511
S4	1.45	24.14	25.59	2.87	36.21	39.08	0.837

Shear in units of kips.
Moment in units of k-ft.

Table 4.4 Stress Increase in Tendons at Peak Load of Specimens S1 and S2

STRESSING SCHEDULE NUMBER	SPECIMEN S1			SPECIMEN S2		
	f_{se}	Δf_{ps}		f_{se}	Δf_{ps}	
		MEAS.	ACI		MEAS.	ACI
W-E Direction						
4	165.27	5.89	25.0	175.29	3.23	22.7
15	163.18	8.78	25.0	173.79	4.62	22.7
3	168.83	9.50	25.0	170.82	4.01	22.7
14	166.67	11.62	25.0	177.24	4.08	22.7
COLUMN → 11	170.75	12.63	25.0	182.02	5.20	22.7
COLUMN → 1	164.42	10.05	25.0	184.07	3.38	22.7
COLUMN → 12	171.24	11.94	25.0	182.76	3.43	22.7
13	163.95	8.89	25.0	175.10	3.50	22.7
2	154.98	11.09	25.0	166.38	3.43	22.7
16	173.40	9.01	25.0	186.31	3.80	22.7
5	173.97	8.74	25.0	177.61	2.28	22.7
N-S Direction						
COLUMN → 10	158.37	0.90		192.08	0.86	
COLUMN → 9	152.12	1.51		185.58	1.06	
7	158.25	0.52		178.73	0.73	
6	164.27	-0.07		178.08	0.07	
8	62.12	-0.59		184.66	0.12	

Stress in units of ksi.

Table 4.5 Stress Increase in Tendons at Peak Load of Specimens S3 and S4

STRESSING SCHEDULE NUMBER		SPECIMEN S3			SPECIMEN S4		
		f_{se}	Δf_{ps}		f_{se}	Δf_{ps}	
			MEAS.	ACI		MEAS.	ACI
W-E Direction							
	4	185.58	9.41	44.5	183.89	2.04	48.9
COLUMN →	1	183.71	13.68	44.5	188.61	6.99	48.9
COLUMN →	2	179.74	14.07	44.5	197.23	5.53	48.9
	3	184.91	8.53	44.5	176.77	3.65	48.9
N-S Direction							
COLUMN →	7	181.26	0.67		161.06	0.72	
COLUMN →	10	184.49	0.18		173.67	0.28	
COLUMN →	5	189.46	-0.73		173.77	0.64	
	8	177.89	-0.09		180.12	-0.31	
	6	169.83	0.29		174.33	0.05	
	9	183.50	-0.23		176.21	0.22	

Stress in units of ksi.

Table 5.1 Comparison of Measured and Predicted Shear Strength Using ACI Model

SPECIMEN	PREDICTED SHEAR STRENGTH				MEASURED STRENGTH		MODE OF FAILURE
	$v_{cw} = 3.5\sqrt{f'_c} + 0.3f_{pc}$		$v_c = 4\sqrt{f'_c}$				
	V_u	M_u	V_u	M_u	V_u	M_u	
S1	10.58	40.02	7.76	28.74	12.98	49.62	Flexure
S2	18.17	44.93	12.38	30.45	18.71	46.27	Shear
S3	13.47	33.17	12.13	29.83	15.10	37.24	Flexure
S4	22.80	34.90	20.68	31.72	25.59	39.08	Shear

Ultimate shear V_u in units of kips.
Ultimate moment M_u in units of k-ft.

Table 5.2 Comparison of Measured and Predicted Flexural Strength Using ACI Model

SPECIMEN	M_u		f_s		f_{ps}	
	MEASURED	ACI 318-77	MEASURED	ACI 318-77	MEASURED	ACI 318-77
S1	49.62	47.02	83.33	72.73	176.8	192.0
S2	46.27	46.37	75.15	72.73	181.1	199.7
S3	37.24	34.87	90.76	72.73	194.9	228.0
S4	39.08	36.91	78.94	72.73	191.2	235.5

Ultimate moment M_u in units of k-ft.
Stress in units of ksi.

Table 5.3 Measured and Predicted Stress Increase in Tendons of Specimens S1, S2, S3 and S4

SPECIMEN	MEASURED Δf_{ps}	PREDICTED Δf_{ps} USING MEASURED ROTATION	BOND-SLIP MODEL MEASURED ϵ_s	BOND-SLIP MODEL $\epsilon_c = 0.003$	MODIFIED TAM & PANNELL $R = \phi\epsilon_c$; $\phi = 9$	ACI 318-77 Eq. (5.2)
S1	12.63 10.05 11.94	11.67	12.06	6.72	12.61	25.0
S2	5.20 3.38 3.43	5.37	5.06	-	-	22.7
S3	13.68 14.07	12.61	13.84	8.24	12.61	44.5
S4	6.99 5.53	8.22	5.22	-	-	48.9

Stress in units of ksi.

Table 5.4 Measured and Predicted Stress Increase in Tendons of Specimens Tested by Other Investigators

REFERENCE	l/h	MEASURED Δf_{ps}	PREDICTED Δf_{ps} USING MEASURED DEFLECTION	PREDICTED Δf_{ps} MODIFIED TAM & PANNELL $R = \phi\epsilon_c$; $\phi = 9$	PREDICTED Δf_{ps} ACI 318-77 Eq. (5.2)	LOADING
33	28	25.0	25.6	14.51	18.63	RU1: SIMPLY SUPPORTED BEAM, MID-POINT LOADING, PEAK LOAD
33	28	18.6	19.3	14.58	18.63	RU2: SIMPLY SUPPORTED BEAM, MID-POINT LOADING, PEAK LOAD
23	45	5.3	4.6	5.87	26.05	SLAB I: 3 x 3 PANEL SLAB, UNIFORM LOADING, TEST 110, TENDON N2
44	45	11.7	10.4	11.65	20.3	SLAB III: 2 x 2 PANEL SLAB, UNIFORM LOADING, TEST 308, TENDON T6
44	45	18.7	15.2	18.65	20.3	SLAB III: 2 x 2 PANEL SLAB, UNIFORM LOADING, TEST 308, TENDON T2
36	45	61.0	76.0	26.76	51.0	M1: SIMPLY SUPPORTED RIBBED, ONE-WAY SLAB, 2 POINT LOADS, 2 LOAD STEPS BEYOND δ_{ACI}
36	37	77.2	95.0	32.38	44.5	M2: SIMPLY SUPPORTED RIBBED, ONE-WAY SLAB, 2 POINT LOADS, PEAK LOAD
36	29	67.0	82.0	41.66	52.2	M3: SIMPLY SUPPORTED RIBBED, ONE-WAY SLAB, 2 POINT LOADS, 2 LOAD STEPS BEYOND δ_{ACI}
36	29	57.0	75.0	40.78	39.5	M4: SIMPLY SUPPORTED ONE-WAY SLAB, 2 POINT LOADS, 3 LOAD STEPS BEYOND δ_{ACI}
11	26.7	27.0	55.0	27.59	16.0	SLAB 1: SIMPLY SUPPORTED ONE-WAY SLAB, 2 POINT LOADS, PEAK LOAD
11	26.7	32.0	61.0	33.56	24.0	SLAB 2: SIMPLY SUPPORTED ONE-WAY SLAB, 2 POINT LOADS, PEAK LOAD
11	26.7	38.0	45.0	37.86	63.0	SLAB 3: SIMPLY SUPPORTED ONE-WAY SLAB, 2 POINT LOADS, PEAK LOAD
11	20.0	31.0	56.0	38.77	17.0	SLAB 4: SIMPLY SUPPORTED ONE-WAY SLAB, 2 POINT LOADS, PEAK LOAD
11	20.0	42.0	62.0	45.62	26.0	SLAB 5: SIMPLY SUPPORTED ONE-WAY SLAB, 2 POINT LOADS, PEAK LOAD
11	20.0	51.0	48.0	50.71	71.0	SLAB 6: SIMPLY SUPPORTED ONE-WAY SLAB, 2 POINT LOADS, PEAK LOAD
11	13.3	37.0	60.0	44.00	17.0	SLAB 7: SIMPLY SUPPORTED ONE-WAY SLAB, 2 POINT LOADS, PEAK LOAD
11	13.3	47.0	66.0	50.00	24.0	SLAB 8: SIMPLY SUPPORTED ONE-WAY SLAB, 2 POINT LOADS, PEAK LOAD
11	13.3	58.0	58.0	50.0	64.0	SLAB 9: SIMPLY SUPPORTED ONE-WAY SLAB, 2 POINT LOADS, PEAK LOAD

Stress in units of ksi.

Table 5.5 Measured and Predicted Strengths Using Beam Analogy

	MEASURED STRENGTH		BEAM ANALOGY			
			$v_{cw} = 3.5\sqrt{f'_c} + 0.3f_{pc}$		$v_c = 4\sqrt{f'_c}$	
SPECIMEN	V_u	M_u	V_u	M_u	V_u	M_u
S1	12.98	49.62	12.23	46.90	12.15	46.30
S2	18.71	46.27	19.54	48.35	18.54	45.87
S3	15.10	37.24	17.73	43.83	16.80	41.50
S4	25.59	39.08	28.47	43.40	25.64	39.16

Ultimate shear V_u in units of kips.
Ultimate moment M_u in units of k-ft.

Table 5.6 Measured and Predicted Strength Using Beam Analogy of Hawkins's Specimen No. 2

	MEASURED STRENGTH		BEAM ANALOGY	
SPECIMEN	V_u	M_u	V_u	M_u
2	30.8	37.0	32.77	39.32

Ultimate shear V_u in units of kips.
Ultimate moment M_u in units of k-ft.

Table 5.7 Calculated Yield Moment/Unit Length for the Use in Yield Line Models

SPECIMEN	X DIRECTION		Y DIRECTION				$\mu = \frac{m_x + m'_x}{m_y + m'_y}$	$\frac{\mu}{1+\mu}$	$\frac{1-\mu}{1+\mu}$	Σm
	m_x	m'_x	m_y	m'_y	$m_x + m'_x$	$m_y + m'_y$				
S1	10.54	7.23	5.71	1.86	17.77	7.57	2.35	0.70	-0.40	25.34
S2	10.31	7.26	6.24	2.02	17.57	8.26	2.13	0.68	-0.36	25.83
S3	6.39	2.92	8.80	2.81	9.31	11.61	0.80	0.44	0.11	20.92
S4	6.51	2.98	8.69	2.85	9.49	11.54	0.82	0.45	0.10	21.03

Moment/unit length in units of k-ft/ft.

Table 5.8 Measured and Predicted Connection Strengths Using Yield Line Theory

	MEASURED STRENGTH		FOLDING-TYPE YIELD LINE		LOCAL FAILURE YIELD LINE	
SPECIMEN	V_u	M_u	V_u	M_u	V_u	M_u
S1	12.98	49.62	11.95	47.82	15.43	59.42
S2	18.71	46.27	18.96	46.90	22.98	56.95
S3	15.10	37.24	14.77	36.93	18.43	45.57
S4	25.59	39.08	25.95	39.62	27.20	41.50

Ultimate shear V_u in units of kips.
Ultimate moment M_u in units of k-ft.

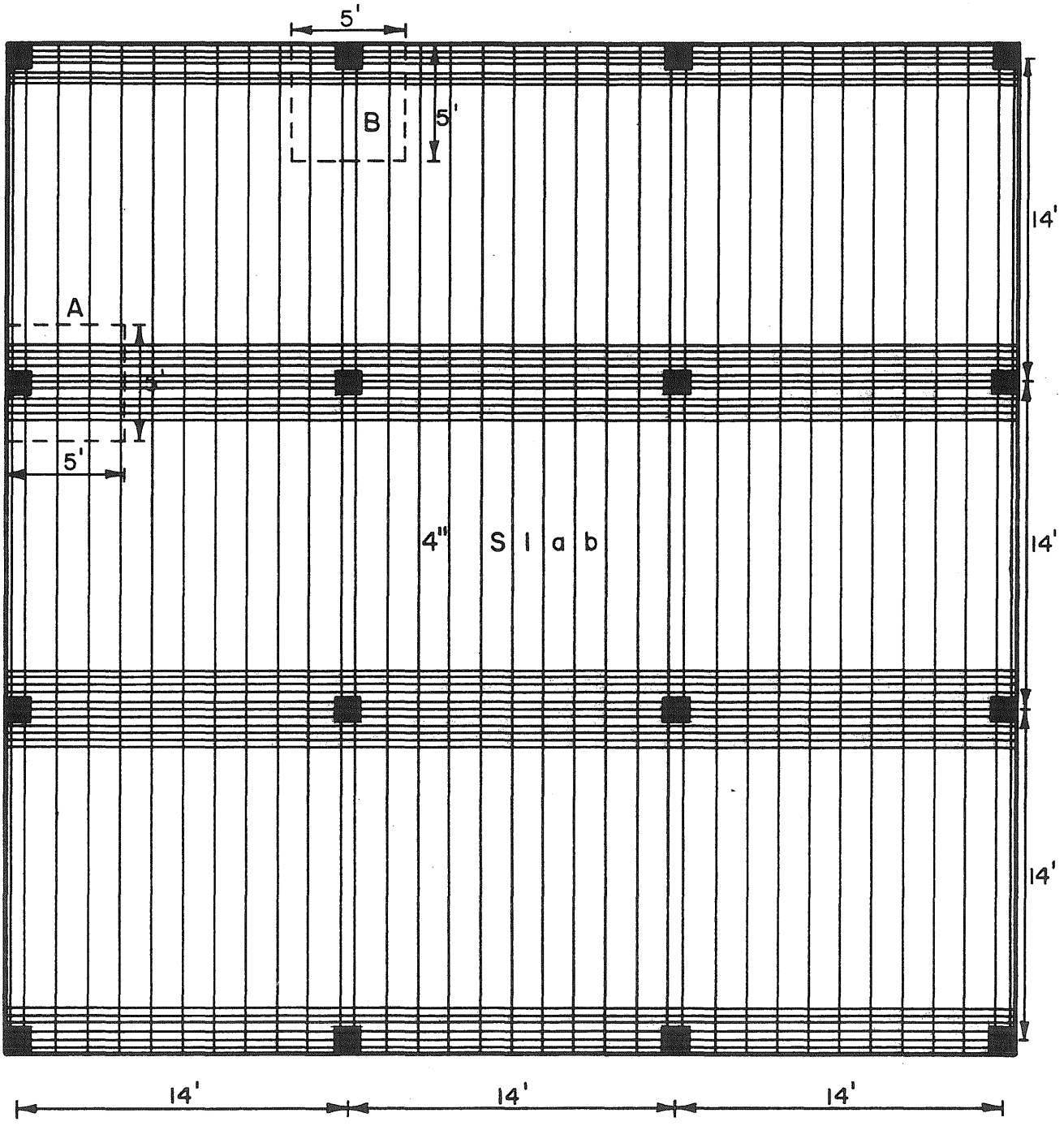

Fig. 1.1 Two-Thirds Scale Model of Prestressed Concrete Slab

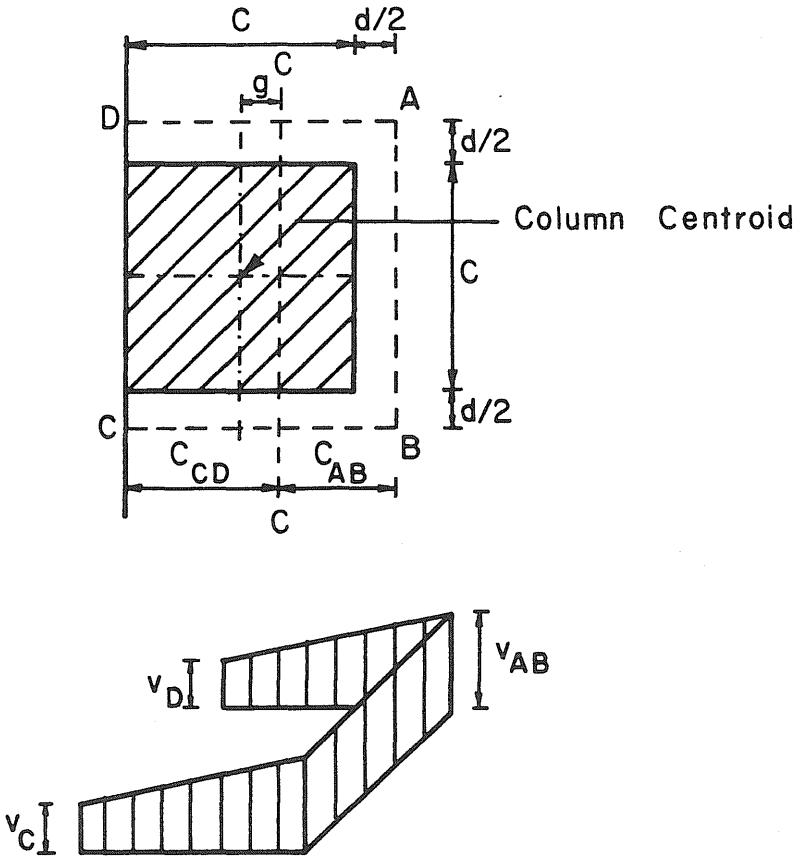

Fig. 2.1 Assumed Distribution of Shear Stress for Exterior Column Connections

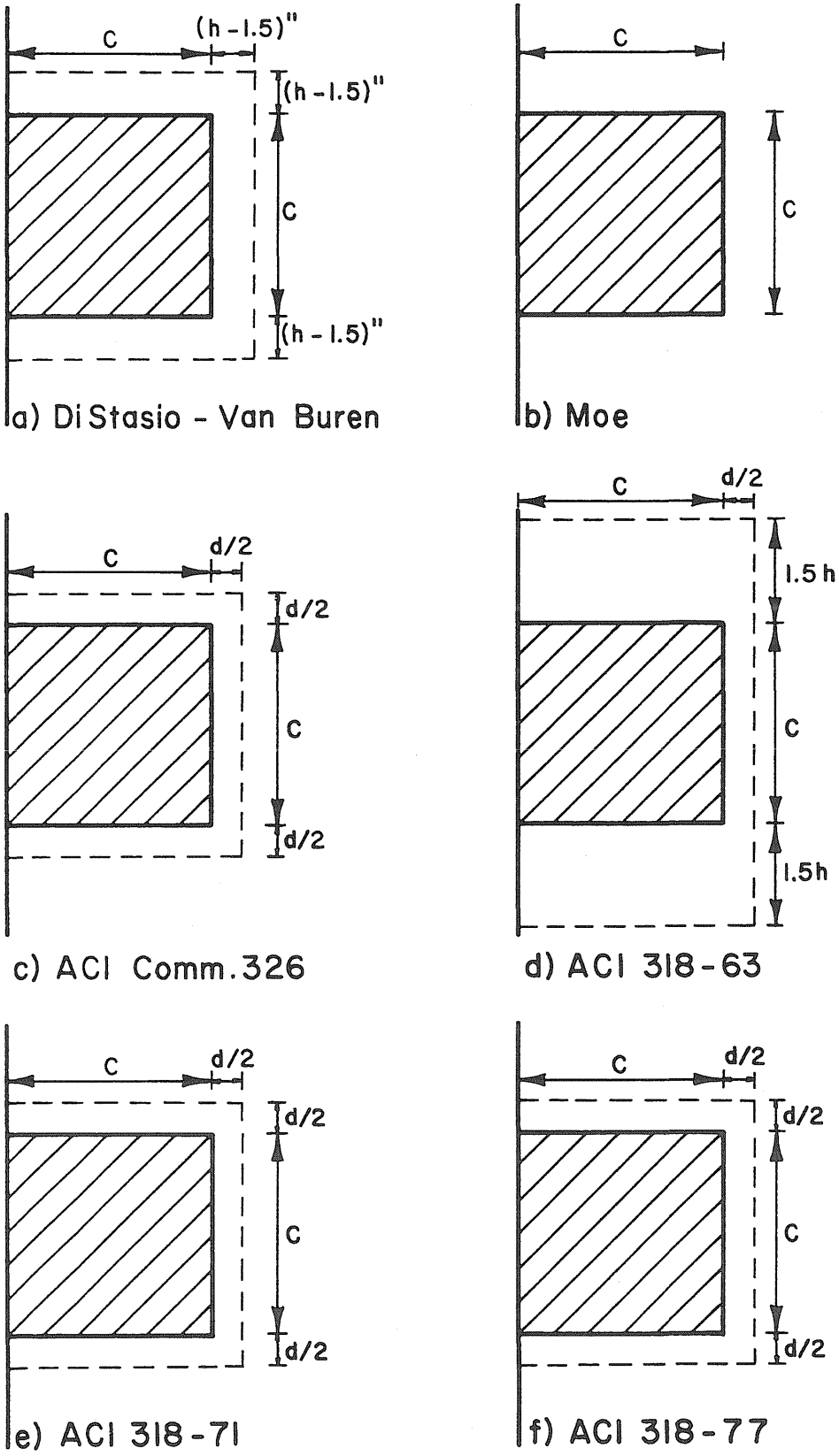

Fig. 2.2 Assumed Critical Sections for Six Failure Models

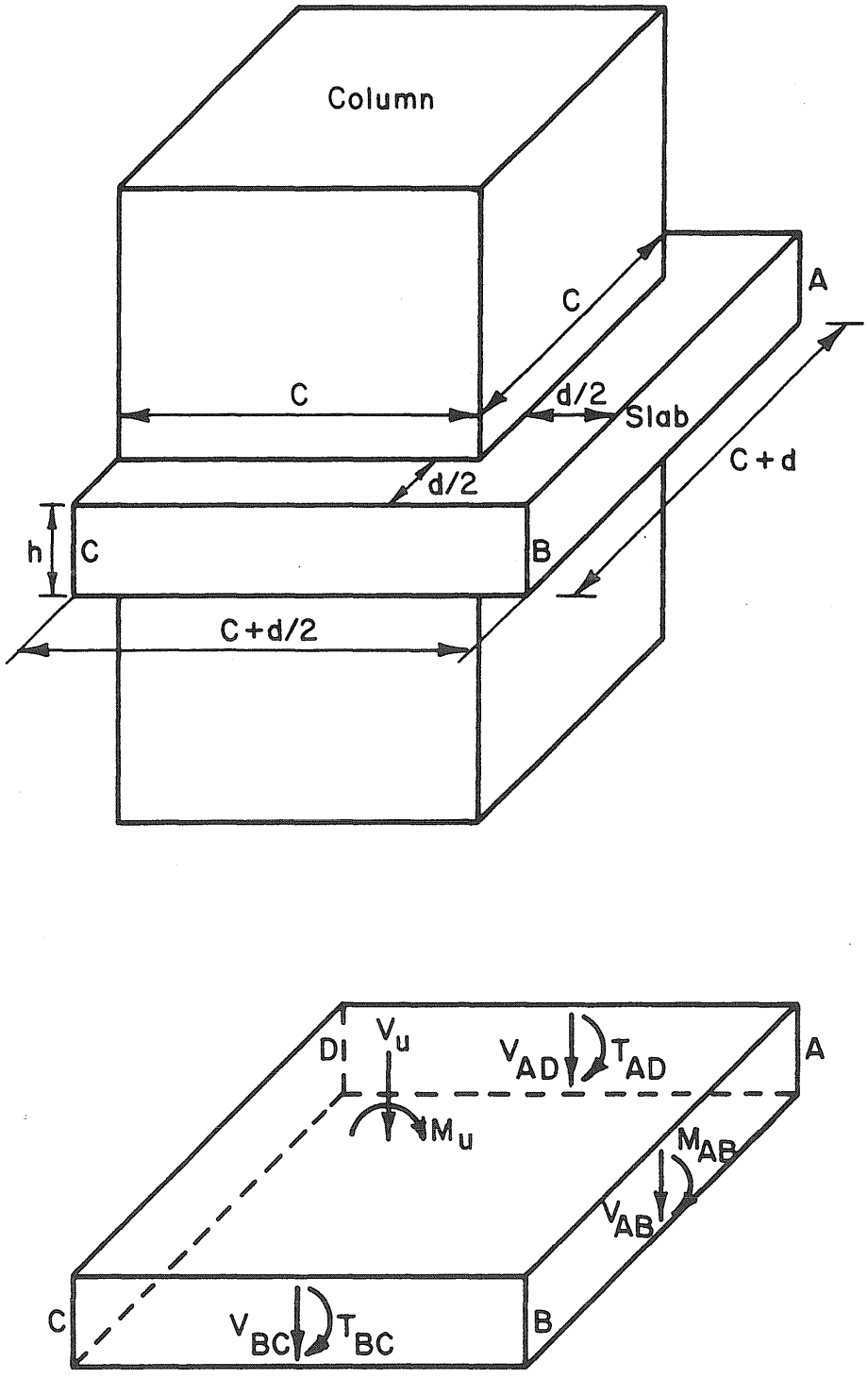

Fig. 2.3 Critical Section and Actions at Exterior Slab-Column Connection

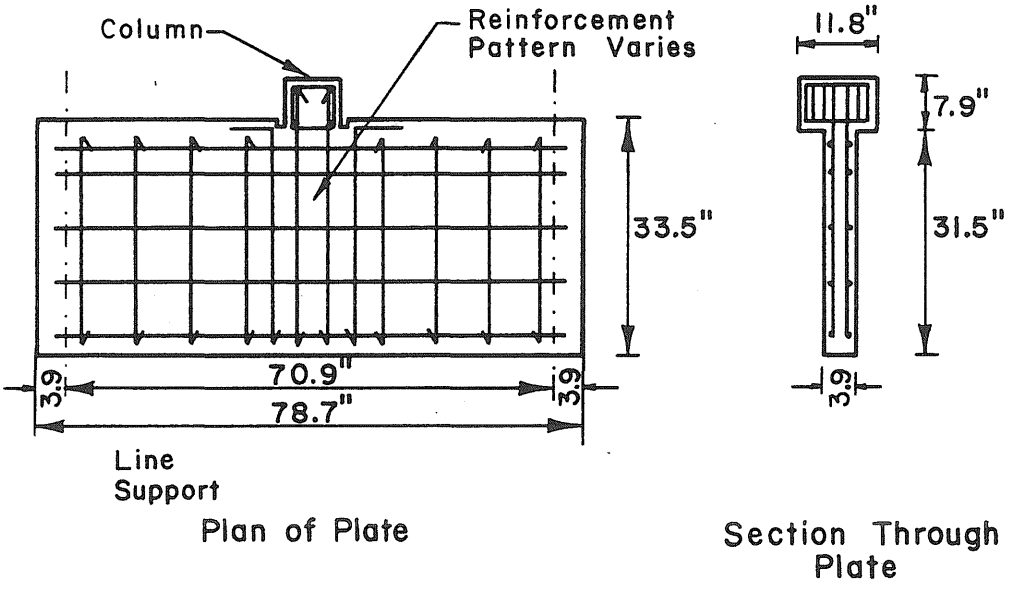

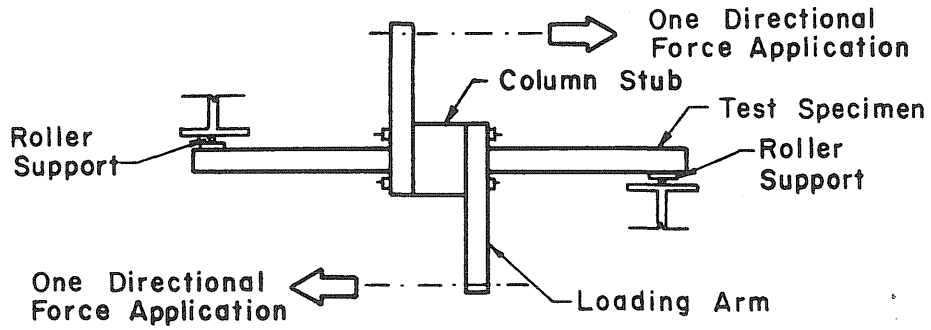

Loading Setup

Fig. 2.4 Kanoh and Yoshizaki's Loading Setup

	D, IN.
S 1	42
S 2	24
S 3	24
S 4	12

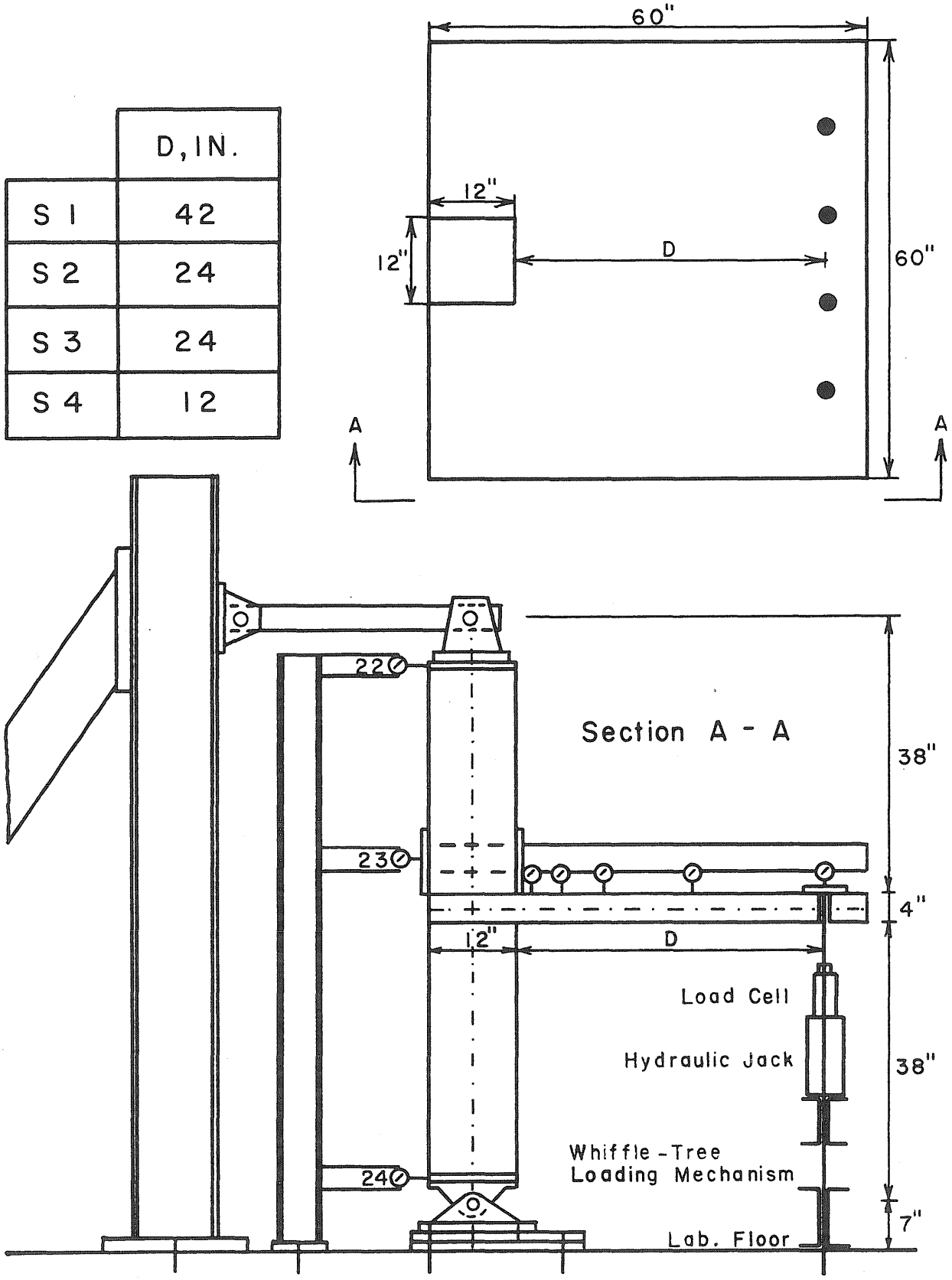

Fig. 3.1 Plan and Elevation of the Test Specimen

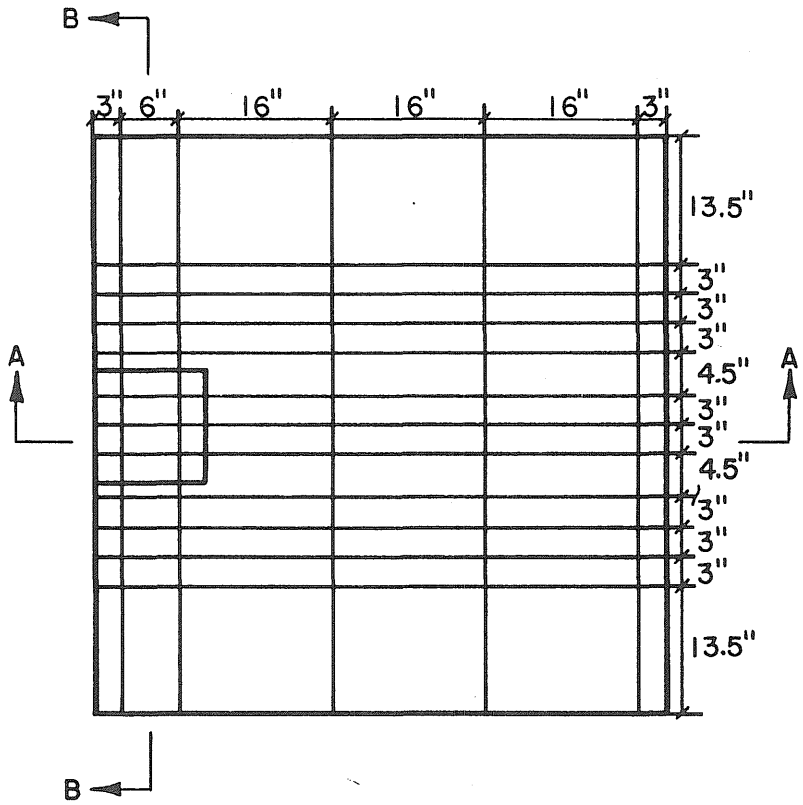

S1 & S2

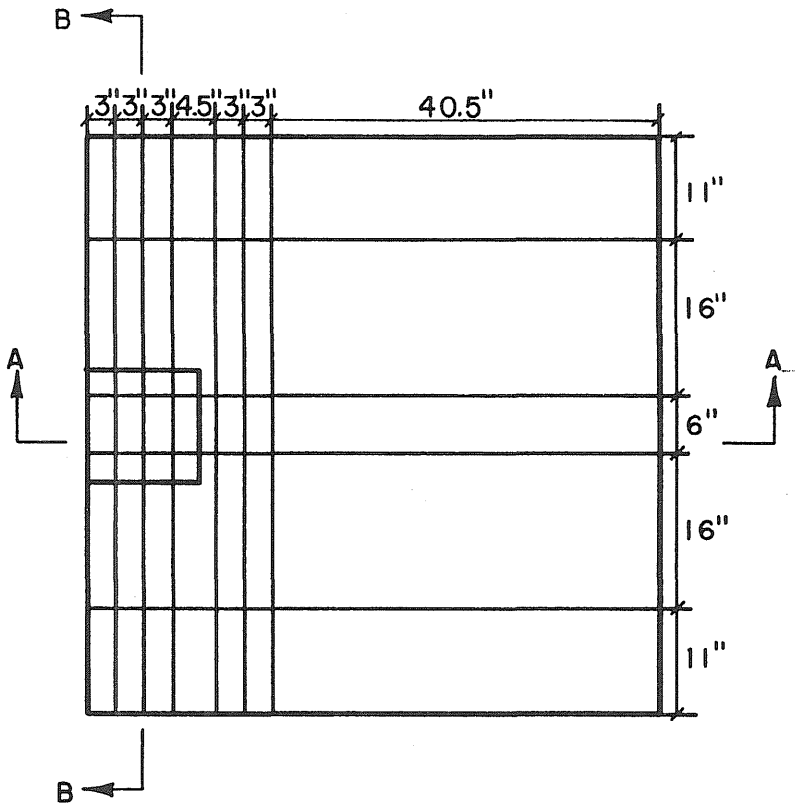

S3 & S4

All Tendons: 3/8" Diameter 7-Wire Strands

Fig. 3.2 Tendon Arrangement

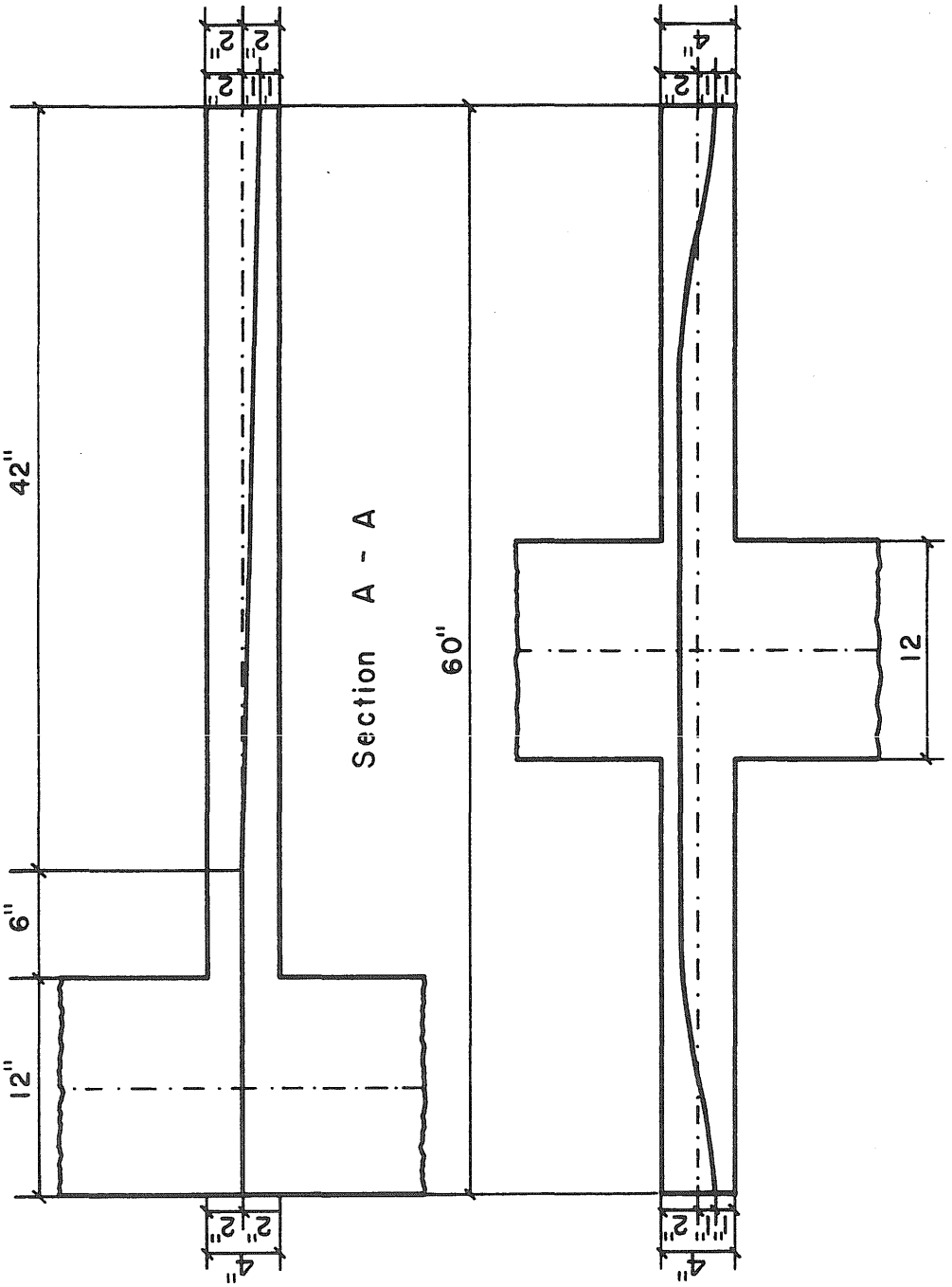

Fig. 3.3 Tendon Profile

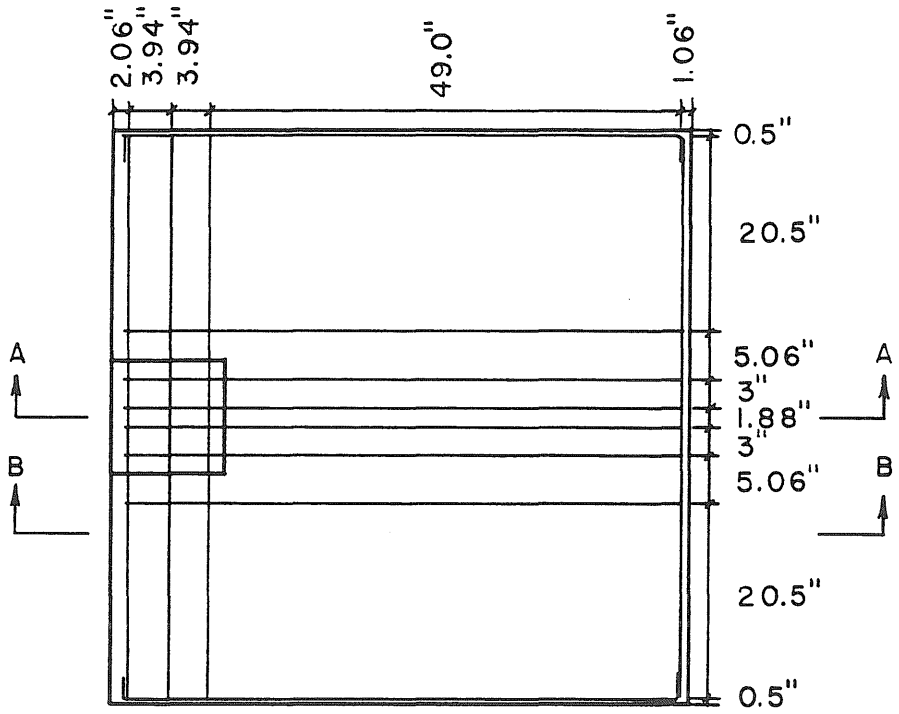

Bonded Reinforcement: No. 3 Deformed Bars

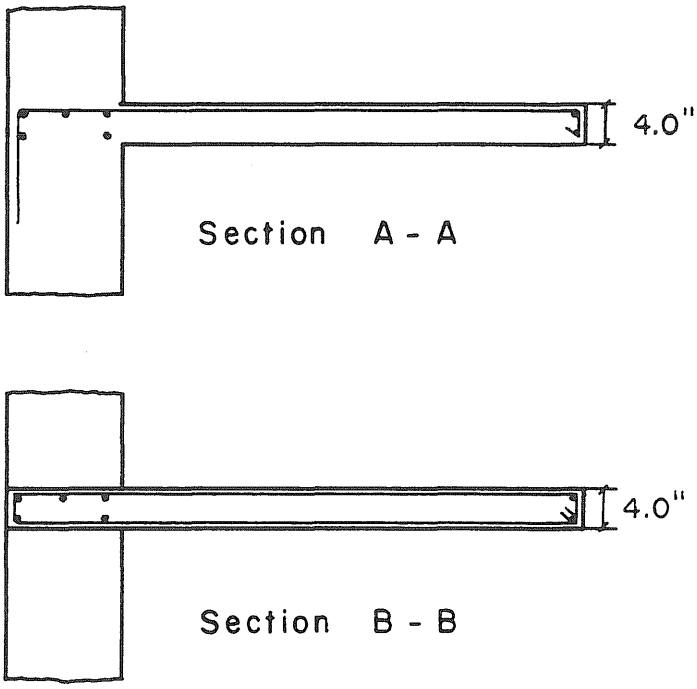

Fig. 3.4 Bonded Reinforcement in the Slab

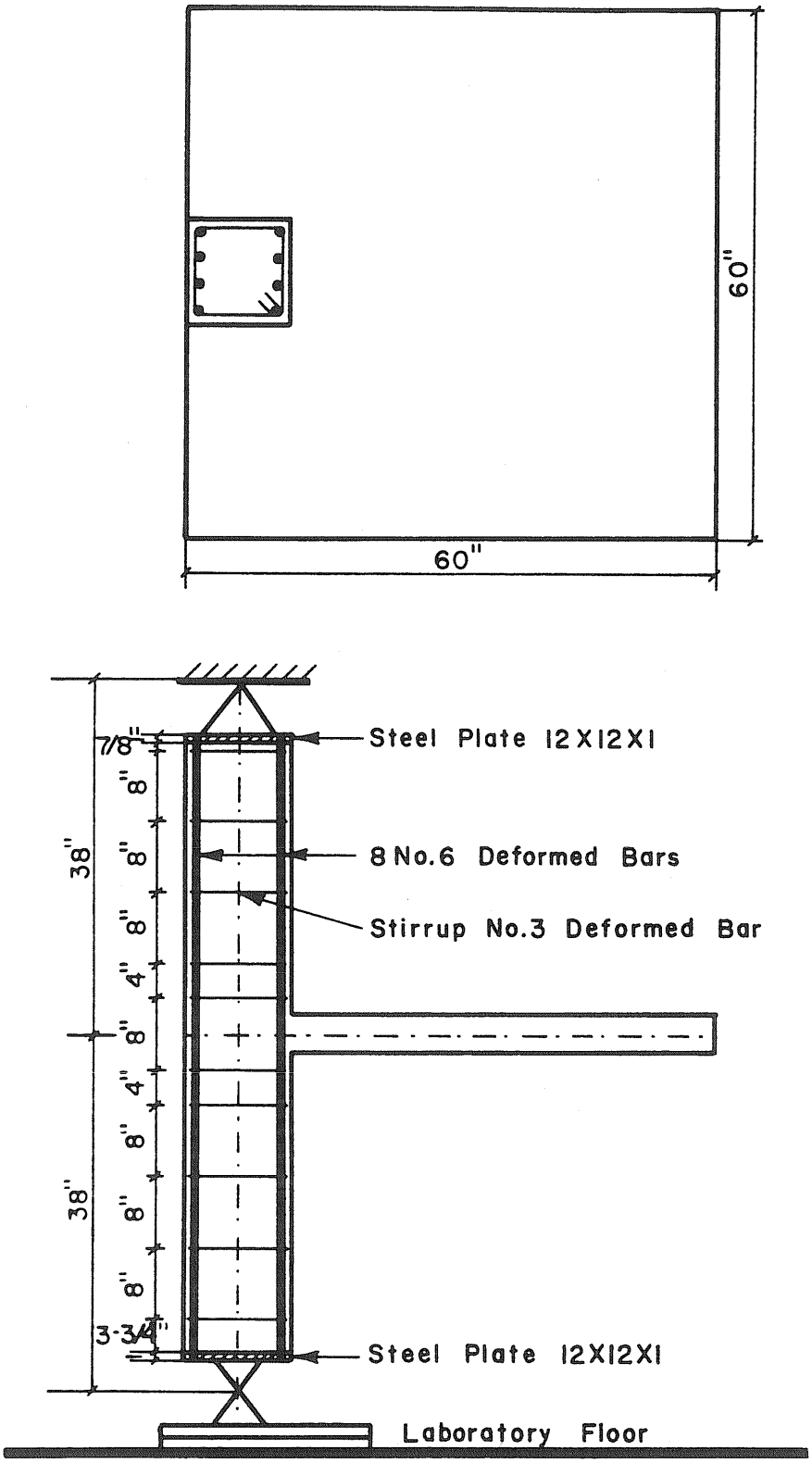

Fig. 3.5 Reinforcement in the Column

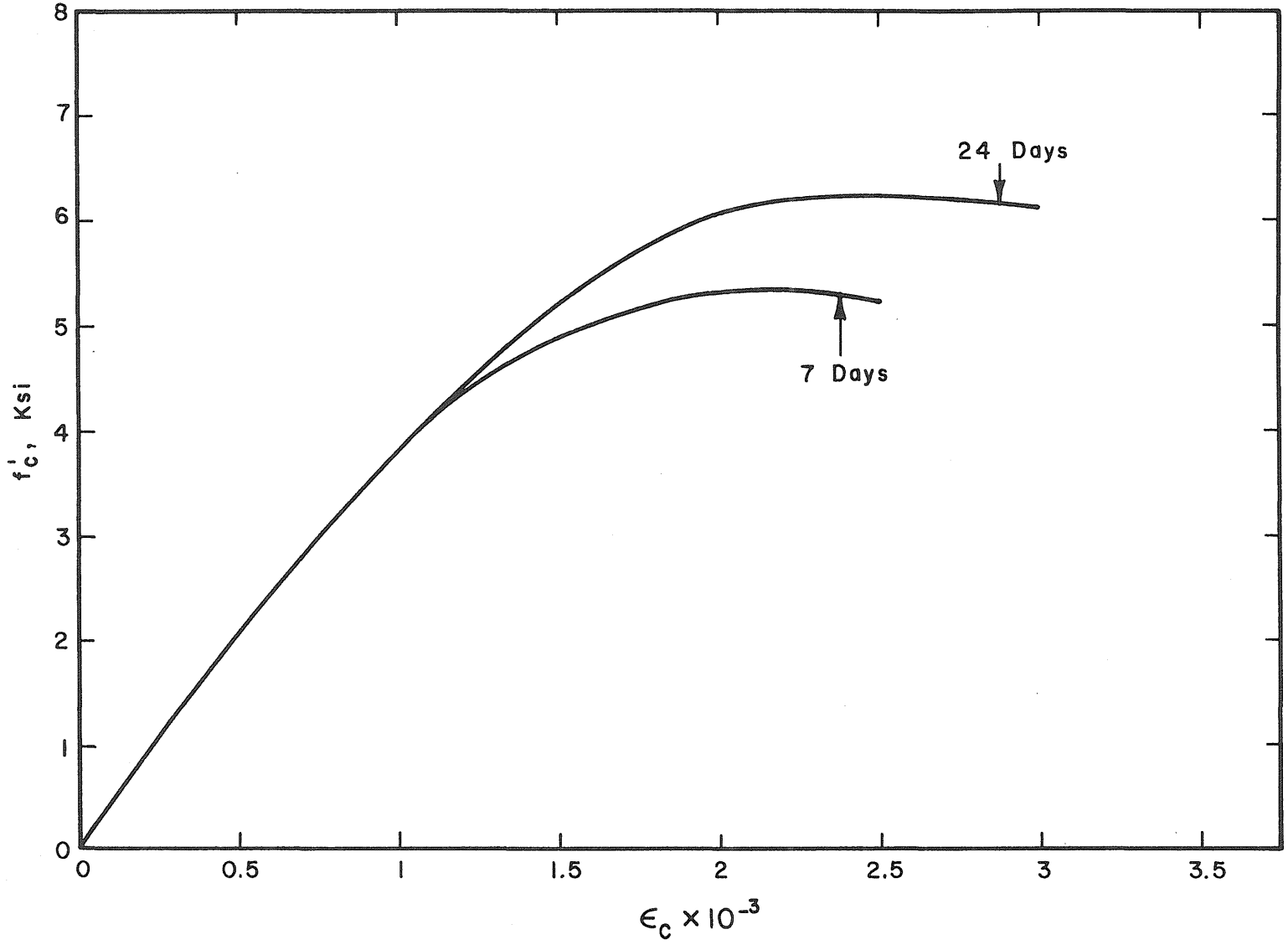

Fig. 3.6 Typical Stress-Strain Curve for the Concrete

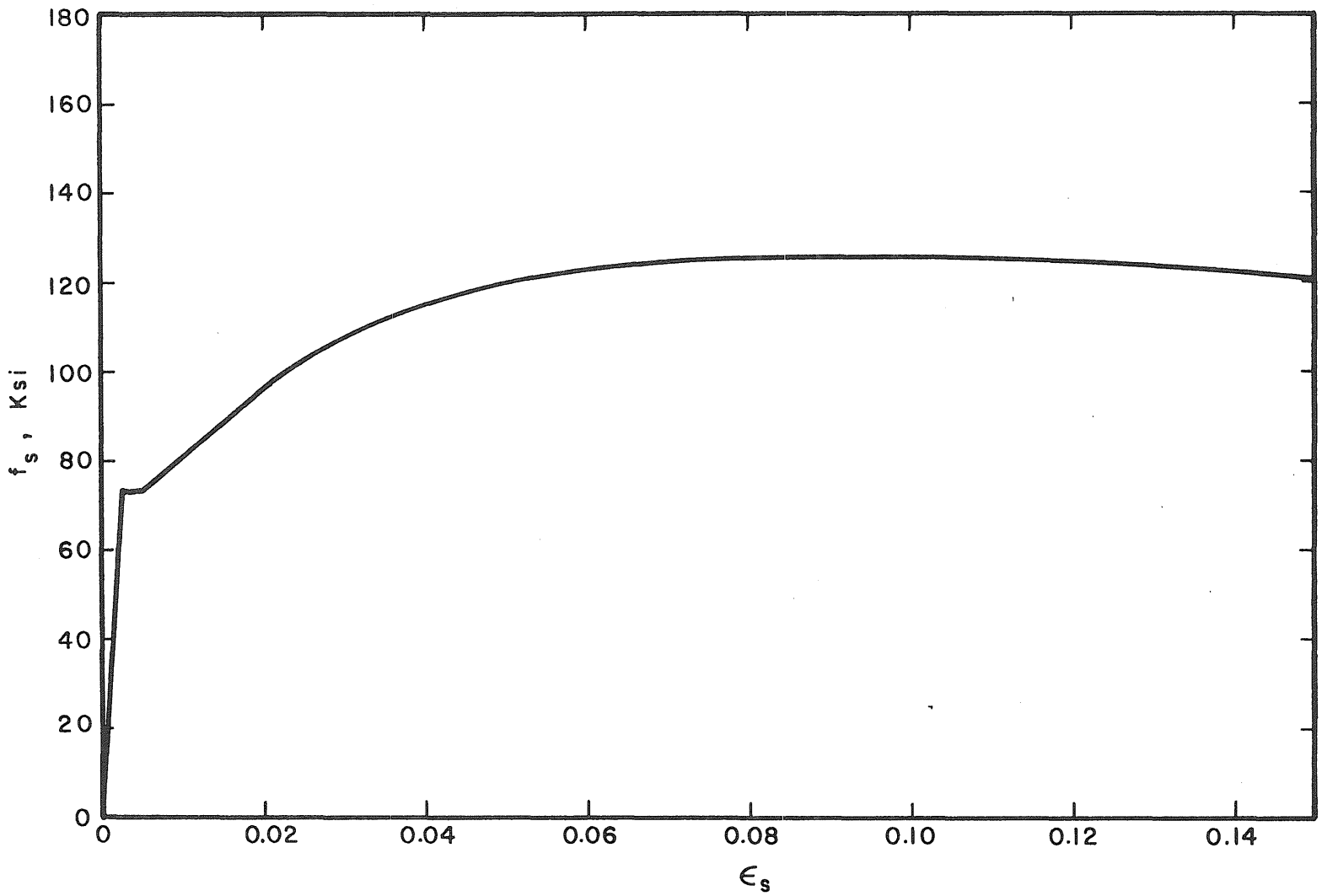

Fig. 3.7 Typical Stress-Strain Curve for the Bonded Reinforcing Steel

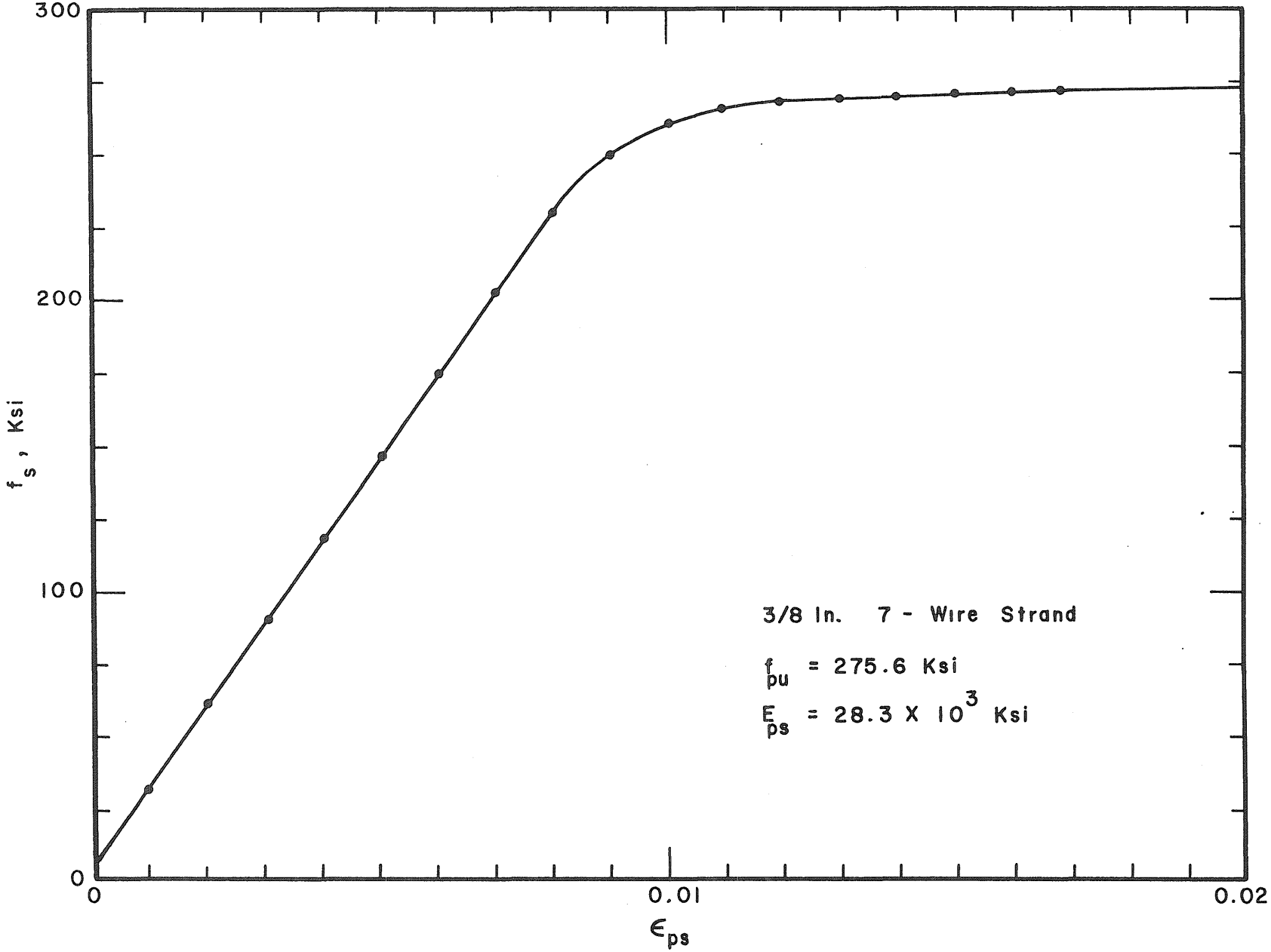

Fig. 3.8 Typical Stress-Strain Curve for the Prestressing Tendon

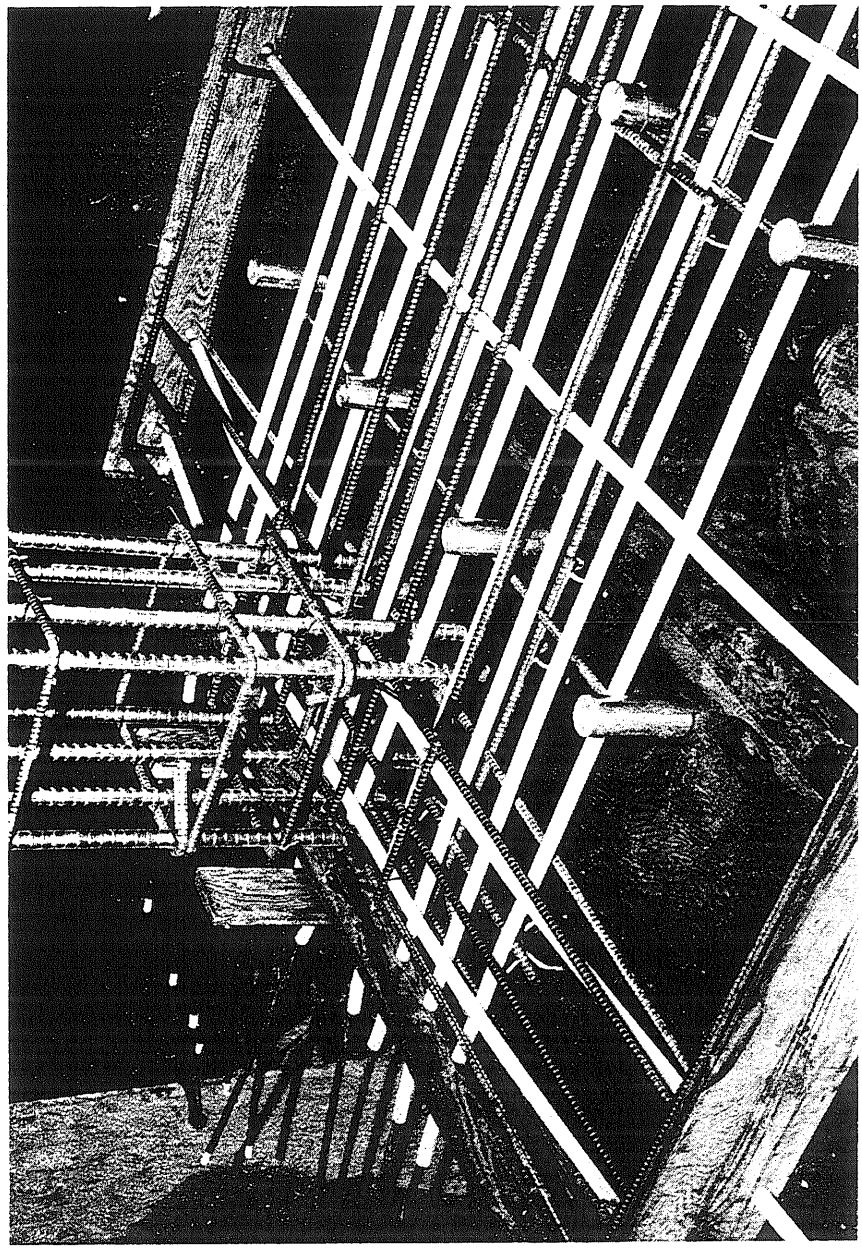

Fig. 3.9 Arrangement of Reinforcement of Specimens S1 and S2

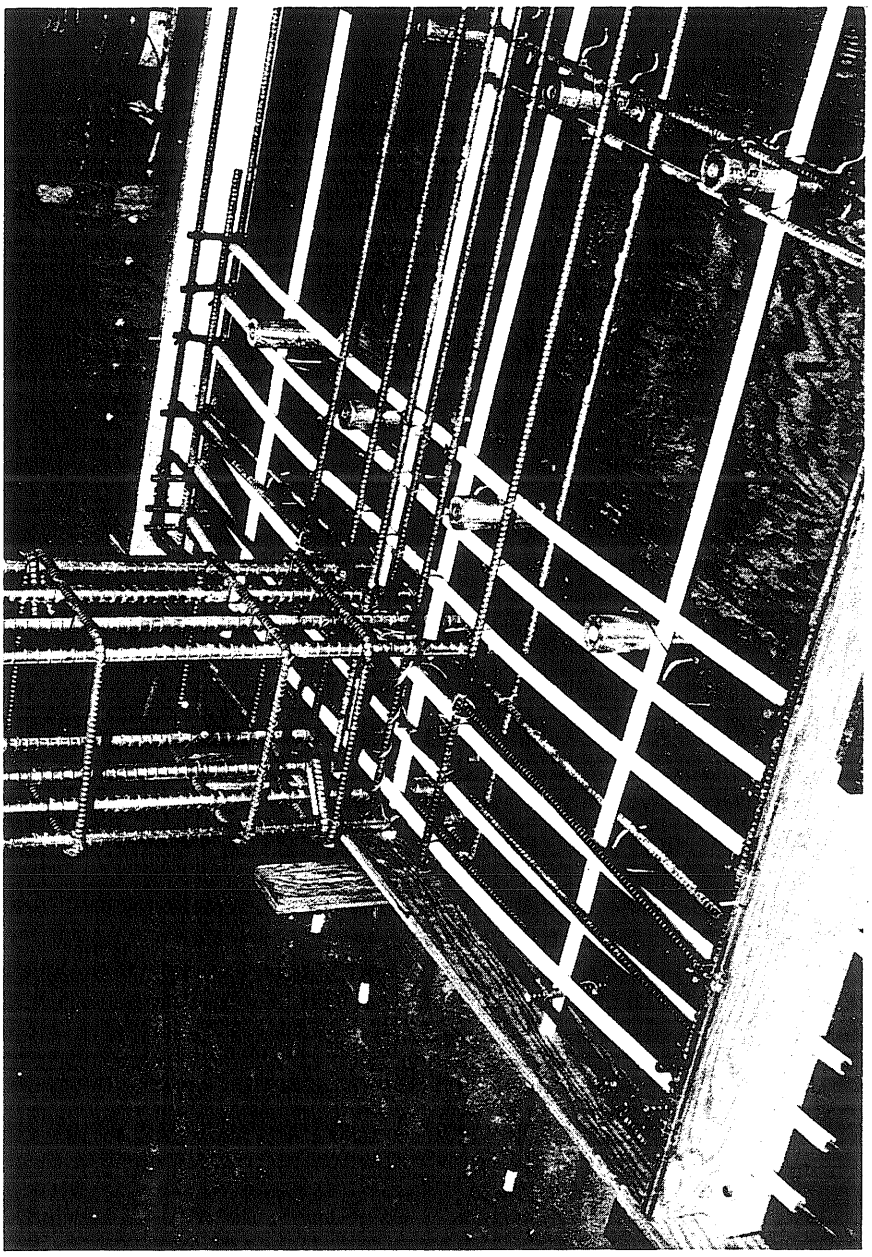

Fig. 3.10 Arrangement of Reinforcement of Specimens S3 and S4

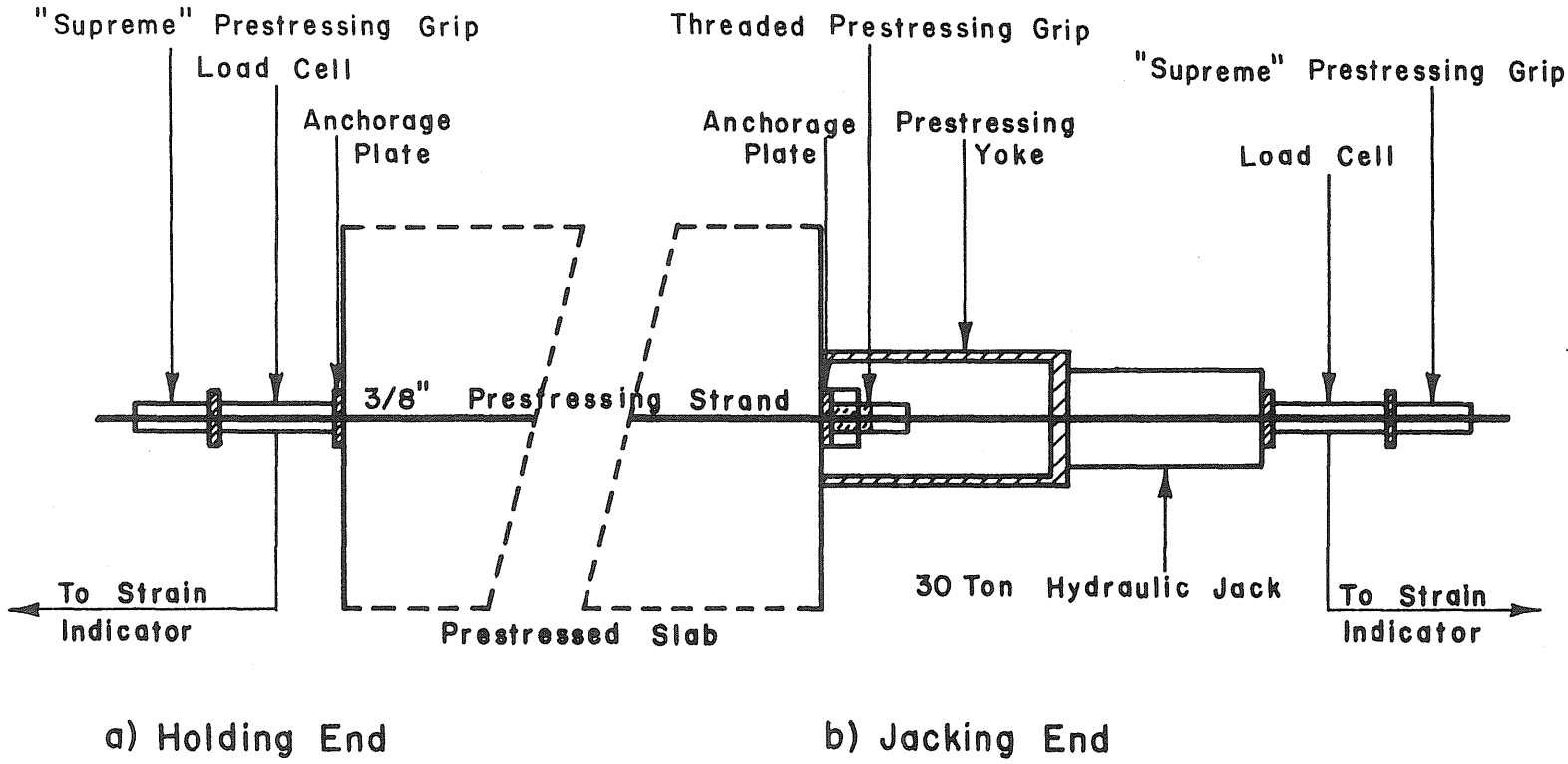

Fig. 3.11 Prestressing Setup

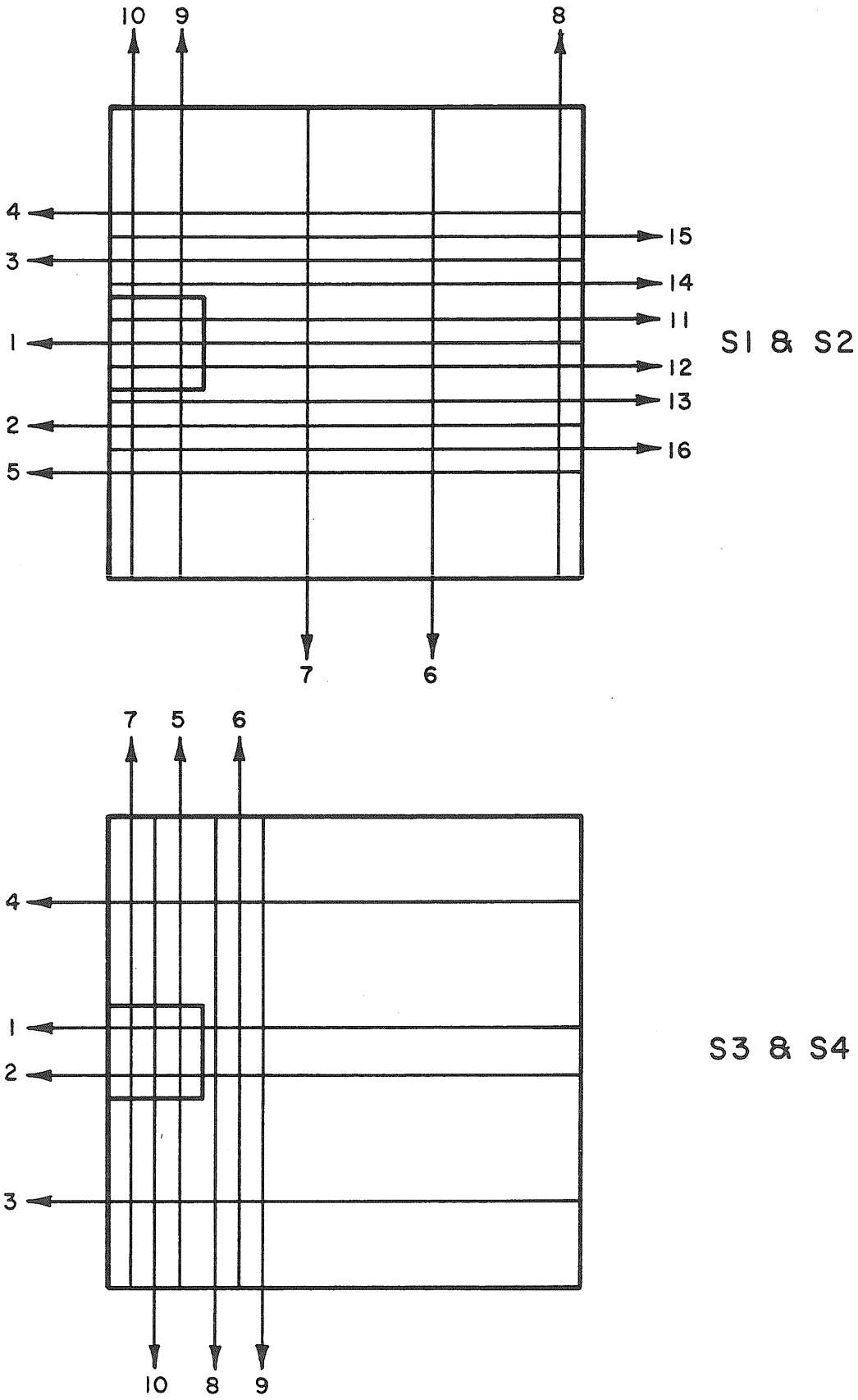

Fig. 3.12 Stressing Schedule

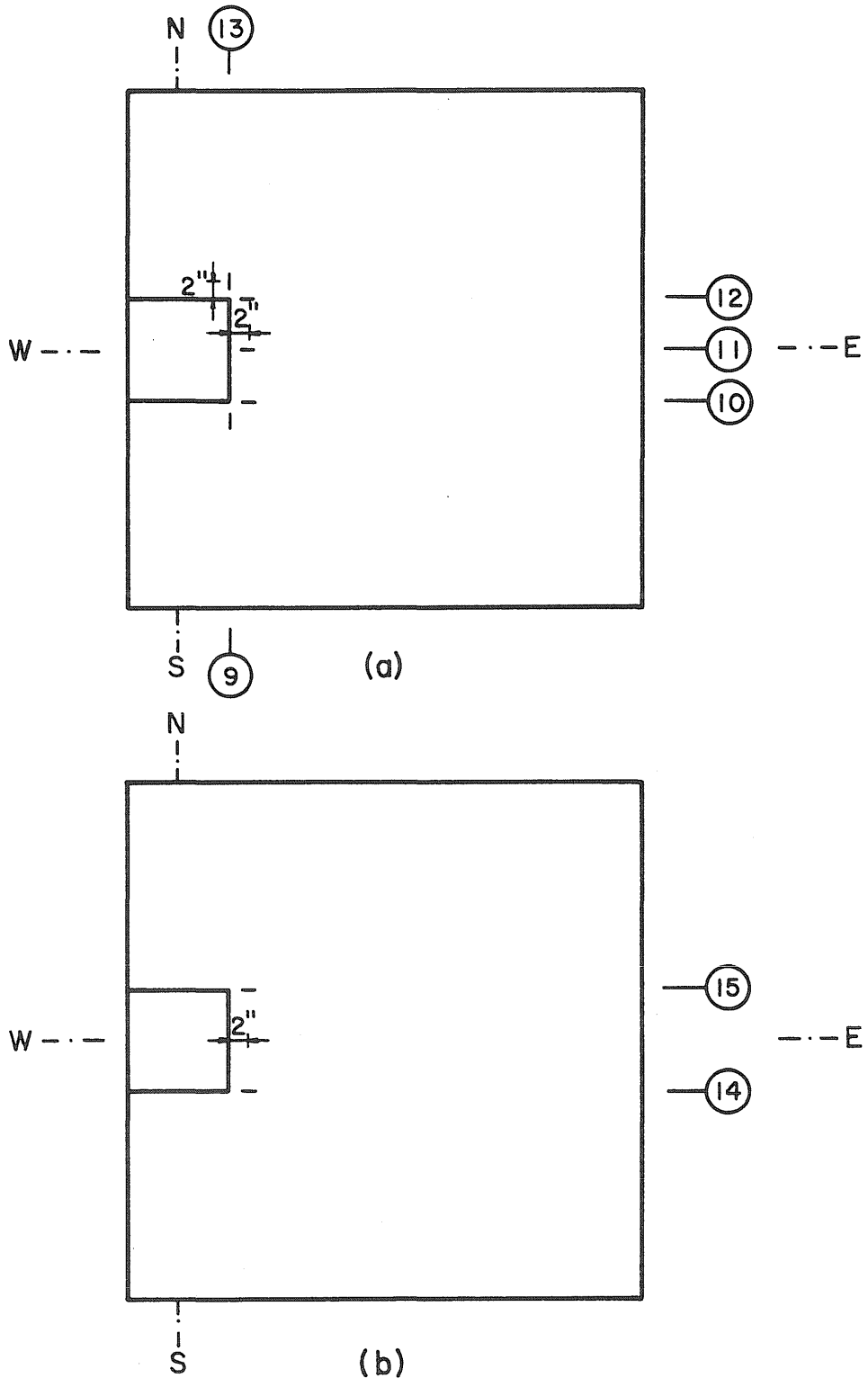

Fig. 3.13 Location of Strain Gages on the Concrete Surfaces: (a) Bottom Surface; (b) Top Surface

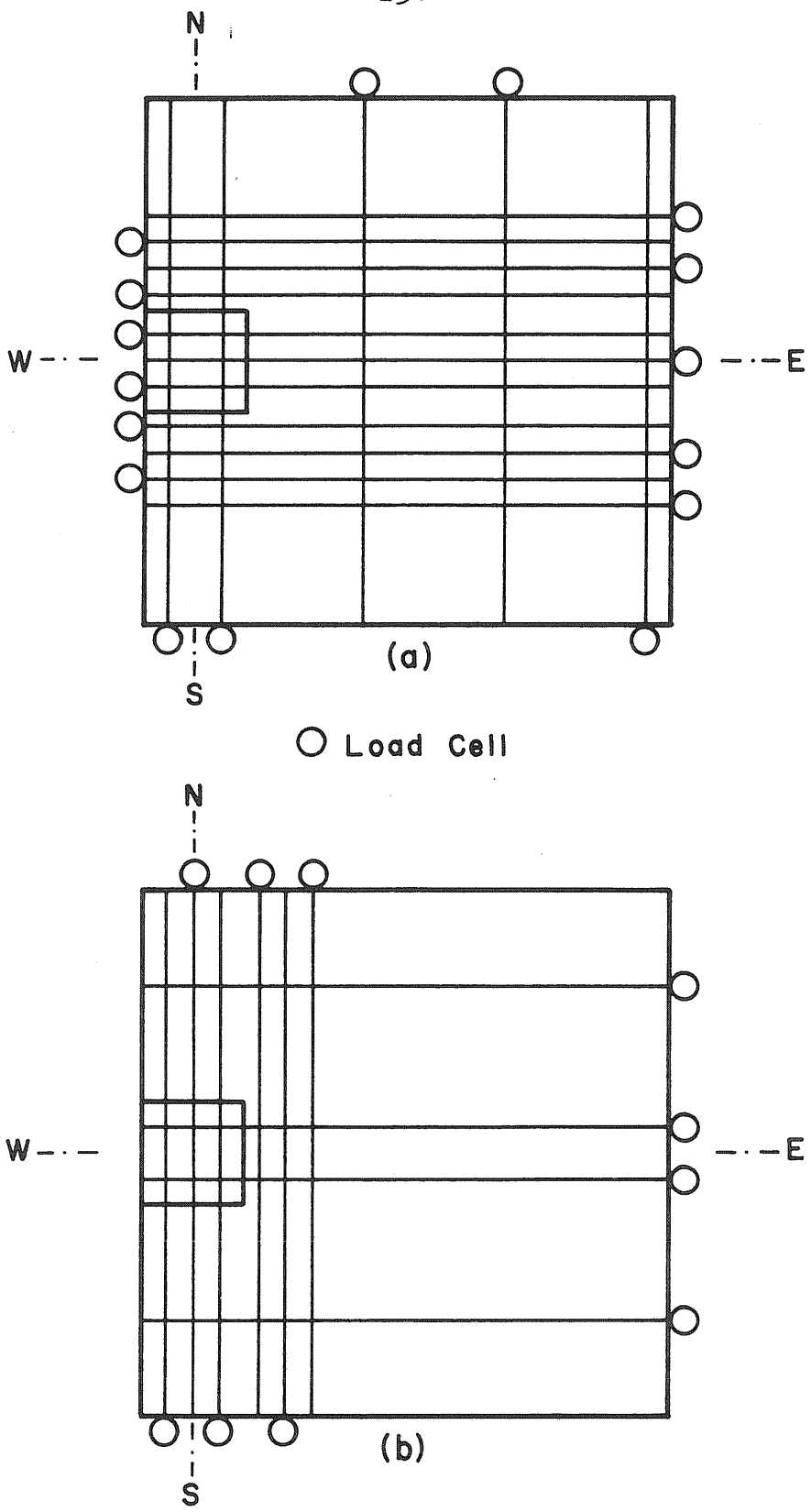

Fig. 3.14 Location of Load Cells on Tendons: (a) S1 and S2; (b) S3 and S4

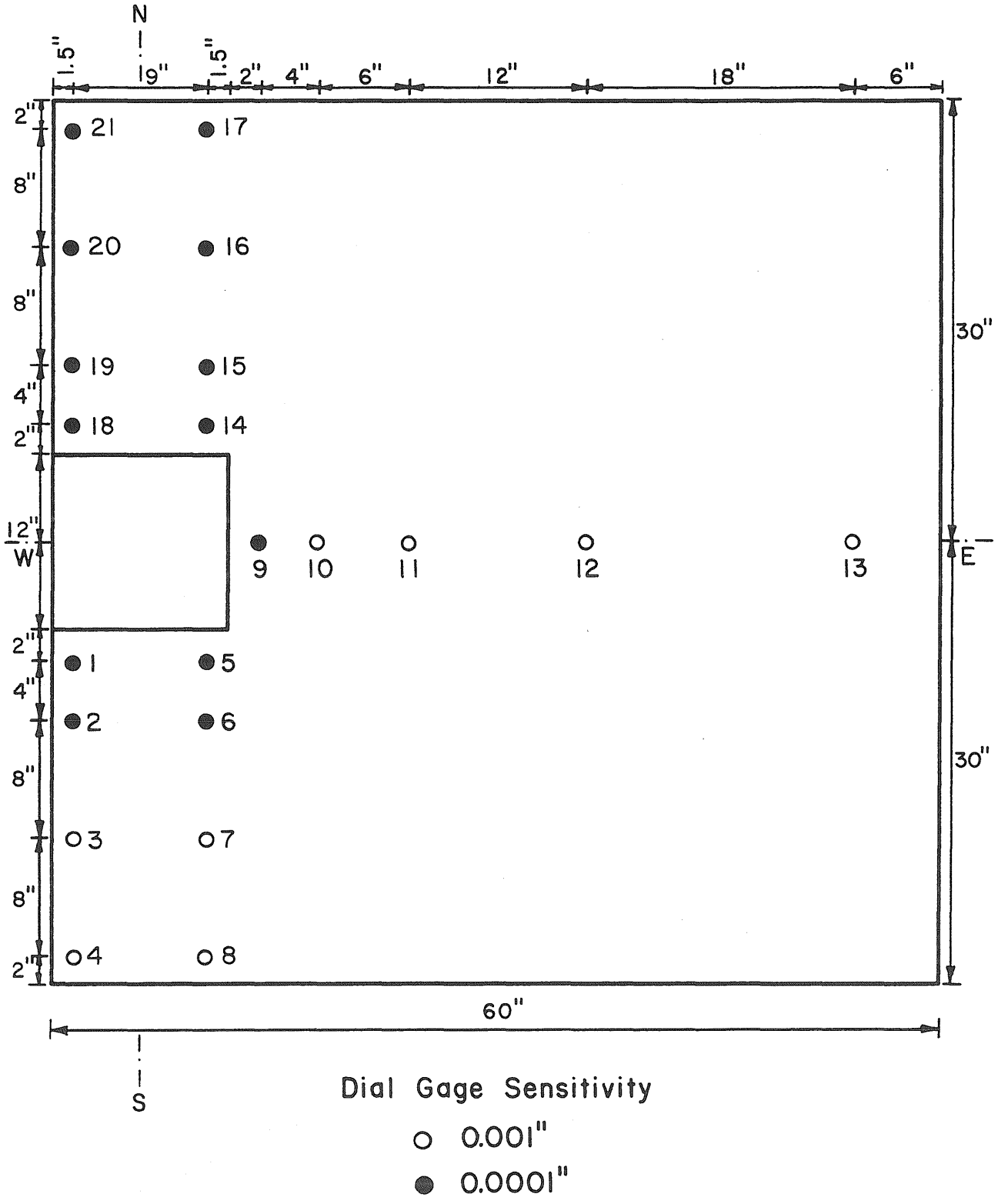

Fig. 3.15 Location of Mechanical Dial Gages

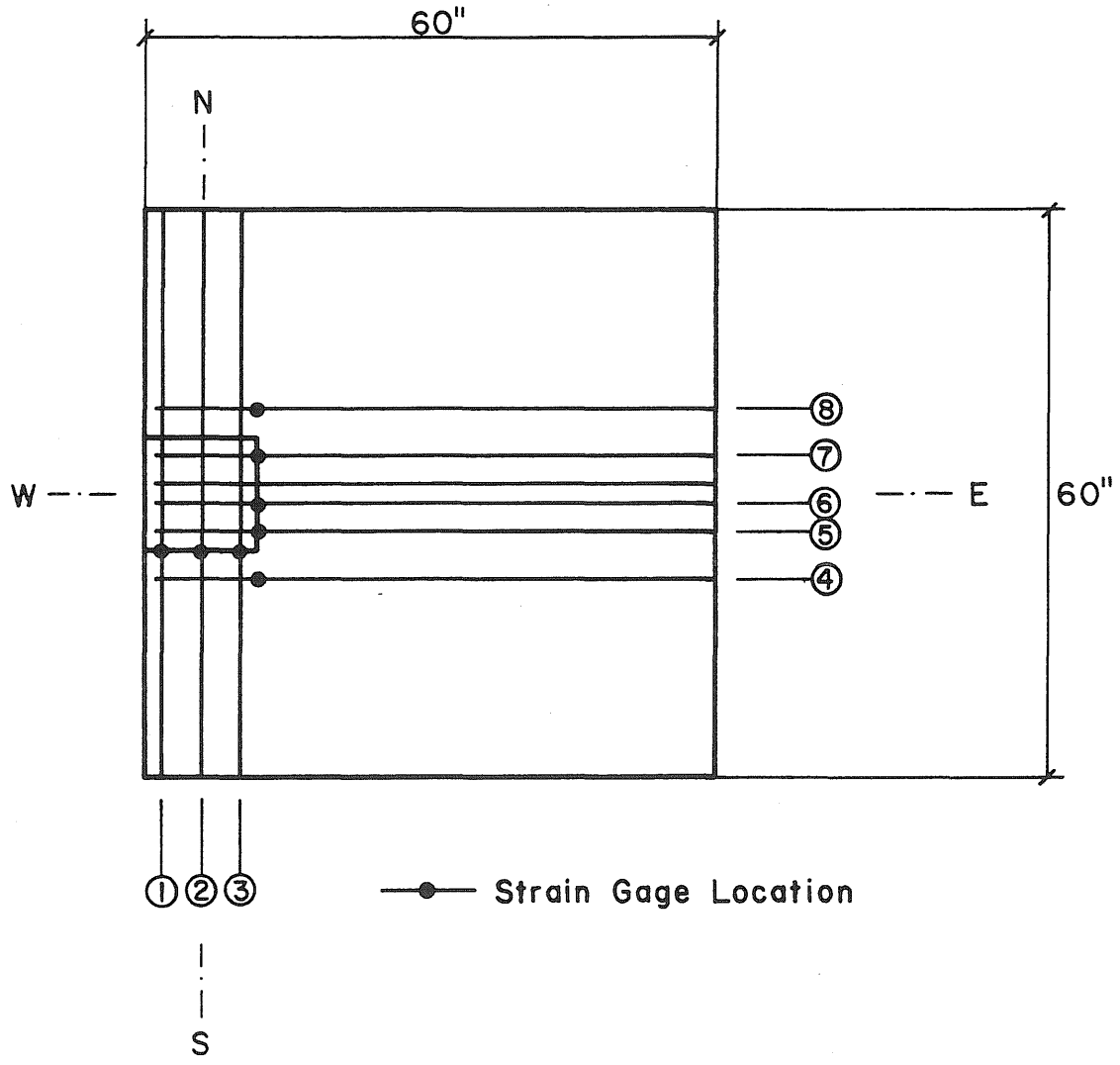

Fig. 3.16 Location of Strain Gages on the Bonded Reinforcement

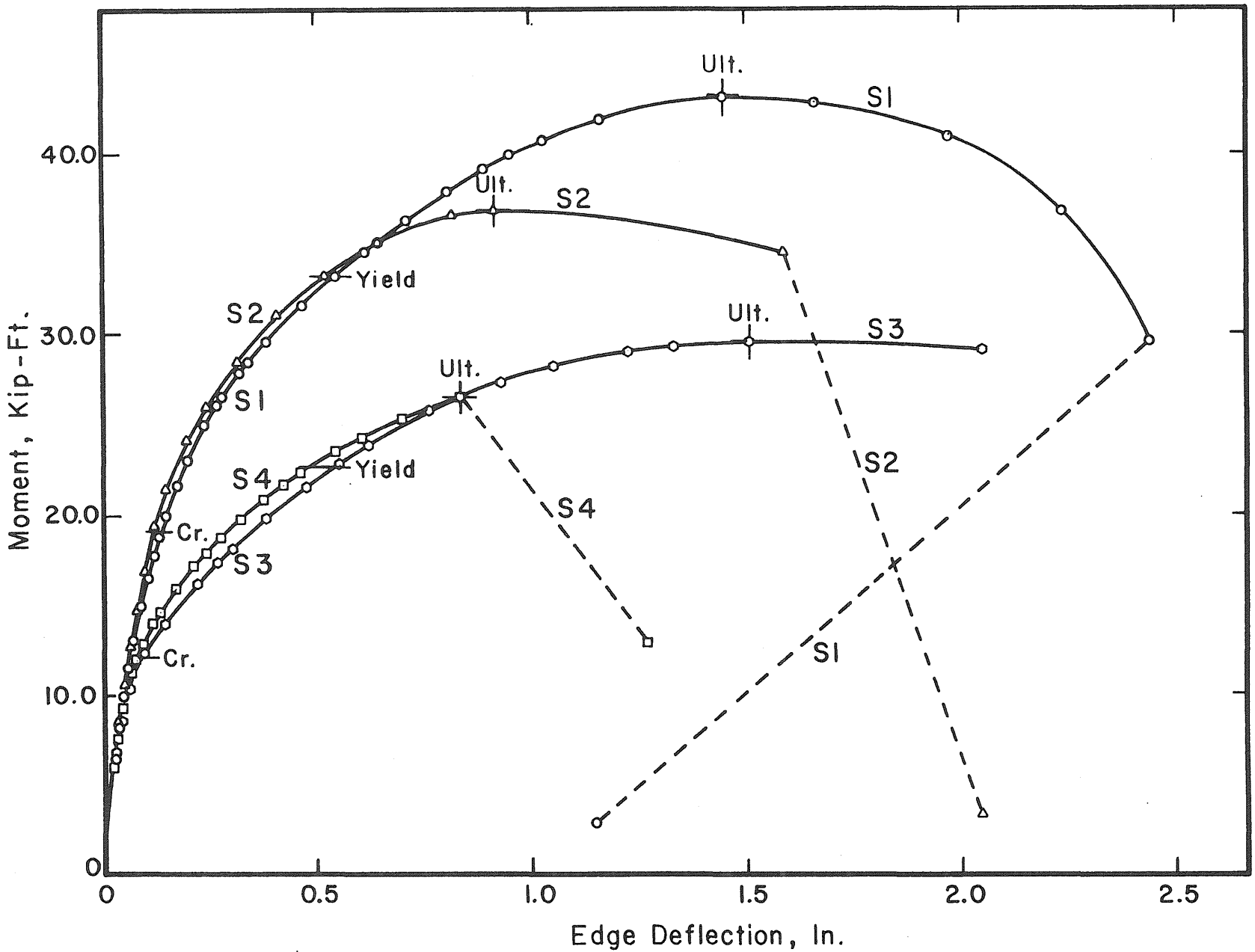

Fig. 4.1 Moment-Deflection Relationships for All Specimens

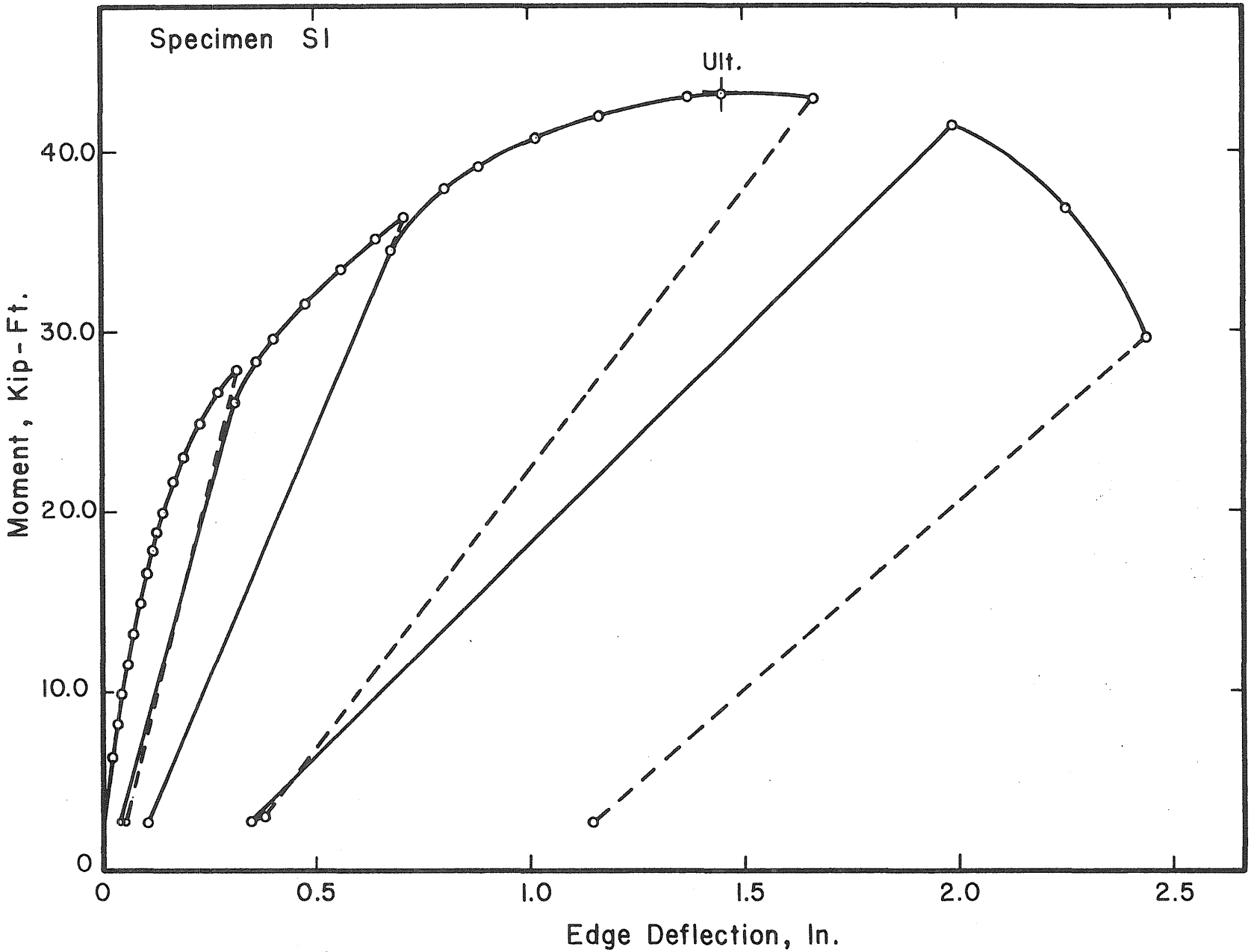

Fig. 4.2 Moment-Deflection Relationship for Specimen S1

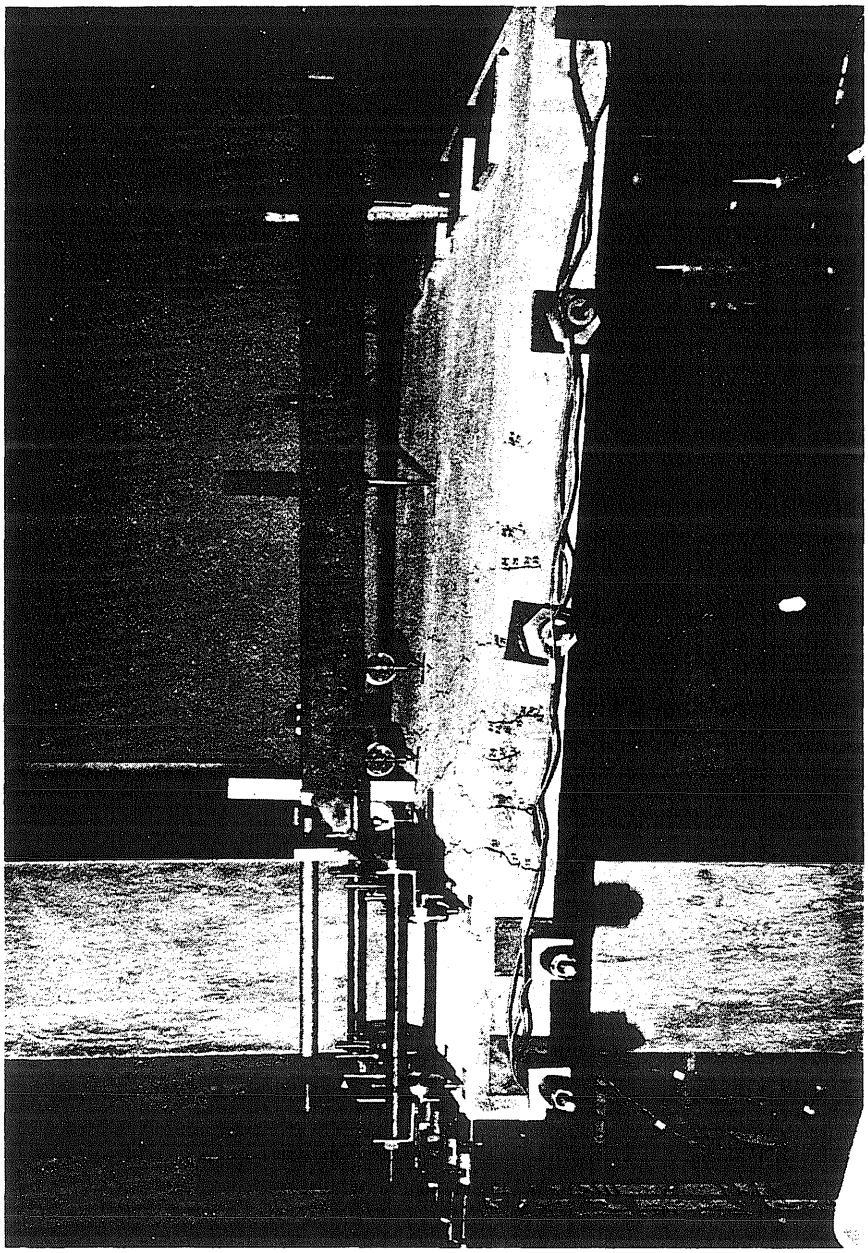

Fig. 4.3 Specimen S1 at Completion of Testing

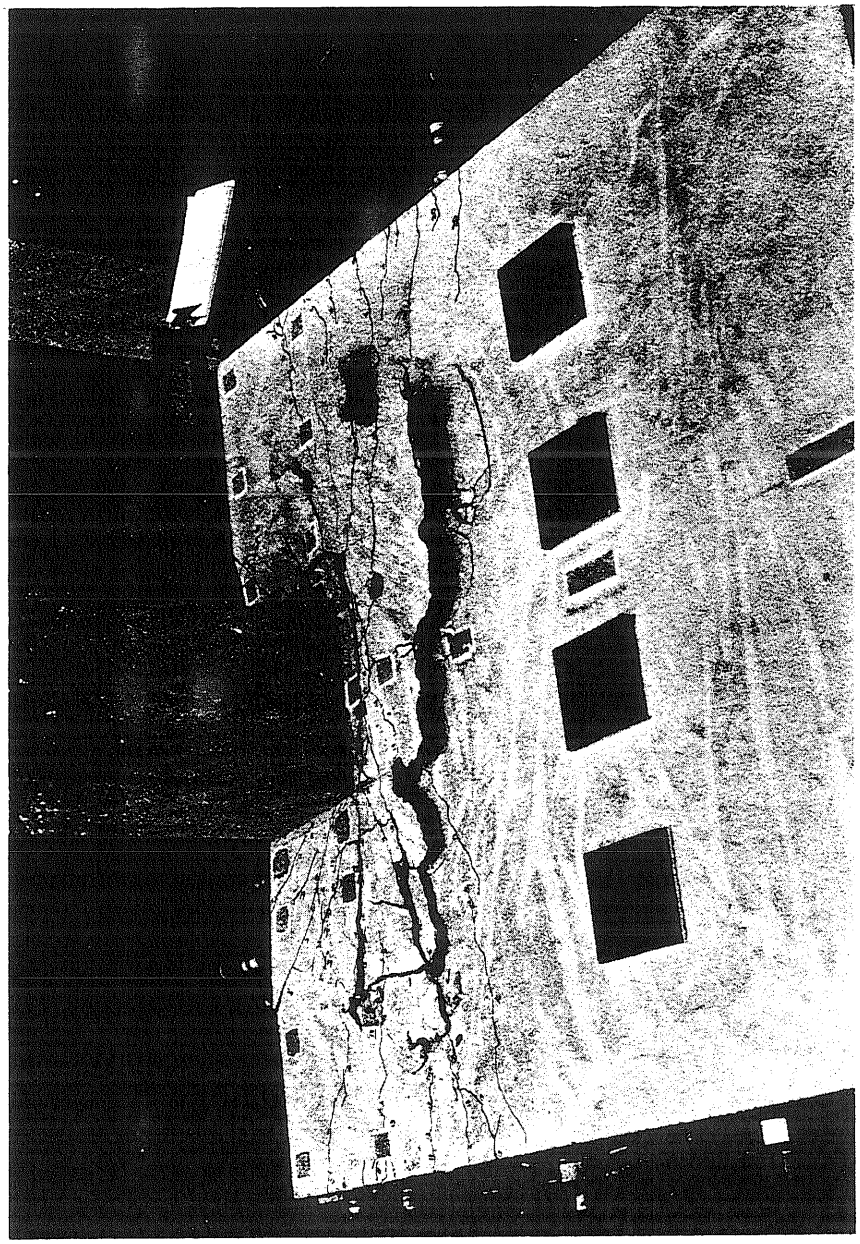

Fig. 4.4 Specimen S2 at Completion of Testing

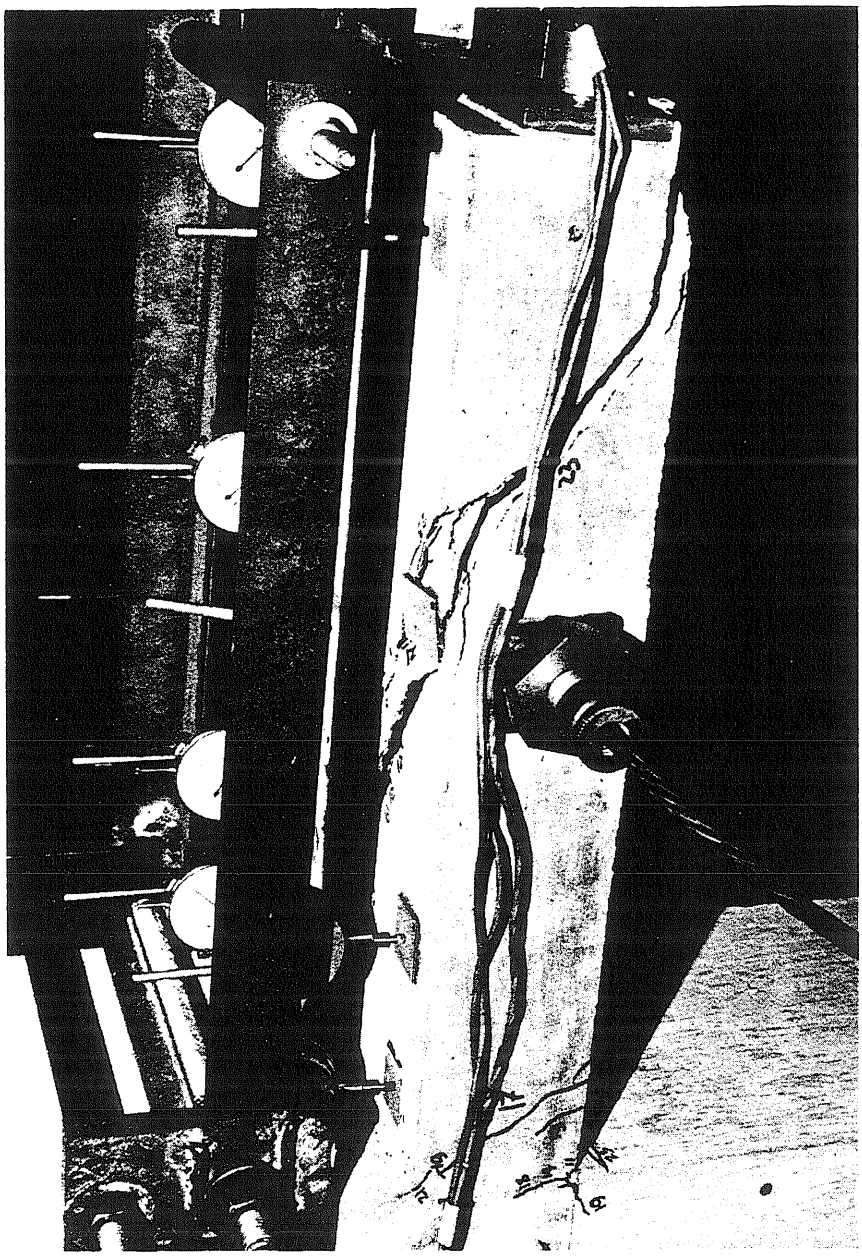

Fig. 4.5 Specimen S3 at Completion of Testing

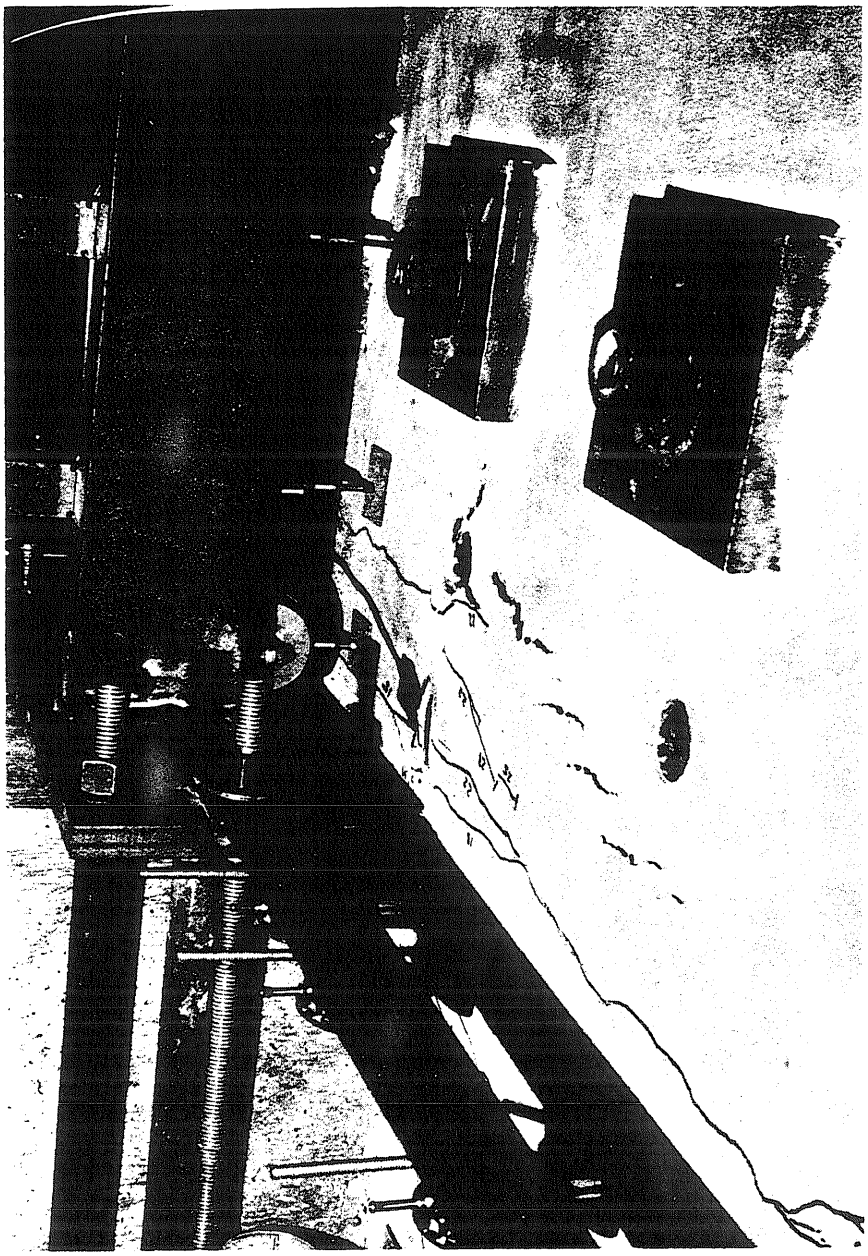

Fig. 4.6 Specimen S4 at Completion of Testing

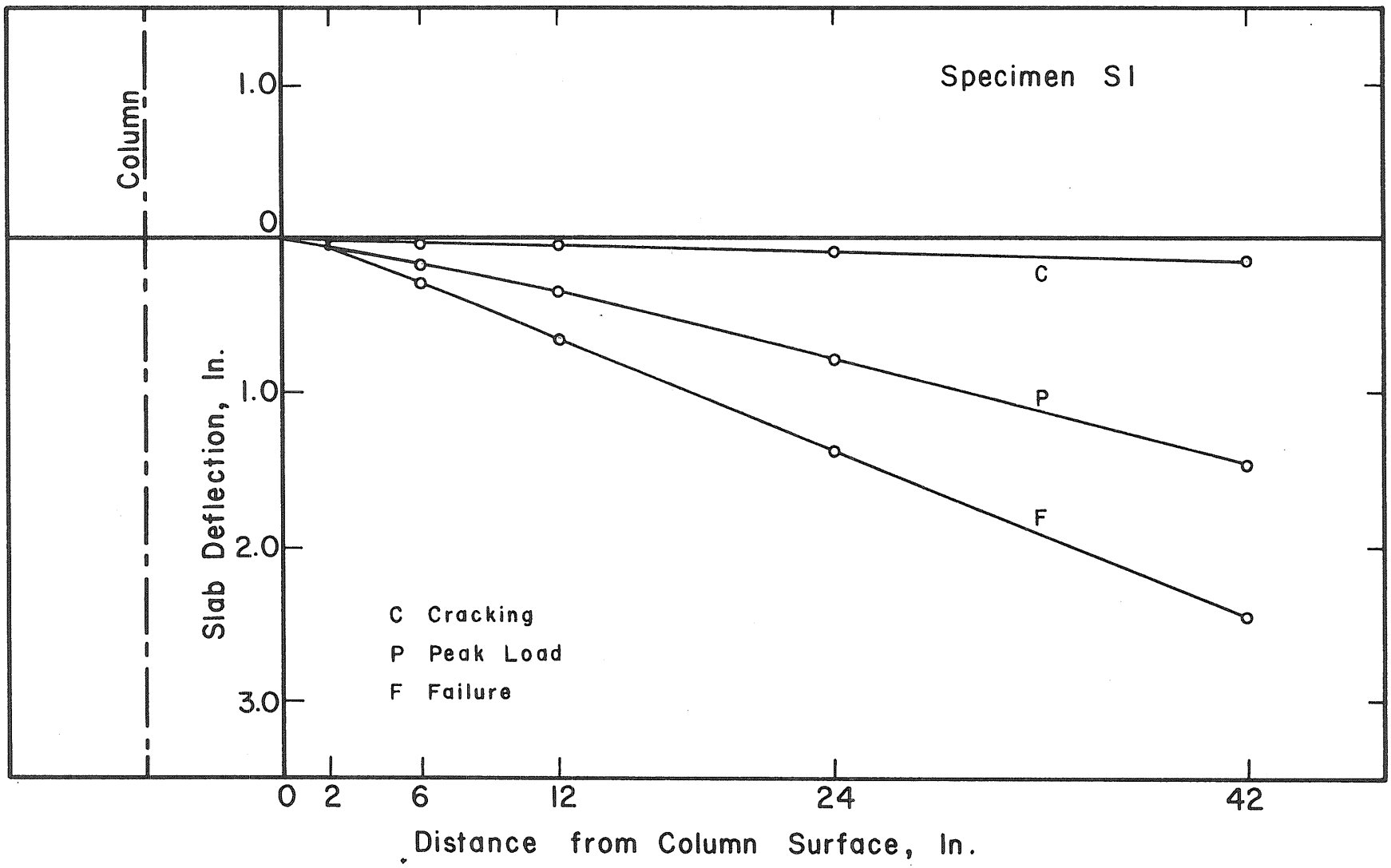

Fig. 4.7 Deflection Profiles of Specimen S1

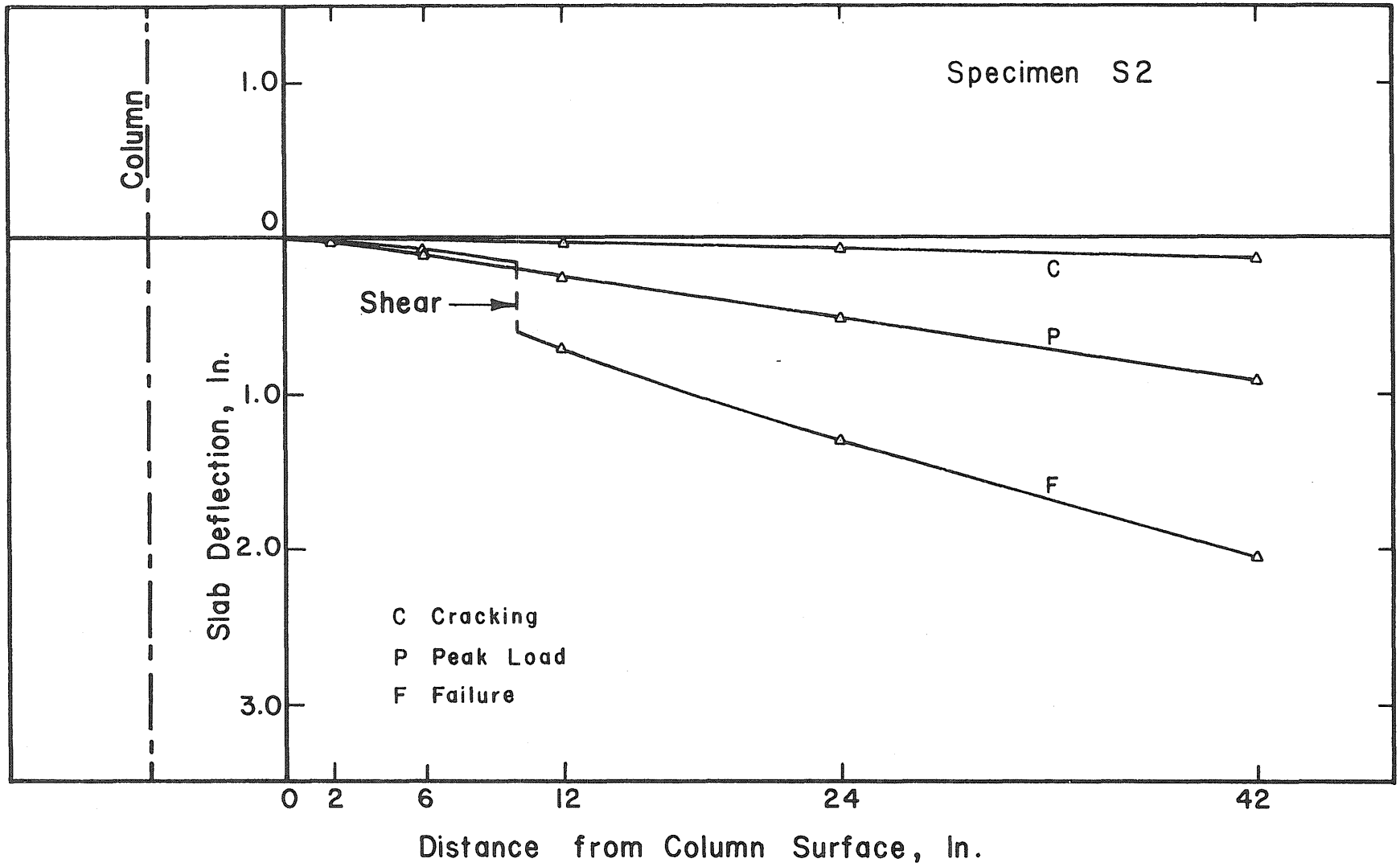

Fig. 4.8 Deflection Profiles of Specimen S2

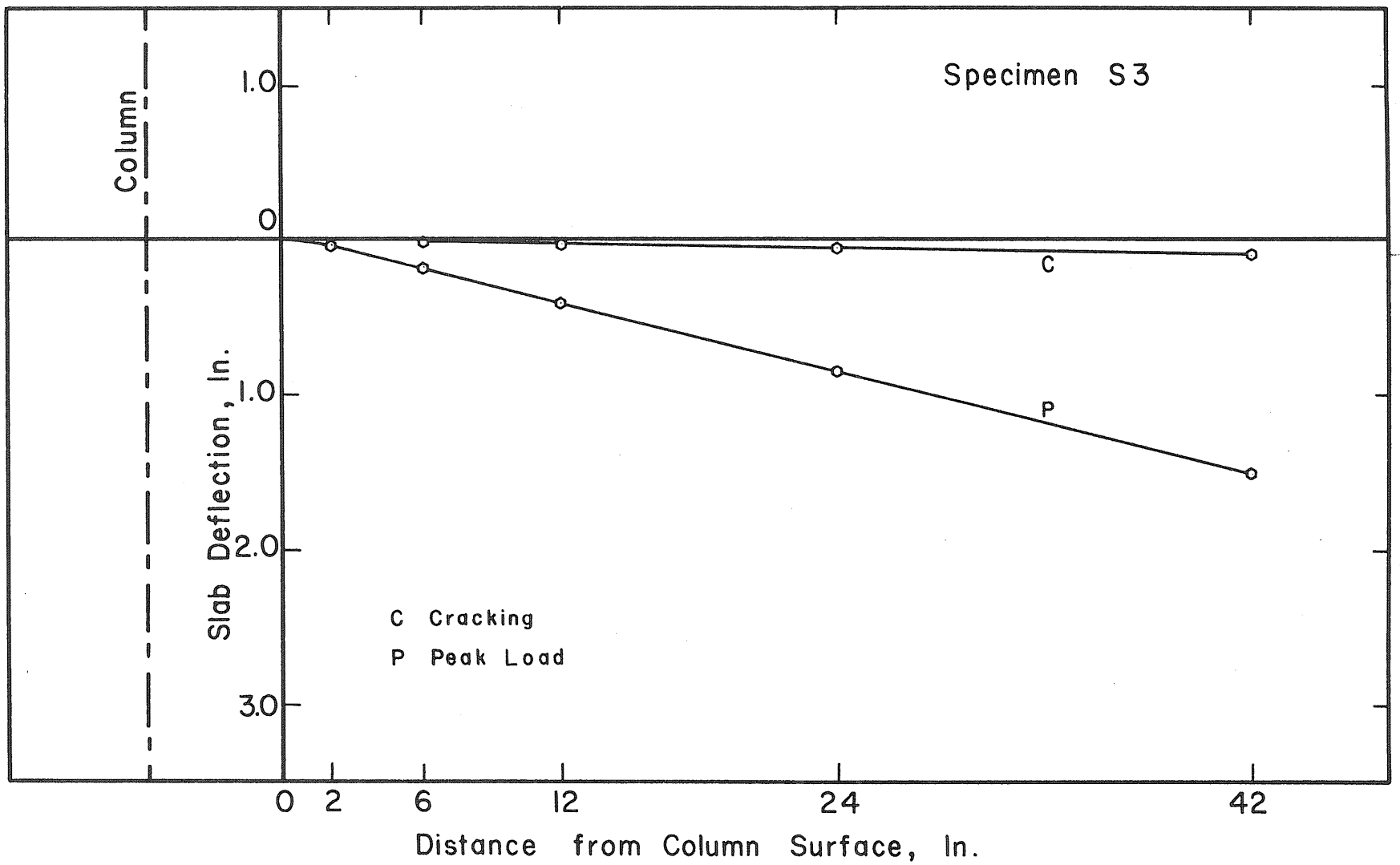

Fig. 4.9 Deflection Profiles of Specimen S3

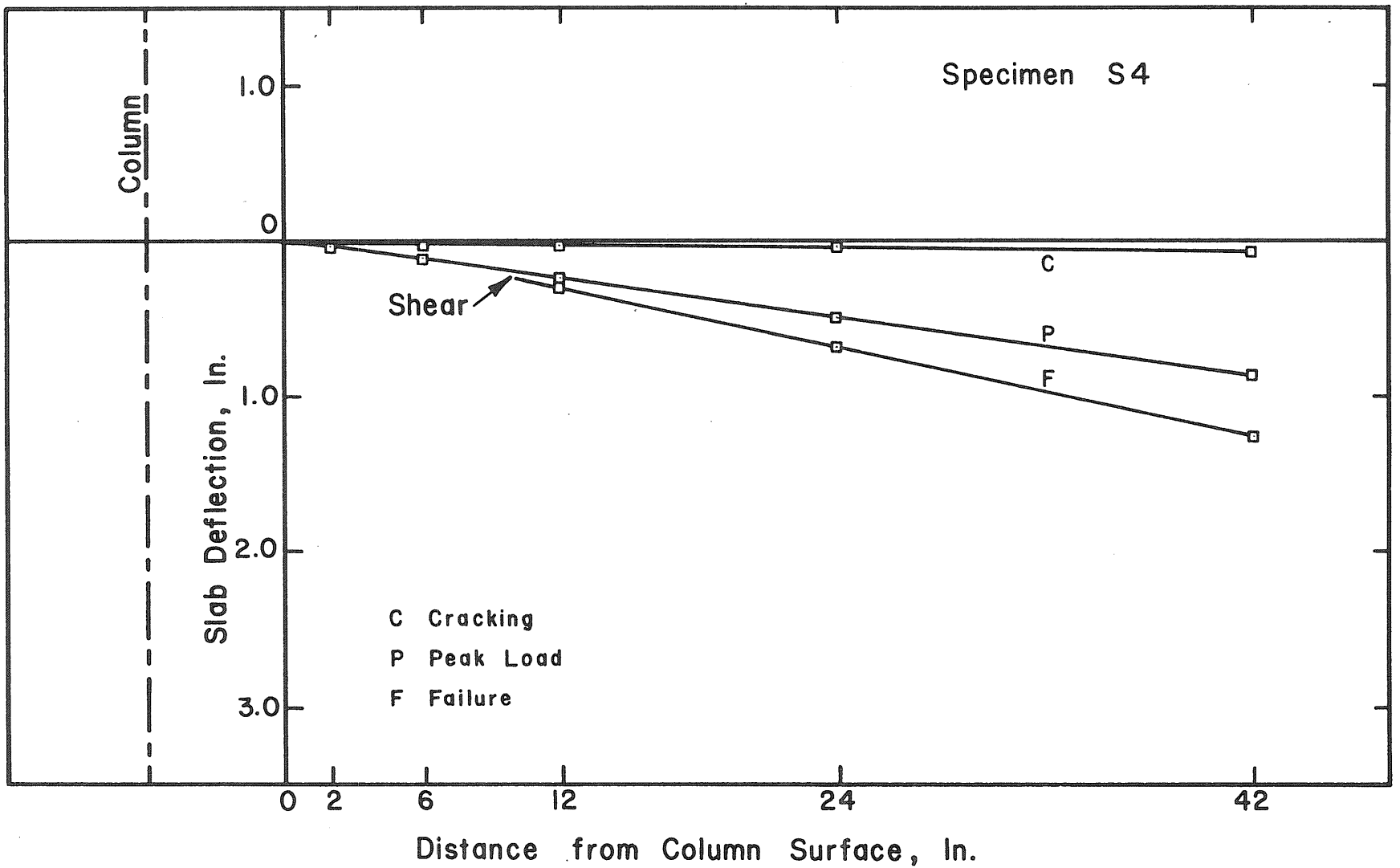

Fig. 4.10 Deflection Profiles of Specimen S4

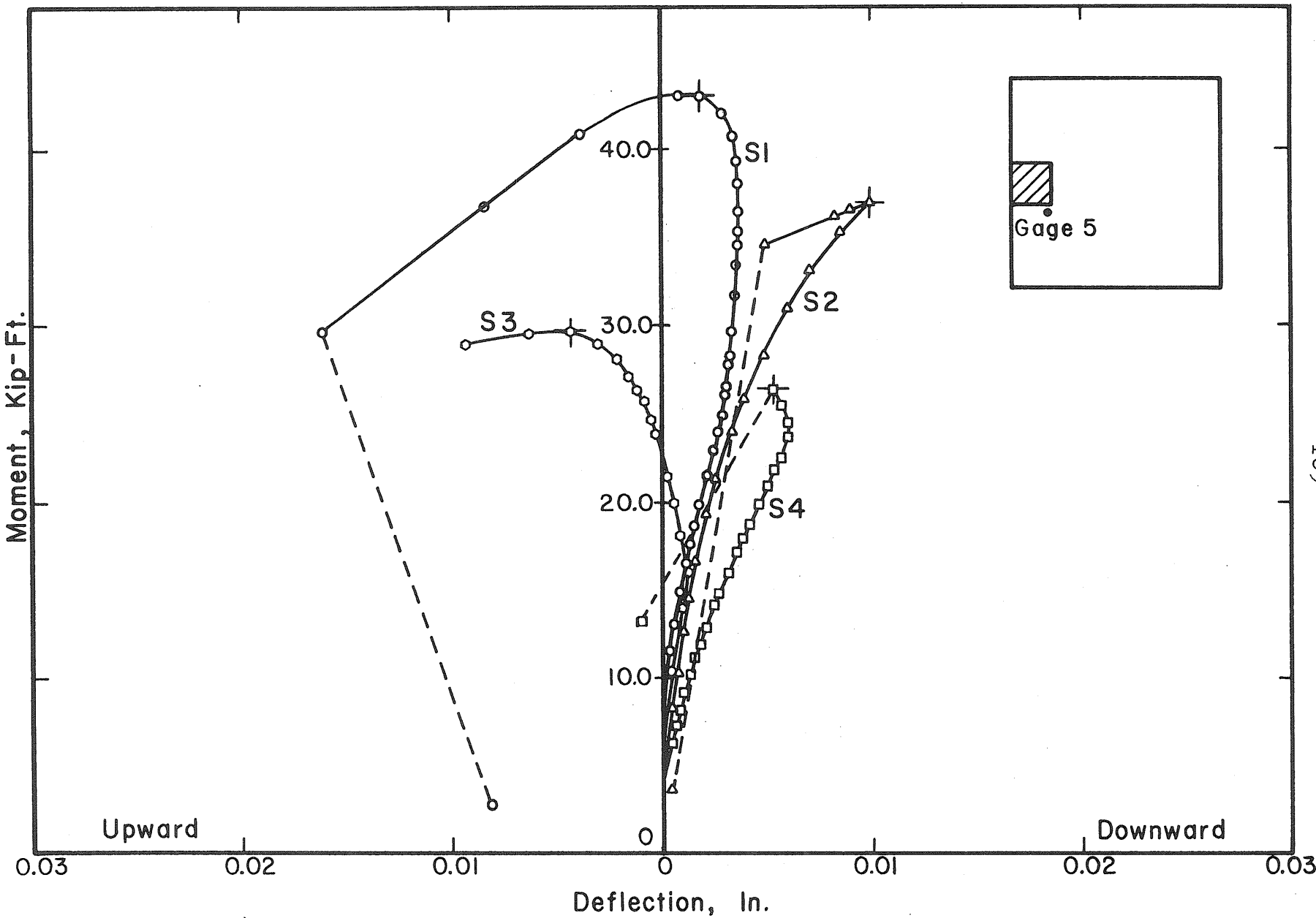

Fig. 4.11 Moment vs. Deflection at Dial Gage No. 5 for All Specimens

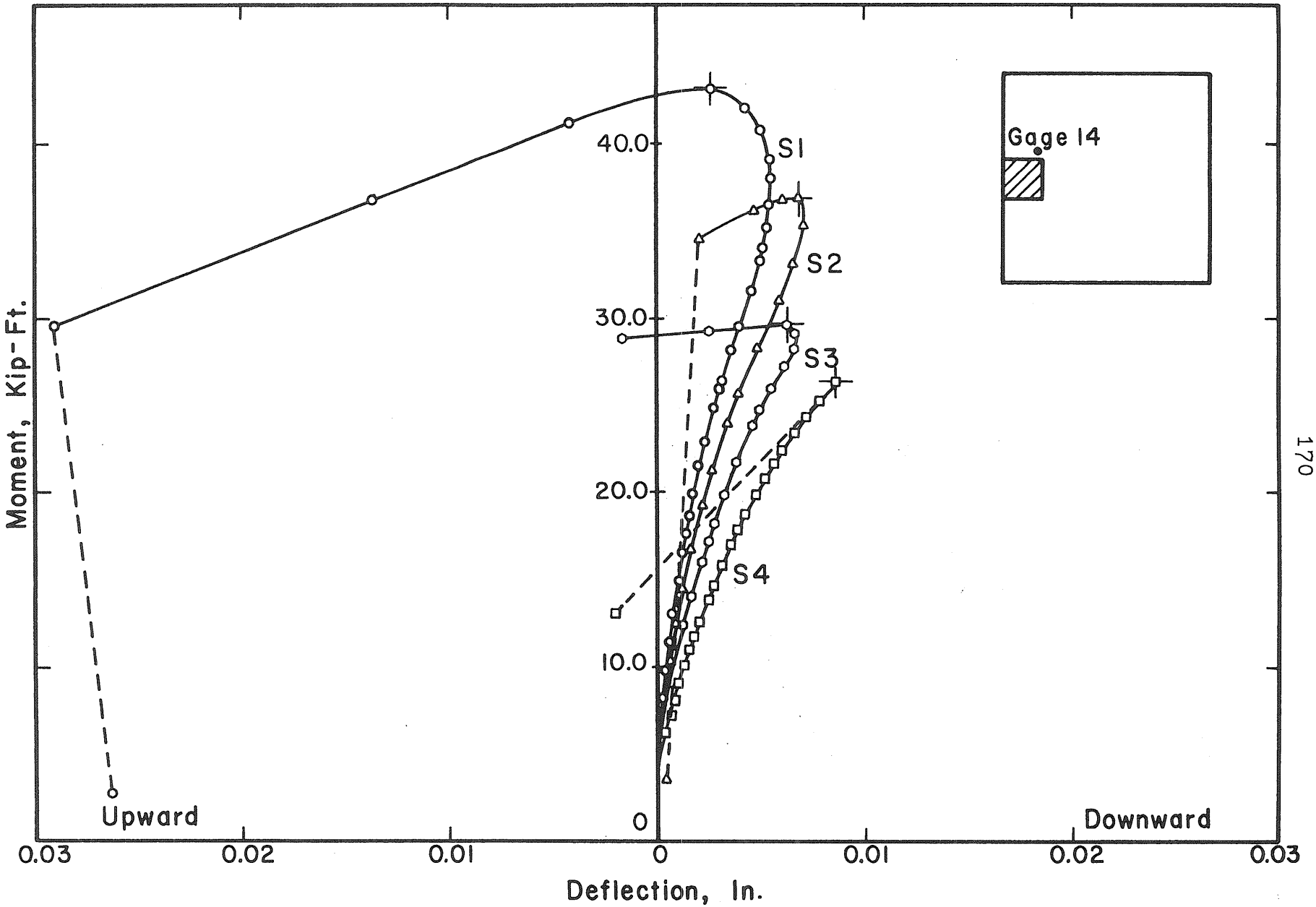

Fig. 4.12 Moment vs. Deflection at Dial Gage No. 14 for All Specimens

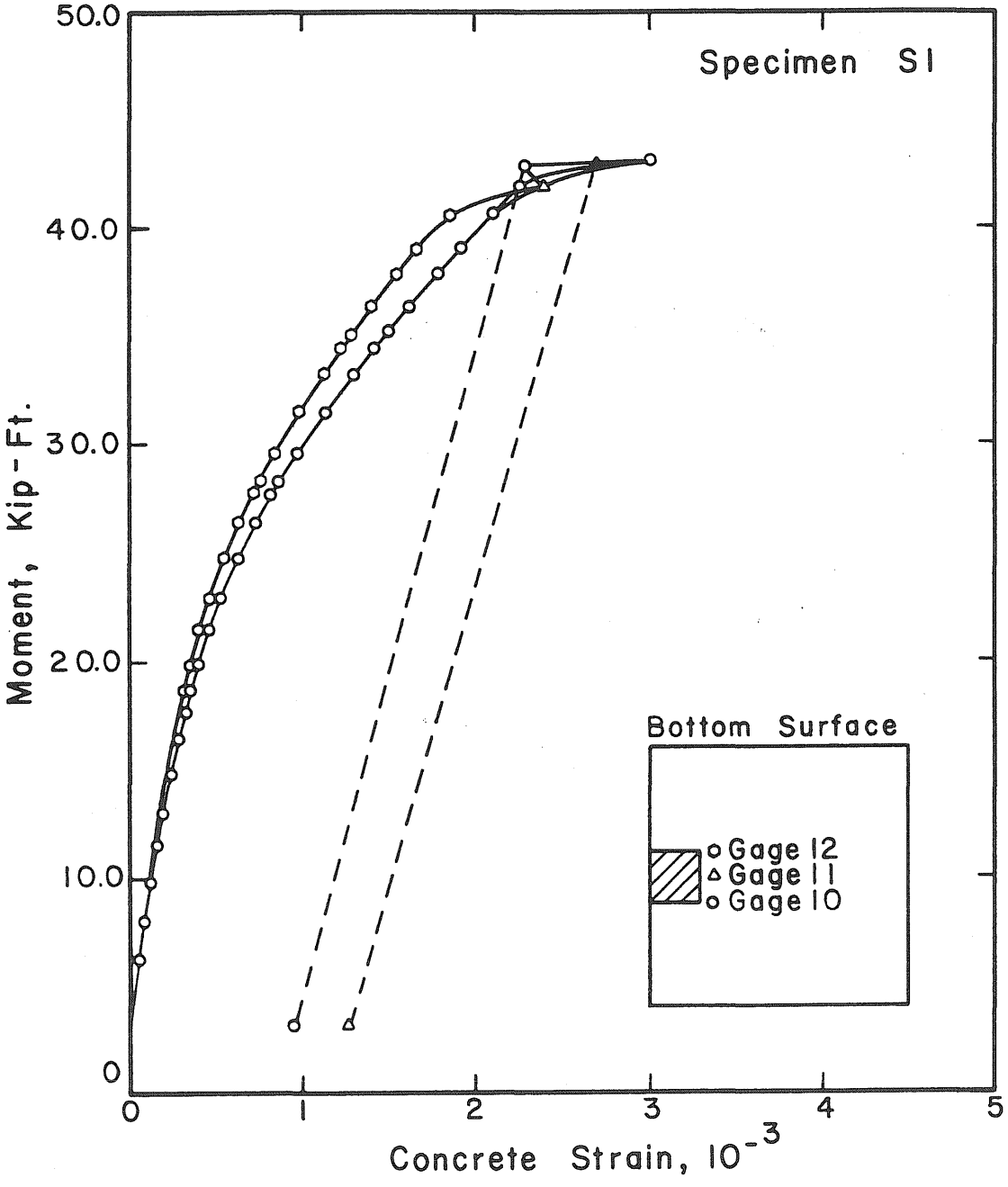

Fig. 4.13 Moment vs. Concrete Strain at the Bottom Surface of Specimen S1

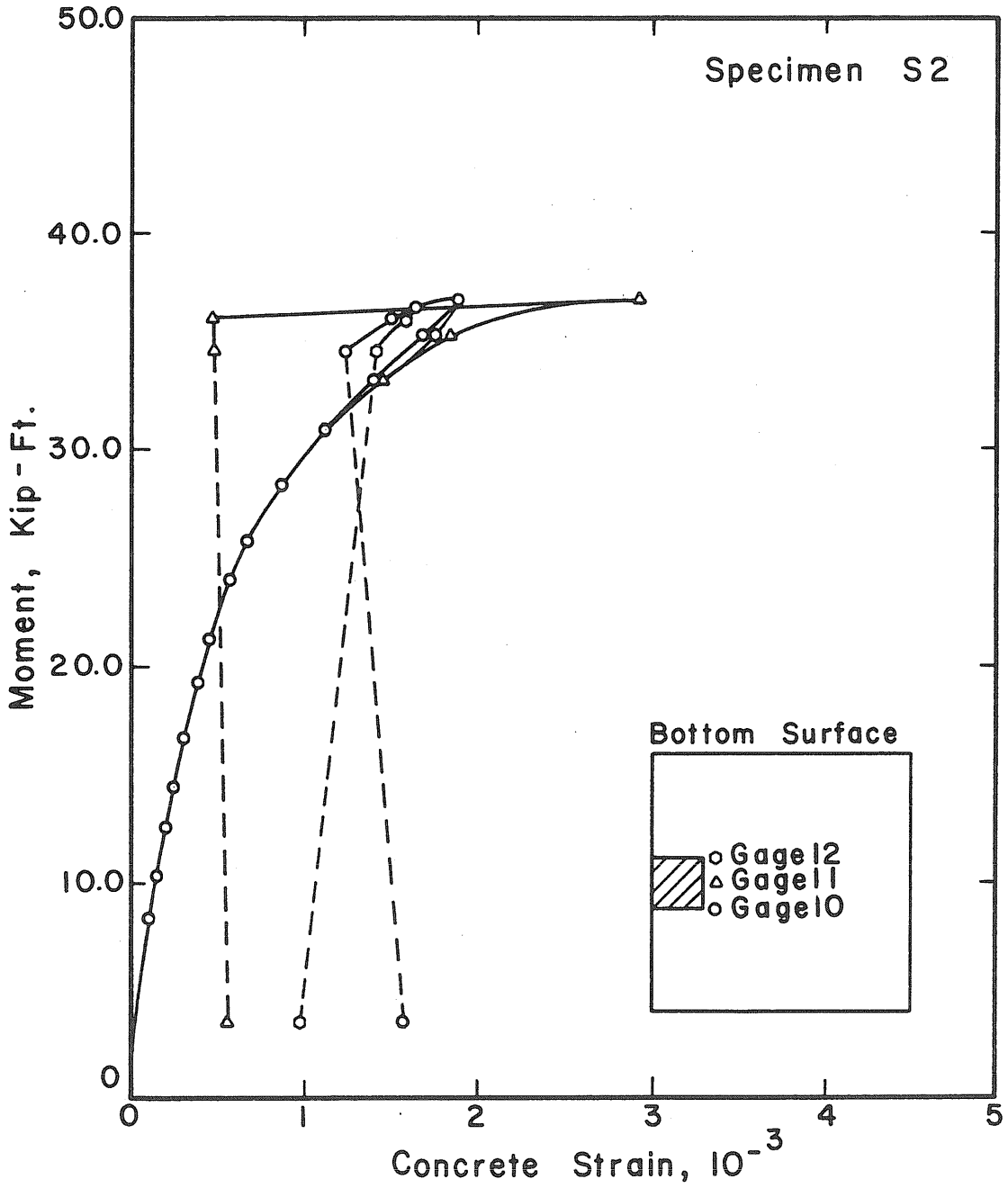

Fig. 4.14 Moment vs. Concrete Strain at the Bottom Surface of Specimen S2

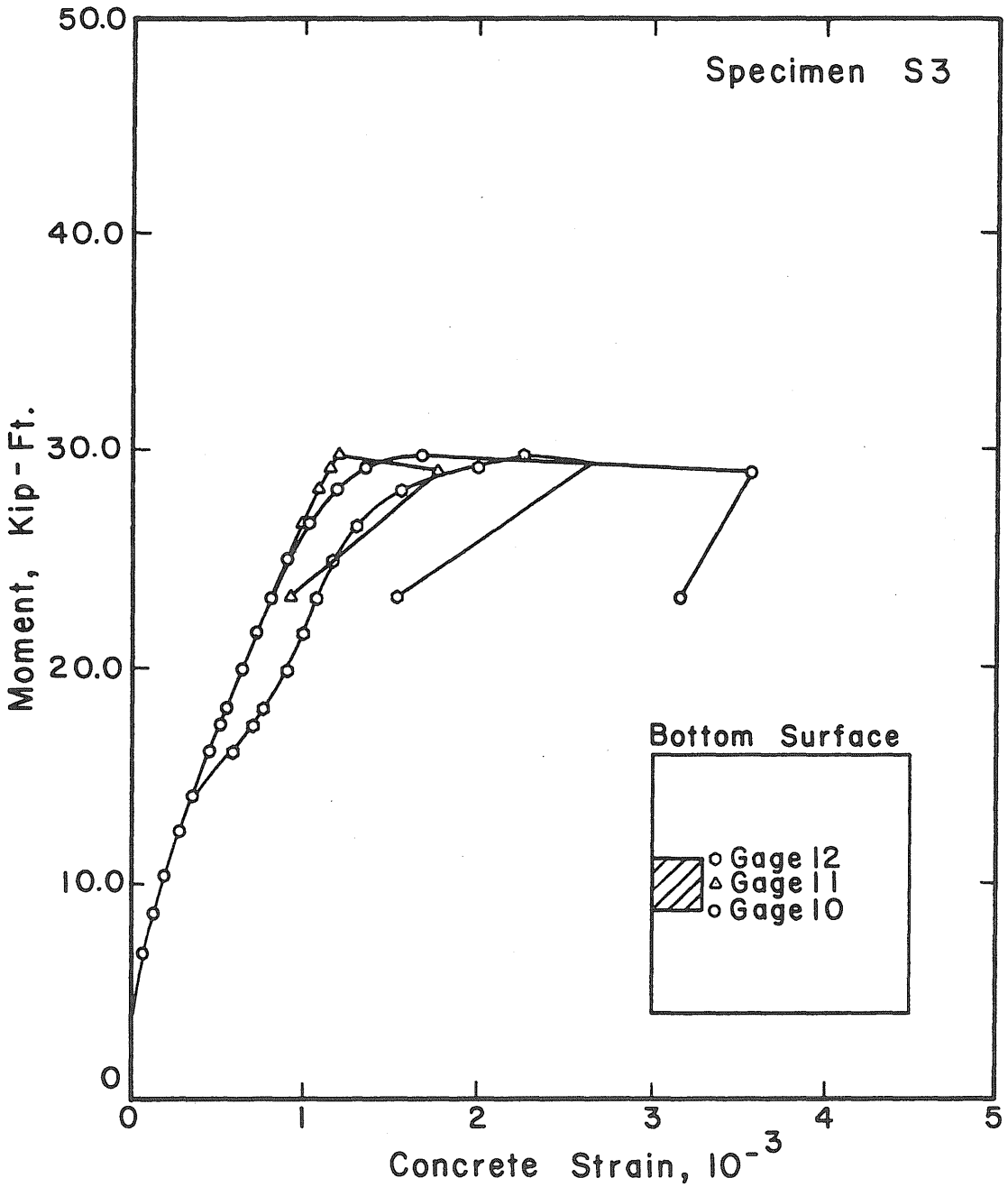

Fig. 4.15 Moment vs. Concrete Strain at the Bottom Surface of Specimen S3

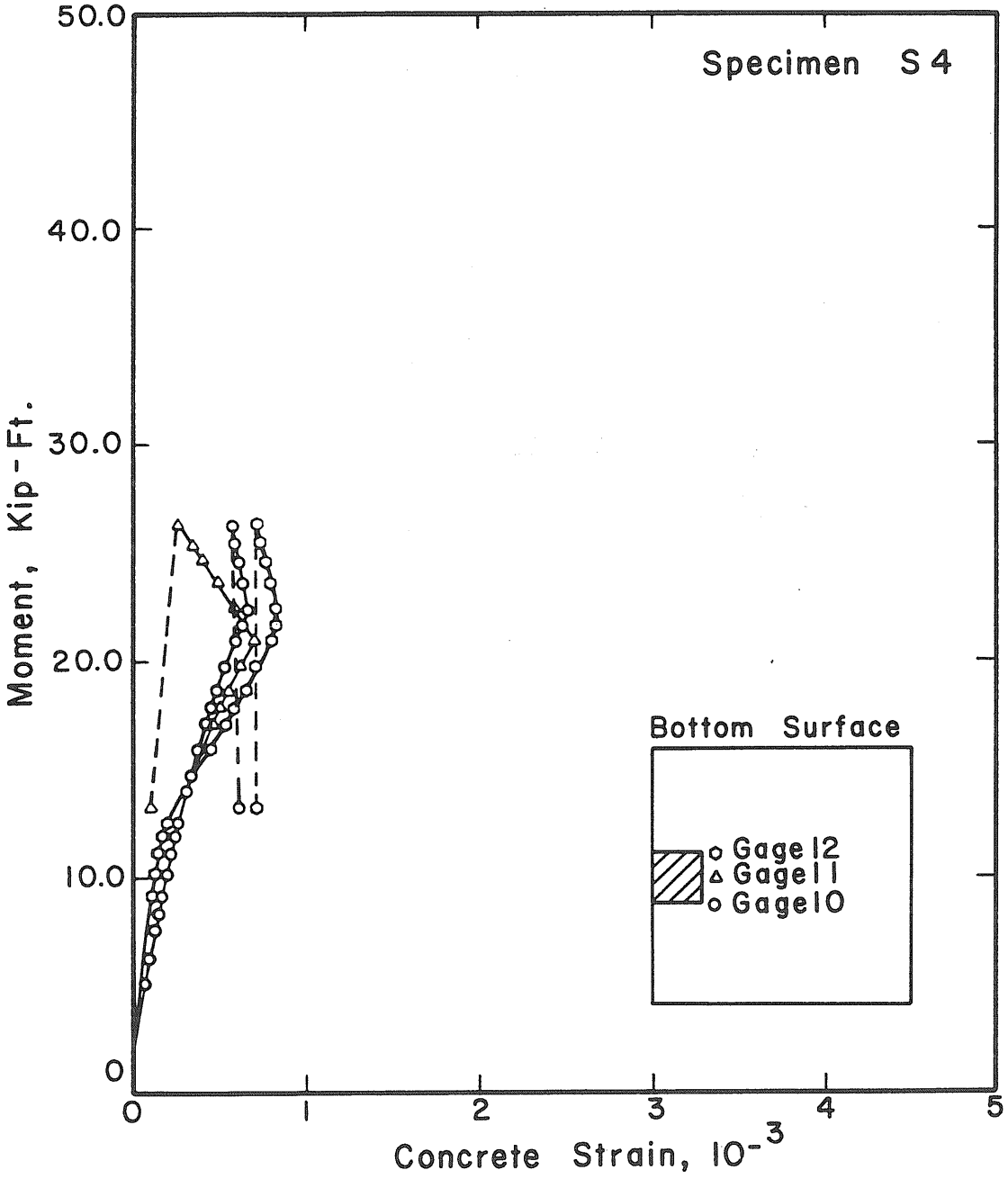

Fig. 4.16 Moment vs. Concrete Strain at the Bottom Surface of Specimen S4

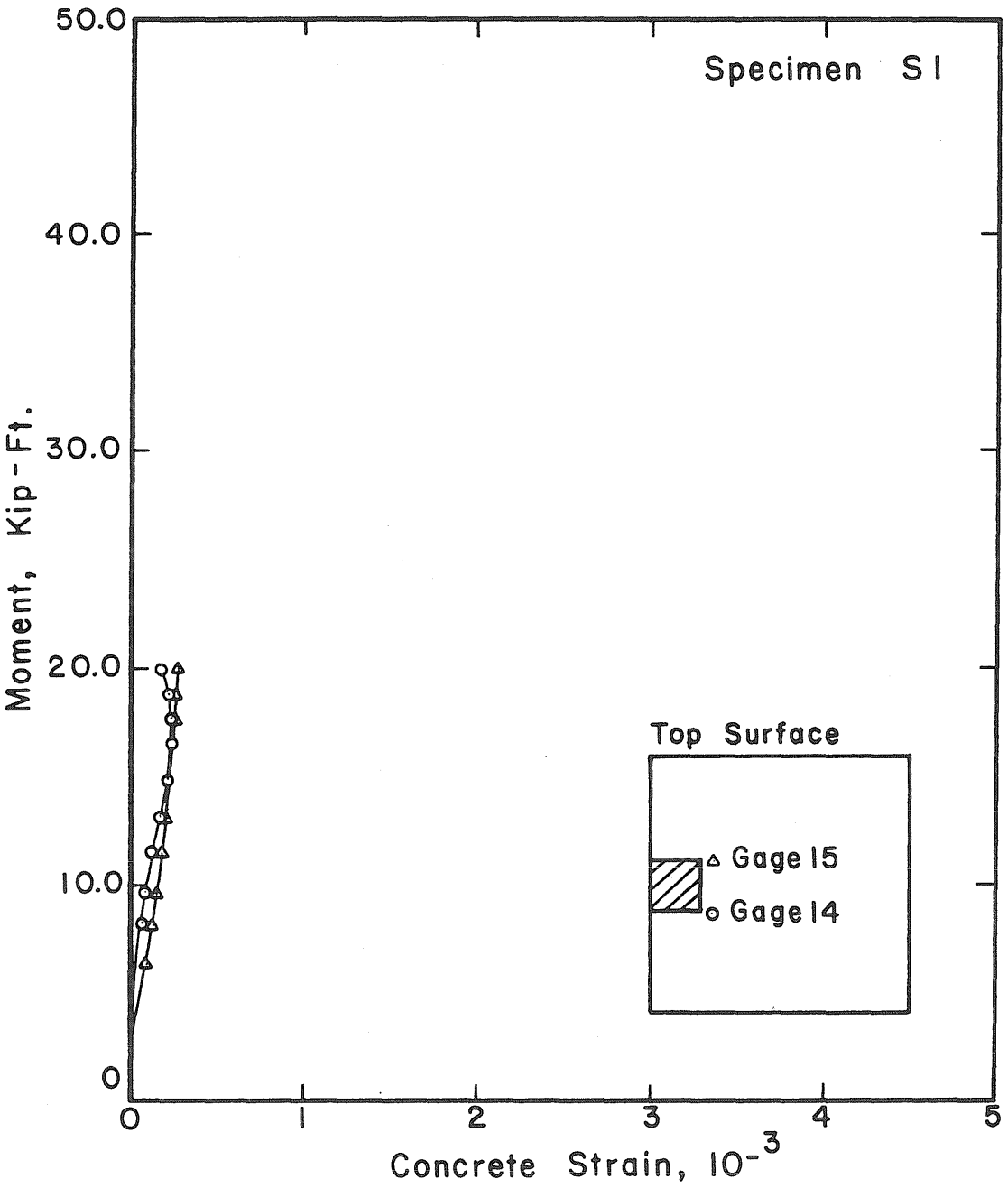

Fig. 4.17 Moment vs. Concrete Strain at the Top Surface of Specimen S1

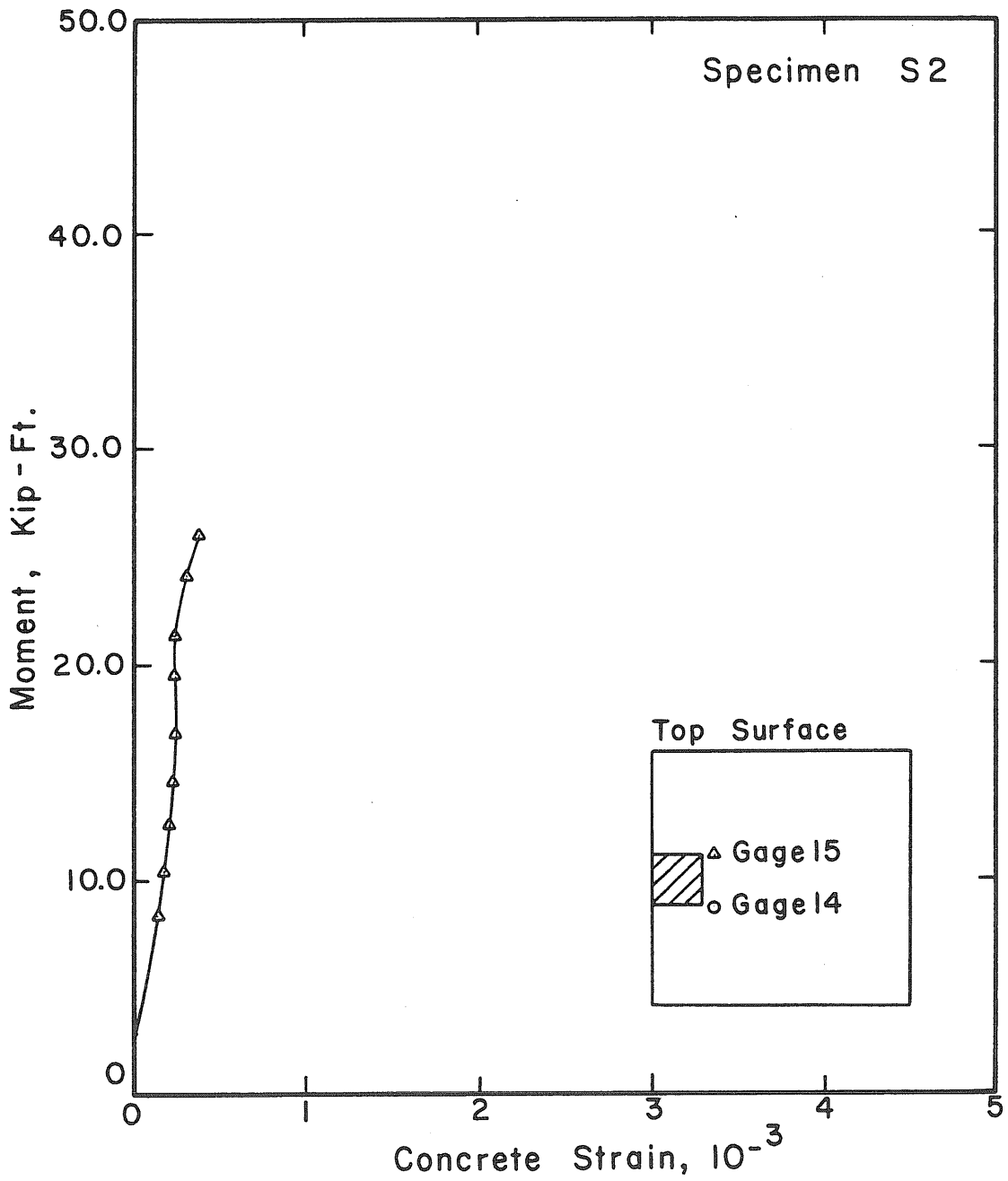

Fig. 4.18 Moment vs. Concrete Strain at the Top Surface of Specimen S2

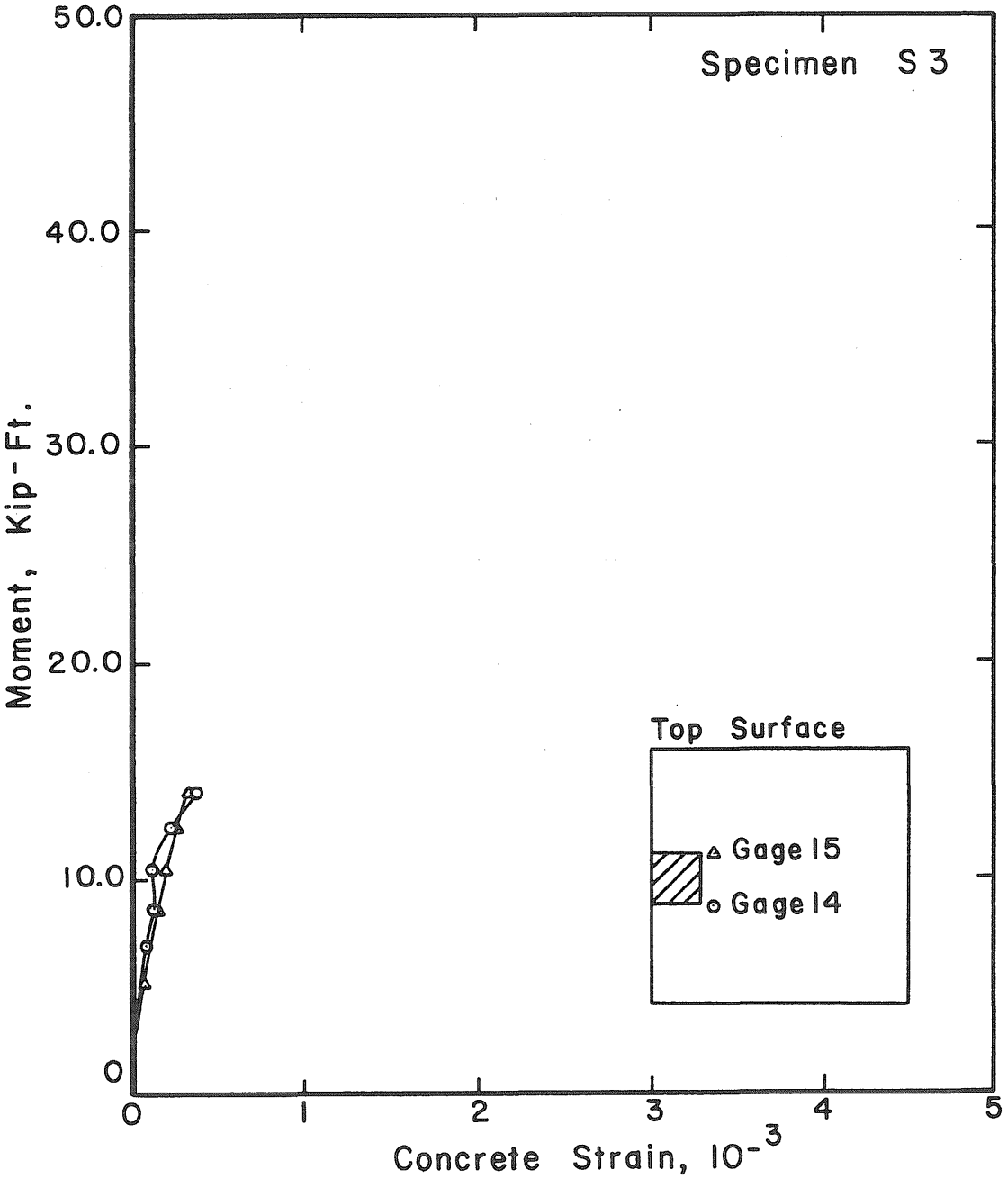

Fig. 4.19 Moment vs. Concrete Strain at the Top Surface of Specimen S3

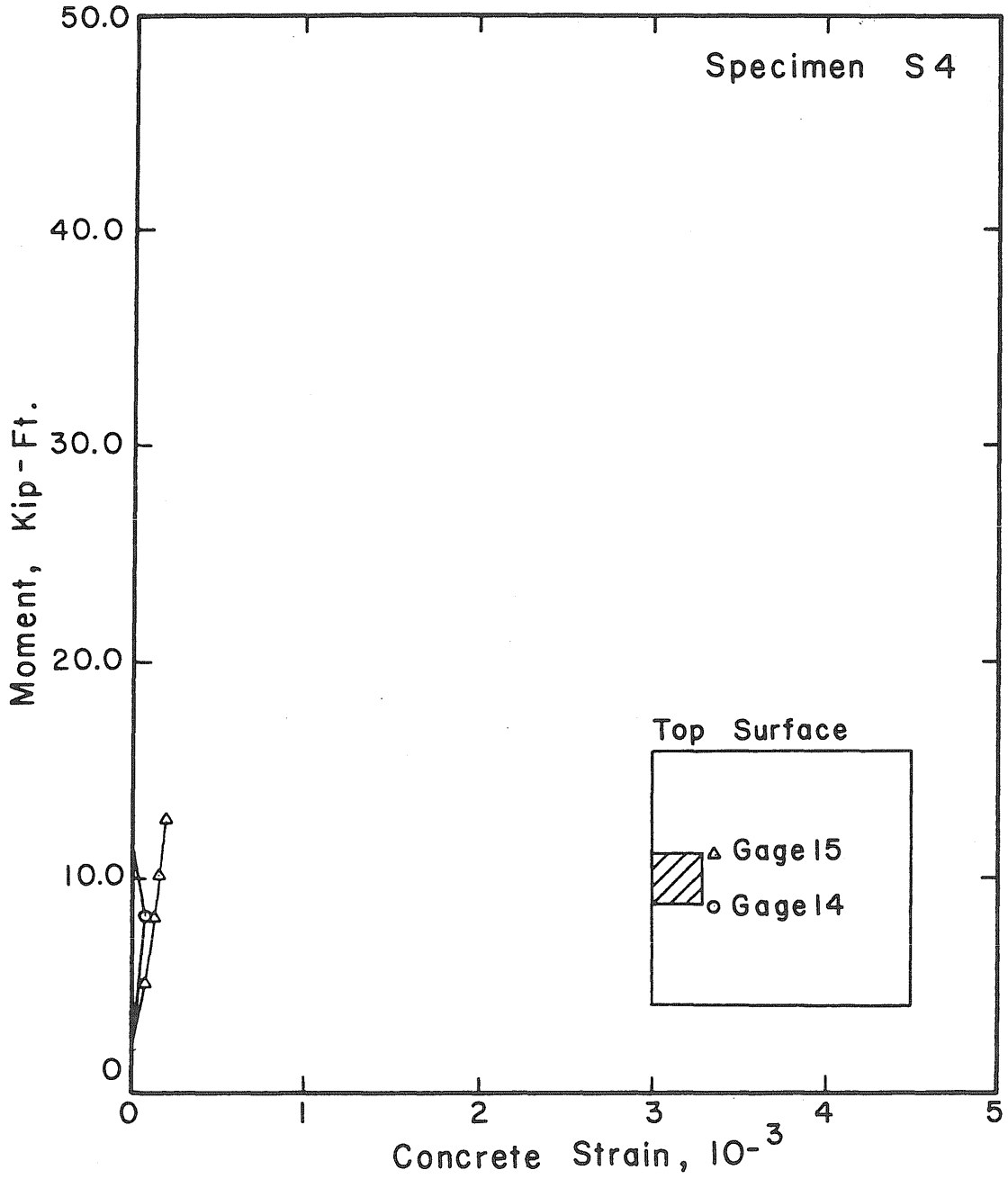

Fig. 4.20 Moment vs. Concrete Strain at the Top Surface of Specimen S4

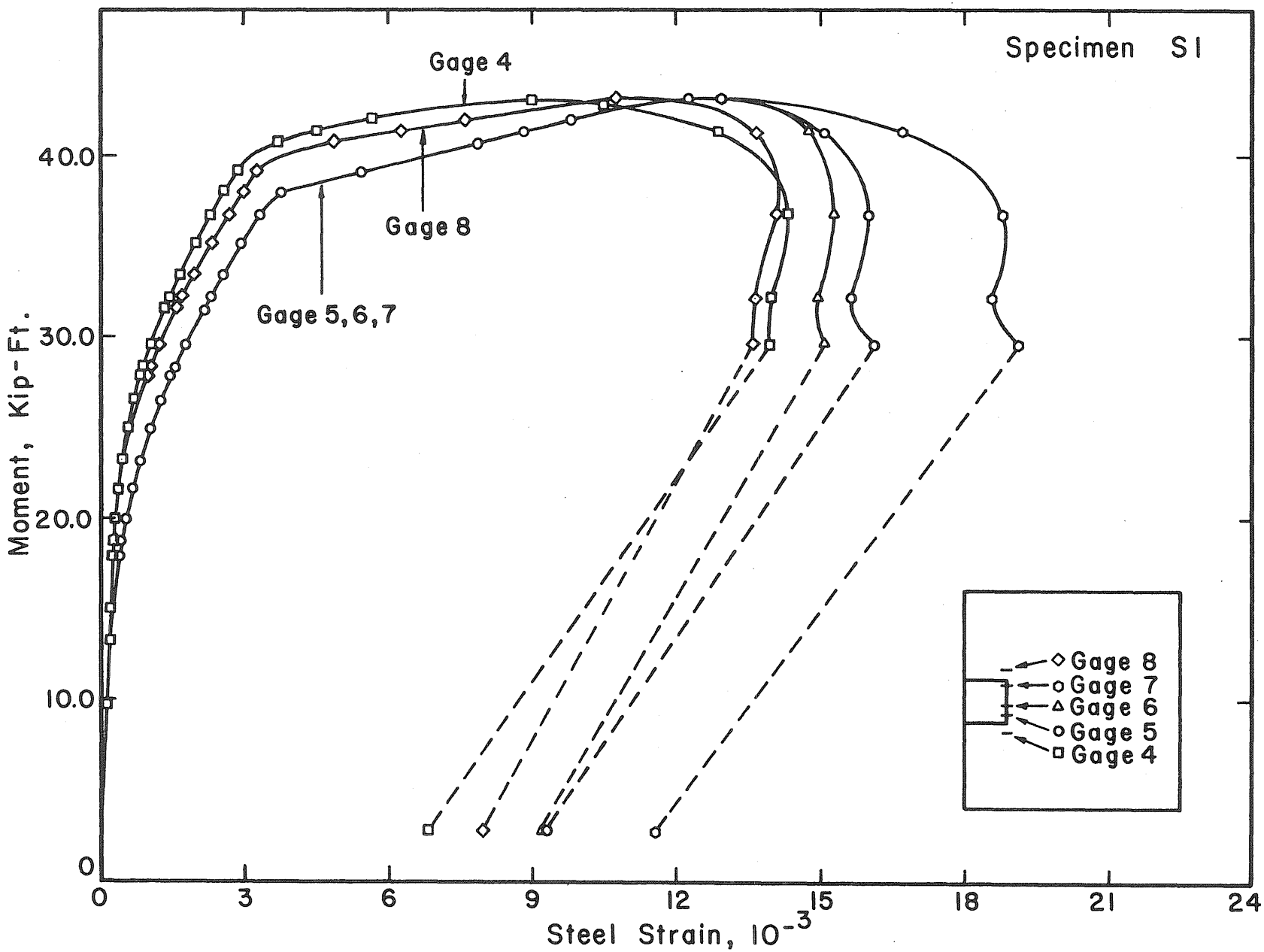

Fig. 4.21 Moment vs. Steel Strain of Specimen S1

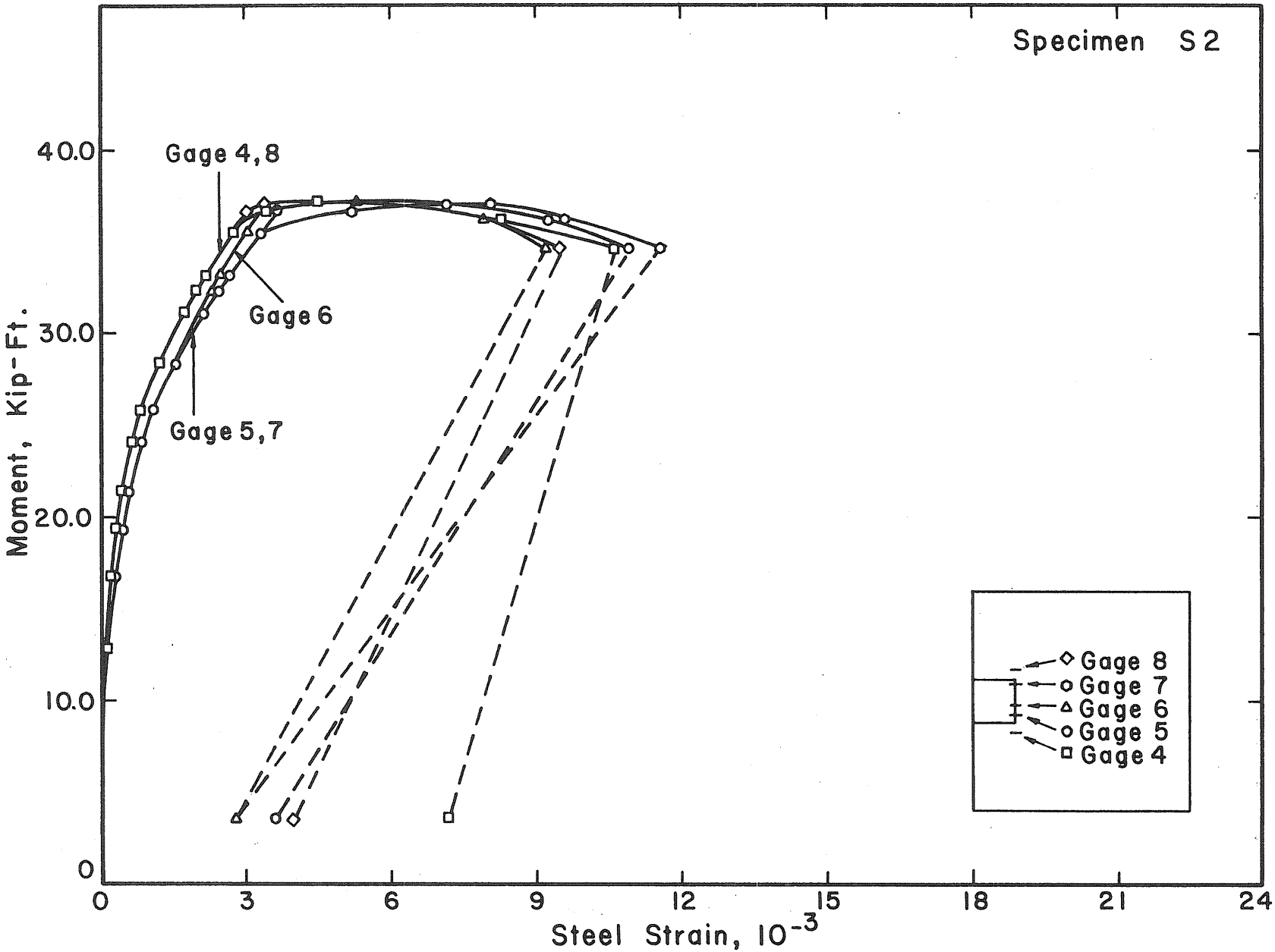

Fig. 4.22 Moment vs. Steel Strain of Specimen S2

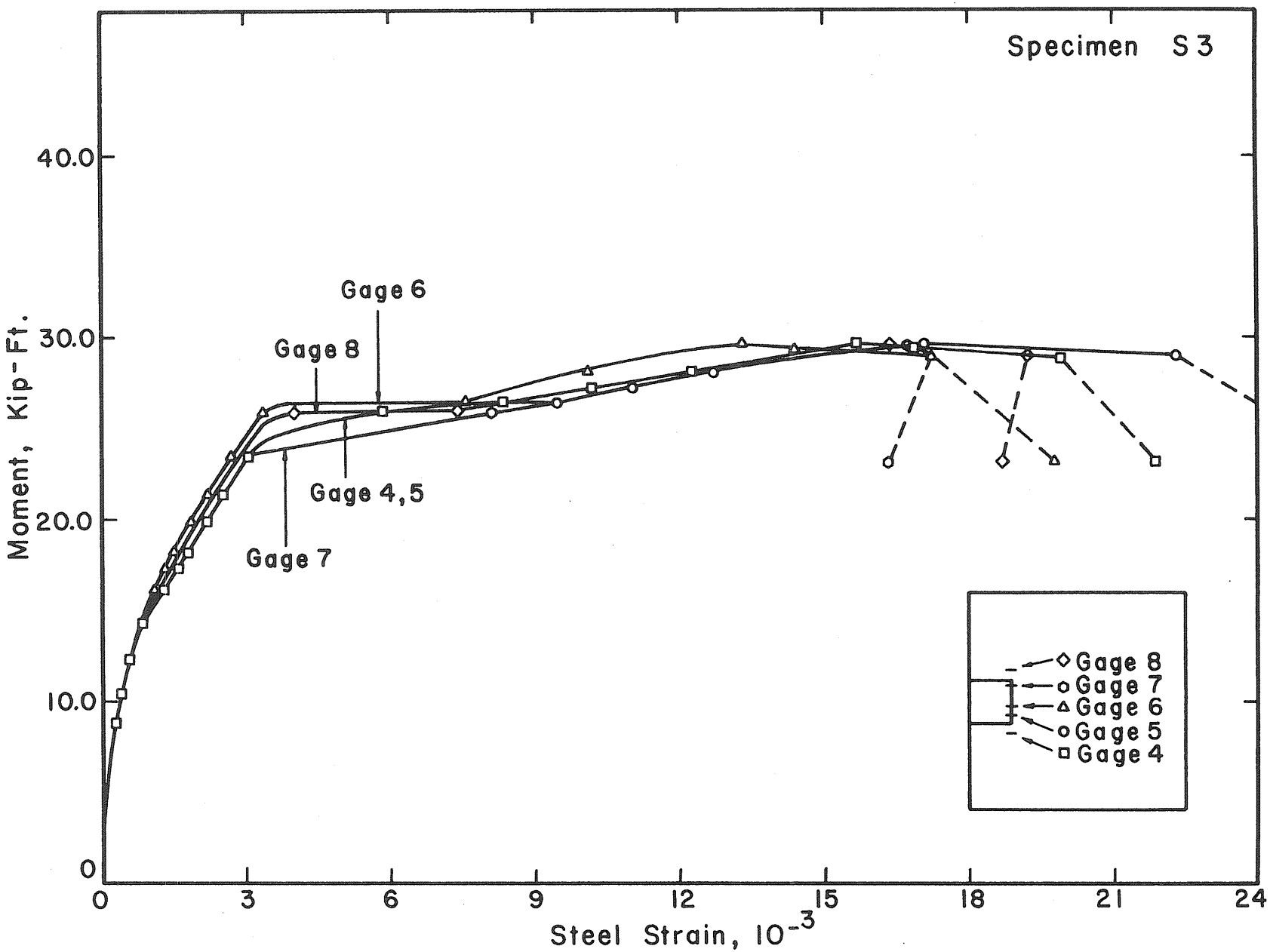

Fig. 4.23 Moment vs. Steel Strain of Specimen S3

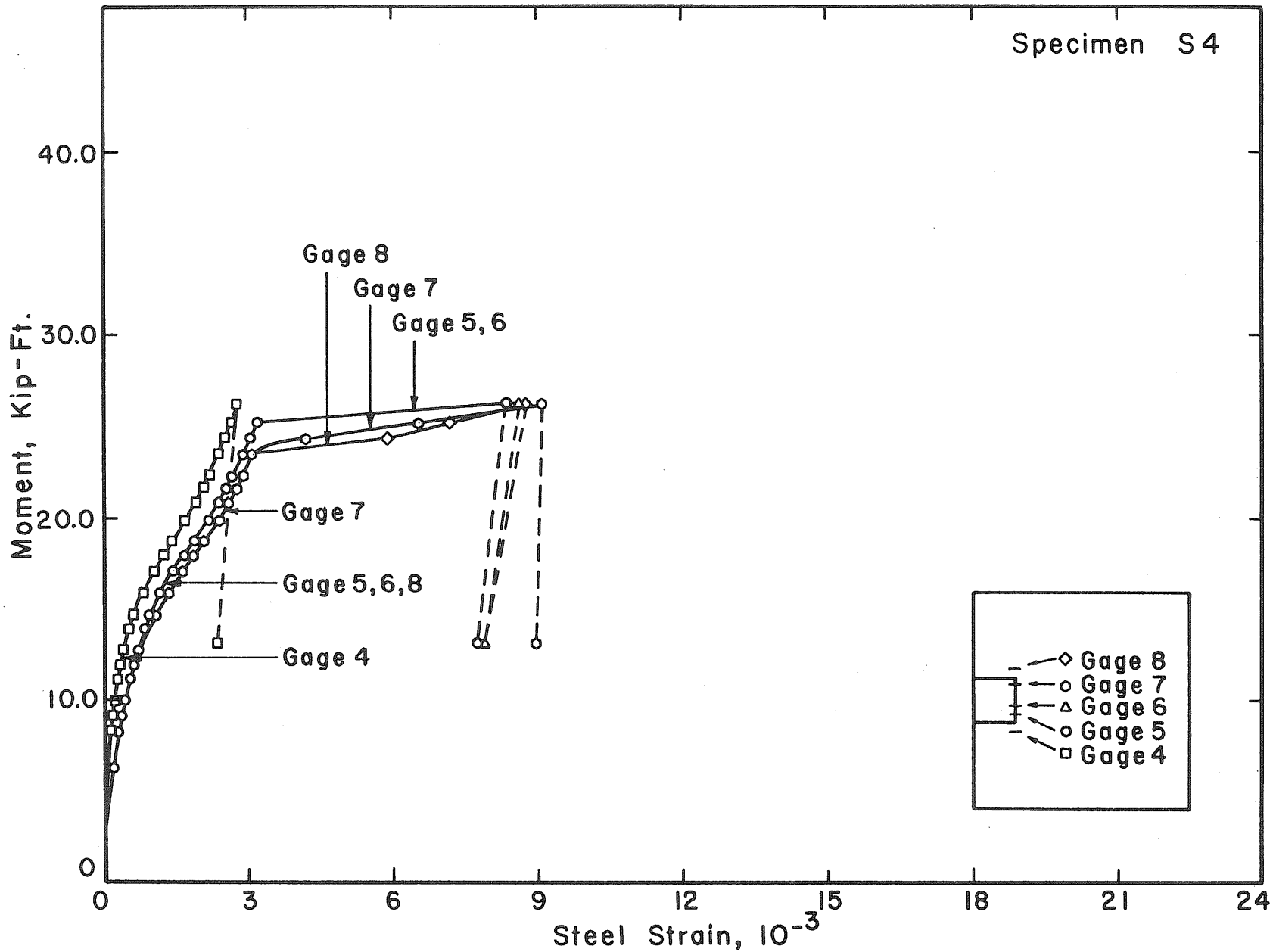

Fig. 4.24 Moment vs. Steel Strain of Specimen S4

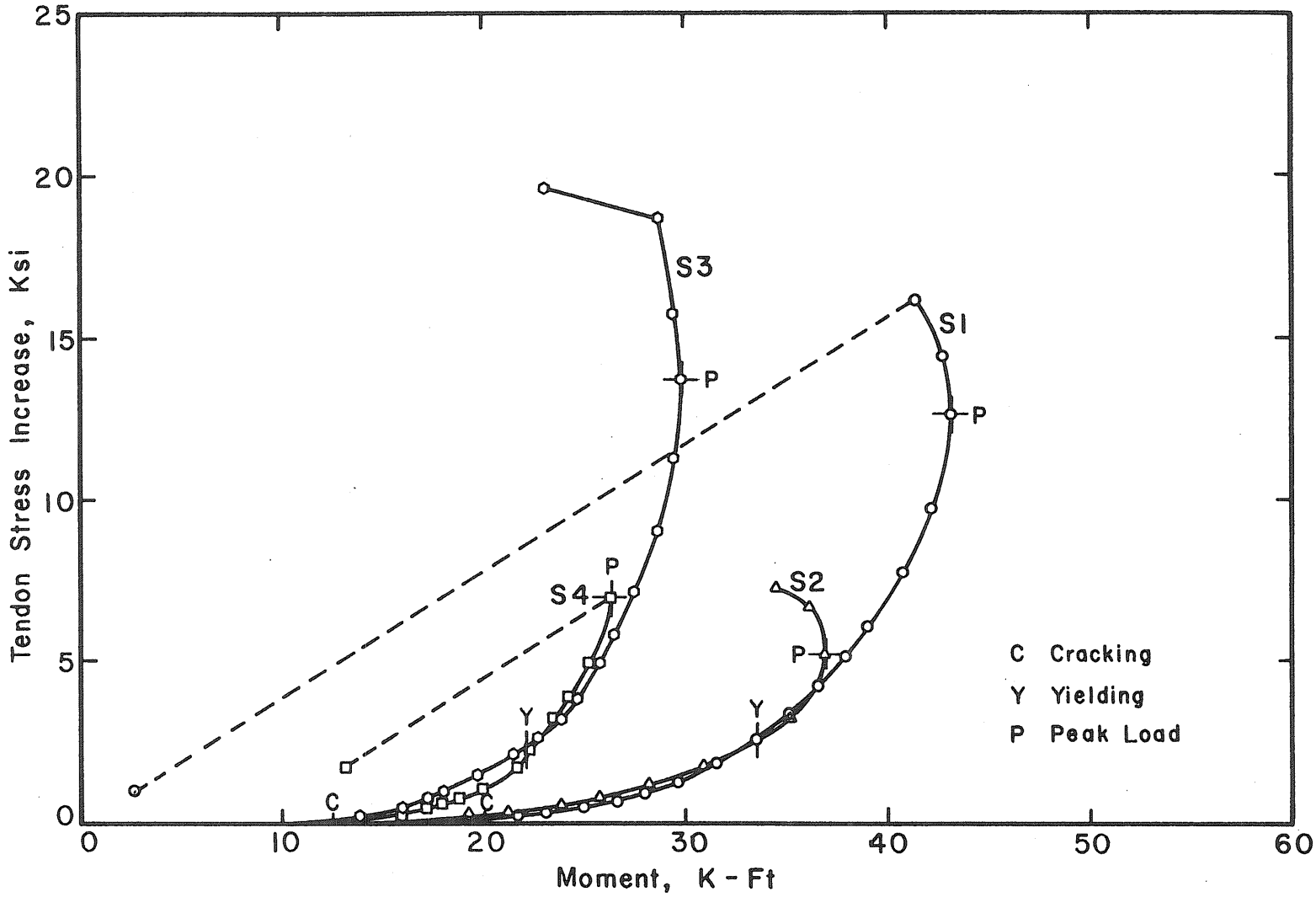

Fig. 4.25 Tendon Stress Increase vs. Moment for Tendons Passing Through Column

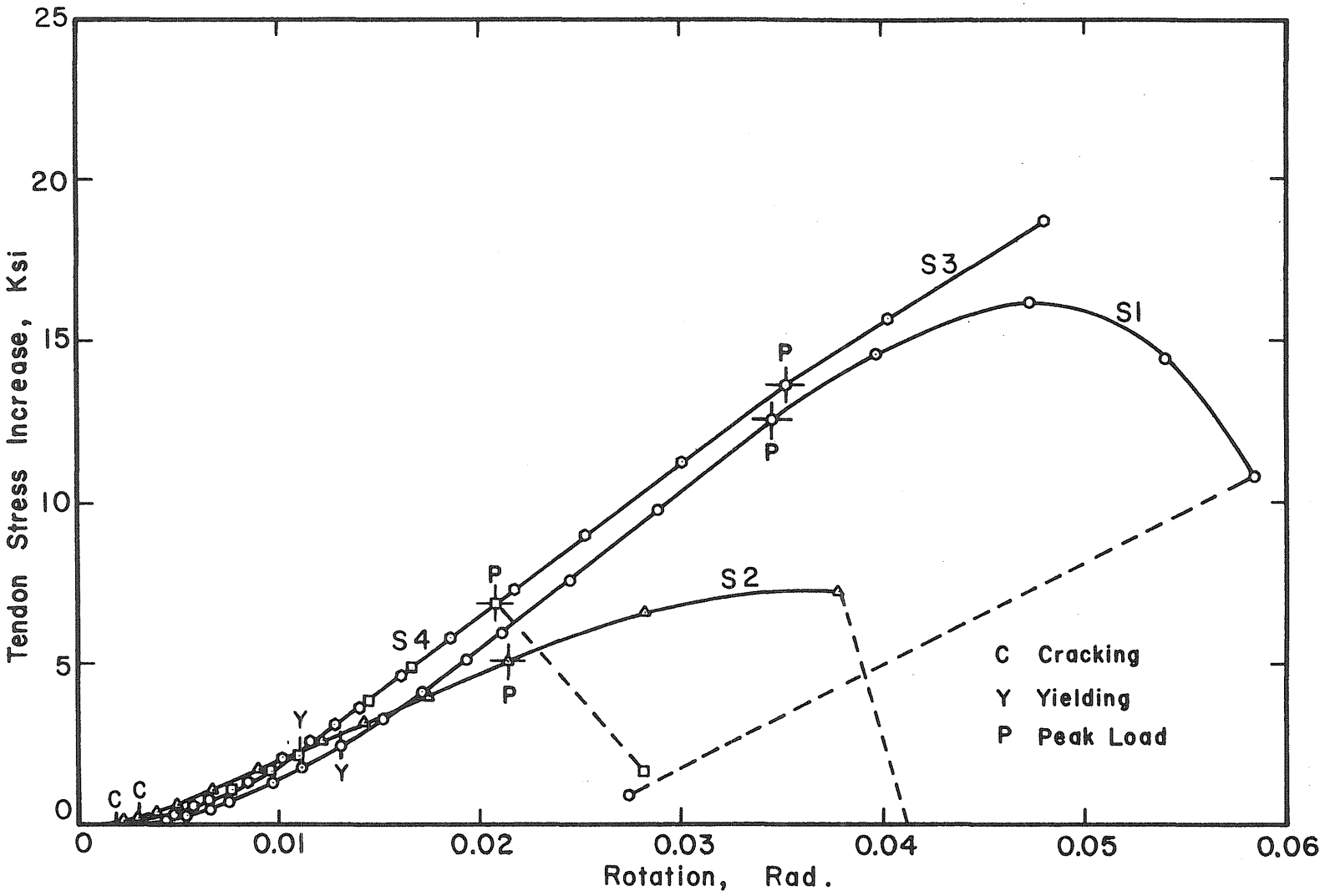

Fig. 4.26 Tendon Stress Increase vs. Rotation for Tendons Passing Through Column

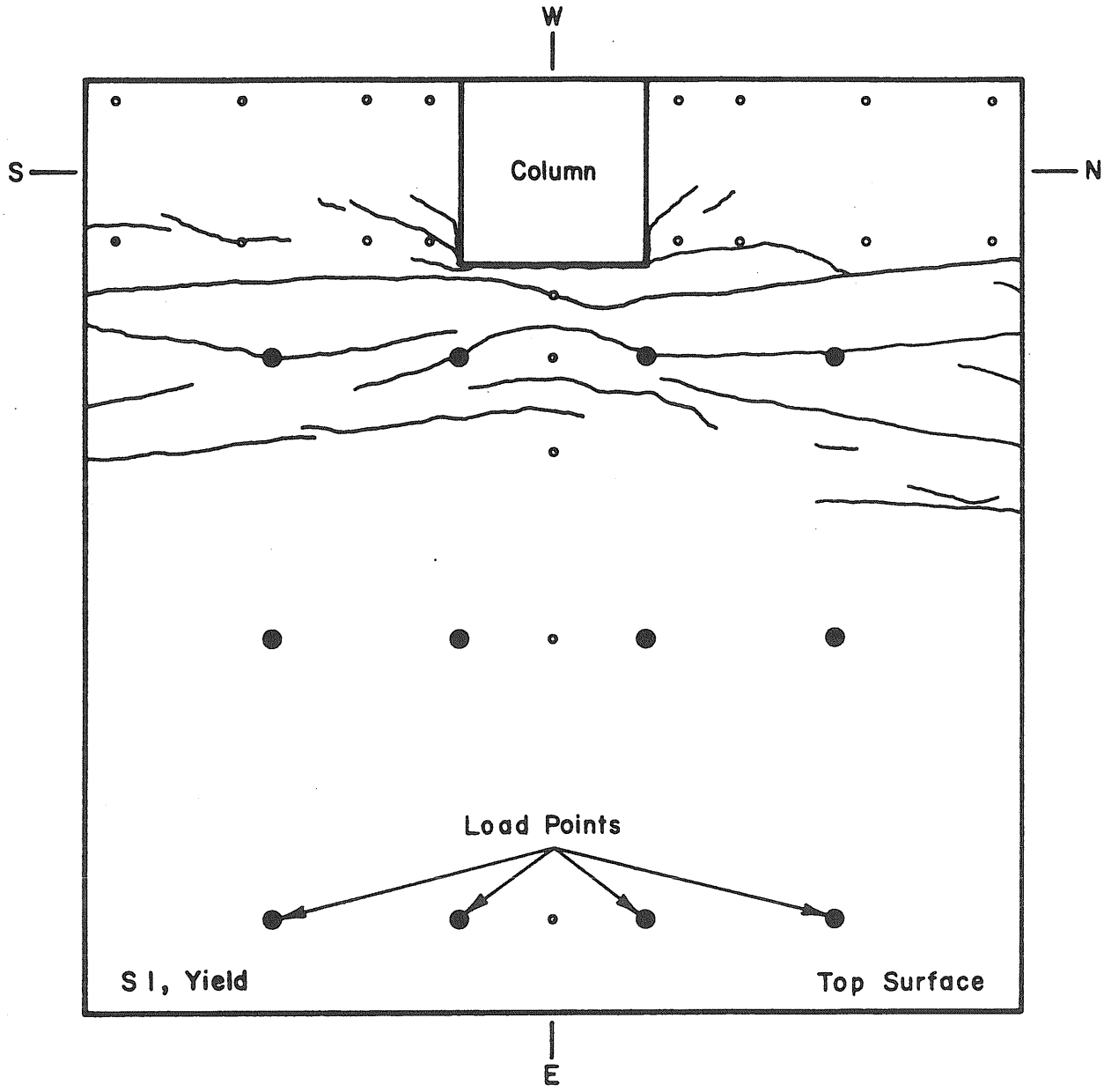

Fig. 4.27 Crack Pattern at Yield on the Top Surface of Specimen S1

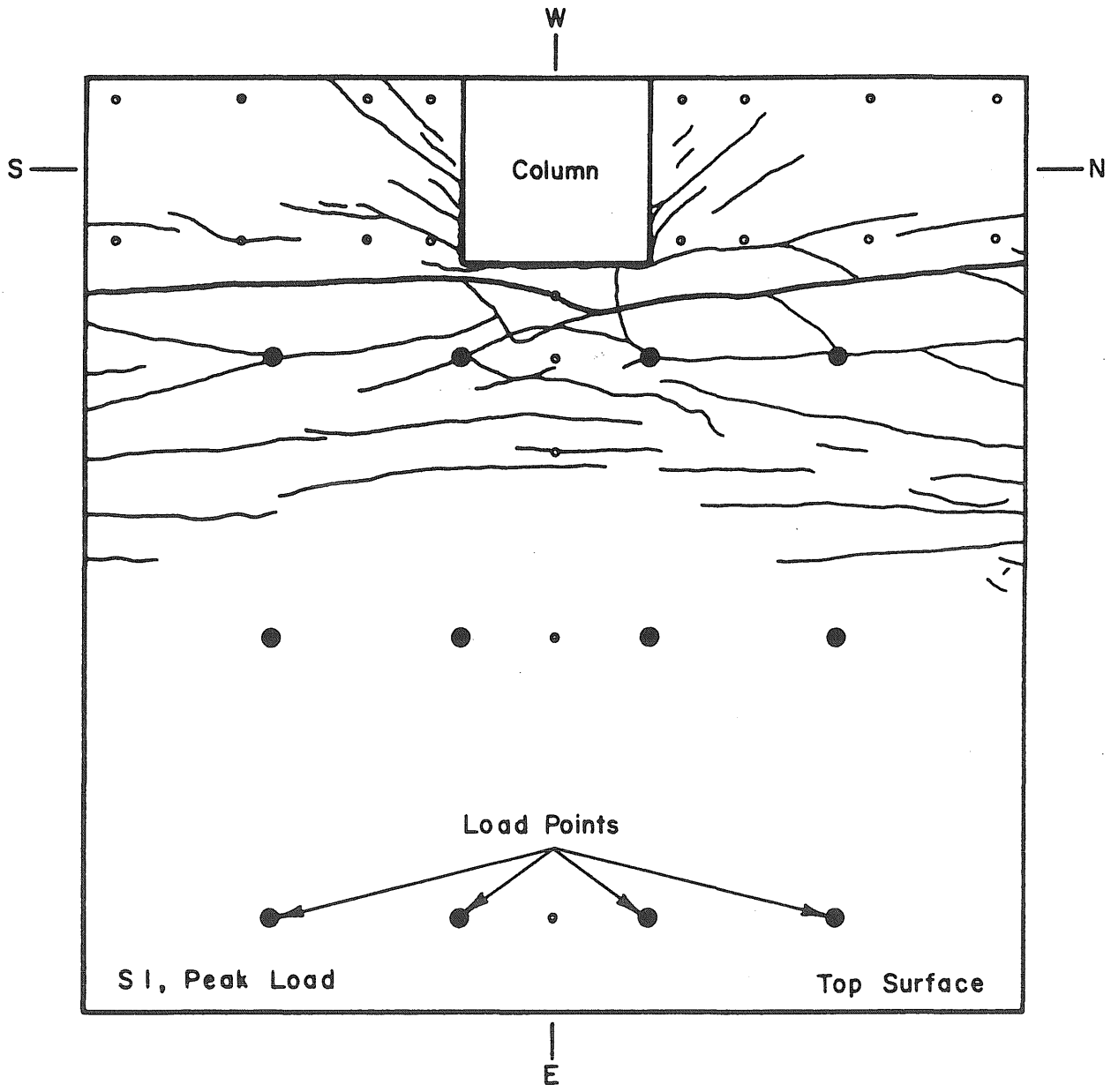

Fig. 4.28 Crack Pattern at Peak Load on the Top Surface of Specimen S1

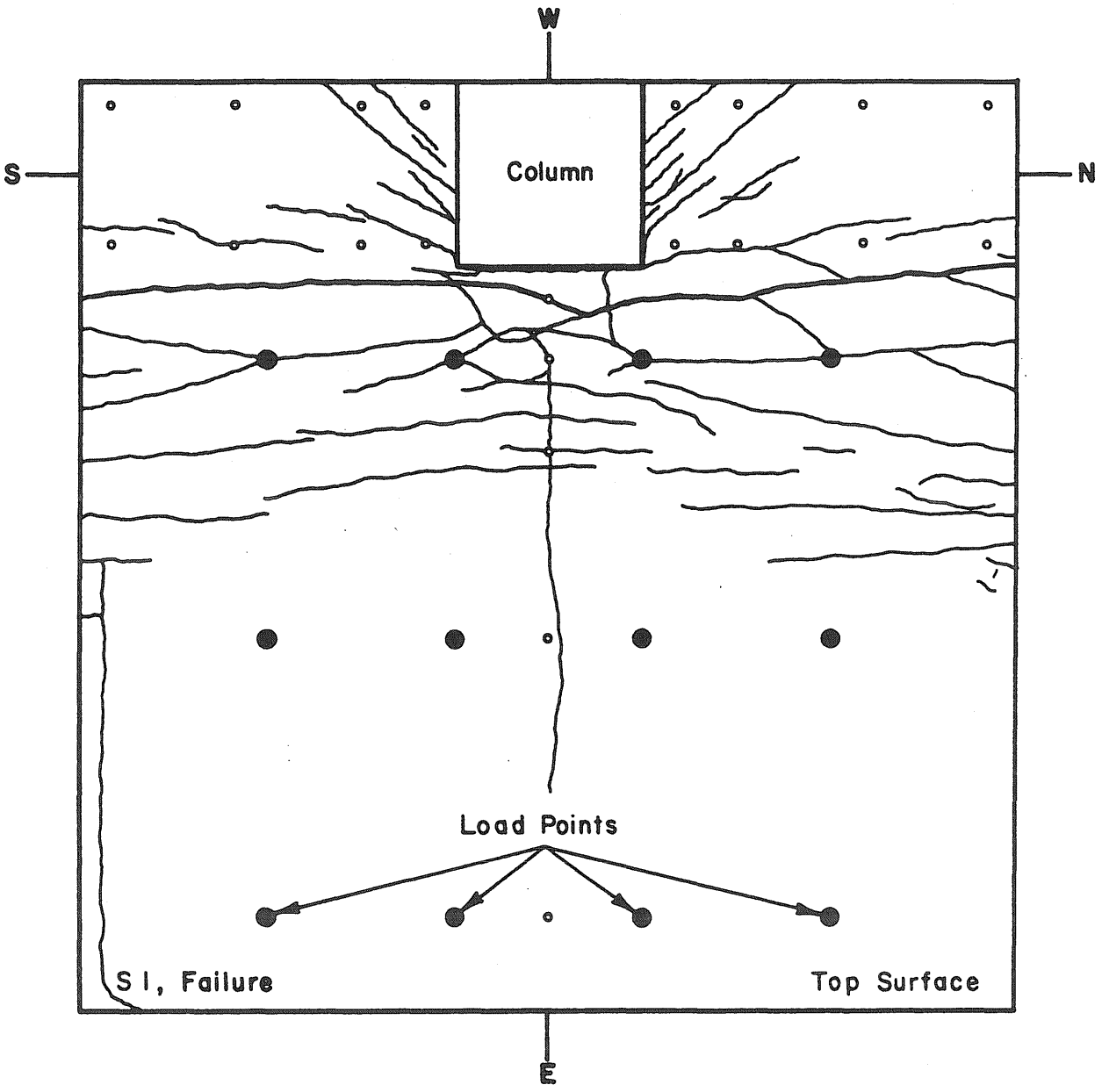

Fig. 4.29 Crack Pattern at Failure on the Top Surface of Specimen S1

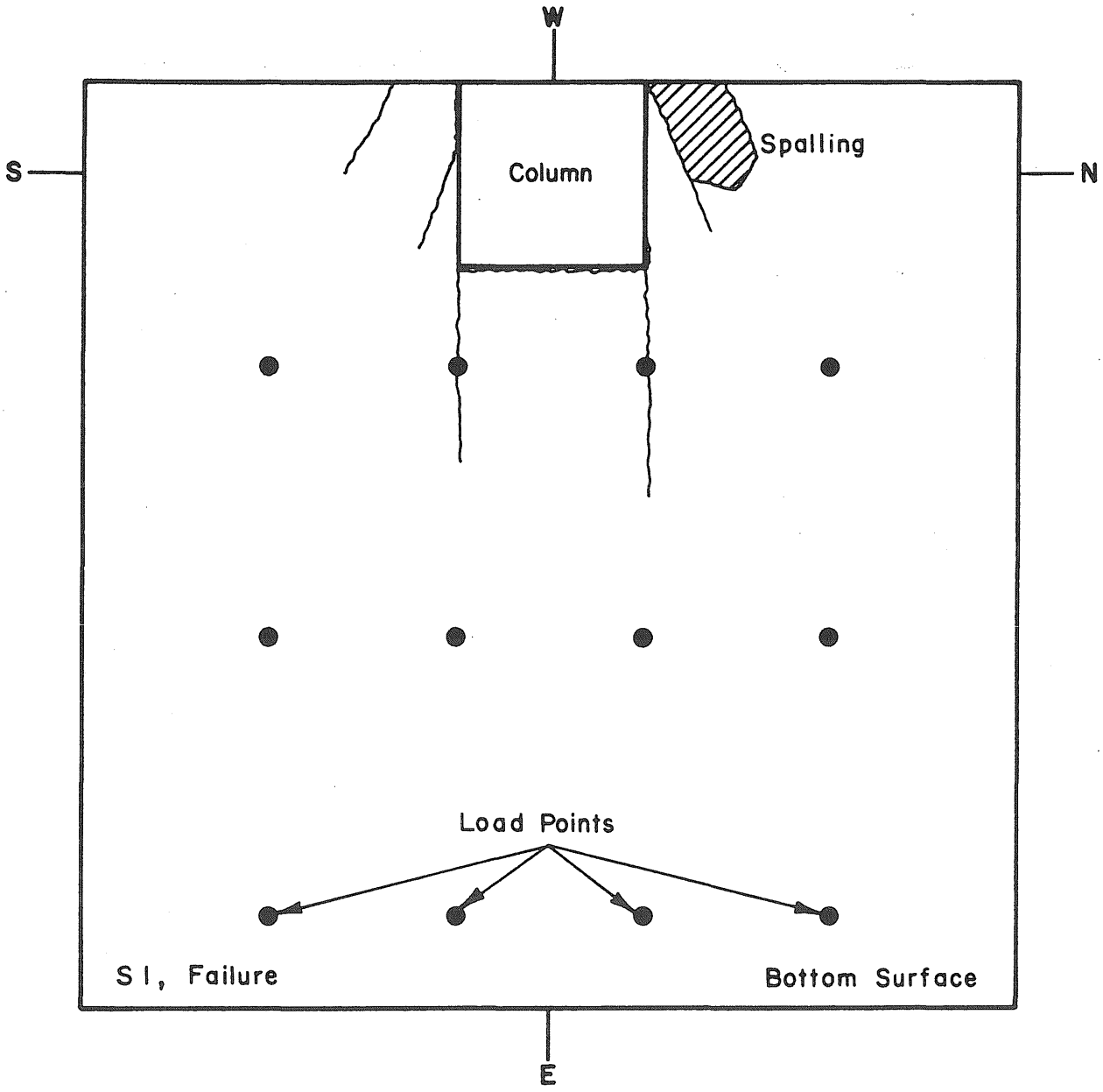

Fig. 4.30 Crack Pattern at Failure on the Bottom Surface of Specimen S1

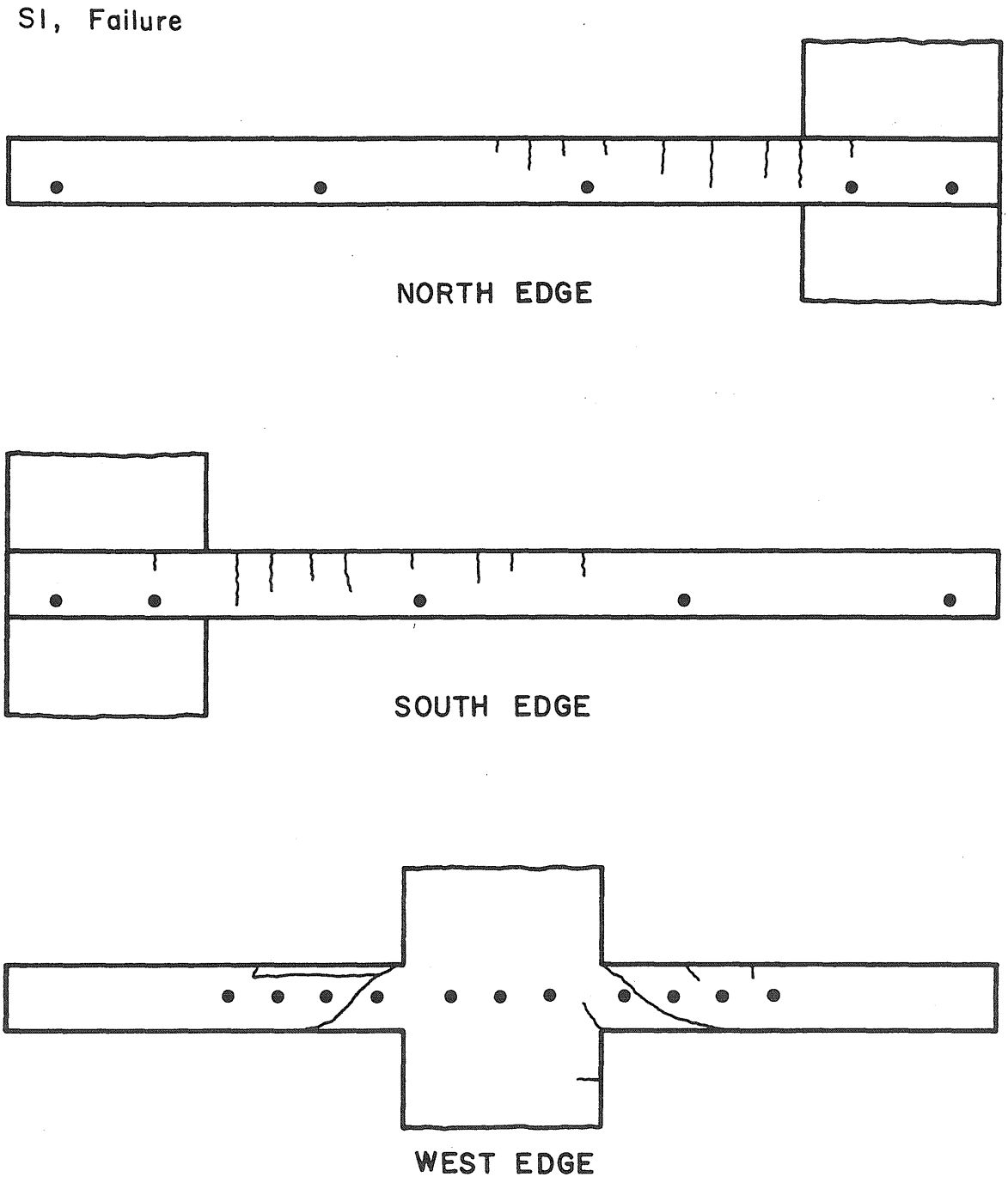

Fig. 4.31 Crack Pattern at Failure on the North, South and West Edges of Specimen S1

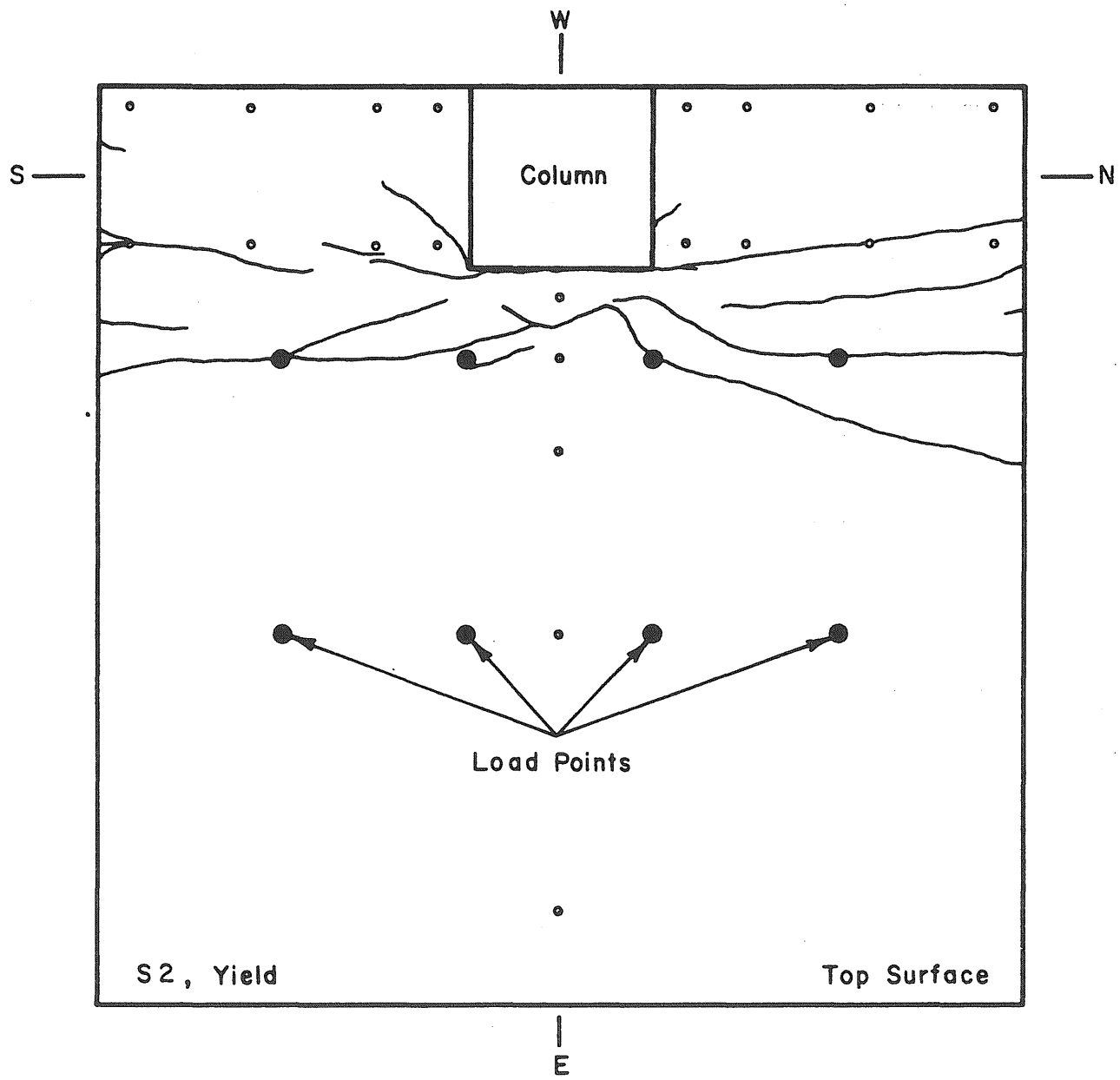

Fig. 4.32 Crack Pattern at Yield on the Top Surface of Specimen S2

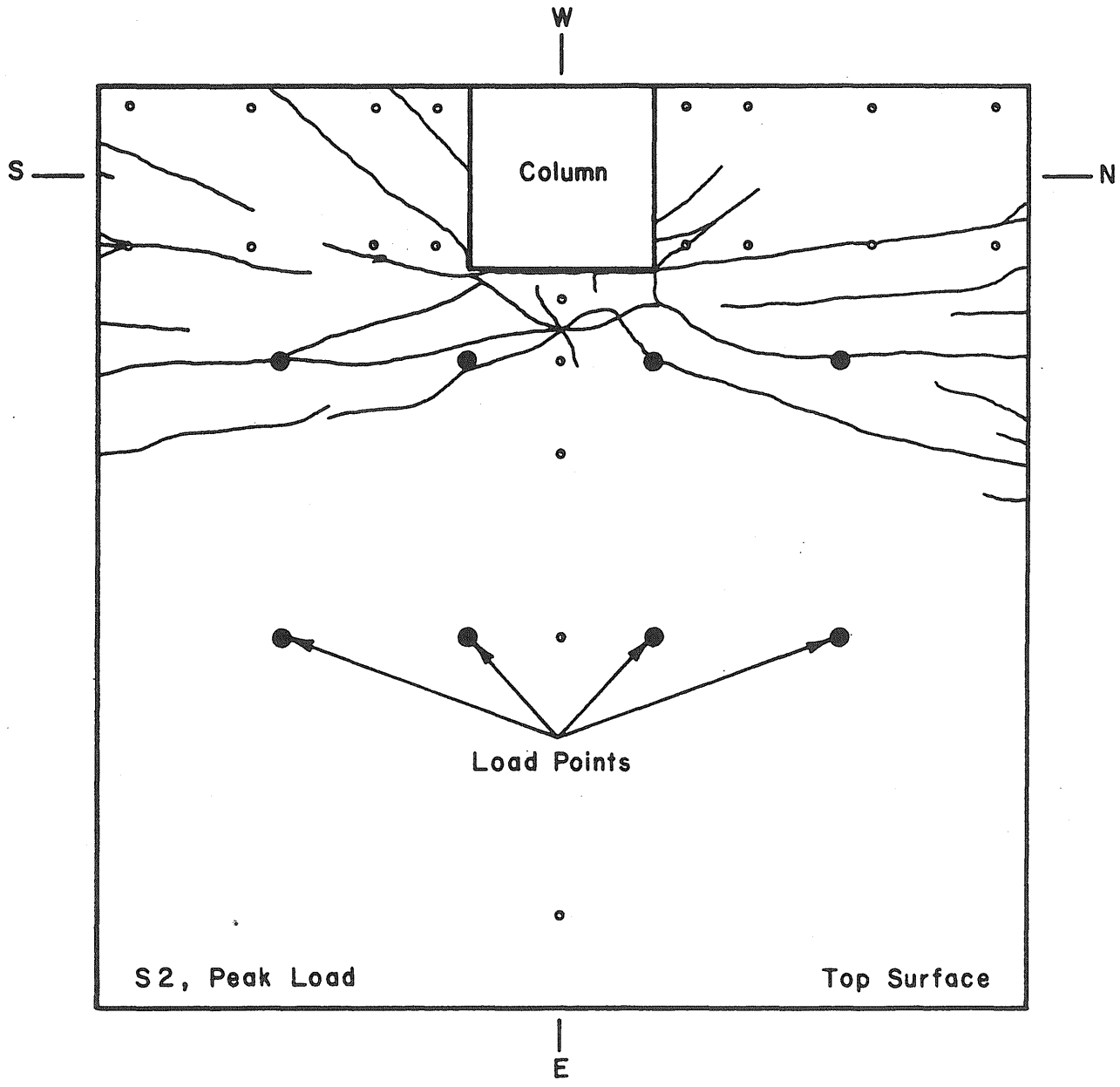

Fig. 4.33 Crack Pattern at Peak Load on the Top Surface of Specimen S2

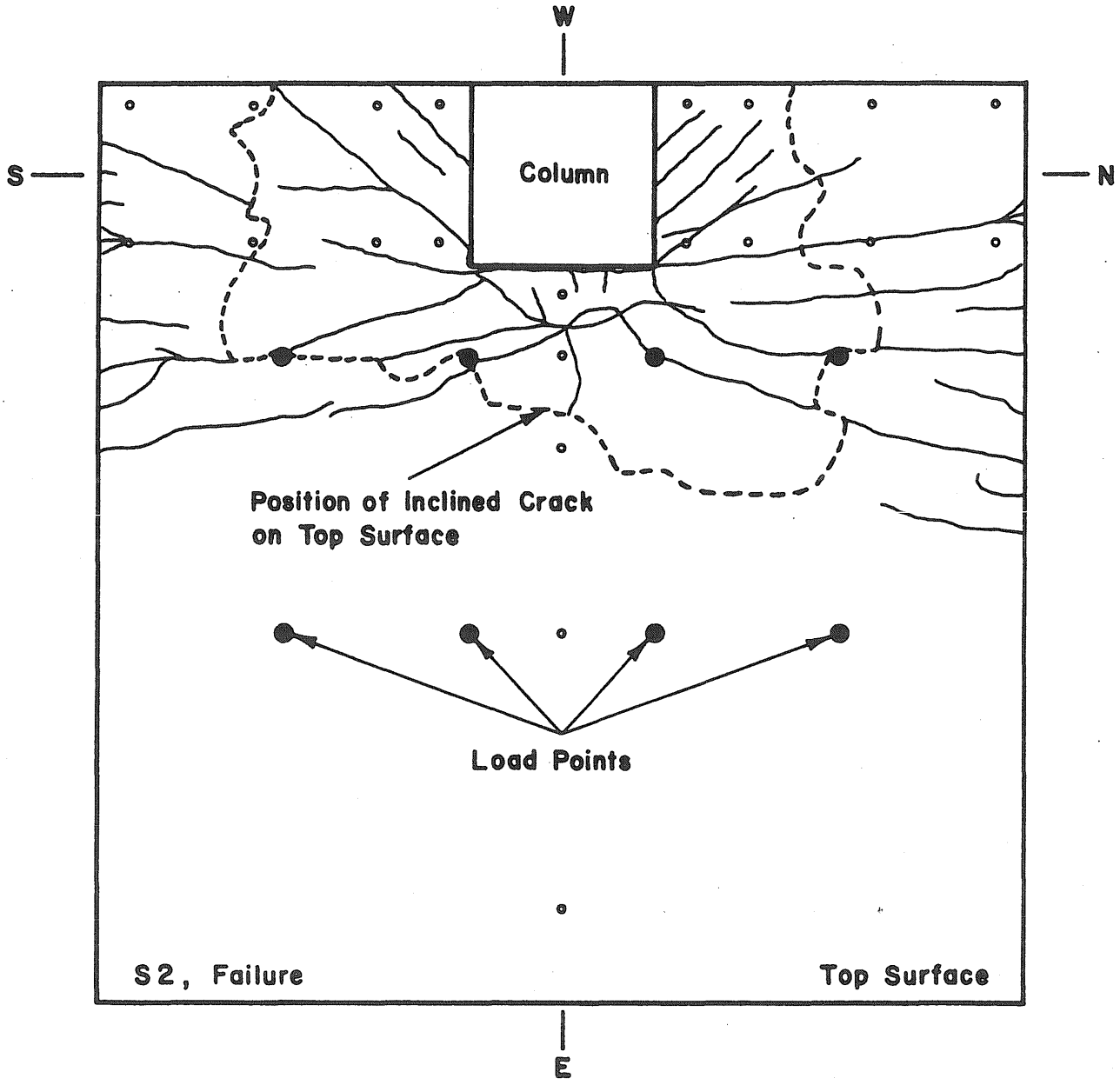

Fig. 4.34 Crack Pattern at Failure on the Top Surface of Specimen S2

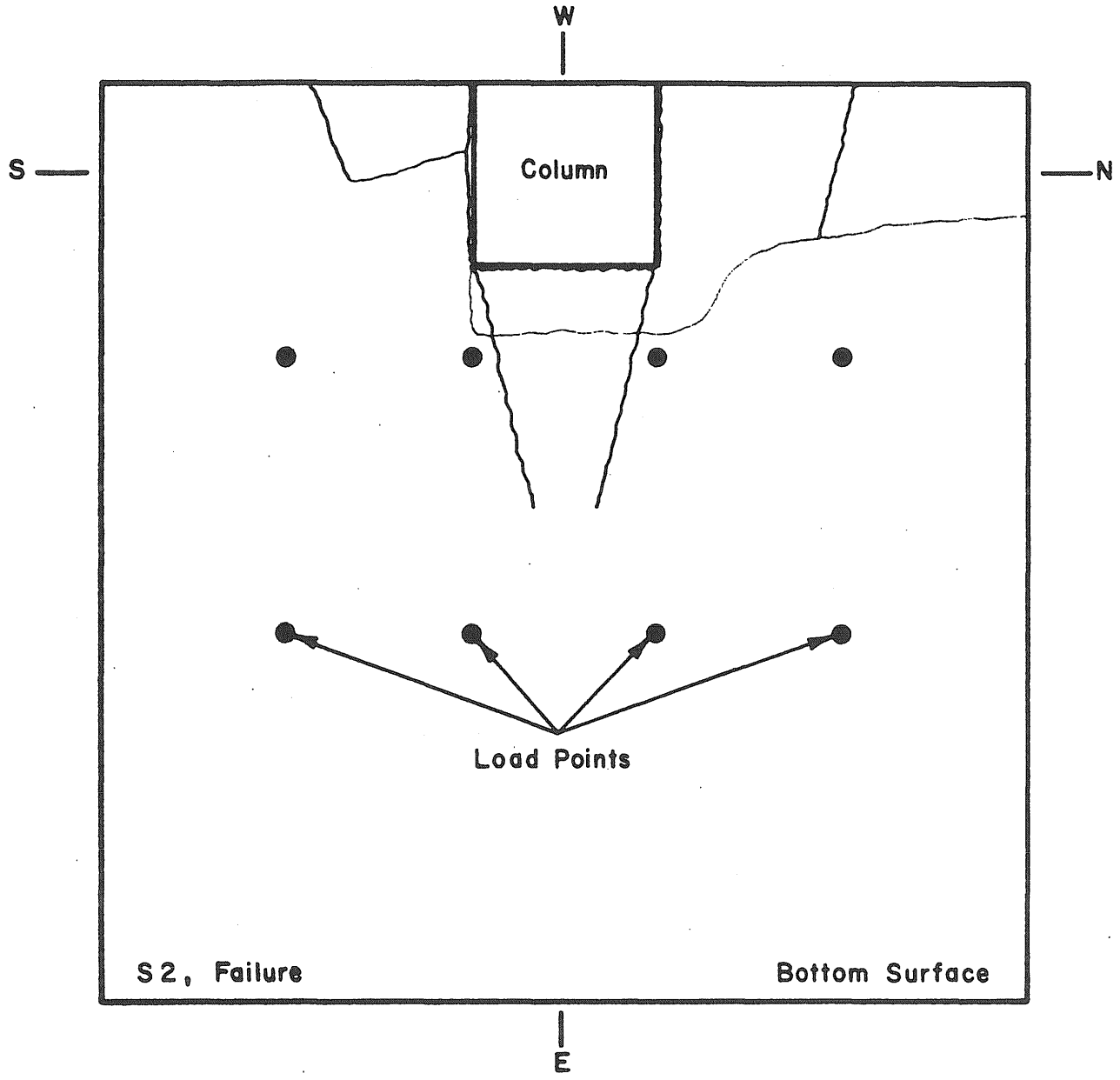

Fig. 4.35 Crack Pattern at Failure on the Bottom Surface of Specimen S2

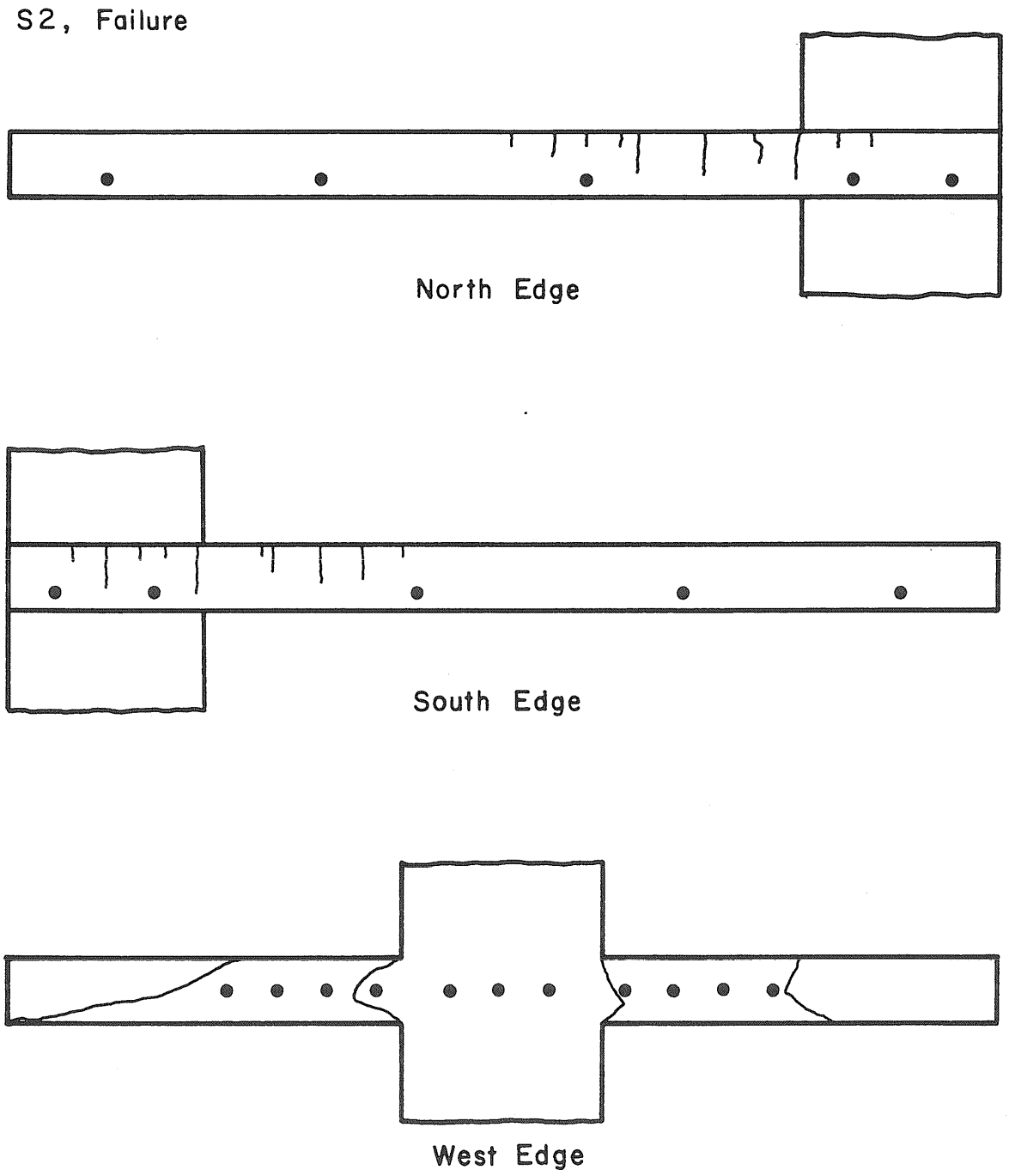

Fig. 4.36 Crack Pattern at Failure on the North, South and West Edges of Specimen S2

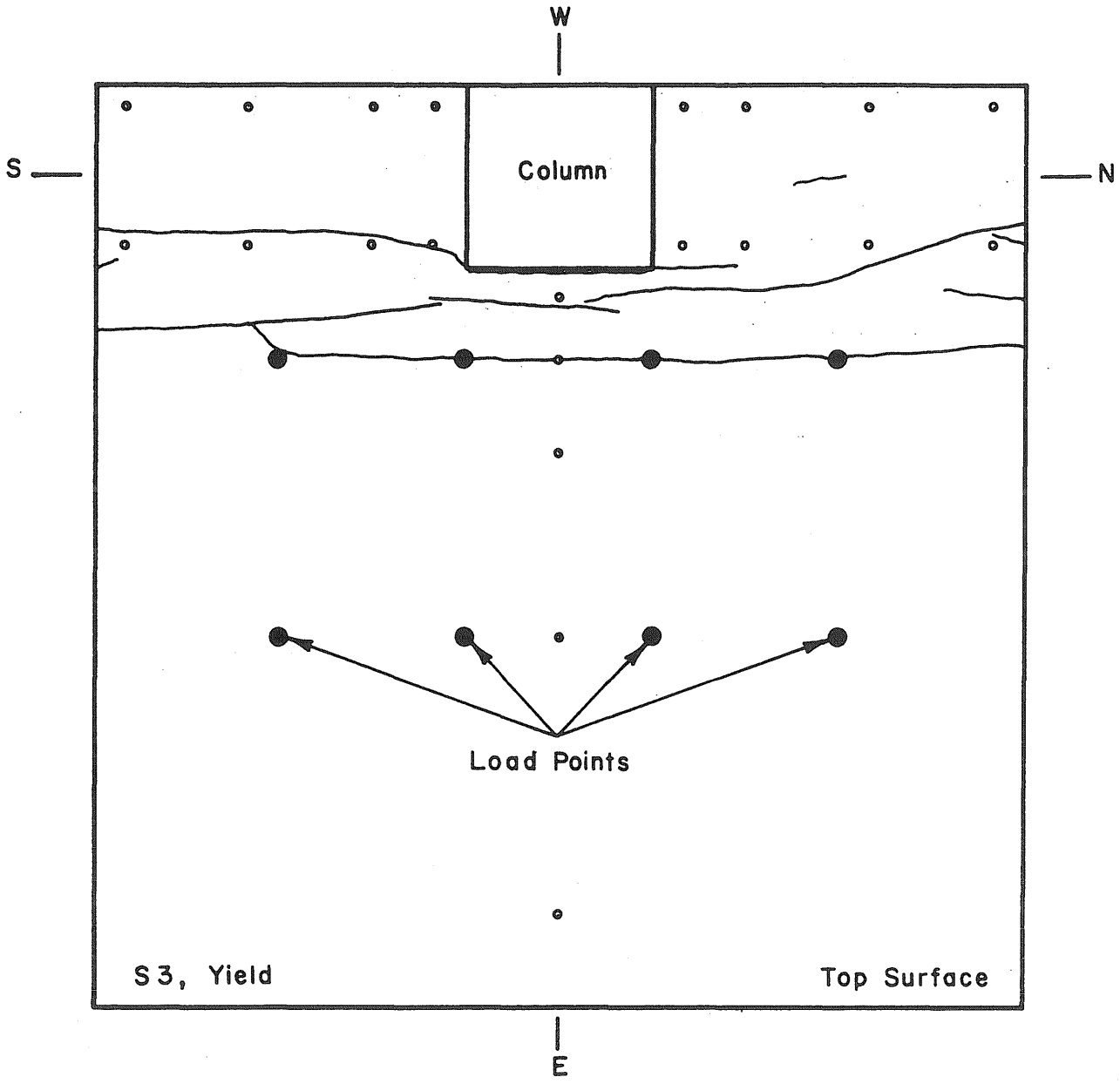

Fig. 4.37 Crack Pattern at Yield on the Top Surface of Specimen S3

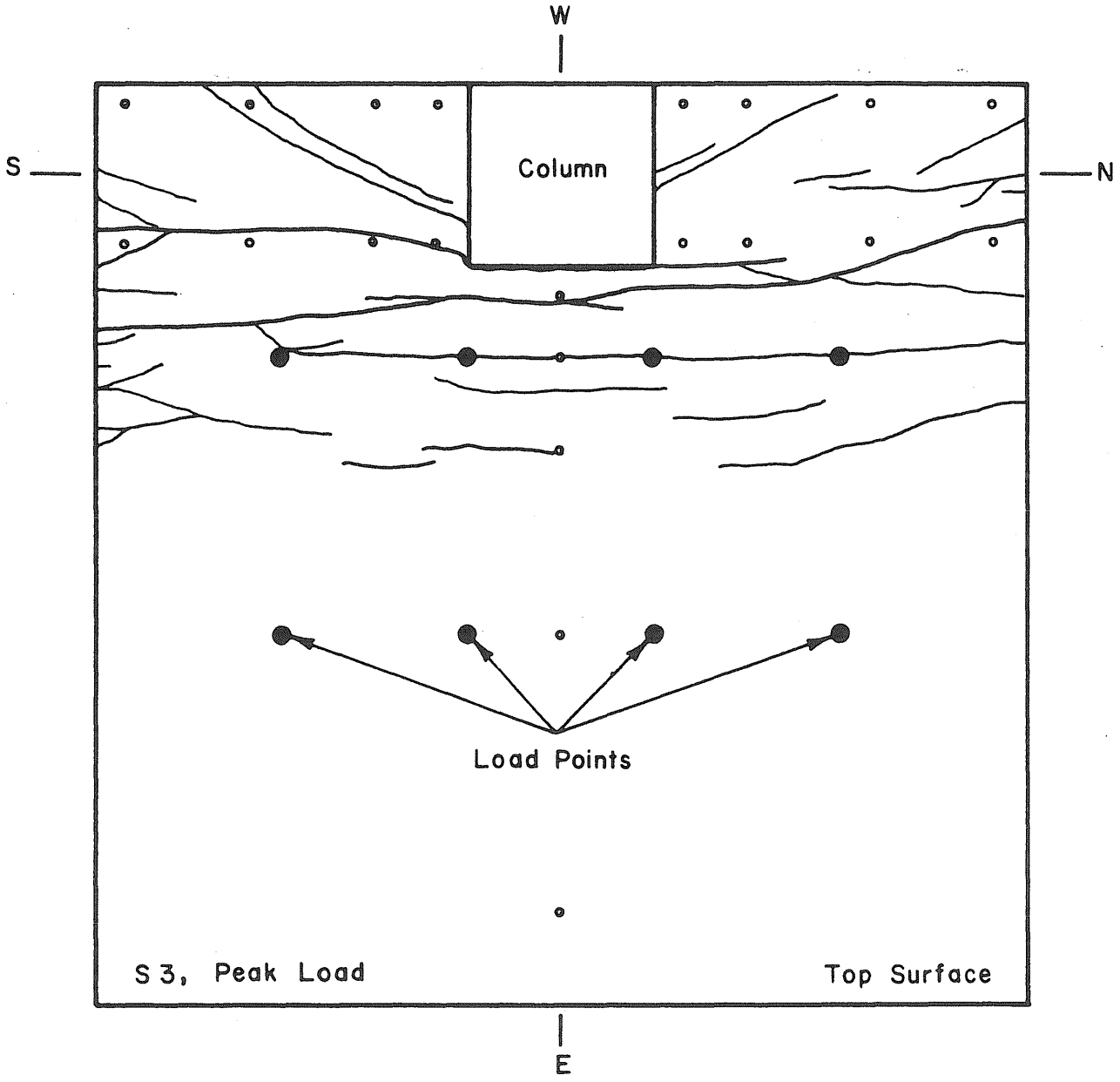

Fig. 4.38 Crack Pattern at Peak Load on the Top Surface of Specimen S3

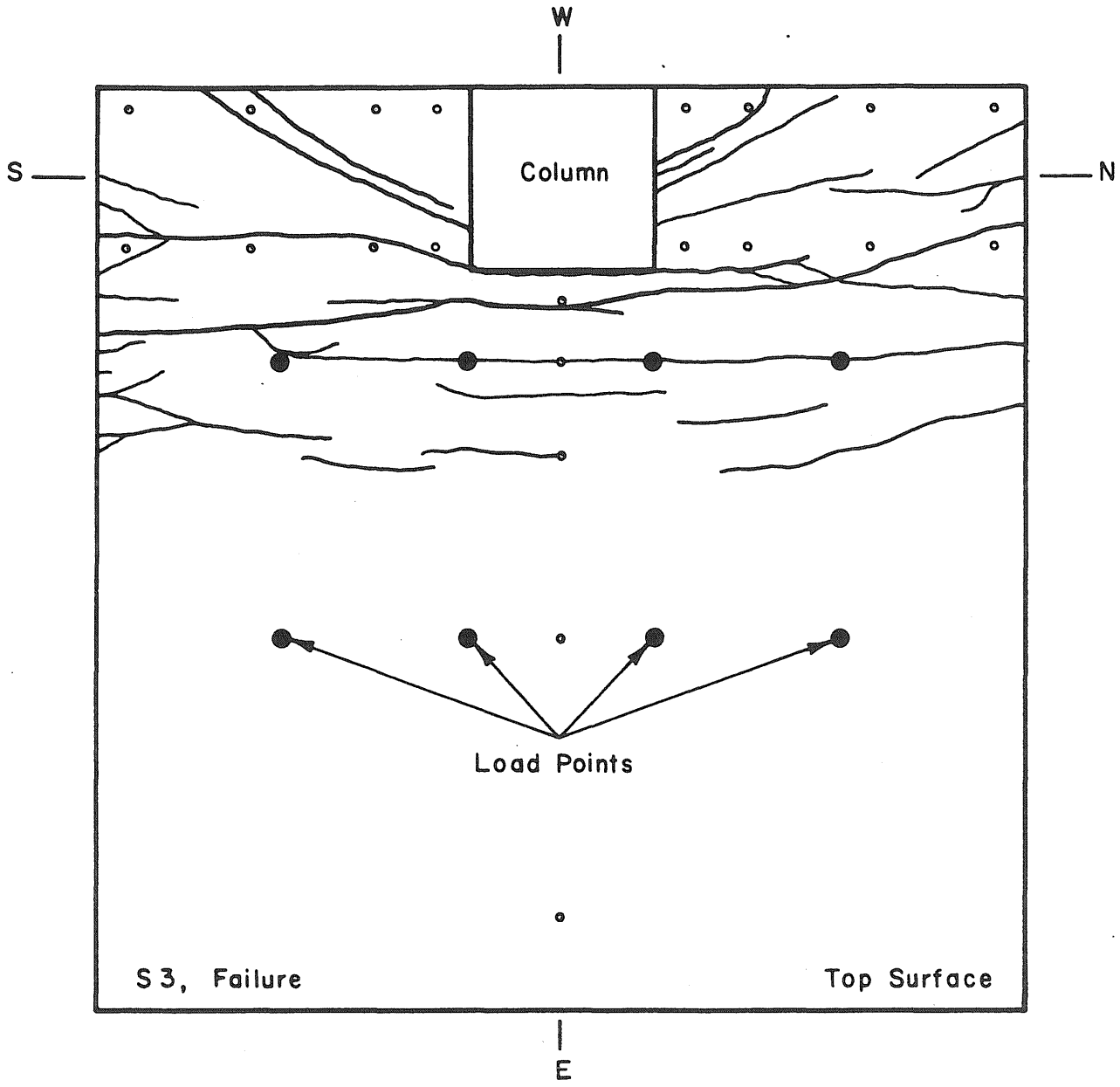

Fig. 4.39 Crack Pattern at Failure on the Top Surface of Specimen S3

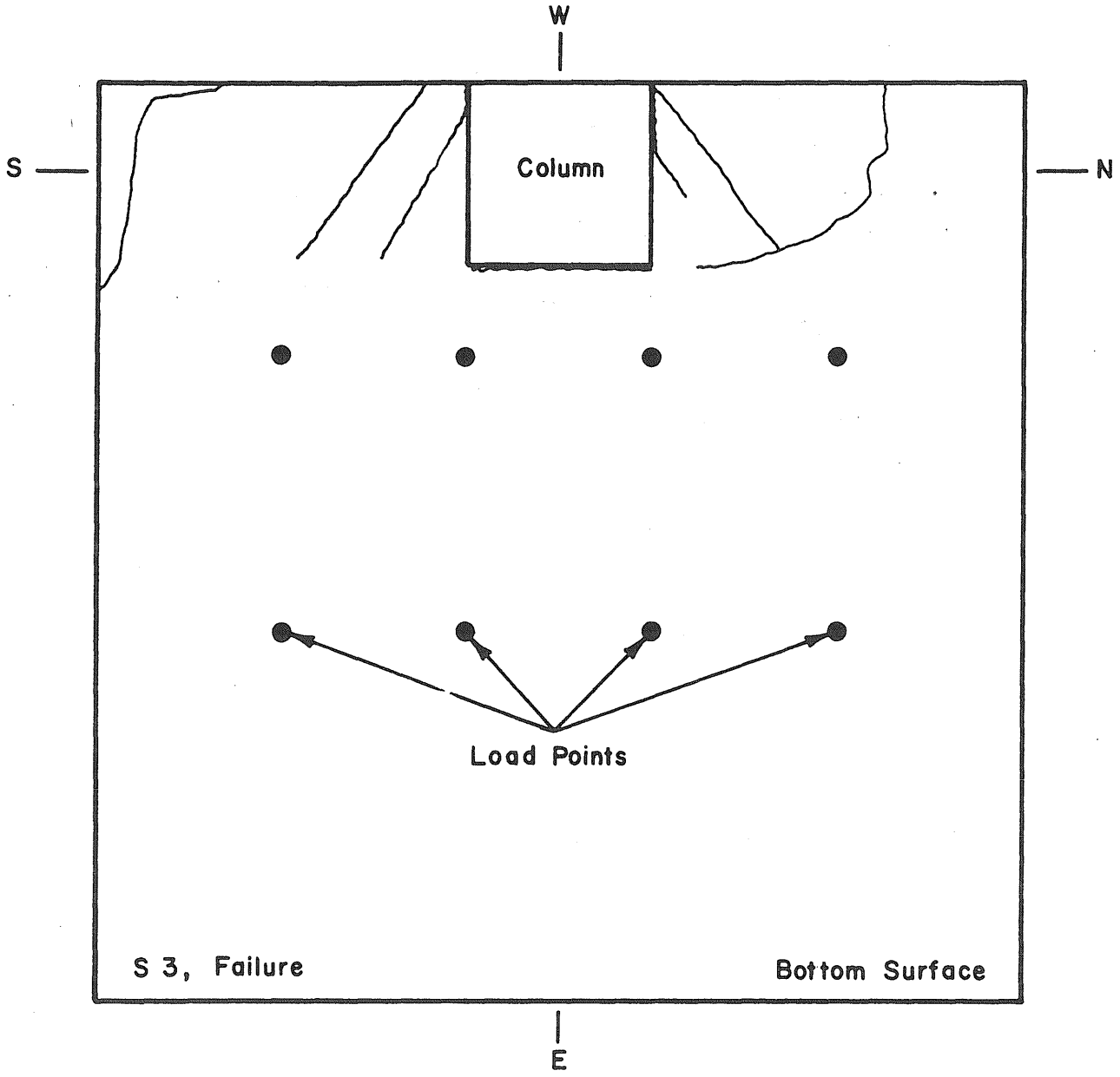

Fig. 4.40 Crack Pattern at Failure on the Bottom Surface of Specimen S3

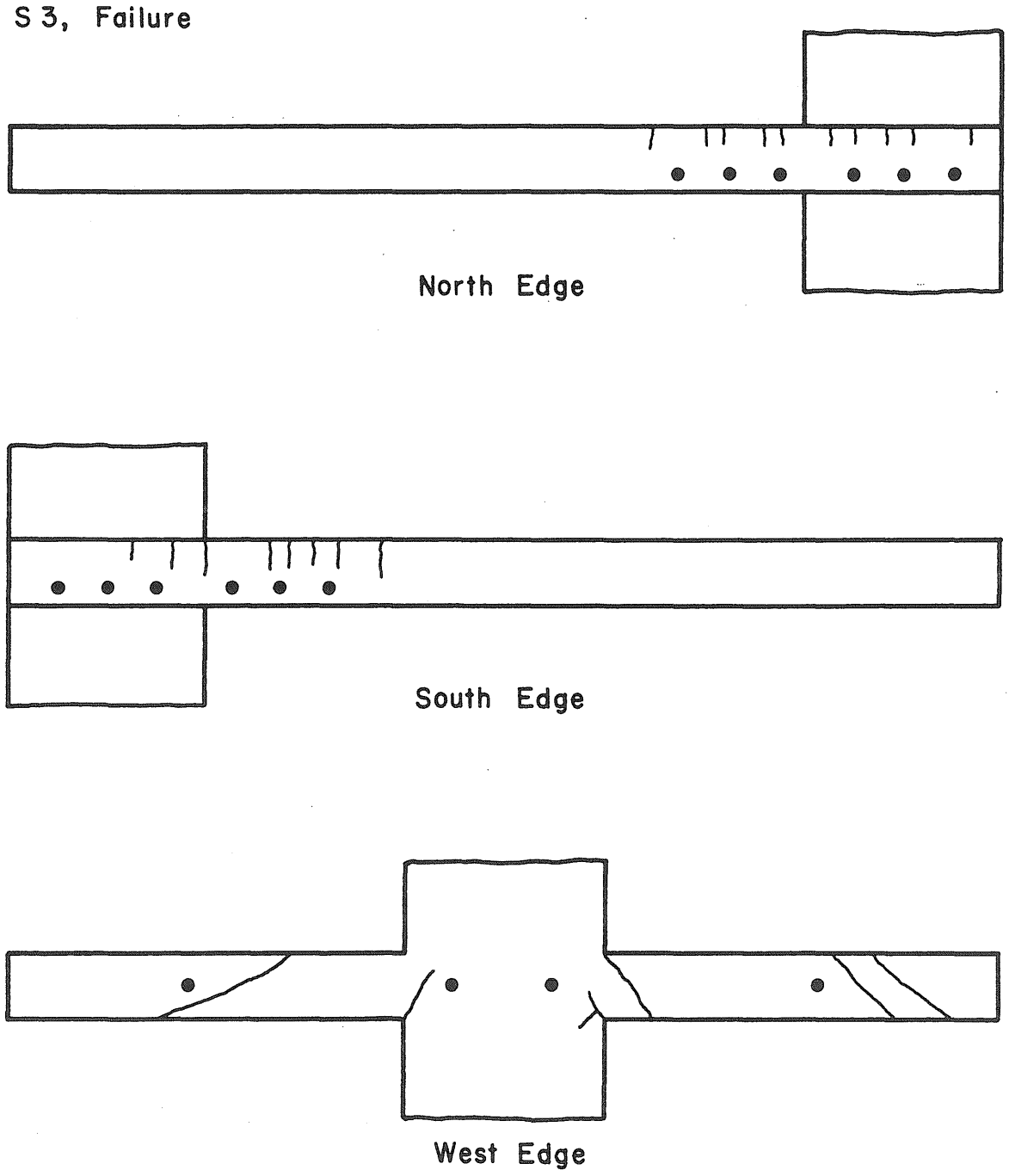

Fig. 4.41 Crack Pattern at Failure on the North, South and West Edges of Specimen S3

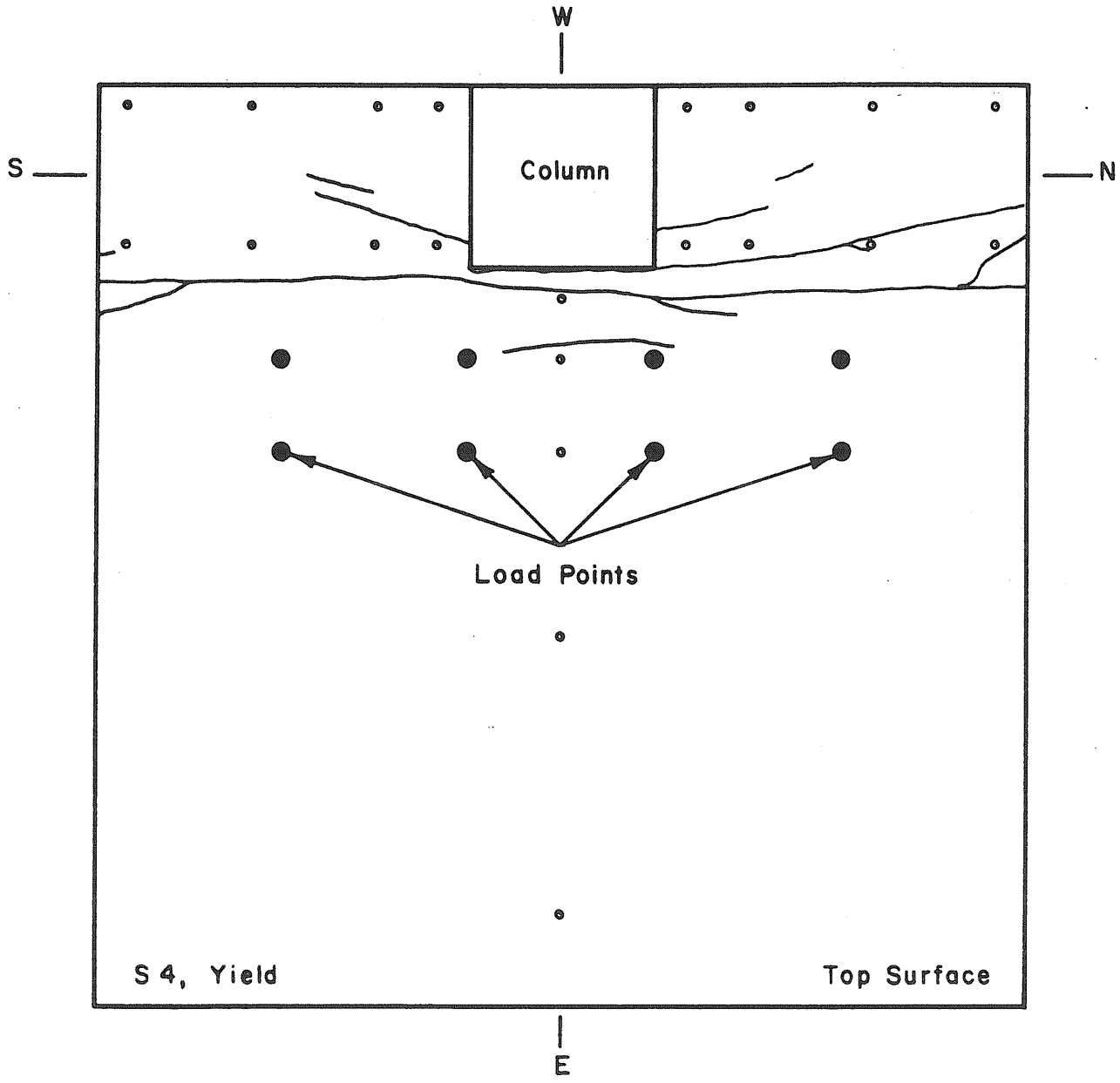

Fig. 4.42 Crack Pattern at Yield on the Top Surface of Specimen S4

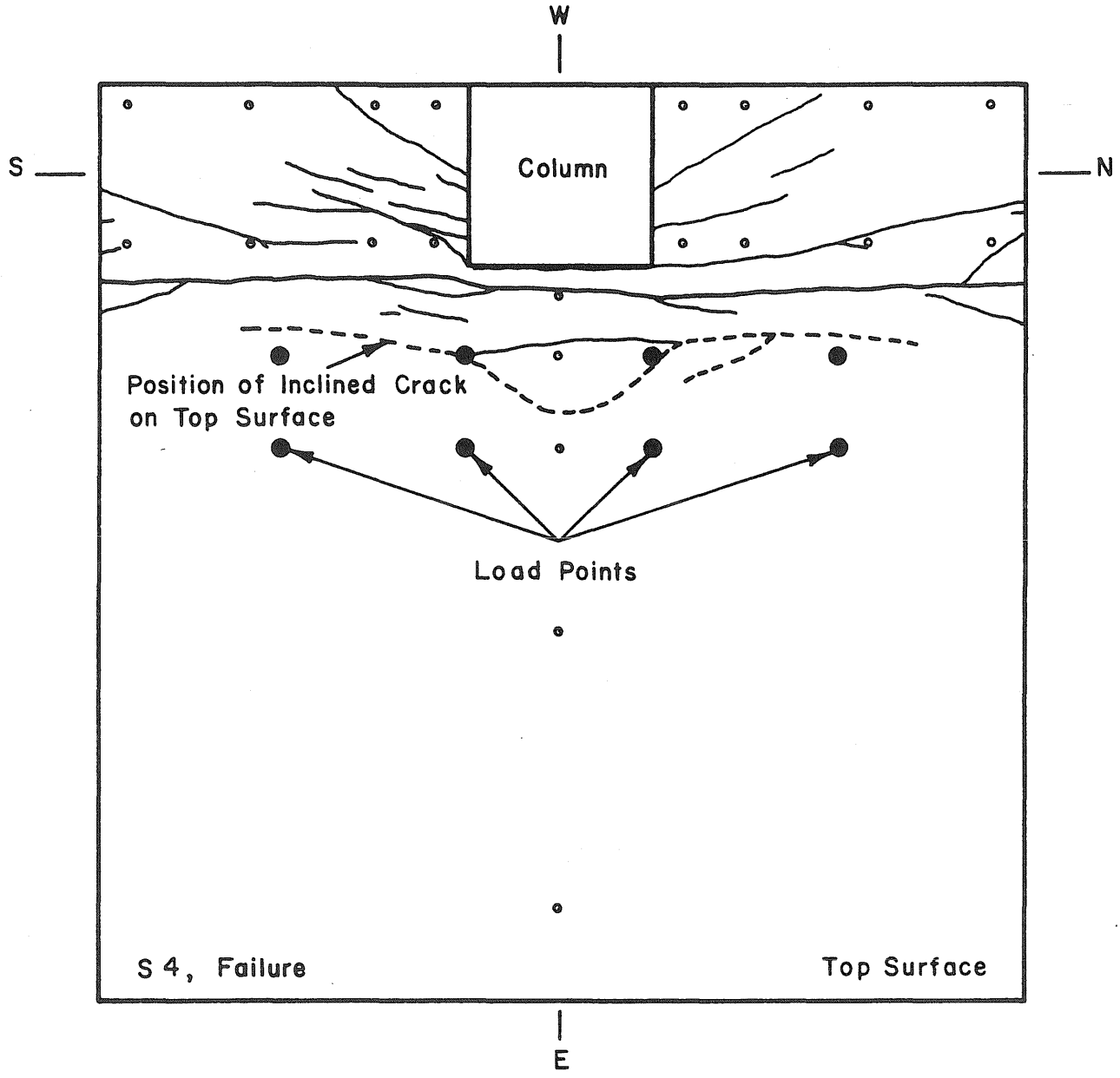

Fig. 4.43 Crack Pattern at Failure on the Top Surface of Specimen S4

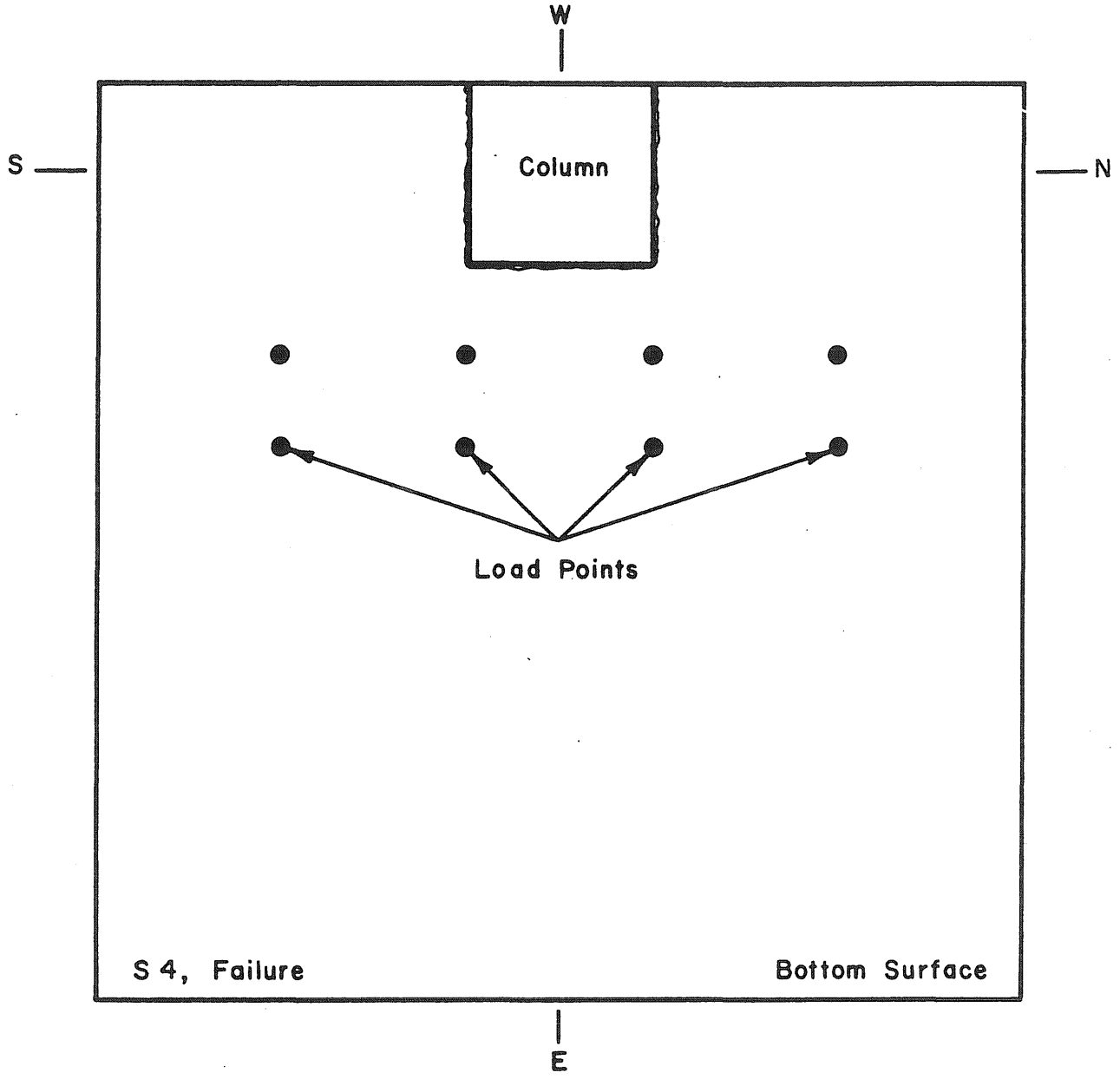

Fig. 4.44 Crack Pattern at Failure on the Bottom Surface of Specimen S4

S4, Failure

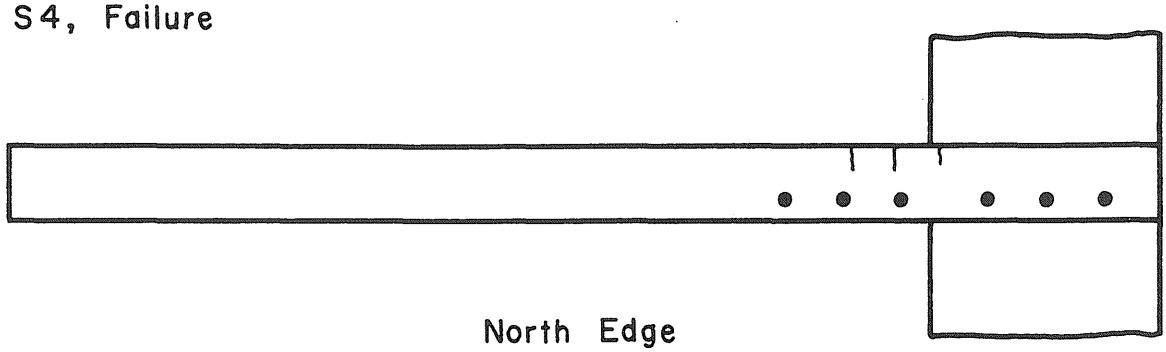

North Edge

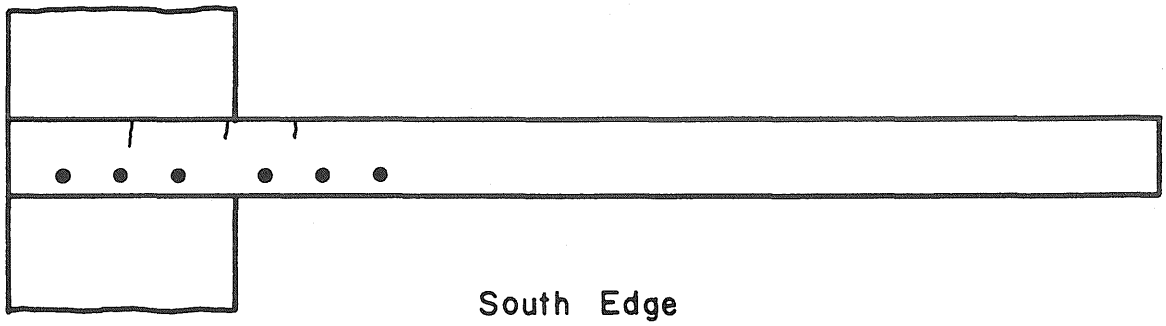

South Edge

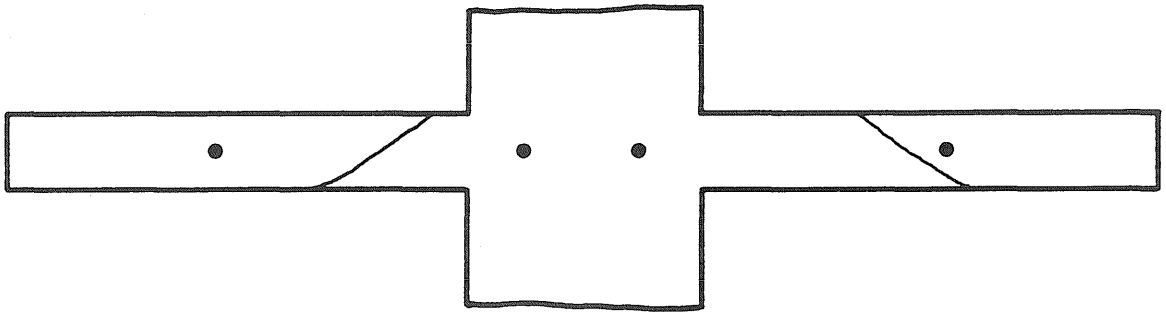

West Edge

Fig. 4.45 Crack Pattern at Failure on the North, South and West Edges of Specimen S4

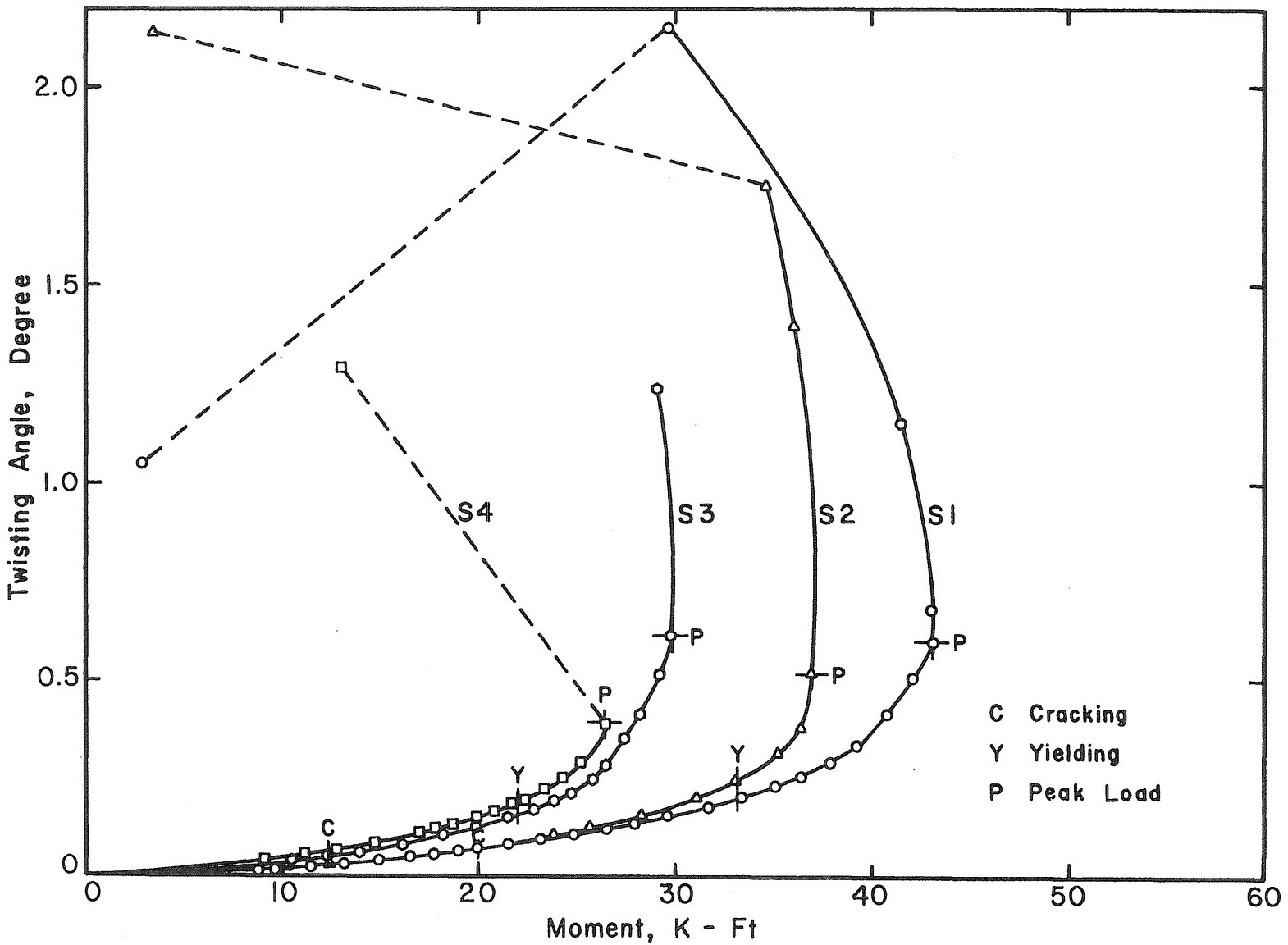

Fig. 4.46 Twisting Angle vs. Moment for All Specimens

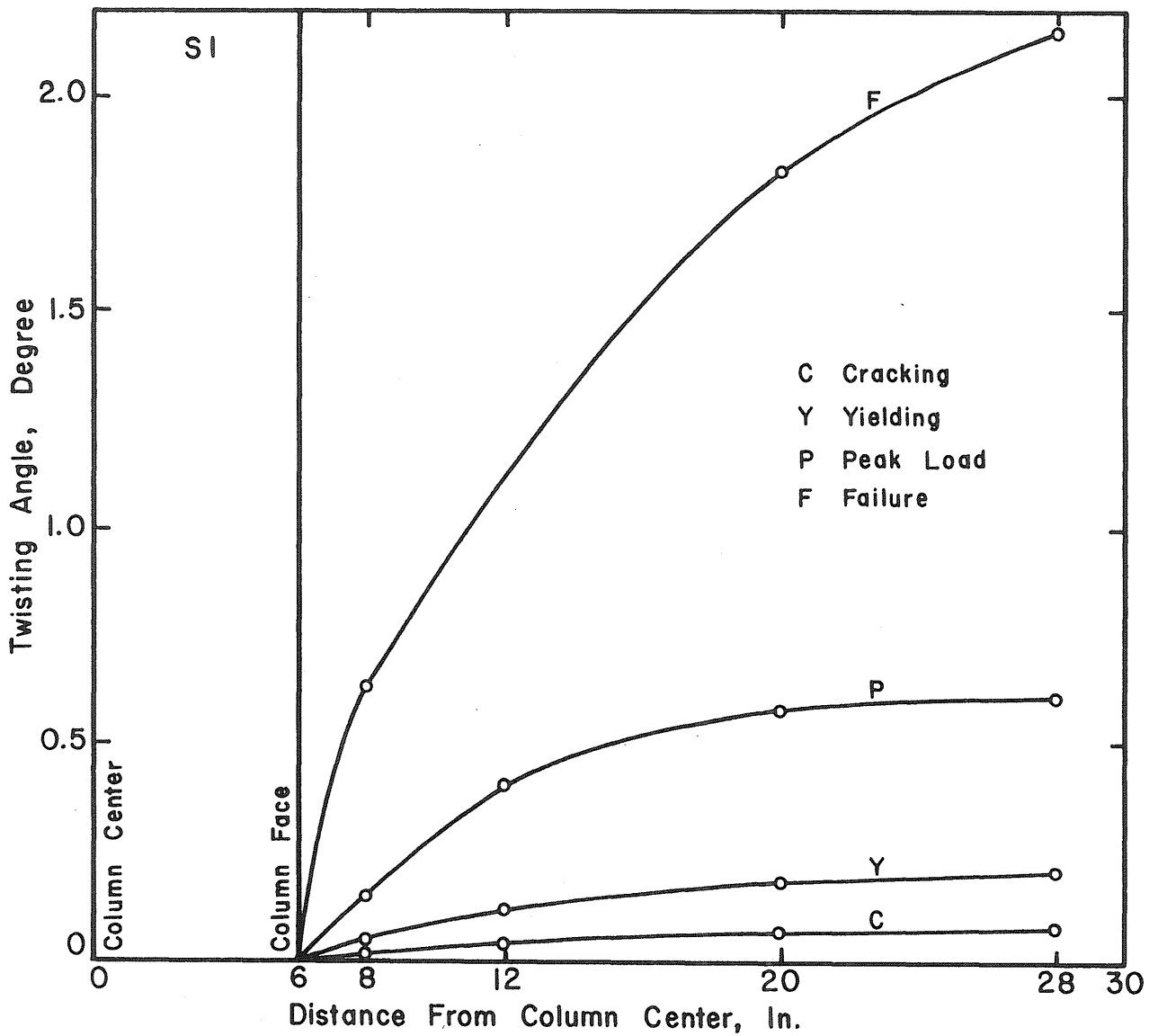

Fig. 4.47 Variation of Twisting Angles Along the Edges of Specimen S1

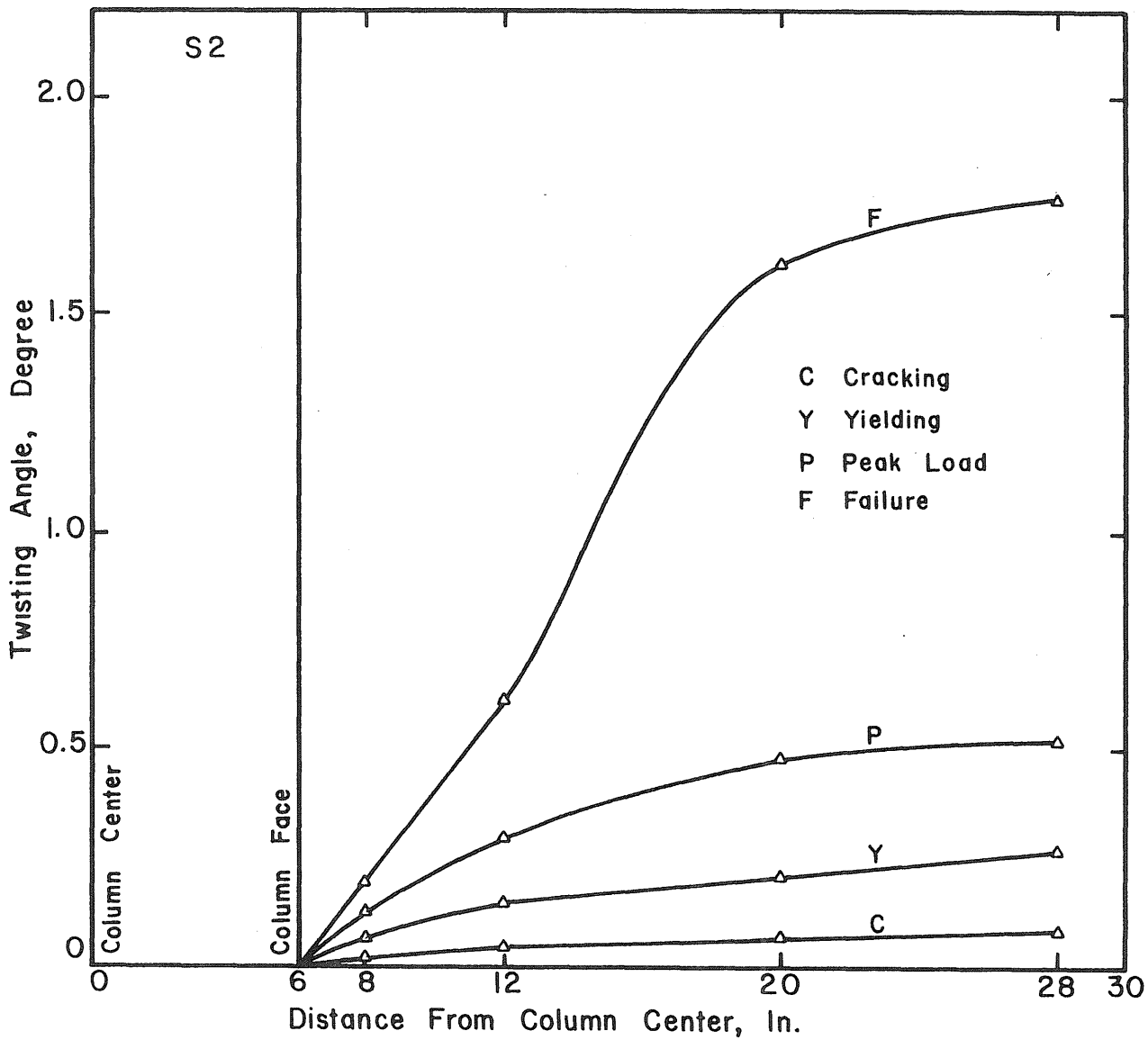

Fig. 4.48 Variation of Twisting Angles Along the Edges of Specimen S2

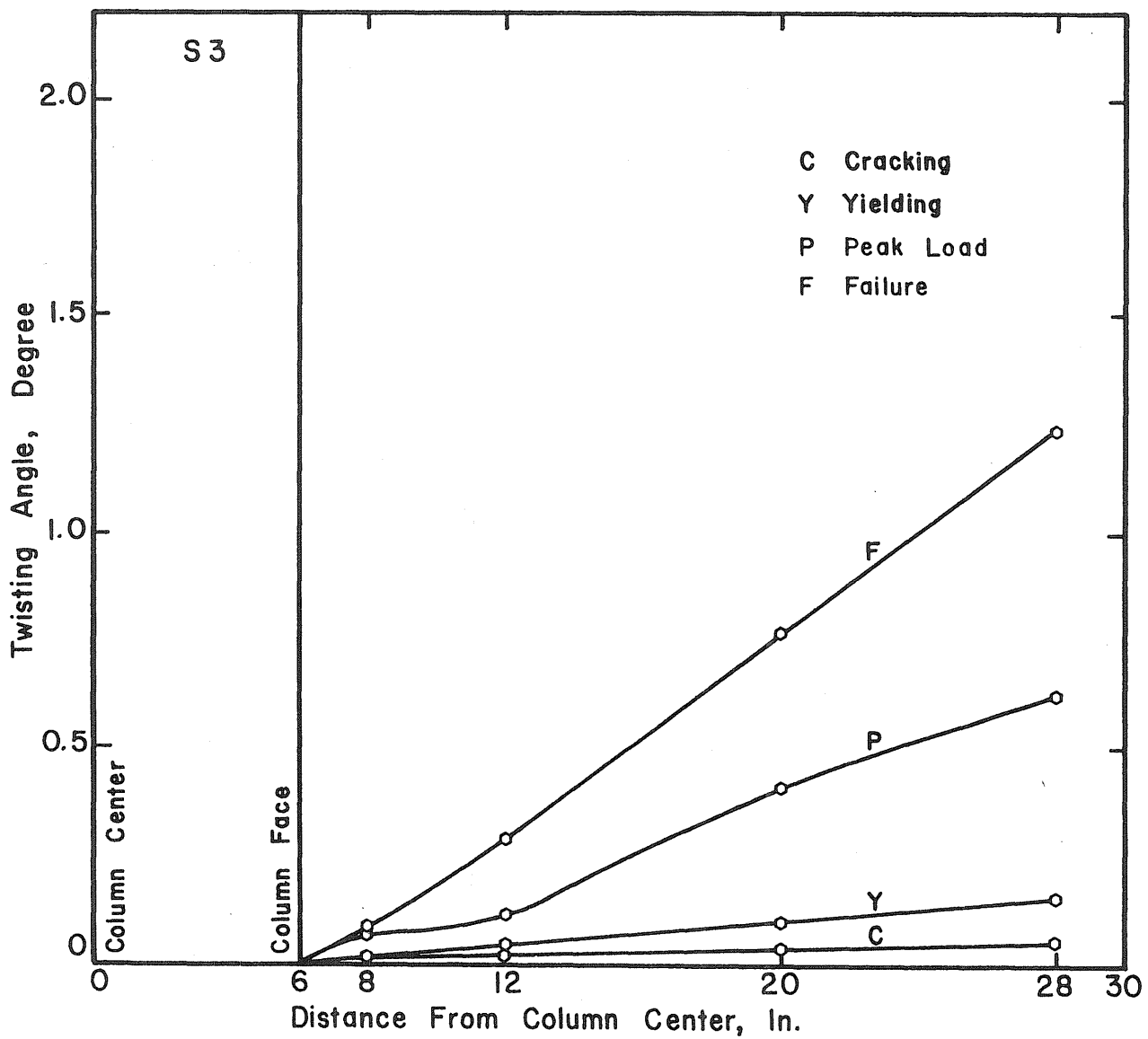

Fig. 4.49 Variation of Twisting Angles Along the Edges of Specimen S3

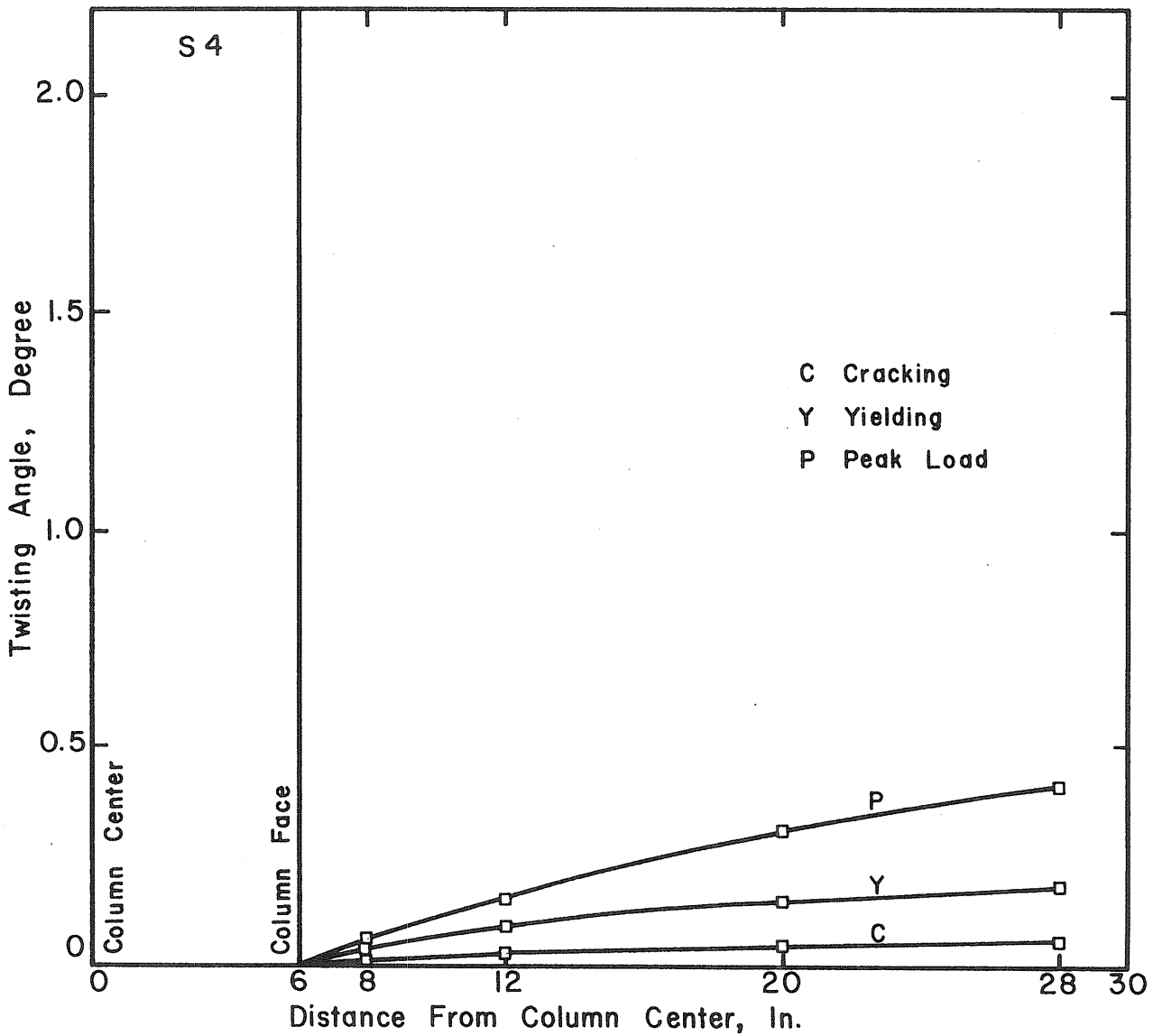

Fig. 4.50 Variation of Twisting Angles Along the Edges of Specimen S4

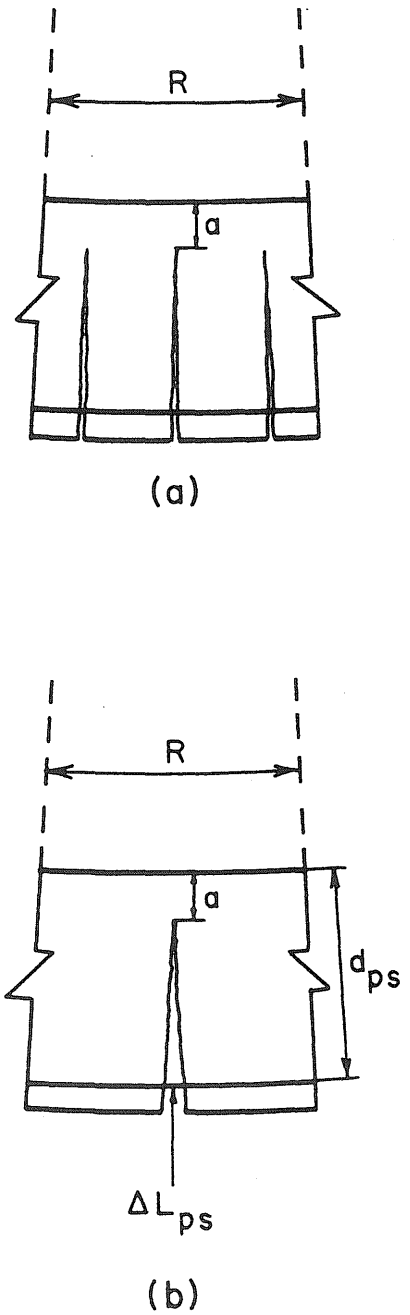

Fig. 5.1 Assumed Crack Model for Predicting the Increase in Unbonded Tendon Stress: (a) Actual Crack Distribution; (b) Assumed Crack Distribution

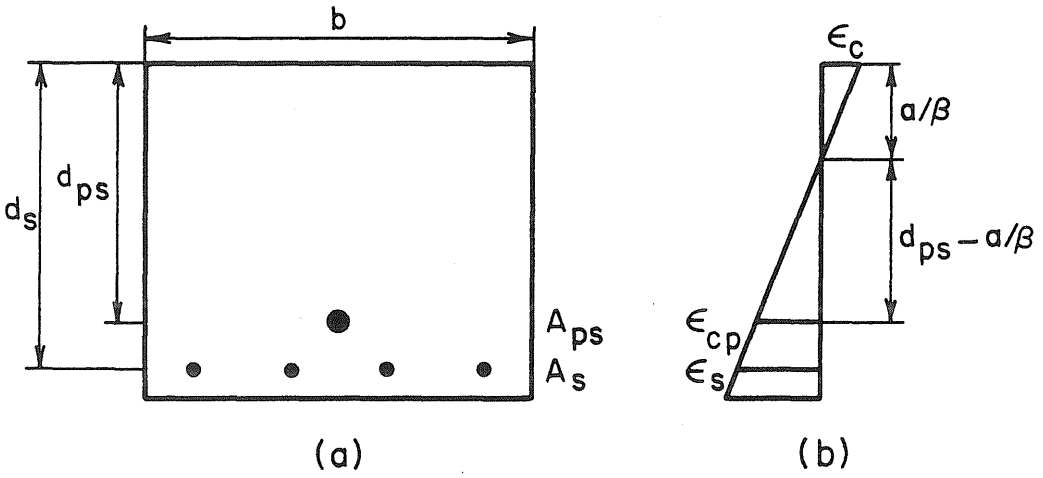

Fig. 5.2 Strain Distribution for Prestressed Concrete Member: (a) Cross-Section of Member; (b) Strain Distribution

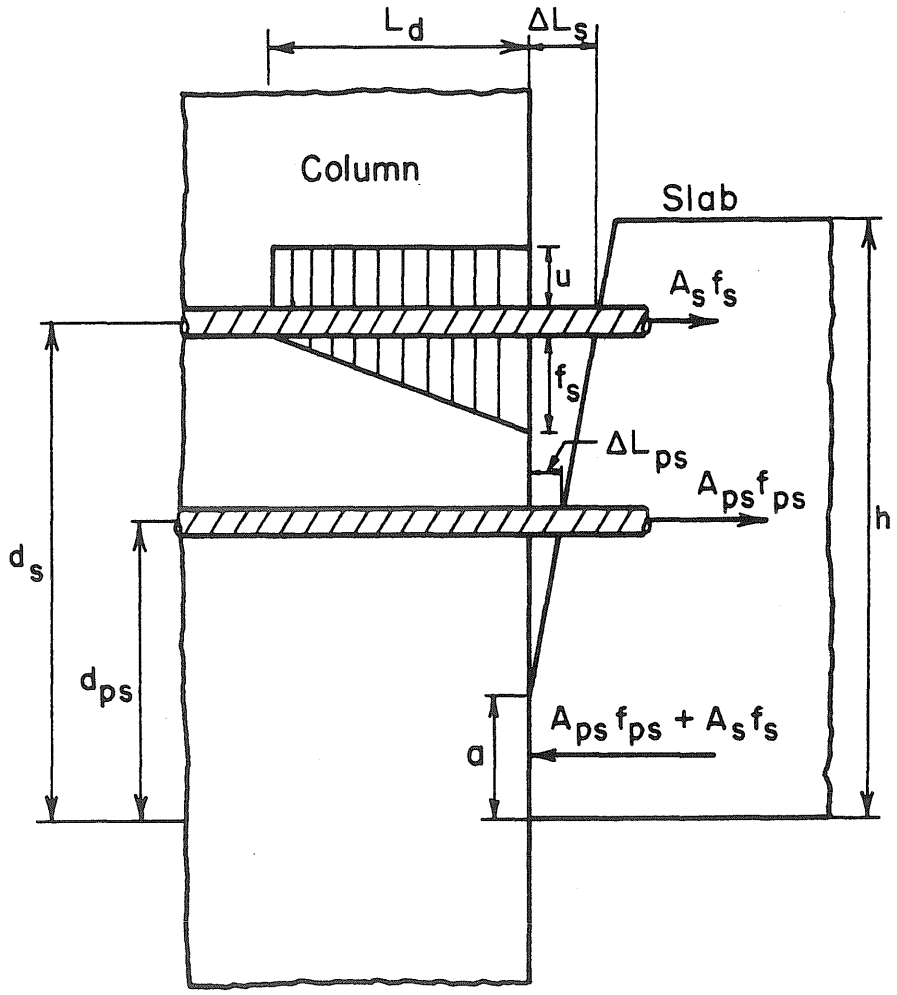

Fig. 5.3 Bond-Slip Model

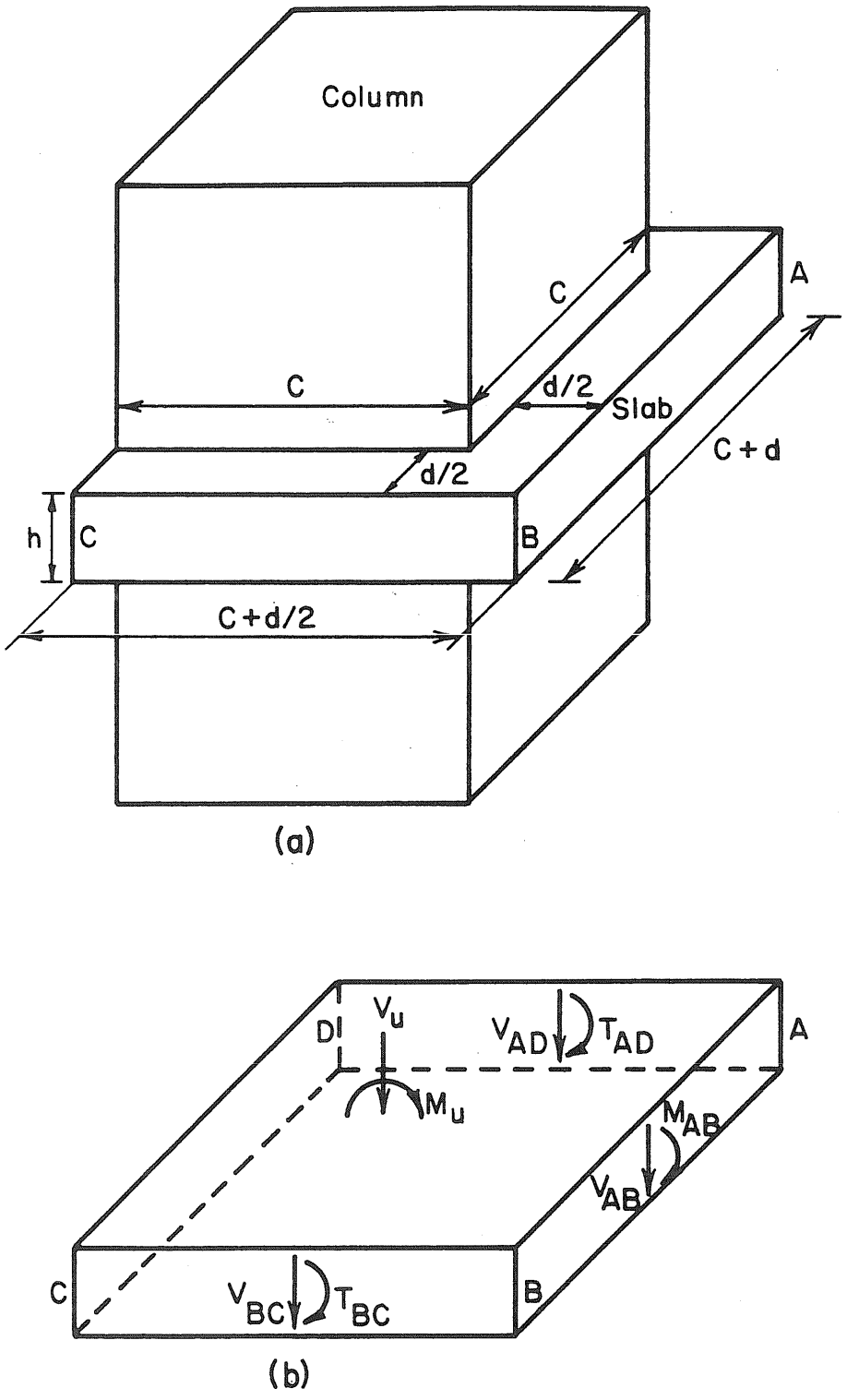

Fig. 5.4 Critical Section and Actions at Exterior Slab-Column Connection

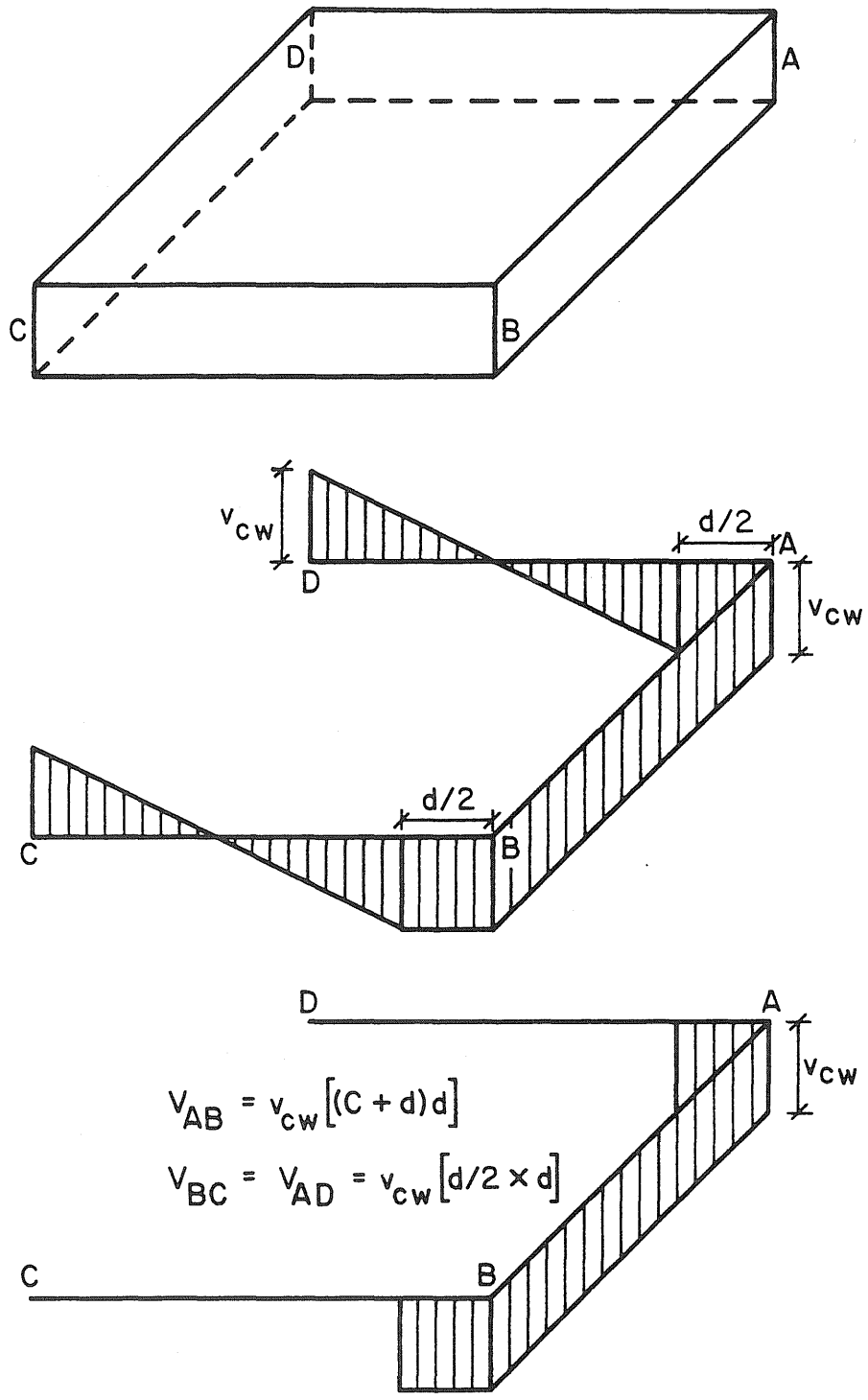

Fig. 5.5 Shear Distribution at the Critical Section for Over-Reinforced Member

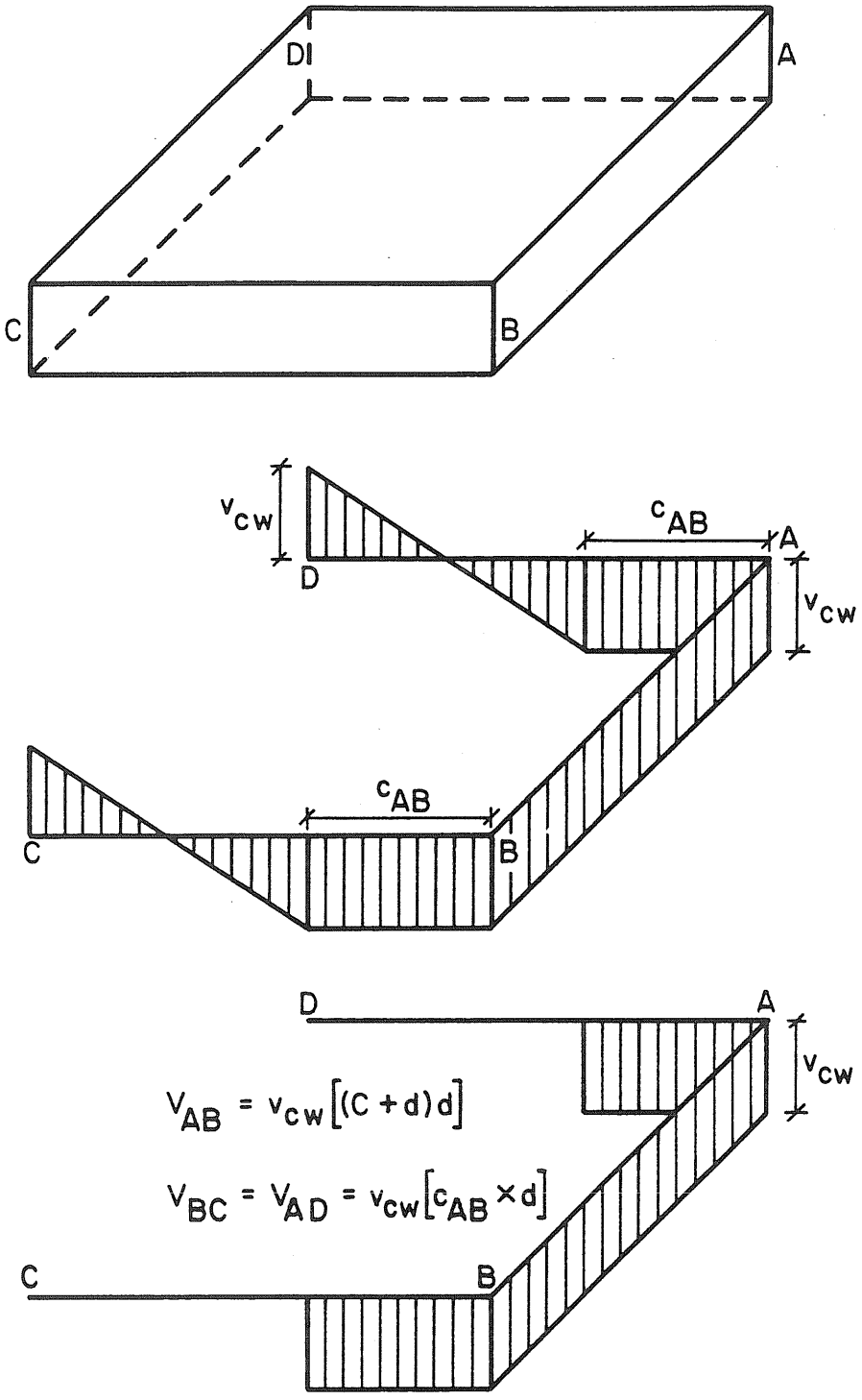

Fig. 5.6 Shear Distribution at the Critical Section for Under-Reinforced Member

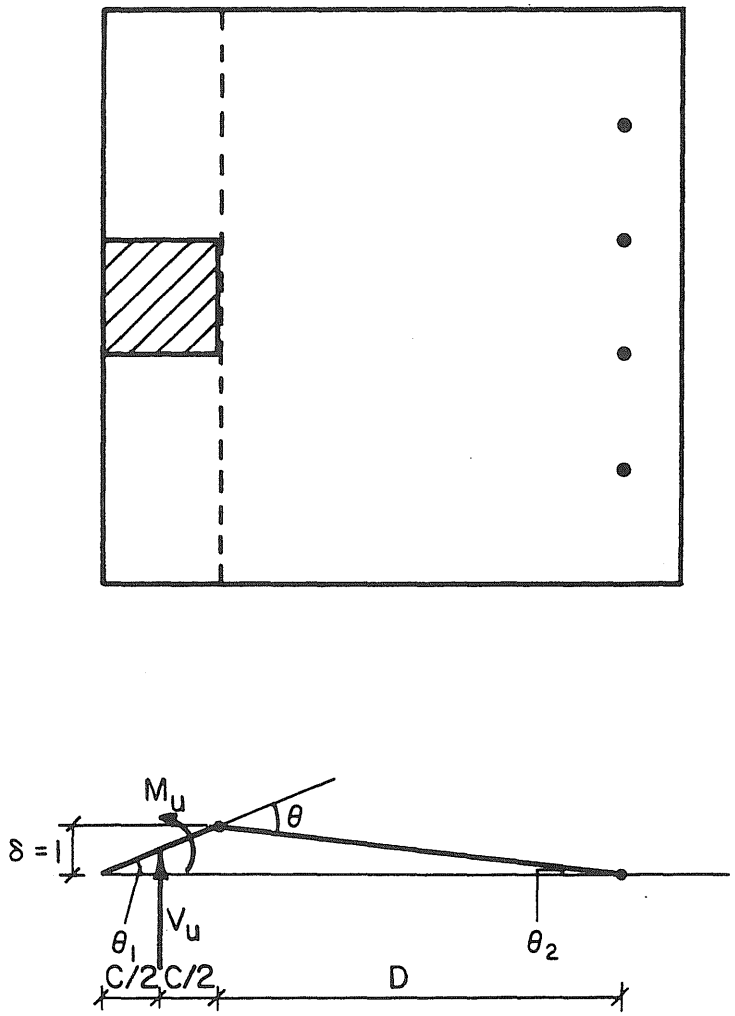

Fig. 5.7 Folding-Type Yield Line Pattern

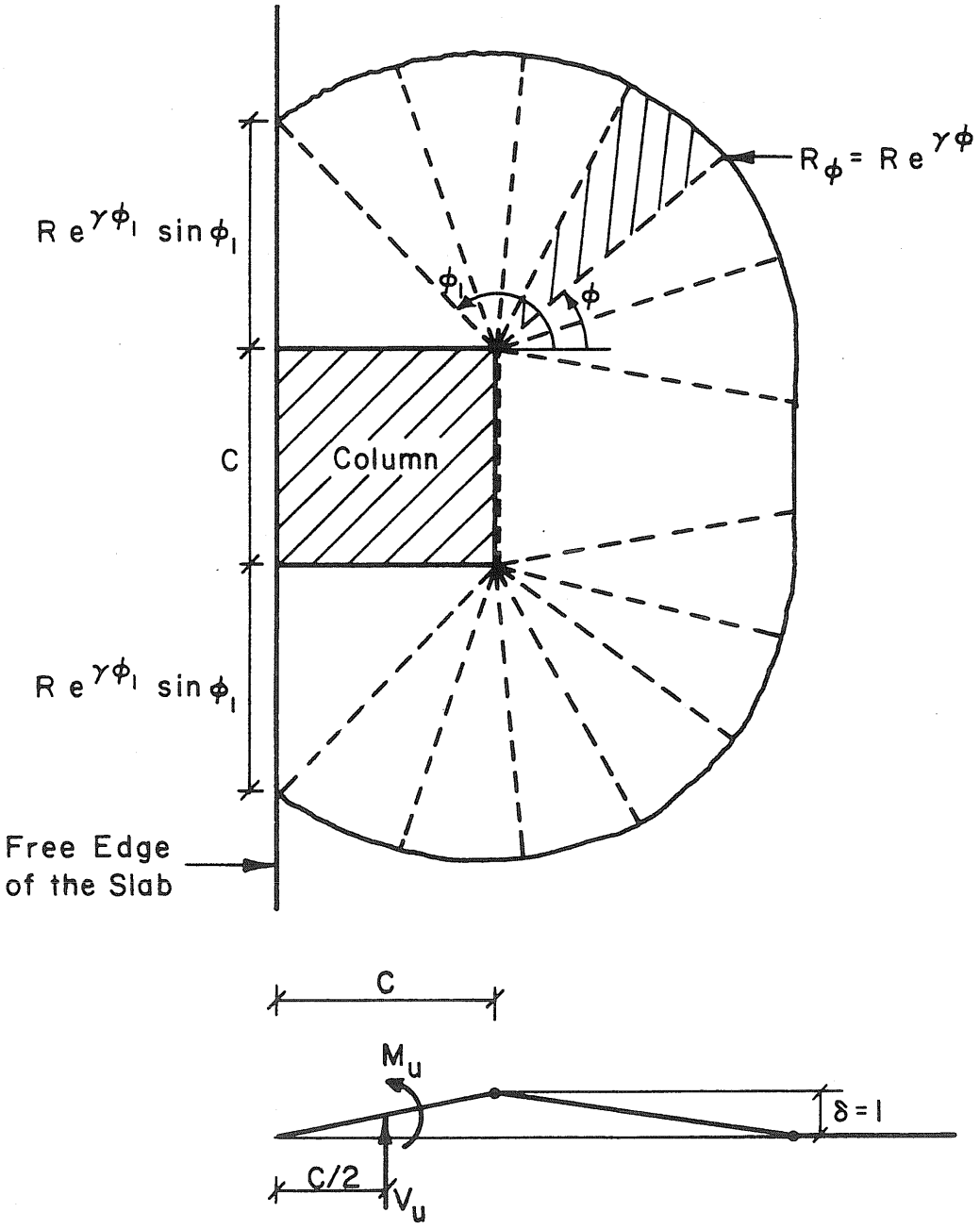

Fig. 5.8 Local Yield Line Pattern

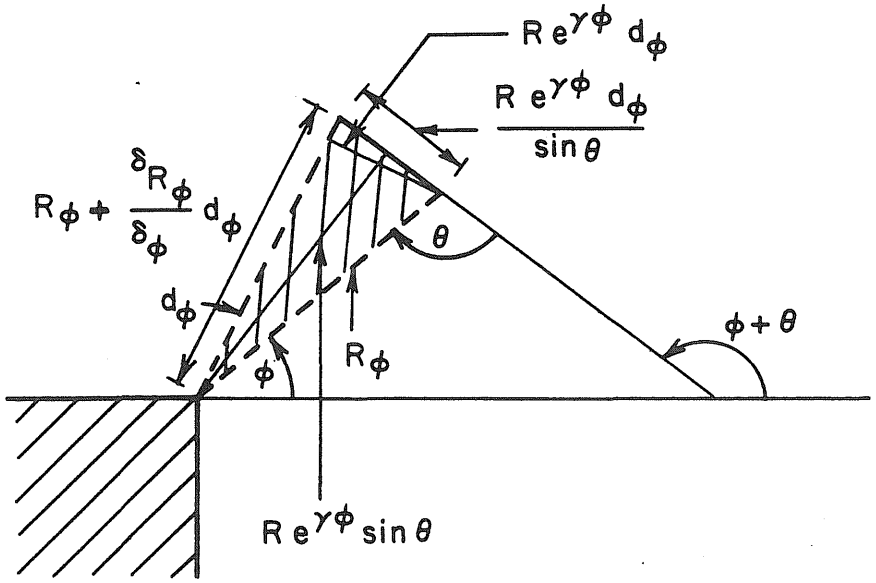

Fig. 5.9 One Segment of the Fan-Shaped Yield Line

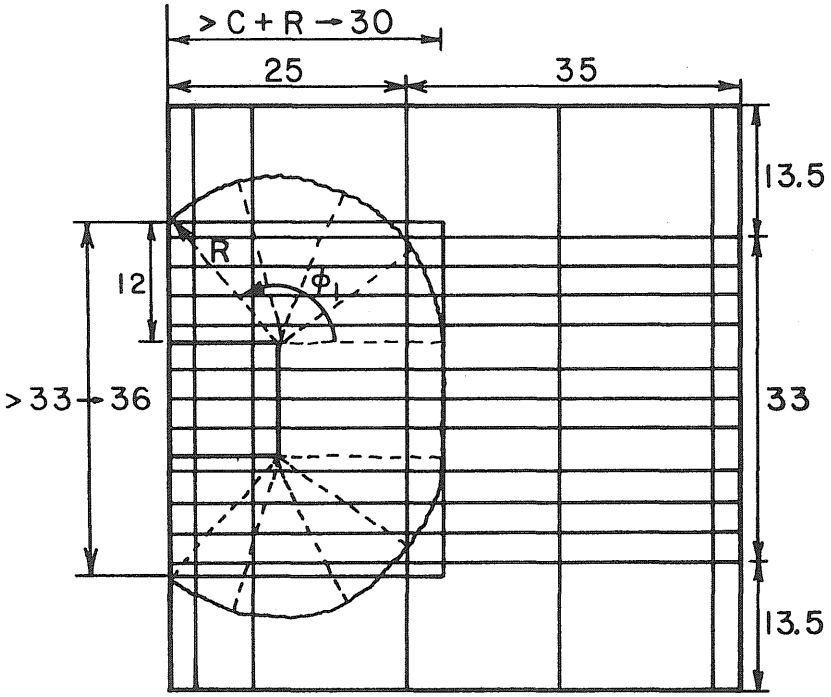

S1 & S2

R = 16.97"

ϕ_1 = 2.36 rad.

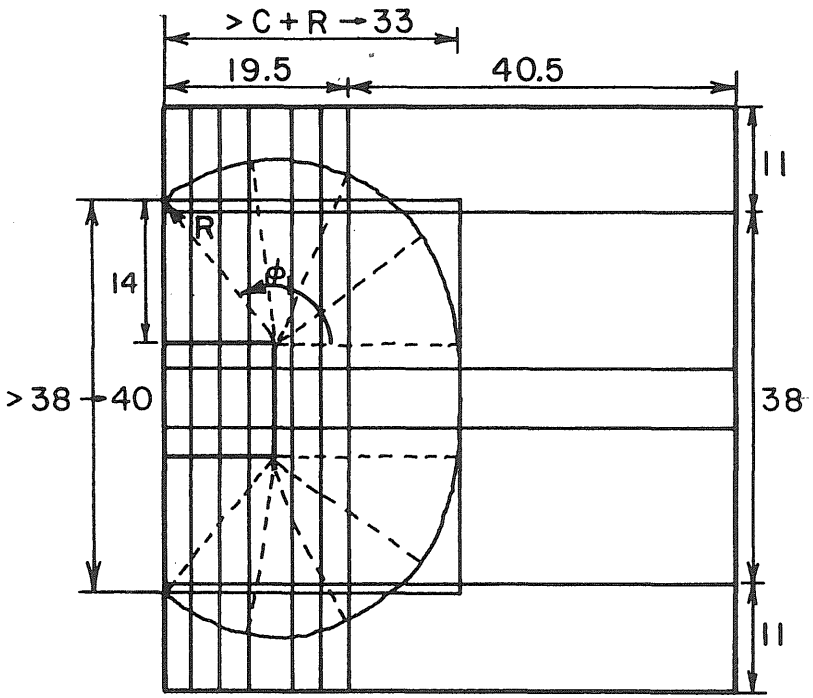

S 3 & S 4

R = 18.44"

ϕ_1 = 2.28 rad.

Fig. 5.10 Local Yield Line Patterns for S1, S2 and S3, S4

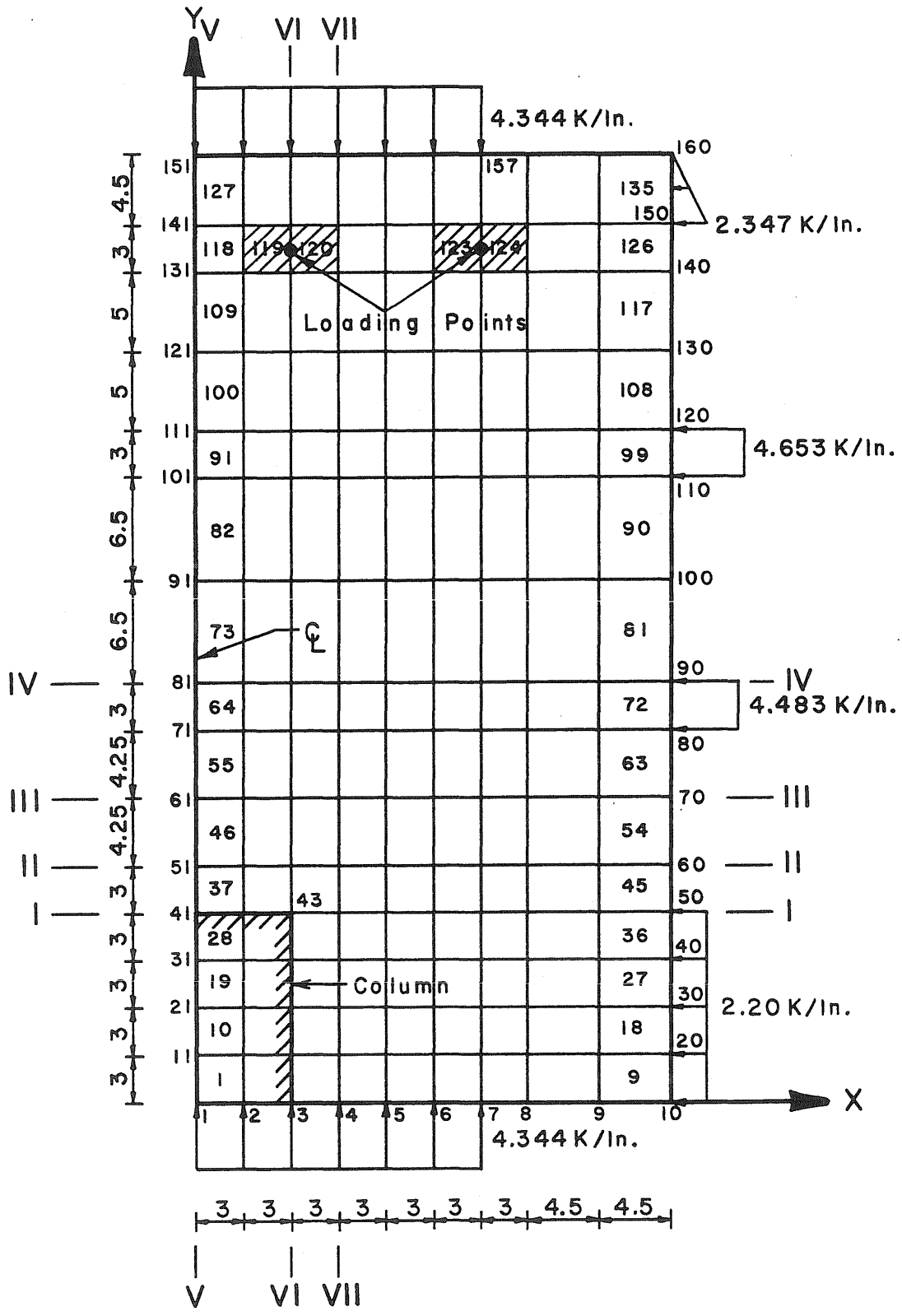

Fig. 5.11 Finite Element Mesh for Half of Specimen S1

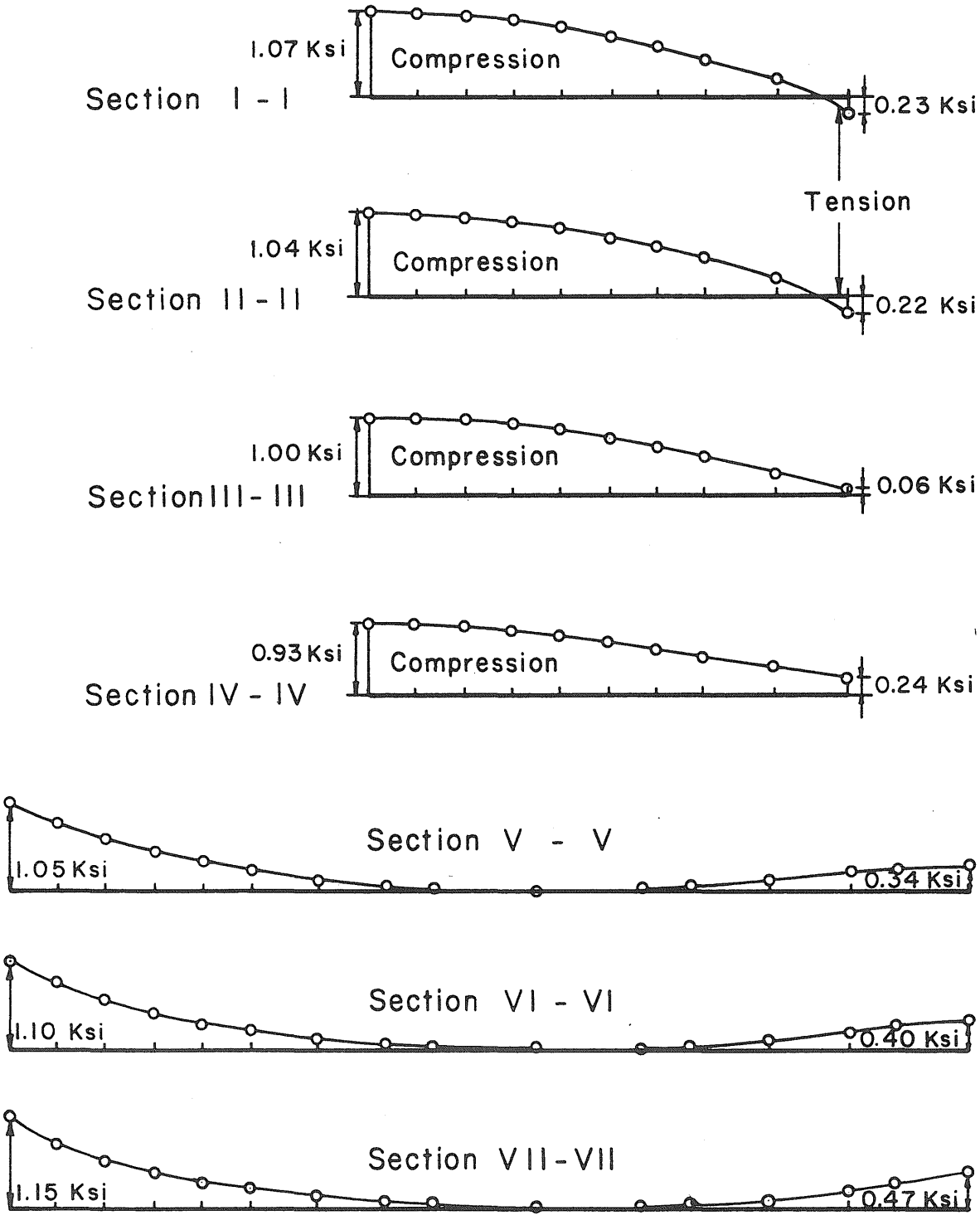

Fig. 5.12 Stress Distribution at the Top Surface of the Slab Due to Prestress Forces Only

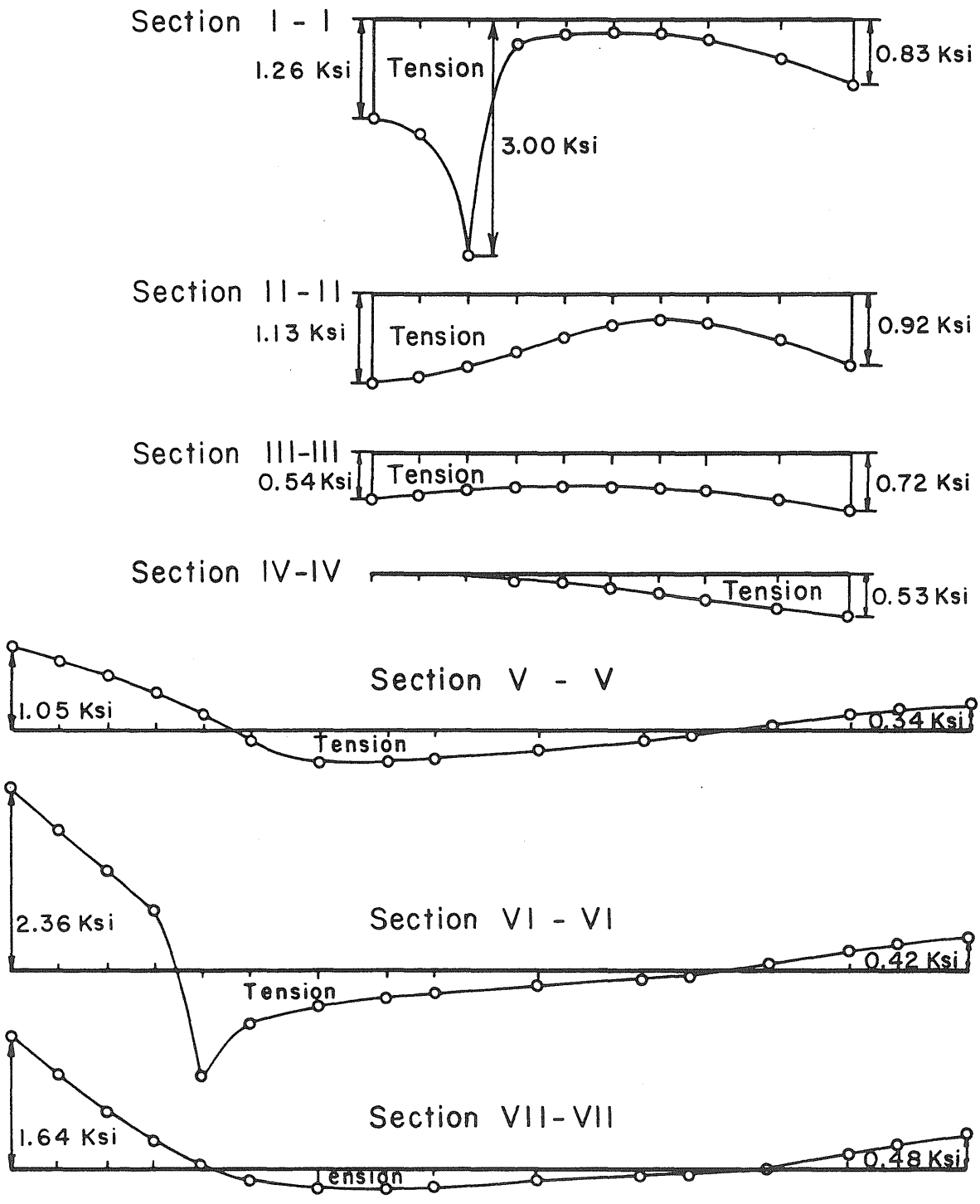

Fig. 5.13 Stress Distribution at the Top Surface of the Slab Due to Prestress Forces, Dead Load and Applied Loads

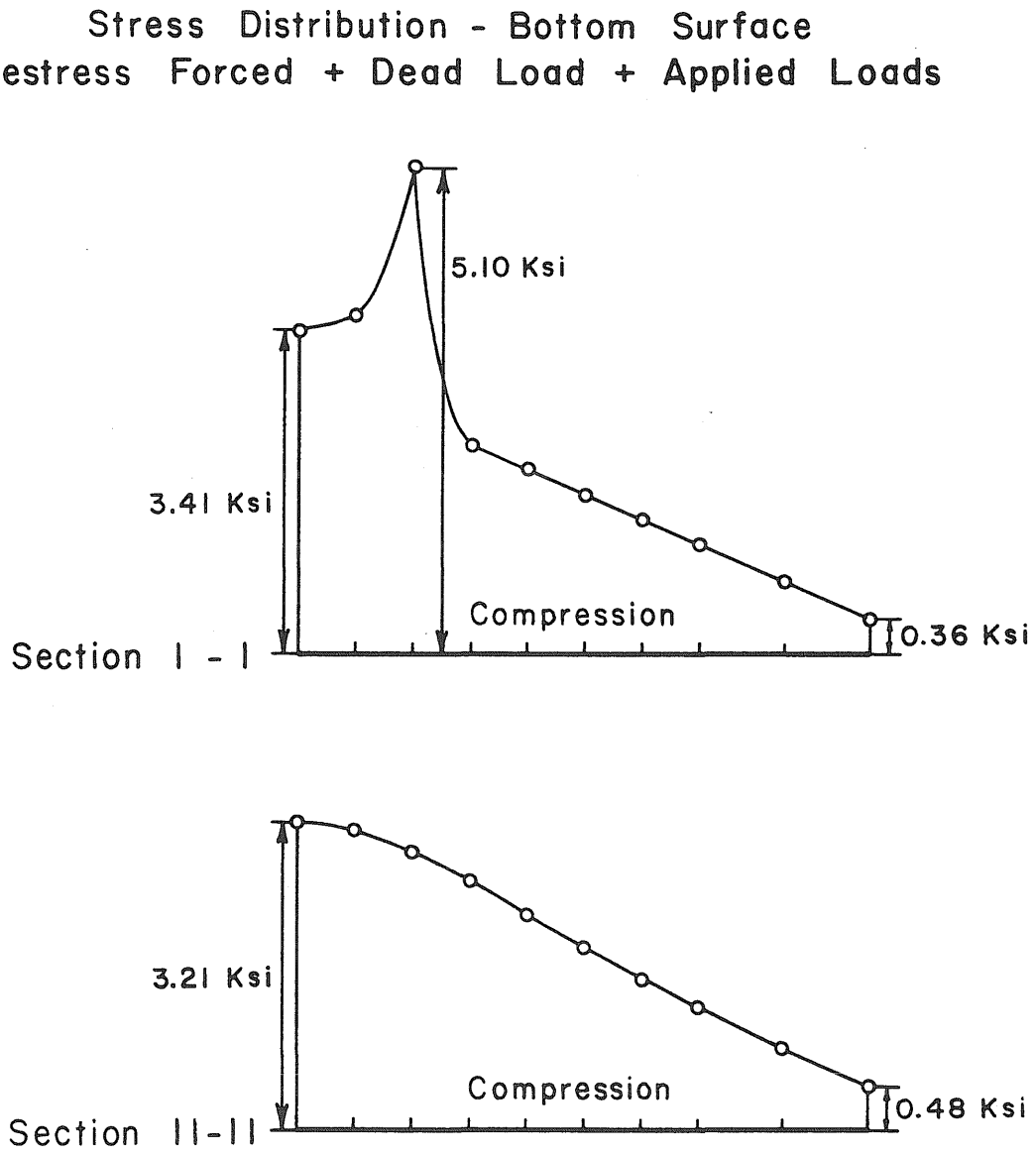

Fig. 5.14 Stress Distribution at the Bottom Surface of the Slab Due to Prestress Forces, Dead Load and Applied Loads

APPENDIX

NOTATION

A_c = area of concrete at assumed critical section

A_{ps} = area of prestressed reinforcement

A_s = area of nonprestressed bonded reinforcement

a = depth of equivalent rectangular stress block

b = width of section being considered

C = size of square column

C_1 = size of rectangular column, measured in the direction of the span for which moments are being determined

C_2 = size of rectangular column, measured transverse to the direction of the span for which moments are being determined

C_{AB} = distance from face AB of the critical section to centroidal axis CC

C_{CD} = distance from points C and D of the critical section to centroidal axis CC

D = distance from face of column to location of applied load

= nominal diameter of steel bar

d = effective depth of prestressed concrete slab, but not less than 0.8h

d_{ps} = distance from extreme compression fiber to centroid of prestressed reinforcement

d_s = distance from extreme compression fiber to centroid of nonprestressed bonded reinforcement

E = east

E_c = modulus of elasticity of concrete

E_{ps} = modulus of elasticity of prestressed reinforcement

E_s = modulus of elasticity of nonprestressed reinforcement

e = base of Napierian logarithms

f'_c = specified compressive strength of concrete

f_{pc} = average compressive stress in concrete due to effective prestress force only

f_{ps} = ultimate stress in prestressed reinforcement

f_{pu} = specified tensile strength of prestressing tendons

f_{py} = specified yield strength of prestressing tendons

f_r = modulus of rupture of concrete

f_{se} = effective stress in prestressed reinforcement at time of interest

f_t = tensile strength of concrete

f_y = specified yield strength of nonprestressed reinforcement

g = distance between the centroidal axis of the critical section, CC, and the centroidal axis of the column

h = overall thickness of the slab

J_c = property of assumed critical section analogous to polar moment of inertia

K = γ_v

= fraction of unbalanced moment transferred by eccentricity of shear at slab-column connections

= value defined by Eq. (5.72)

L = width of specimen

L_d = development length

L_{ps} = length of prestressing tendon

M_{AB} = ultimate resisting moment for face AB of the critical section

M_u = ultimate unbalanced bending moment, acting about the centroidal axis of the column section

m = negative yield moment per unit length

m' = positive yield moment per unit length

N = north

P_s = prestressing tendon force

R = dimension of yield fan in direction of bending

= rotation along a yield line

R_ϕ = radius of fan-shaped yield line

S = south

T_{AD} = ultimate resisting torsional moment acting on face AD of the critical section

T_{BC} = ultimate resisting torsional moment acting on face BC of the critical section

T_u = ultimate torsional capacity of rectangular prestressed beam

u = bond stress

V_{AB} = shear force acting on face AB of the critical section

V_{AD} = shear force acting on face AD of the critical section

V_{BC} = shear force acting on face BC of the critical section

V_{cw} = nominal shear strength provided by concrete when diagonal cracking results from excessive principal tensile stress in web

V_p = vertical component of effective prestress force at section

V_u = ultimate shear force, acting about the centroidal axis of the column section

v_{AB} = shear stress on face AB of the critical section

v_C = shear stress at point C of the critical section

v_D = shear stress at point D of the critical section

v_c = permissible shear stress carried by concrete

v_t = maximum torsional shear stress

W = west

W_h = plastic hinge width

x = shorter overall dimension of rectangular part of cross section

y = longer overall dimension of rectangular part of cross section

α = shape factor

β_1 = ratio of equivalent depth a to neutral axis depth

β_c = ratio of long side to short side of column

γ = $1/\tan\theta$

γ_v = fraction of unbalanced moment transferred by eccentricity of shear at slab-column connections

ϵ = strain

ϵ_c = limit of concrete strain

ϵ_{cp} = strain in concrete at tendon level

ϵ_{ps} = total strain in tendon at ultimate

ϵ_{s} = strain in bonded reinforcement

ϵ_{se} = strain in tendon due to effective prestress

θ = angle between radial and circumferential yield lines

= rotation along a folding-type yield line

μ = coefficient of orthotropy

ρ_p = ratio of prestressed reinforcement

ϕ = angle measured from X axis

ϕ = plastic hinge width parameter

$$\omega = \frac{\frac{A_s}{bd} f_y}{f'_c}$$

$$\omega_p = \frac{\frac{A_{ps}}{bd} f_{ps}}{f'_c}$$

REFERENCES

1. ACI Committee 318, "Building Code Requirements for Reinforced Concrete (ACI 318-77)," American Concrete Institute, Detroit, 1977.

2. ACI Committee 318, "Commentary on Building Code Requirements for Reinforced Concrete (ACI 318-77)," American Concrete Institute, Detroit, 1977.

3. ACI Committee 318, "Building Code Requirements for Reinforced Concrete (ACI 318-71)," American Concrete Institute, Detroit, 1971.

4. ACI Committee 318, "Building Code Requirements for Reinforced Concrete (ACI 318-63)," American Concrete Institute, Detroit, 1963.

5. ACI-ASCE Committee 326, "Shear and Diagonal Tension. Part 3-Slabs and Footings," Journal of the American Concrete Institute, Vol. 59, No. 3, March, 1962, pp. 352-396.

6. ACI-ASCE Committee 423, "Tentative Recommendations for Prestressed Concrete Flat Plates," Journal of the American Concrete Institute, Vol. 71, No. 2, February, 1974, pp. 61-71.

7. ASCE-ACI Committee 426, "The Shear Strength of Reinforced Concrete Members-Slabs," Journal of the Structural Division, ASCE, Vol. 100, No. ST8, August, 1974, pp. 1543-1591.

8. ASCE-ACI Committee 426, "Suggested Revisions to Shear Provisions for Building Codes," Journal of the American Concrete Institute, Vol. 74, No. 9, September, 1977, pp. 458-469.

9. Burns, N.H., and Hemakom, R., "Test of a Scale Model Post-Tensioned Flat Plate," Journal of the Structural Division, ASCE, Vol. 103, No. ST6, June, 1977, pp. 1237-1255.

10. Charney, F.A., "Strength and Behavior of a Partially Prestressed Concrete Slab with Unbonded Tendons," thesis presented to The University of Texas, at Austin, Texas, in 1976, in partial fulfillment of the requirements for the degree of Master of Science.

11. Cooke, N., Park, R., and Yong, P., "Flexural Strength of Prestressed Concrete Members with Unbonded Tendons," Journal of the Prestressed Concrete Institute, Vol. 26, No. 6, November-December, 1981, pp. 52-80.

12. Criswell, M.E., "Strength and Behavior of Reinforced Concrete Slab-Column Connections Subjected to Static and Dynamic Loadings," December, 1970, U.S. Army Engineer Waterways Experiment Station, Vicksburg, Mississippi, Technical Report N-70-1 (Final Report).

13. Criswell, M.E., and Hawkins, N.M., "Shear Strength of Slabs-Basic Principles and Their Relation to Current Methods of Analysis," Shear in Reinforced Concrete, ACI Special Publication SP-42, American Concrete Institute, Detroit, 1974, pp. 641-676.

14. "Design of Post-Tensioned Slabs," Post-Tensioning Institute, Phoenix, Arizona, 1977.

15. DiStasio, J., and Van Buren, M.P., "Transfer of Bending Moment between Flat Plate Floor and Column," Journal of the American Concrete Institute, Vol. 57, No. 3, September, 1960, pp. 299-314.

16. Gesund, H., and Goli, H.B., "Limit Analysis of Flat-Slab Buildings for Lateral Loads," Journal of the Structural Division, ASCE, Vol. 105, No. ST11, November, 1979, pp. 2187-2202.

17. Goli, H.B., and Gesund, H., "Flexural Strength of Flat Slabs at Exterior Columns," to be published in the Journal of the Structural Division, ASCE.

18. Hanson, N.W., and Hanson, J.M., "Shear and Moment Transfer between Concrete Slabs and Columns," Journal of the PCA Research and Development Laboratories, PCA, Vol. 10, No. 1, January, 1968, pp. 2-16.

19. Hawkins, N.M., "Shear Strength of Slabs with Moments Transferred to Columns," Shear in Reinforced Concrete, ACI Special Publication SP-42, American Concrete Institute, Detroit, 1974, pp. 817-846.

20. Hawkins, N.M., "Lateral Load Resistance of Unbonded Post-Tensioned Flat Plate Construction," Journal of the Prestressed Concrete Institute, Vol. 26, No. 1, January-February, 1981, pp. 94-116.

21. Hawkins, N.M., and Corley, W.G., "Transfer of Unbalanced Moment and Shear from Flat Plates to Columns," Cracking, Deflection, and Ultimate Load of Concrete Slab Systems, ACI Special Publication SP-30, American Concrete Institute, Detroit, 1971, pp. 147-176.

22. Hawkins, N.M., Criswell, M.E., and Roll, F., "Shear Strength of Slabs without Shear Reinforcement," Shear in Reinforced Concrete, ACI Special Publication SP-42, American Concrete Institute, Detroit, 1974, pp. 677-720.

23. Hemakom, R., "Strength and Behavior of Post-Tensioned Flat Plates with Unbonded Tendons," thesis presented to The University of Texas, at Austin, Texas, in 1975, in partial fulfillment of the requirements for the degree of Doctor of Philosophy.

24. Hsu, T.T.C., "Torsion of Structural Concrete-Uniformly Prestressed Rectangular Members without Web Reinforcement," Journal of the Prestressed Concrete Institute, Vol. 13, No. 2, April, 1968, pp. 34-44.

25. Islam, S., and Park, R., "Tests on Slab-Column Connections with Shear and Unbalanced Flexure," Journal of the Structural Division, ASCE, Vol. 102, No. ST3, March, 1976, pp. 544-568.

26. Kanoh, Y., and Yoshizaki, S., "Strength of Slab-Column Connections Transferring Shear and Moment," Journal of the American Concrete Institute, Vol. 76, No. 3, March, 1979, pp. 461-478.

27. Kosut, G.M., "Shear Strength of a Post-Tensioned Concrete Flat Plate at the Column Connections," thesis presented to The University of Texas, at Austin, Texas, in 1977, in partial fulfillment of the requirements for the degree of Master of Science.

28. Lin, T.Y., and Burns, N.H., Design of Prestressed Concrete Structures, John Wiley and Sons, 1981.

29. Long, A.E., and Bond, D., "Punching Failure of Reinforced Concrete Slabs," Proceedings, Institution of Civil Engineers, London, England, May, 1967, pp. 109-136.

30. Lopez, L.A., Dodds, R.H., Rehak, D.R., and Urzua, J., "Polo-Finite: A Structural Mechanics System for Linear and Nonlinear Analysis," Civil Engineering Systems Laboratory, University of Illinois at Urbana-Champaign, and Department of Civil Engineering and the Academic Computer Center, University of Kansas, Lawrence, Kansas.

31. Mast, P.E., "Plate Stresses at Columns Near the Free Edge," Journal of the American Concrete Institute, Vol. 67, No. 11, November, 1970, pp. 898-902.

32. Masterson, D.M., and Long, A.E., "The Punching Strength of Slabs, A Flexural Approach Using Finite Elements," Shear in Reinforced Concrete, ACI Special Publication SP-42, American Concrete Institute, Detroit, 1974, pp. 747-768.

33. Mattock, A.H., Yamakazi, J., and Kattula, B.T., "Comparative Study of Prestressed Concrete Beams, with and without Bond," Journal of the American Concrete Institute, Vol. 68, No. 2, February, 1971, pp. 116-125.

34. Moe, J., "Shearing Strength of Reinforced Concrete Slabs and Footings under Concentrated Loads," Development Department Bulletin D47, Portland Cement Association, April, 1961.

35. Mojtahedi, S., and Gamble, W.L., "Ultimate Steel Stresses in Unbonded Prestressed Concrete," Journal of the Structural Division, ASCE, Vol. 104, No. ST7, July, 1978, pp. 1159-1165.

36. Mojtahedi, S., and Gamble, W.L., "Preliminary Tests of Span-Depth Ratio Effects in Post-Tensioned Concrete," unpublished report.

37. Morrison, D.G., and Sozen, M.A., "Response of Reinforced Concrete Plate-Column Connections to Dynamic and Static Horizontal Loads," Civil Engineering Series, Structural Research Series No. 490, University of Illinois, Urbana, April, 1981.

38. Pannell, F.N., "The Ultimate Moment of Resistance of Unbonded Prestressed Concrete Beams," Magazine of Concrete Research, Vol. 21, No. 66, March, 1969, pp. 43-54.

39. Park, R., and Gamble, W.L., Reinforced Concrete Slabs, John Wiley and Sons, 1980.

40. Park, R., and Islam, S., "Strength of Slab-Column Connections with Shear and Unbalanced Flexure," Journal of the Structural Division, ASCE, Vol. 102, No. ST9, September, 1976, pp. 1879-1901.

41. Tam, A., and Pannell, F.N., "The Ultimate Moment of Resistance of Unbonded Partially Prestressed Reinforced Concrete Beams," Magazine of Concrete Research, Vol. 28, No. 97, December, 1976, pp. 203-208.

42. Trongtham, N., and Hawkins, N.M., "Moment Transfer to Columns in Unbonded Post-Tensioned Prestressed Concrete Slabs," Report SM 77-3, Department of Civil Engineering, University of Washington, Seattle, Washington, October, 1977.

43. Warwaruk, J., Sozen, M.A., and Siess, C.P., "Strength and Behavior in Flexure of Prestressed Concrete Beams," University of Illinois Engineering Experimental Station Bulletin No. 464, Urbana, Illinois, August, 1962.

44. Winter, C.V., "Flexural Behavior of a Post-Tensioned Flat Plate with Unbonded Tendons," thesis presented to The University of Texas, at Austin, Texas, in 1978, in partial fulfillment of the requirements for the degree of Master of Science.

45. Zaghlool, E.R.F., and de Paiva, H.A.R., "Tests of Flat-Plate Corner Column-Slab Connections," Journal of the Structural Division, ASCE, Vol. 99, No. ST3, March, 1973, pp. 551-572.

46. Zia, P., and McGee, W.D., "Torsion Design of Prestressed Concrete," Journal of the Prestressed Concrete Institute, Vol. 19, No. 2, March-April, 1974, pp. 46-65.